



QA: NA

December 2003

Technical Basis Document No. 6: Waste Package and Drip Shield Corrosion

Revision 1

Prepared for:

U.S. Department of Energy

Office of Civilian Radioactive Waste Management

Office of Repository Development

1551 Hillshire Drive

Las Vegas, Nevada 89134-6321

Prepared by:

Bechtel SAIC Company, LLC

1180 Town Center Drive

Las Vegas, Nevada 89144

Under Contract Number

DE-AC28-01RW12101

CONTENTS

		Page
1.	INTRODUCTION	1-1
1.1	WASTE PACKAGE AND DRIP SHIELD MATERIALS SELECTION, DESIGN, AND FABRICATION	1-4
1.2	INTEGRATED MODEL FOR WASTE PACKAGE AND DRIP SHIELD DEGRADATION	1-6
1.3	NOTE REGARDING THE STATUS OF SUPPORTING TECHNICAL INFORMATION.....	1-10
2.	THERMAL OPERATING REGIMES FOR WASTE PACKAGE AND DRIP SHIELD	2-1
2.1	EXPECTED IN-DRIFT ENVIRONMENT.....	2-1
2.2	RELATION OF IN-DRIFT CHEMICAL MODEL RESULTS TO CORROSION TESTING ENVIRONMENTS	2-3
3.	LONG-TERM THERMAL AGING OF ALLOY 22 IN THE REPOSITORY	3-1
3.1	MODEL DEVELOPMENT	3-1
3.2	KINETICS OF TRANSFORMATION IN A NICKEL-CHROMIUM- MOLYBDENUM ALLOY SURROGATE FOR ALLOY 22.....	3-1
3.3	EXPERIMENTAL RESULTS.....	3-5
3.4	MODEL CONFIDENCE.....	3-9
3.5	SUMMARY	3-10
4.	WASTE PACKAGE OUTER SHELL OXIDATION AND CORROSION IN DRYOUT REGIME.....	4-1
4.1	DRY OXIDATION ABOVE DELIQUESCENCE POINT	4-1
4.2	CORROSION UNDERNEATH DELIQUESCENT BRINES	4-2
5.	GENERAL CORROSION OF THE WASTE PACKAGE OUTER SHELL	5-1
5.1	LONG-TERM WEIGHT LOSS MEASUREMENTS.....	5-1
5.2	GENERAL CORROSION MODEL.....	5-4
5.3	UNCERTAINTY ANALYSIS OF GENERAL CORROSION RATE DATA.....	5-6
5.4	TIME-DEPENDENT GENERAL CORROSION BEHAVIOR OF THE WASTE PACKAGE OUTER SHELL	5-6
5.5	OTHER FACTORS INFLUENCING GENERAL CORROSION OF WASTE PACKAGE OUTER SHELL MATERIAL	5-7
5.6	SUMMARY OF GENERAL CORROSION OF WASTE PACKAGE OUTER SHELL	5-12
6.	LOCALIZED CORROSION OF ALLOY 22 IN AGGRESSIVE BRINES EVOLVED IN THE TRANSITION REGIME	6-1
6.1	CRITERION FOR LOCALIZED CORROSION.....	6-1
6.2	LONG-TERM OPEN-CIRCUIT CORROSION POTENTIAL DATA ANALYSIS.....	6-2

CONTENTS (Continued)

	Page
6.3 CYCLIC POTENTIODYNAMIC POLARIZATION TECHNIQUES.....	6-7
6.4 CURRENT APPROACH TO MODELING LOCALIZED CORROSION	6-9
6.5 LOCALIZED CORROSION INITIATION MODEL	6-18
6.6 CONSERVATISM IN THE LOCALIZED CORROSION MODEL FOR THE WASTE PACKAGE OUTER SHELL	6-21
6.7 LOCALIZED CORROSION PENETRATION RATE MODEL.....	6-21
7. LOCALIZED CORROSION OF ALLOY 22 IN CALCIUM-CHLORIDE-FREE BRINES EXPECTED IN THE TRANSITION- AND LOW-TEMPERATURE REGIMES (FREQUENCY GREATER THAN OR EQUAL TO 90 PERCENT).....	7-1
8. THE EFFECTS OF GAMMA RADIOLYSIS IN TRANSITION AND LOW-TEMPERATURE REGIMES	8-1
9. STRESS CORROSION CRACKING AND PREVENTION THROUGH STRESS MITIGATION OF THE WASTE PACKAGE OUTER SHELL	9-1
9.1 INITIAL ASSESSMENT OF ALLOY 22 STRESS CORROSION CRACKING SUSCEPTIBILITY OVER RANGE OF POTENTIAL AND ACCELERATED WASTE PACKAGE OUTER SHELL ENVIRONMENTS.....	9-1
9.2 PREDICTIVE MODELS FOR STRESS CORROSION CRACKING INITIATION AND PROPAGATION.....	9-3
9.3 THRESHOLD STRESS INTENSITY FACTOR.....	9-8
9.4 PREVENTION OF STRESS CORROSION CRACKING THROUGH MITIGATION OF RESIDUAL TENSILE STRESS IN CLOSURE WELD	9-10
9.5 IMPACT OF CORROSION ON STRESS-MITIGATED WELD (COMPRESSIVE LAYER).....	9-16
10. DEGRADATION OF DRIP SHIELD MATERIALS	10-1
10.1 BACKGROUND ON TITANIUM GRADE 7 AND CORROSION MODELING	10-1
10.2 DRY OXIDATION.....	10-4
10.3 GENERAL CORROSION.....	10-5
10.4 LOCALIZED CORROSION	10-9
10.5 INFLUENCE OF FLUORIDE ON THE CORROSION OF TITANIUM GRADE 7	10-11
10.6 INFLUENCE OF CALCIUM CHLORIDE ON LOCALIZED CORROSION OF TITANIUM GRADE 7.....	10-12
10.7 ENVIRONMENTALLY ASSISTED CRACKING OF THE DRIP SHIELD.....	10-13
10.7.1 Stress Corrosion Cracking of Drip Shield.....	10-13
10.7.2 Hydrogen-Induced Cracking of Drip Shield	10-14
10.8 OTHER FACTORS POTENTIALLY AFFECTING DRIP SHIELD CORROSION	10-15
10.9 SUMMARY OF DEGRADATION OF DRIP SHIELD MATERIALS	10-17

CONTENTS (Continued)

	Page
11. CONCLUSIONS.....	11-1
11.1 THERMAL REGIMES.....	11-1
11.2 DEGRADATION MODES	11-2
11.3 RADIOLYSIS.....	11-4
11.4 MICROBIALLY INFLUENCED CORROSION.....	11-4
11.5 OTHER POTENTIAL DRIP SHIELD DEGRADATION MODES.....	11-4
12. REFERENCES	12-1
12.1 DOCUMENTS CITED.....	12-1
12.2 CODES, STANDARDS, AND REGULATIONS.....	12-9
12.3 DATA, LISTED BY DATA TRACKING NUMBER	12-9
APPENDIX A — MEASUREMENT OF CORROSION RATES OF WASTE PACKAGE MATERIALS (RESPONSE TO CLST 1.07 AIN-1)	A-1
APPENDIX B — DISTRIBUTION OF STRESSES (RESPONSE TO CLST 1.13 AND GEN 1.01 (COMMENT 120))	B-1
APPENDIX C — ROCKFALL AND DEAD-WEIGHT EFFECTS (RESPONSE TO CLST 1.14).....	C-1
APPENDIX D — EFFECTS OF FABRICATION ON THE SUSCEPTIBILITY OF ALLOY 22 AND TITANIUM GRADE 7 TO CORROSION AND STRESS CORROSION CRACKING (RESPONSE TO CLST 1.15 AND GEN 1.01 (COMMENT 119))	D-1
APPENDIX E — THERMAL PROFILE OF THE WASTE PACKAGE MATERIAL DUE TO INDUCTION ANNEALING (RESPONSE TO CLST 1.16)	E-1
APPENDIX F — STRESS MEASURE FOR ASSESSING THE SUSCEPTIBILITY OF VARIOUS ENGINEERED BARRIER SYSTEM MATERIALS TO STRESS CORROSION CRACKING (RESPONSE TO RDTME 3.18)	F-1
APPENDIX G — QUANTIFICATION OF THE RESISTANCE OF ALLOY 22 AND TITANIUM-7 TO ENVIRONMENTALLY ASSISTED CRACKING PHENOMENA (RESPONSE TO CLST 1.12 AND GEN 1.01 (COMMENTS 9, 10, 119, AND 120)).....	G-1
APPENDIX H — EXPECTED BEHAVIOR OF ALPHA TITANIUM ALLOYS (RESPONSE TO CLST 6.02 AIN-1 AND CLST 6.03 AIN-1)	H-1

INTENTIONALLY LEFT BLANK

FIGURES

	Page
1-1. Components of the Postclosure Technical Basis for the License Application	1-4
1-2. Typical Waste Package Types That Will Be Used for the Storage of Spent Nuclear Fuel and High-Level Radioactive Waste	1-5
1-3. Systematic Interactions between the In-Drift Environment and the Drip Shield and Waste Package Outer Shell Resulting in the Occurrence of Various Degradation Modes.....	1-7
2-1. Typical Waste Package Temperature Histories	2-1
2-2. Typical In-Drift Relative Humidity Histories.....	2-2
3-1. Time-Temperature-Transformation Diagram for Ternary Alloy Nickel–21.1 Chromium–13.5 Molybdenum	3-2
3-2. Calculated Isothermal Time-Temperature-Transformation for a Face-Centered Cubic-Based Matrix of a Ternary Ni–21.1Cr–7.5Mo (in Weight Percent) Alloy (Surrogate for Alloy 22) Transforming into the oP6-Ordered Phase for 2, 10, and 15 Percent Transformation Rates.....	3-3
3-3. Calculated Isothermal Time-Temperature-Transformation for a Face-Centered Cubic-Based Matrix of a Ternary Ni–21.1Cr–13.5Mo (in Weight Percent) Alloy (Surrogate for Alloy 22) Transforming into the P Phase for 2, 10, and 15 Percent Transformation Rates.....	3-4
3-4. Calculated Isothermal Time-Temperature-Transformation for a Face-Centered Cubic-Based Matrix of a Ternary Ni–21.1Cr–13.5Mo (in Weight Percent) Alloy (Surrogate for Alloy 22) Transforming into the σ Phase for 2, 5, and 10 Percent Transformation Rates.....	3-5
3-5. Precipitation of Tetrahedrally Close Packed Phases in Alloy 22 Base Metal as a Function of Time and Temperature	3-6
3-6. Precipitation of Tetrahedrally Close Packed Phases at Alloy 22 Grain Boundaries as a Function of Time and Temperature	3-7
3-7. Microhardness (Hv) Measurements on Aged Alloy 22 Base Metal Shown as a Function of Time and Temperature and Indicative of Long-Range Ordering.....	3-8
3-8. Tetrahedrally Close Packed Phase Precipitation Kinetics for Alloy 22 Gas Tungsten Arc Weld as a Function of Temperature.....	3-9
4-1. Thermogravimetric Analysis Data Comparing the Weight Gains of Alloy 825 and Alloy 22 at 150°C and 22.5 Percent Relative Humidity	4-3
4-2. Localized Corrosion of Alloy 825 Underneath a Deliquescent Brine	4-4
4-3. Scanning Electron Microscope View of the White Precipitates on the Alloy 22 Surface (Shown in Figure 4-2) Formed from the Deliquescent Brine.....	4-4
5-1. Corrosion Rates for Alloy 22 Weight-Loss Coupons in Simulated Acidified Water, Simulated Concentrated Water, and Simulated Dilute Water.....	5-3
5-2. Corrosion Rates for Alloy 22 Crevice Coupons in Simulated Acidified Water, Simulated Concentrated Water, and Simulated Dilute Water	5-3

FIGURES (Continued)

	Page
5-3. Cumulative Distribution Function of R_o of Base-Case General Corrosion Rate for Alloy 22 Waste Package Outer Shell at 60°C.....	5-4
5-4. Temperature Dependence of Corrosion Rates for Alloy 22 for Various Metallurgical Conditions and Sample Configurations and in a Wide Range of Test Solutions	5-5
5-5. Calculated Model Outputs of the Base-Case Temperature-Dependent General Corrosion Model, Based on the Crevice Sample Data at 25°C, 50°C, 75°C, 100°C, 125°C, and 150°C.....	5-6
5-6. Time-Dependent General Corrosion Rate of Alloy 22.....	5-7
5-7. Comparison of Corrosion Rates from 24-Hour Polarization Resistance Measurements of Mill-Annealed, As-Welded, and As-Welded Plus Aged Alloy 22 Multiple Crevice Assembly Samples in 5 M CaCl ₂ Brines at Varying Temperatures.....	5-11
5-8. Comparison of Corrosion Rates from 24-Hour Polarization Resistance Measurements of Mill-Annealed, As-Welded, and As-Welded Plus Aged Alloy 22 Multiple Crevice Assembly Samples in 5 M CaCl ₂ + 0.5 M Ca(NO ₃) ₂ Brines at Varying Temperatures.....	5-12
6-1. Open-Circuit Corrosion Potential Measurements for Samples of Alloy 22 in Three Types of Long Term Corrosion Test Facility Solutions (Simulated Dilute Water, Simulated Acidified Water, and Simulated Concentrated Water), as a Function of Time.....	6-3
6-2. Open-Circuit Corrosion Potential Measurements for Samples of Alloy 22 in Simulated Acidified Water, at Different Conditions, and as a Function of Time	6-4
6-3. Open-Circuit Corrosion Potential Measurements for Samples of Alloy 22 in CaCl ₂ Solutions, with Various Concentrations and Inhibitor Levels, and as a Function of Time.....	6-5
6-4. Open-Circuit Corrosion Potential for Alloy 22, with Various Sample Configurations, Metallurgical Conditions, and Chloride Concentration, after Exposure for Extended Periods.....	6-6
6-5. Hypothetical Cyclic Potentiodynamic Polarization Curves for 316L, Alloy 22, and Titanium in High-Chloride Solutions	6-7
6-6. Cyclic Potentiodynamic Polarization Data for Alloy 22 in Simulated Saturated Water at 120°C.....	6-8
6-7. Cyclic Potentiodynamic Polarization Data for Type 316L Stainless Steel in Simulated Saturated Water at 120°C (Noncreviced Disc Sample).....	6-9
6-8. Cyclic Potentiodynamic Polarization Data for Creviced Alloy 22 (DEA 3229) in 5 M CaCl ₂ Brine at 45°C without NO ₃ ⁻ Inhibitor.....	6-11
6-9. Cyclic Potentiodynamic Polarization Data for Creviced Alloy 22 (DEA 3219) in 5 M CaCl ₂ Brine at 90°C without NO ₃ ⁻ Inhibitor.....	6-12
6-10. Cyclic Potentiodynamic Polarization Data for Creviced Alloy 22 (DEA 3236) in 5 M CaCl ₂ Brine at 120°C without NO ₃ ⁻ Inhibitor.....	6-12

FIGURES (Continued)

	Page
6-11. Effect of Long-Term Exposure on the Open-Circuit Corrosion Potential of Alloy 22 in High-Temperature CaCl ₂ Brine	6-13
6-12. Critical Potentials of Creviced Alloy 22 Samples in CaCl ₂ Brines, without NO ₃ ⁻ Inhibitor, and at Temperatures Ranging from 45°C to 120°C	6-13
6-13. Cyclic Potentiodynamic Polarization Data for Creviced Alloy 22 (DEA 3102) in 5 M CaCl ₂ Brine at 90°C with NO ₃ ⁻ Inhibitor.....	6-14
6-14. Cyclic Potentiodynamic Polarization Data for Creviced Alloy 22 (DEA 3127) in 7 M CaCl ₂ Brine at 130°C with NO ₃ ⁻ Inhibitor.....	6-14
6-15. Effect of Long-Term Exposure on the Open-Circuit Corrosion Potential of Alloy 22 in High-Temperature CaCl ₂ Brine with Nitrate Inhibitor	6-15
6-16. Critical Potentials of Creviced Alloy 22 Samples in CaCl ₂ Brines, with NO ₃ ⁻ Inhibitor, and at Temperatures Ranging from 60°C to 170°C	6-15
6-17. Critical Potentials of Creviced Alloy 22 Samples in CaCl ₂ Brines, with NO ₃ ⁻ Inhibitor, and at Temperatures Ranging from 60°C to 170°C	6-16
6-18. Localized Corrosion during Cyclic Potentiodynamic Polarization of Alloy 22 Multiple Crevice Assembly in 5 M CaCl ₂ Brine at 105°C, with and without Inhibition by NO ₃ ⁻ Anion	6-17
6-19. Localized Corrosion during Cyclic Potentiodynamic Polarization of Alloy 22 Disk in 9 M CaCl ₂ Brine at 150°C, with and without Inhibition by NO ₃ ⁻ Anion (Specimens DEA 596 and DEA 597)	6-17
6-20. Model Results for Crevice Corrosion Susceptibility of the Waste Package Outer Shell as a Function of Temperature for 10 M Chloride, pH 7, and 1 M Nitrate (NO ₃ /Cl ratio = 0.1)	6-20
6-21. Model Results for Crevice Corrosion Susceptibility of the Waste Package Outer Shell as a Function of Temperature for 10 M Chloride, pH 3, and 1 M Nitrate (NO ₃ /Cl ratio = 0.1)	6-20
7-1. Cyclic Potentiodynamic Polarization of Alloy 22 in Basic Saturated Water at 100°C, Showing a 550 mV Margin between the Short-Term Open-Circuit Corrosion Potential and the Anodic Oxidation Peak	7-2
7-2. Long-Term Open-Circuit Corrosion Potential for Alloy 22 in Basic Saturated Water at 105°C, Showing that the Corrosion Potential Reaches a Stable, Constant Value of below 150 mV after 2 Years	7-2
7-3. Cyclic Potentiodynamic Polarization of Alloy 22 in Simulated Acidified Water at 90°C, Showing a 650 mV Margin between the Short-Term Open-Circuit Corrosion Potential and the Breakdown Potential	7-3
7-4. Long-Term Open-Circuit Corrosion Potential for Alloy 22 in Simulated Acidified Water at 90°C, Showing that the Corrosion Potential Reaches a Stable, Constant Value of below 400 mV after 2 Years	7-4
7-5. Cyclic Potentiodynamic Polarization of Alloy 22 in Simulated Concentrated Water at 90°C, Showing a 500 mV Margin between the Short-Term Open-Circuit Corrosion Potential and the Anodic Oxidation Peak	7-5

FIGURES (Continued)

	Page
7-6. Long-Term Open-Circuit Corrosion Potential for Alloy 22 in Simulated Concentrated Water at 90°C, Showing that the Corrosion Potential Reaches a Stable, Constant Value of below 0 mV versus Ag/AgCl after More than 2 Years.....	7-6
9-1. Predicted Crack-Growth Rate for the Stress Corrosion Cracking of Alloy 22 in Basic Saturated Water at 110°C as a Function of Stress Intensity Factor, and for Bounding Values of the Repassivation Parameter (n)	9-7
9-2. Measured Residual Tensile Stress in Alloy 22 Weld Region with and without Laser-Shock-Peening	9-11
9-3. Site Recommendation and License Application Waste Package Closure Lid Designs	9-12
9-4. Hoop Stress versus Depth for the Stress-Mitigated Outer Lid of the Waste Package Outer Shell at Various Angles	9-13
9-5. Stress Intensity Factor versus Depth for the Stress-Mitigated Outer Lid of the Waste Package Outer Shell	9-13
9-6. Predictions of the Hoop Stress ($\theta = 0$) as a Function of Depth in the Stress-Mitigated Outer Weld of the Waste Package Outer Shell	9-14
9-7. Residual Stress Distribution in Welded Alloy 22 Plates with Laser-Shock Peening Stress Mitigation	9-15
9-8. Residual Stress Distribution in Welded Alloy 22 Plates with Controlled Plasticity Burnishing Stress Mitigation	9-16
10-1. Relationship between the Relevant Titanium Alloys.....	10-3
10-2. Corrosion Modes and Modeling Approaches in <i>General Corrosion and Localized Corrosion of the Drip Shield</i>	10-4
10-3. Distribution of General Corrosion Rates of Titanium Grade 16: (a) Long Term Corrosion Test Facility 1-Year Weight Loss Samples and (b) 1-Year Crevice Samples	10-6
10-4. Distribution of General Corrosion Rates of Titanium Grade 16: (a) Long Term Corrosion Test Facility 5-Year Weight Loss Specimens and (b) 5-Year Crevice Specimens	10-8
10-5. Titanium Grade 7 in Simulated Saturated Water at 120°C (NEA031s)	10-10
10-6. Plot of the Median ΔE and -4σ Confidence Interval Surface versus pH and Absolute Temperature at $[Cl^-] = 3 \text{ mol/L}$ (a) and versus pH and Base 10 Logarithm of Chloride Ion Concentration at $T = 300 \text{ K}$ for Titanium Grade 7 Using an Absolute Temperature of 380 K	10-11

TABLES

	Page
1-1. Key Technical Issue Agreements Addressed in this Report.....	1-2
2-1. Drift Crown Seepage Water Limiting Compositions and Probabilities of Their Formation, the Associated Brine Type, and the Corresponding Corrosion Test Solutions	2-7
2-2. Target Composition of Standard Test Media Based on J-13 Well Water.....	2-8
2-3. Brines from Dust Deposited on the Waste Packages, Including Bromide, the Probabilities of Their Formation, the Associated Brine Type, and the Corresponding Corrosion Test Solutions.....	2-9
5-1. Alterations in Corrosion Rates and Potentials Associated with Microbial Degradation.....	5-9
6-1. Bounding Rates for Localized Corrosion for Alloy 22 (Distribution).....	6-22
9-1. Slow Strain Rate Test Results for Annealed Alloy 22 (Strain Rate of 1.66×10^{-6} per second)	9-2
9-2. Determination of the Slip-Dissolution Film-Rupture Model Parameters for Alloy 22 in Basic Saturated Water at 110°C	9-6
9-3. Threshold Stress Intensity Factor (K_{ISCC}) Distribution for Alloy 22 in 110°C Basic Saturated Water.....	9-8
9-4. Estimates of the Time-to-Failure (t_f) for Stress-Mitigated Closure Weld	9-17
10-1. American Society for Testing and Materials Specifications for Chemical Composition Requirements (Weight Percent) for Relevant Titanium Alloys	10-2
10-2. American Society for Testing and Materials Specifications for Mechanical Properties of Relevant Titanium Alloys in this Report.....	10-2
10-3. Dry Oxidation Titanium Oxide Thickness: Measured versus Calculated Using Equation 10-2.....	10-5
10-4. Summary of 1-Year and 5-Year Corrosion Data Comparison.....	10-7
10-5. General Corrosion Rates of Titanium Grade 7 in Selected Test Media Containing High Concentrations of Chlorides of Ca^{2+} , Mg^{2+} , and Fe^{3+} Ions at Elevated Temperature	10-13

INTENTIONALLY LEFT BLANK

ACRONYMS AND ABBREVIATIONS

AIN	additional information needed
AMR	analysis and modeling report
BSW	basic saturated water
CLST	Container Life and Source Term
DOE	U.S. Department of Energy
GEN	General Agreement
KTI	Key Technical Issue
LA	license application
LTCTF	Long Term Corrosion Test Facility
MIC	microbially influenced corrosion
NRC	U.S. Nuclear Regulatory Commission
PWR	pressurized water reactor
RDTME	Repository Design and Thermal-Mechanical Effects
SAW	simulated acidified water
SCC	stress corrosion cracking
SCW	simulated concentrated water
SDW	simulated dilute water
SSC	silver/silver chloride (Ag/AgCl)
SSW	simulated saturated water
TSPA	total system performance assessment

INTENTIONALLY LEFT BLANK

1. INTRODUCTION

This report provides a discussion of the degradation processes and long-term performance of waste packages and drip shields within the repository system. This report responds to Key Technical Issue (KTI) agreements (listed in Table 1-1) raised by the U.S. Nuclear Regulatory Commission (NRC) related to the adequacy of the representation of the testing environments and processes affecting the integrity of the waste package and drip shield during the repository regulatory period. It describes the degradation models, corrosion testing and treatment of uncertainty, appropriate for the environmental conditions predicted for the repository.

This technical basis document provides a summary of the likely behavior of the waste package and drip shield in the repository after the permanent closure of the facility. This document is one in a series of technical basis documents prepared for each feature of the repository system relevant to predicting the likely postclosure performance of the repository. The relationship of waste package and drip shield performance (Process VI. Waste Package and Drip Shield Corrosion) to the other components is illustrated in Figure 1-1.

Appendices to this technical basis document are intended to allow for a transparent and direct response to each KTI agreement. Each appendix addresses one or more of the KTI agreements. If agreements apply to similar aspects of the waste package or drip shield degradation process, they were grouped in a single appendix. In some cases, appendices provide detailed discussions of data, analyses, or information related to the further conceptual understanding presented in this technical basis document.

A technical basis document on the in-drift chemical environment will provide the information on the evolution of the environment on the waste package and drip shield during the regulatory performance period. Based on the chemical environment described in that technical basis document, this report discusses the corrosion models developed, corrosion-related testing, and an assessment of other degradation processes. Section 1 discusses the materials selection and design and the integrated degradation model for the waste package and the drip shield. Section 2 provides a description of the waste package and drip shield surface environments. The evolution of this local in-drift environment depends upon the interaction between warm waste packages, rocks in the drift wall, seepage water, dust deposits, and humidity. Section 2 describes these interactions and the resulting water compositions on the surface of the drip shield and waste package in sufficient detail to set the stage for subsequent sections. Sections 3 through 9 describe the various degradation processes and the models that address them. Section 10 addresses the integrity of the drip shield. Section 11 provides the conclusions derived from the individual models and their integration. Appendices A through H address specific KTIs associated with this technical basis document.

Table 1-1. Key Technical Issue Agreements Addressed in this Report

KTI/AIN/GEN Code	Wording
CLST 1.07	Provide documentation for the alternative methods to measure corrosion rates of the waste package materials (e.g., ASTM G-102 testing) or provide justification for the current approach. DOE will document the alternative methods of corrosion measurement in the revision of Alloy 22 AMR (ANL-EBS-MD-000003), prior to license application.
CLST 1.07 AIN-1	The use of appropriate standards should be adopted and exceptions should be properly justified. If a standard is mentioned but not used in its entirety, DOE should indicate specifically which parts of the code will be used (example, G1 is used for identification of equipment, G1 is used for data interval, etc.). Better justification for not using alternative techniques is needed. If such a justification cannot be provided, then DOE must provide details on the alternative techniques to be used for corrosion rate measurements.
CLST 1.12	Provide the documentation for Alloy 22 and titanium for the path forward items listed on slides 34 and 35. DOE will provide the documentation in a revision to AMRs (ANL-EBS-MD-000005 and ANL-EBS-MD-000006) prior to LA.
CLST 1.13	Provide the data that characterizes the distribution of stresses due to laser peening and induction annealing of Alloy 22. DOE will provide the documentation in a revision to AMR (ANL-EBS-MD-000005) prior to LA.
CLST 1.14	Provide the justification for not including the rockfall effect and deadwood from drift collapse on SCC of the waste package and drip shield. DOE will provide the documentation for the rockfall and dead-weight effects in the next revision of the SCC AMR (ANL-EBS-MD-000005) prior to LA.
CLST 1.15	Provide the documentation for Alloy 22 and titanium for the path forward items listed on slide 39. DOE will provide documentation for Alloy 22 and Ti path forward items on slide 39 in a revision to the SCC and General and Localized Corrosion Analysis and Model Reports (ANL-EBS-MD-000003, ANL-EBS-MD-000004, ANL-EBS-MD-000005) by license application.
CLST 1.16	Provide the documentation on the measured thermal profile of the waste package material due to induction annealing. DOE stated that the thermal profiles will be measured during induction annealing, and the results will be reported in the next stress corrosion cracking analysis model report (ANL-EBS-MD-000005) prior to LA.
RDTME 3.18	Provide a technical basis for a stress measure that can be used as the equivalent uniaxial stress for assessing the susceptibility of the various EBS materials to stress corrosion cracking. The proposed stress measure must be consistent and compatible with the methods proposed by the DOE to assess SCC of the containers in WAPDEG and in accordance with the agreements reached at the Container Life and Source Term Technical Exchange. DOE will include a detailed discussion of the stress measure used to determine nucleation of stress corrosion cracks in the calculations performed to evaluate waste package barriers and the drip shield against stress corrosion cracking criterion. DOE will include these descriptions in future revisions of the following: Design Analysis for UCF Waste Packages, ANL-UDC-MD-000001, Design Analysis for the Defense High-Level Waste Disposal Container, ANL-DDC-ME-000001, Design Analysis for the Naval SNF Waste Package, ANL-UDC-ME-000001, and Design Analysis for the Ex-Container Components, ANL-XCS-ME-000001. The stresses reported in these documents will be used in WAPDEG and will be consistent with the agreements and associated schedule made at the Container Life and Source Term Technical Exchange (Subissue 1, Agreement 14, Subissue 6, Agreement 1).
CLST 6.02	Provide additional justification for the use of a 400 ppm hydrogen criterion or perform a sensitivity analysis using a lower value. DOE stated that additional justification will be found in the report "Review of Expected Behavior of Alpha Titanium Alloys under Yucca Mountain Condition" TDR-EBS-MD-000015, which is in preparation and will be available in January 2001.

Table 1-1. Key Technical Issue Agreements Addressed in this Report (Continued)

KTI/AIN/GEN Code	Wording
CLST 6.03	Provide the technical basis for the assumed fraction of hydrogen absorbed into titanium as a result of corrosion. DOE stated that additional justification will be found in the report "Review of Expected Behavior of Alpha Titanium Alloys under Yucca Mountain Condition" TDR-EBS-MD-000015, which is in preparation and will be available in January 2001.
CLST 6.02 AIN-1	<ol style="list-style-type: none"> 1. Provide better justification to verify the critical hydrogen concentration chosen is a realistic and representative value for the onset of cracking in Titanium Grade 7. An evaluation of the critical hydrogen concentration for Titanium Grade 24 should also be given. 2. Provide an evaluation of possible detrimental effects of the fluoride on hydrogen uptake and its effects on the critical hydrogen concentration and subsequent cracking. 3. Provide the results for the Titanium Grade 24 structural drip shield components.
CLST 6.03 AIN-1	Provide an evaluation of the possible detrimental effects of fluoride on possible hydrogen uptake rates, as well as enhanced corrosion resulting in higher than currently estimated hydrogen generation rates.
GEN 1.01 Comment 9	<p>Data supporting the residual stress calculations as a result of welding, after laser peening and after induction annealing are not provided.</p> <p>Basis: The distribution of residual stresses in the waste package final closure welds is based on Finite element modeling. Details of the Model are provided in the <i>Stress Corrosion Cracking of the Drip Shield, the Waste Package Outer Barrier, and the Stainless Steel Structured Material</i> AMR. The effects of induction annealing on the residual stresses in the final closure are detailed in the <i>Residual Stress Minimization of Waste Packages from Induction Annealing</i> AMR. Several assumptions are made in the models that are not supported by data. These include the assumed temperature profile during welding, the cooling rates during welding and the residual stress during induction annealing.</p> <p>The distribution of residual stress in the inner closure weld after laser peening is estimated in the SSPA using a shot-peened Incoloy 908 specimen. The technical basis for using a shot-peened specimen is not provided. Differences in the residual stress mitigation methods (i.e. mechanical shot-peening vs. laser peening) may result in significantly different stress distributions.</p>
GEN 1.01 (Comment 10)	<p>The modified stress corrosion cracking parameters are based in recent tests that may not consider the range of possible environments and the effects of fabrication processes.</p> <p>Basis: The SSPA uses modified parameters for the stress corrosion cracking including the repassivation rate for the slip dissolution model and the minimum threshold stress for stress corrosion cracking. The SSPA indicates that these new parameters are based on recent data. The particular importance is the change in the minimum threshold stress which has been increased from 20-30 to 80-90 percent of the yield strength. The value of this parameter which is used in the model abstraction as the critical parameter for the occurrence of SCC is likely to be dependent on several factors that have not been investigated such as chemical composition of the environment and the effects of fabrication processes (only a limited number of cold worked and welded specimens has been evaluated).</p>
GEN 1.01 (Comment 119)	In p. 7-9 DOE claimed that NRC accepted the slip dissolution model. The DOE must supply the reference for this acceptance.
GEN 1.01 (Comment 120)	Page 7-11, the use of the triangular distribution for the residual stress uncertainty dictates that the endpoints of the distribution are well known. Showing the data compared to the distribution would support the selection of a triangular distribution.

NOTE: AMR = analysis and modeling report; DOE = U.S. Department of Energy; LA = license application; EBS = engineered barrier system; SNF = spent nuclear fuel; SCC = stress corrosion cracking.

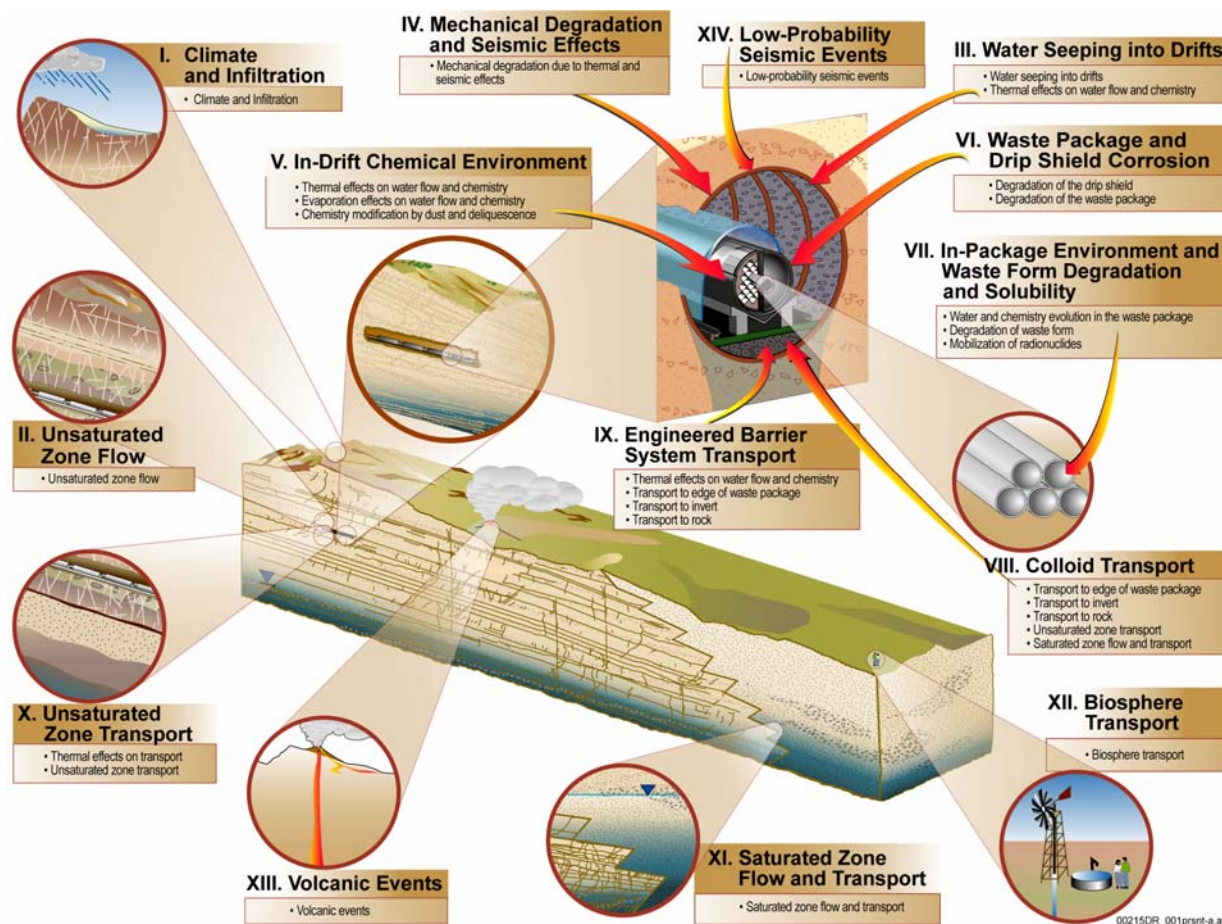


Figure 1-1. Components of the Postclosure Technical Basis for the License Application

1.1 WASTE PACKAGE AND DRIP SHIELD MATERIALS SELECTION, DESIGN, AND FABRICATION

Spent nuclear fuel and high-level radioactive waste (70,000 MTHM) will be placed in approximately 11,000 waste packages (Figure 1-2). The design for the waste package is based upon double-wall construction (Plinski 2001). The inner wall serves as a structural support and is constructed from Type 316 stainless steel with controls on carbon and nitrogen levels. The corrosion-resistant waste package outer shell is constructed from Alloy 22 (UNS N06022), a high-performance nickel-based alloy. Solution heat treatment of the as-fabricated disposal container is used to remove fabrication-related residual tensile stress (BSC 2003a, Section 8.1). After the waste package is filled with high-level radioactive waste or spent nuclear fuel, at the site hot cell facility, the stainless steel cylinder is sealed and two closure lids made of Alloy 22 will be welded to the container outer shell by gas tungsten arc welding. Because residual weld stress at the closure welds might initiate stress corrosion cracking (SCC), a postweld stress mitigation process will be used to reduce the tensile stress in the outer surface, thereby eliminating the stress initiator. The baseline stress mitigation process is laser-shock peening (also called laser peening). The titanium alloy drip shield is used to prevent seepage water, as well as rocks, from directly impinging on the waste package. They will be installed in the stress-relieved condition, following emplacement of the waste packages in the drifts. The stress relief treatment is used to reduce fabrication-related tensile stress below the SCC initiation threshold.

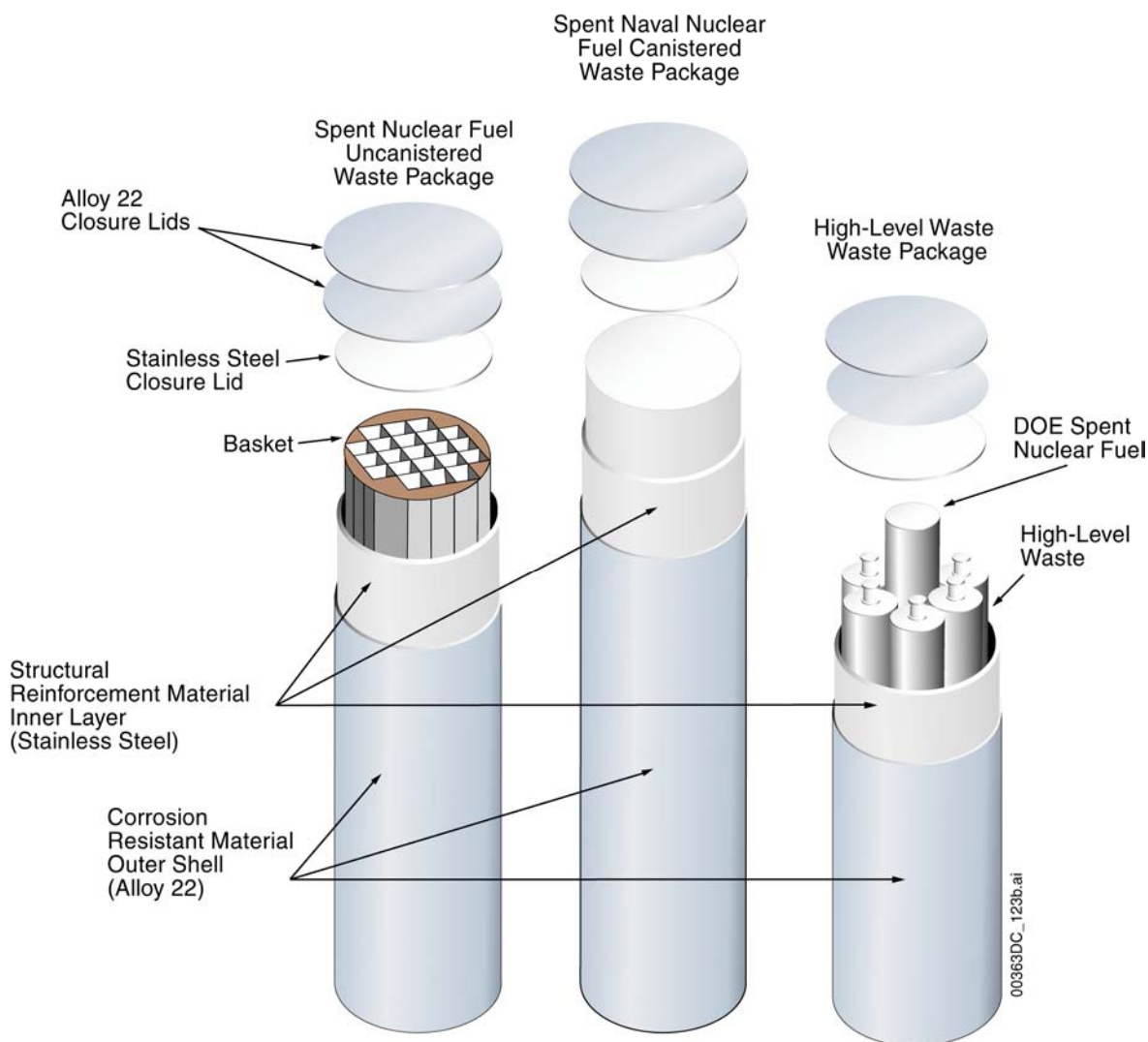


Figure 1-2. Typical Waste Package Types That Will Be Used for the Storage of Spent Nuclear Fuel and High-Level Radioactive Waste

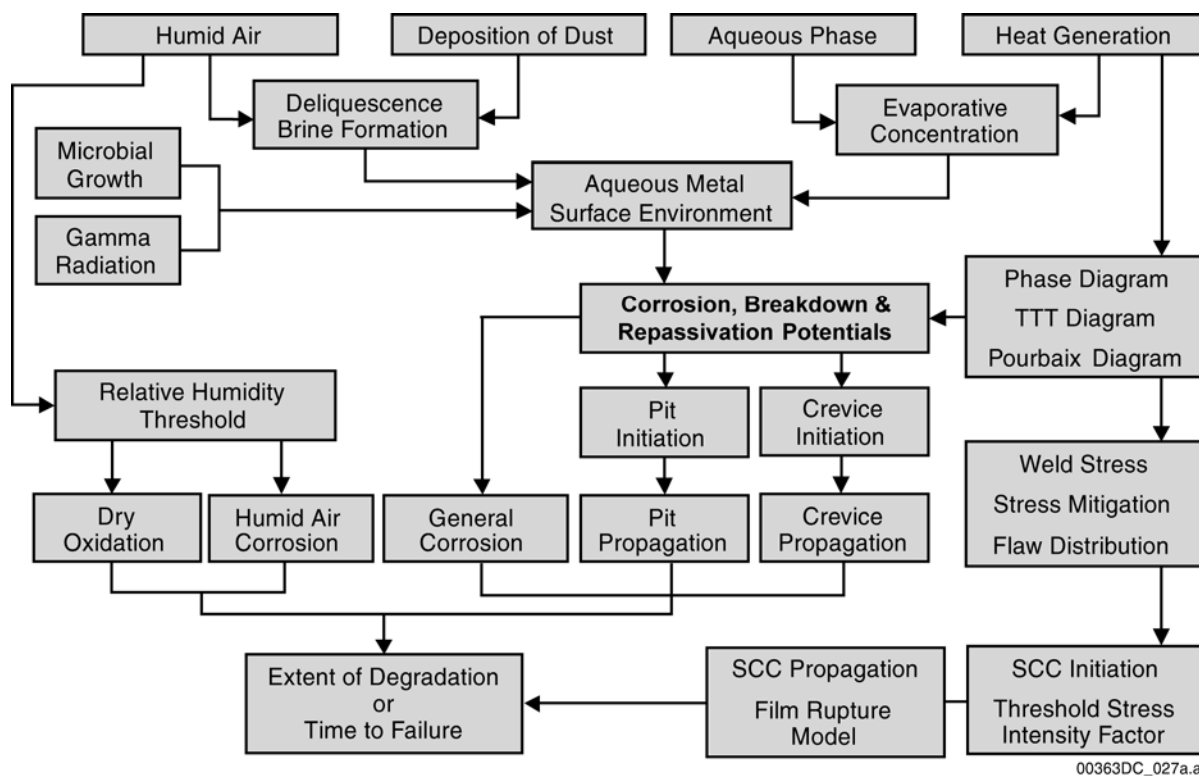
Materials Selection for the Waste Package Outer Shell—Alloy 22 (UNS N06022) was selected for its excellent corrosion resistance in brines and will be used for construction of the outer shell of the waste package. It has already been used for the construction of mockups. It consists of 20.0 to 22.5 percent chromium, 12.5 to 14.5 percent molybdenum, 2.0 to 6.0 percent iron, 2.5 to 3.5 percent tungsten, 2.5 percent (max.) cobalt, 0.015 percent (max.) carbon, and balance nickel (BSC 2003b). Other elements present include phosphorus, silicon, sulfur, and manganese (Treseder et al. 1991). The localized corrosion resistance of Alloy 22 is due to the additions of molybdenum and tungsten, both of which stabilize the passive film at low pH (Hack 1983). The oxides of these elements are insoluble at low pH. Consequently, Alloy 22 is highly resistant to localized attack. Very high repassivation potentials have been observed by some (Gruss et al. 1998), while others have found very low corrosion rates in simulated crevice solutions containing 10 weight percent FeCl_3 (Haynes International 1997). Furthermore, no localized attack of Alloy 22 has been seen in crevices exposed to water compositions representative of

most of those expected in the repository. Such tests have been conducted in the Long Term Corrosion Test Facility (LTCTF) (see Section 5).

Drip Shield Materials—The drip shields will be fabricated using titanium alloys containing small palladium additions to provide corrosion resistance in the anticipated postclosure drift environment. Titanium Grade 7 (UNS R524000), an alpha-phase alloy, was selected for the plate material, which will be supported using higher strength welded ribs and bulkheads made from Titanium Grade 24 (UNS R56405), an alpha-beta alloy. Similar to Alloy 22, based on laboratory test results, literature, and model predictions, these titanium alloys are expected to provide a high level of resistance to the various potential corrosion-related degradation modes, including localized corrosion and hydrogen-induced cracking.

1.2 INTEGRATED MODEL FOR WASTE PACKAGE AND DRIP SHIELD DEGRADATION

Integrated Model—Systematic interactions between the in-drift environment and the drip shield and waste package outer shell result in the occurrence of various degradation modes, which are shown schematically in Figure 1-3. This schematic accounts for a wide range of degradation modes, each operable to varying degrees, depending upon the temperature regime. In the preclosure regime, the walls of the drifts will be kept dry by ventilation air, and no significant degradation of the waste packages is expected. In the postclosure dryout regime (when temperature is greater than or equal to the boiling point of seepage water), potentially relevant high-temperature modes of degradation include dry oxidation and corrosion underneath deliquescent brines (formed by the adsorption of airborne water by dust deposits). In the transition regime (temperature is approximately the boiling point range of seepage water), seepage waters could concentrate on the waste package through evaporation if the drip shield were to fail. The potential modes of attack in these concentrated brines include uniform general corrosion, localized corrosion, and SCC. In the low temperature regime, seepage waters can enter the drift, but the thermal driving force for localized corrosion would be less. The possible modes of attack include general corrosion, localized corrosion, and SCC. Microbially influenced corrosion (MIC) may also occur. These modes of failure are dealt with in this technical basis document, and are illustrated in Figure 1-3. As described in subsequent sections, not every degradation mode represented in Figure 1-3 may occur on either the waste package or the drip shield in the repository (e.g., the drip shield material is not subject to localized corrosion or MIC); however, Figure 1-3 is an illustration of the conceptual model used to consider the possible degradation modes. In addition to these scenarios, other possible events that could lead to failure include seismic and volcanic activity. These scenarios are examined in the technical basis documents on seismic events and igneous events. In addition, effects of combined features, events, and processes are not discussed here.



NOTE: TTT = time-temperature-transformation.

Figure 1-3. Systematic Interactions between the In-Drift Environment and the Drip Shield and Waste Package Outer Shell Resulting in the Occurrence of Various Degradation Modes

Phase Instability—The Titanium Grade 7 drip shield material is a stable alpha (α) phase alloy and possesses outstanding phase stability (BSC 2003c, Section 6.5.3). While Titanium Grade 7 does contain small amounts of alloying elements, most notably palladium, it is essentially pure titanium, which will not form intermetallic compounds under the thermal exposure conditions in the repository. On this basis, Titanium Grade 7 is considered immune to the effects of phase instability under repository exposure conditions.

Alloy 22 is a metastable austenitic alloy, where secondary complex phases can be precipitated at high temperature (BSC 2003d). These intermetallic phases (P , σ , and μ) are rich in those elements responsible for the exceptional corrosion resistance of Alloy 22, and can therefore cause depletion of the passivating elements in close proximity to the precipitates. Such depleted, localized areas may be more susceptible to corrosion than areas where no precipitation has occurred. Furthermore, these precipitates may cause degradation of the mechanical properties. In addition to the higher temperature complex phases, long-range ordering can occur at somewhat lower temperatures and could potentially negatively affect SCC susceptibility. Multicomponent phase diagrams have enabled prediction of the phases that are possible as a function of elemental composition and temperature. Time-temperature-transformation diagrams have been predicted, compared with experimental kinetic measurements, and used to calculate the rate at which deleterious phases (precipitates and long-range ordering) form at time-temperature combinations relevant to the repository. As will be discussed in the Section 3 summary, such predictions indicate insignificant precipitation and long-range ordering for the

mill-annealed and for the as-welded conditions during the 10,000-year simulation period, as long as the temperature is kept below 200°C (or 300°C for shorter times).

Dry Oxidation—Dry oxidation is another high-temperature degradation mode (BSC 2003b; CRWMS M&O 2000a). The reaction of oxygen with Alloy 22, or Titanium Grade 7, can cause a uniform thickening of the oxide layer on the surface. The surface oxide can consist of any of the alloying elements or constituents, although for Alloy 22 a chromium oxide layer has been assumed as the basis of calculations. The rate of metal loss due to dry oxidation at the highest temperature in the repository is insignificant compared to other possible modes of attack. Dry oxidation is not a performance limiting process of the waste package outer shell under the exposure condition expected in the repository and is not considered in the waste package performance analysis for the repository (BSC 2003b, Section 8). Additional details are presented in Section 4.

General Corrosion—General corrosion of the waste package outer shell and the drip shield occurs when the relative humidity at the waste package surface is equal to or greater than the relative humidity threshold ($RH_{threshold}$) for corrosion initiation. The general corrosion rate for the drip shield is temperature independent and does not decrease with exposure time. The general corrosion rate of the waste package outer shell is a function of temperature, expressed with an activation energy using a modified Arrhenius relationship. Because of the very low general corrosion rates of the waste package outer shell for the conditions expected in the repository, waste package performance is not limited by general corrosion during the regulatory period. Additional details are provided in Section 5.

MIC: The drip shield is immune to MIC under the repository exposure conditions (BSC 2003c, Section 6.5.2). The waste package outer shell is potentially subject to MIC when the relative humidity at the waste package surface is equal to or greater than 90 percent. The effect of MIC is represented by an enhancement to the abiotic general corrosion rate of the waste package outer shell (BSC 2003b, Section 8).

Corrosion Underneath Deliquescent Brines—As the temperature begins to decrease during cooling, the possibility exists of concentrated electrolytes developing through the formation of deliquescent brines and the evaporative concentration of seepage waters. Modes of attack experienced in aqueous electrolytes include general corrosion, localized corrosion, and SCC. In the case of general corrosion, the rate of dissolution is uniform over all surfaces and is due to the transport of cations from the metal-oxide interface to the oxide-electrolyte interface, where the formation of soluble metal-containing corrosion products can occur. Cations and anions are transported through the very thin passive oxide barrier film adjacent to the metal surface, with the growth kinetics controlled by diffusion and electric field-driven electromigration (BSC 2003b, Section 6.4.1.1.2).

Localized Corrosion (Pitting and Crevice Corrosion)—Pitting corrosion is any type of distributed, nonuniform corrosive attack of the surface, and is due to the localized failure of the passive film. Such localized failure may be initiated due to surface inclusions of relatively soluble species, the precipitation of small soluble halide crystallites on the passive film, or destabilization of the passive film within occluded areas such as crevices. This destabilization is due to the lowering of pH, which results from the combined effects of differential aeration, the

hydrolysis of dissolved metal cations within the crevice, and the electric field-driven electromigration of aggressive halide anions into the crevice. Localized attack may also occur at sites where precipitation has occurred. Both the drip shield and waste package outer shell are resistant to pitting corrosion under a range of the exposure conditions in the repository.

Crevice may be formed between the waste package and supports, beneath mineral precipitates, corrosion products, dust, rocks, cement, and bio-films, and between layers of the containers. In the absence of inhibitor and buffer ions, the hydrolysis of dissolved metal can lead to the accumulation of H^+ and a corresponding decrease in pH. Electromigration of Cl^- (and other anions) into the crevice must occur to balance cationic charge associated with H^+ ions (Gartland 1997; Walton et al. 1996; Farmer and McCright 1998). These exacerbated conditions can set the stage for subsequent attack of the corrosion resistant material by passive corrosion, pitting (initiation and propagation), SCC, or other mechanisms (Farmer and McCright 1998; Farmer, Lu et al. 2000; Farmer, McCright et al. 2000). Gamma radiolysis may produce hydrogen peroxide, thereby increasing open-circuit corrosion potential (Glass et al. 1986; Kim 1987, 1988, 1999a, 1999b).

The drip shield is not subject to crevice corrosion under the exposure conditions in the repository (BSC 2003c, Section 8.4). The waste package outer shell is not subject to crevice corrosion if the solution contacting the waste package contains significant concentrations of inhibitive ions such as nitrate. The waste package outer shell is, however, potentially susceptible to crevice corrosion if an acidic chloride-containing solution with a low NO_3^-/Cl^- ratio contacts the waste package while it is at elevated temperatures. Additional details are provided in Sections 6 and 7. However, no crevice corrosion was observed after 5-year exposure to a range of brines in the Long Term Corrosion Test Facility.

Stress Corrosion Cracking—SCC is the initiation and propagation of cracks in structural components due to the simultaneous interaction of three factors: metallurgical susceptibility, critical environment, and static (or sustained) tensile stresses. Both Alloy 22 and Titanium Grade 7 are susceptible to SCC under repository exposure conditions. The drip shields (including their fabrication welds) will be fully stress-relief annealed before placement in the drifts (Plinski 2001, Section 8.3.17). Therefore, the drip shield is not subject to SCC upon emplacement in the repository. However, the drip shields are potentially subject to SCC under the action of seismic-induced loading and rockfall. An analysis of the consequence of SCC of the drip shield (BSC 2003a, Section 6.3.7) indicates that stress corrosion cracks in passive alloys such as Titanium Grade 7 tend to be very tight and could be plugged by corrosion products or mineral deposits and, thereby, preventing water transport. Since the primary role of the drip shield is to keep water from contacting the waste package, SCC of the drip shield does not compromise its intended design purpose and is not of significant consequence to repository performance.

Similar to the drip shield, all regions of the waste package (including fabrication welds) except the waste package closure lid welds are stress-relief annealed before the waste packages are loaded with waste (Plinski 2001, Section 8.1.7) and, thus, do not develop residual stress or stress-intensity factors high enough for SCC to occur (BSC 2003a, Section 6.4.2). Residual stress mitigation techniques are applied to the waste package outer closure lid weld region to induce compressive stresses in the outer layers and delay the initiation of crack growth until

these layers are removed by general corrosion processes. The SCC model makes use of a threshold stress for the initiation of stress corrosion cracks on smooth surfaces and a stress-intensity factor threshold for the initiation of crack growth. Manufacturing flaws (e.g., weld defects) are also considered to propagate by SCC. It is conservatively assumed that manufacturing flaws behave like stress corrosion cracks and, thus, only the stress intensity factor threshold for crack growth is applied to the manufacturing flaws.

1.3 NOTE REGARDING THE STATUS OF SUPPORTING TECHNICAL INFORMATION

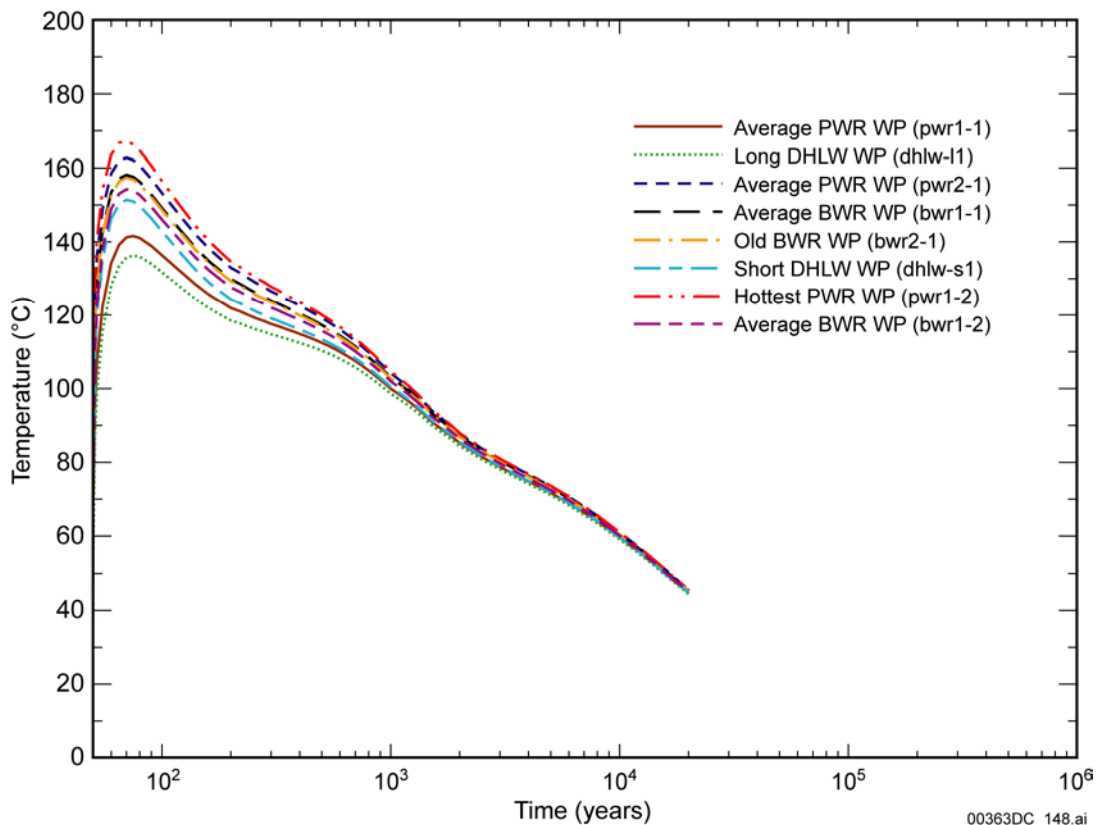
This document was prepared using the most current information available at the time of its development. This technical basis document and its appendices providing KTI agreement responses that were prepared using preliminary or draft information reflect the status of the Yucca Mountain Project's scientific and design bases at the time of submittal. In some cases, this involved the use of draft analysis and model reports and other draft references whose contents may change with time. Information that evolves through subsequent revisions of the analysis and model reports and other references will be reflected in the license application as the approved analyses of record at the time of license application submittal. Consequently, the project will not routinely update either this technical basis document or its KTI agreement appendices to reflect changes in the supporting references prior to submittal of the license application.

2. THERMAL OPERATING REGIMES FOR WASTE PACKAGE AND DRIP SHIELD

2.1 EXPECTED IN-DRIFT ENVIRONMENT

The current repository design enables the repository to operate in three temperature regimes: dryout, transition, and low-temperature. The relevant attributes of each regime are summarized below.

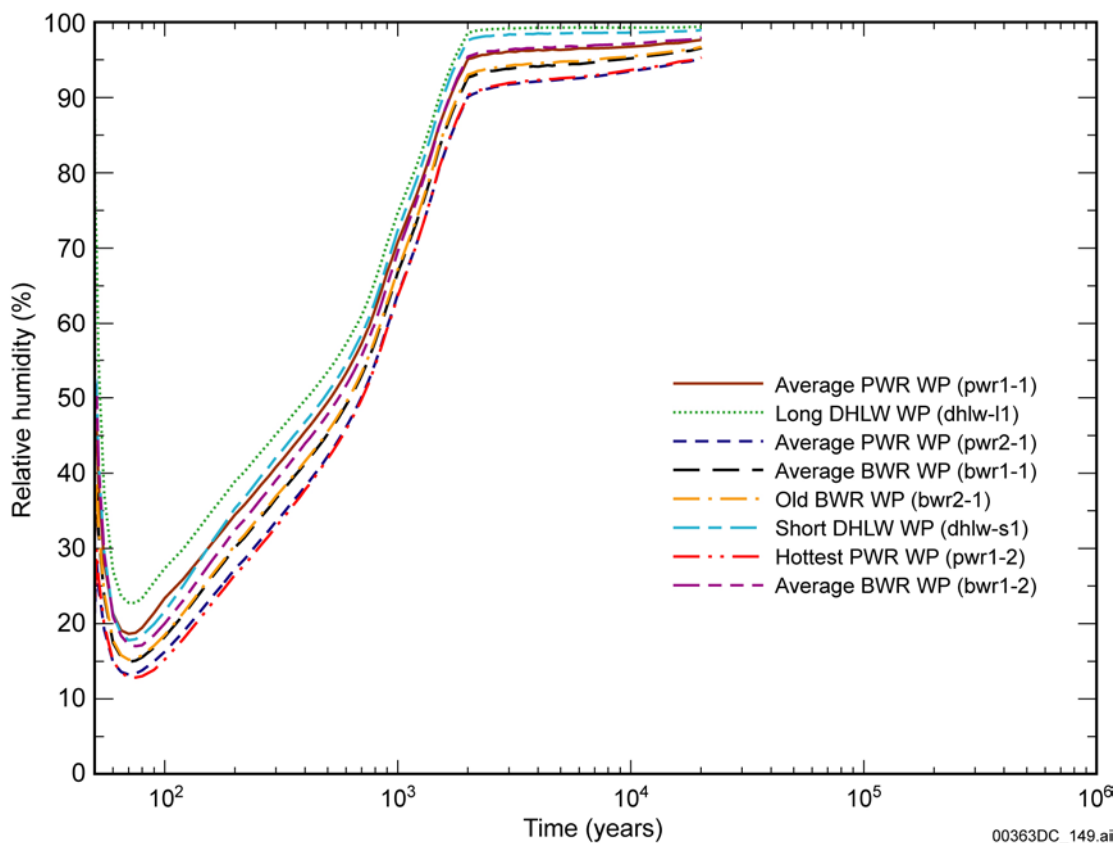
Figures 2-1 and 2-2 show a representative time-temperature and time-relative humidity profile for a variety of waste packages (located near the center of the repository) in the three operational regimes.



Source: BSC 2003e.

NOTE: These histories are plotted for the P3R7C12 location (in the mountain scale thermal-hydrologic model), which is near the center of the repository in the Tptpl1 (tsw35) unit. PWR = pressurized water reactor; WP = waste package; DHLW = defense high-level radioactive waste; BWR = boiling water reactor.

Figure 2-1. Typical Waste Package Temperature Histories



Source: BSC 2003e.

NOTE: These histories are plotted for the P3R7C12 location (in the mountain scale thermal-hydrologic model), which is near the center of the repository in the Tptpl1 (tsw35) unit). PWR = pressurized water reactor; WP = waste package; DHLW = defense high-level radioactive waste; BWR = boiling water reactor.

Figure 2-2. Typical In-Drift Relative Humidity Histories

Dryout—Drift walls will first be dried by ventilation air during the preclosure period. Eventually during postclosure, heat generated by radioactive decay will increase the temperature of waste packages and drift walls above the boiling point of water. Since no significant seepage is expected for drift wall temperatures above the boiling point of water, no aqueous phase corrosion due to seepage is expected (calcium chloride type brines are possible and predicted to occur in this regime, but they occur in the host rock when temperatures are above boiling and seepage into the drift is prevented by the vaporization barrier effect as described in the technical basis document on the in-drift chemical environment). However, depending on the surface temperature and relative humidity conditions, the existence of liquid-phase water on the waste package or drip shield is possible due to the presence of a dust or salt deposit. In the presence of such a deposit, a thin-film liquid phase can be established at a higher temperature and lower relative humidity than otherwise possible. Thus, formation of deliquescent brines in the absence of seepage may occur, and corrosion of the waste package and drip shield is considered in the context of these solutions.

Transition—Seepage into the drifts will become possible as the waste package cools, as the temperature of the drift wall drops below the boiling point of water, and while the waste package

surface temperature is at or above the boiling point of the water. Seepage waters will undergo evaporative concentration on the drip shield surface or the waste package surface at the time when the drip shield seepage diversion function is lost, thereby evolving into either carbonate- or sulfate-type brines. The drip shield will mitigate seepage effects on the waste package and is expected to last through this period, unless there are low-probability seismic events that would shorten its performance lifetime. However, as in the dryout regime, formation of deliquescent brines could occur in this regime.

Low Temperature—As the waste package cools to a temperature below the boiling point of water, the in-drift relative humidity will increase, so evaporated solutions cannot be as concentrated. With further cooling, the temperature will drop to below the threshold for localized corrosion for the repository-relevant environments. This threshold temperature is a function of the presence of beneficial ions, such as nitrates and sulfates.

2.2 RELATION OF IN-DRIFT CHEMICAL MODEL RESULTS TO CORROSION TESTING ENVIRONMENTS

The project has developed an understanding of the in-drift chemical environment for the three regimes described in Section 2.1. The understanding is based on geochemical models and supporting data and analysis appropriate for the repository conditions. A detailed description of the evolution of the chemical environment is provided in the in-drift chemical environment technical basis document, which includes a discussion of the relationship between the geochemical process model results and the chemical environments used in corrosion related testing. A high-level summary of the chemical environment applicable to corrosion related testing extracted from the technical basis document on in-drift chemical environment follows.

The geochemical model developed by the project to characterize the range of expected in-drift environments is presented in *Engineered Barrier System: Physical and Chemical Environment Model* (BSC 2003f). The model output is in the form of lookup tables, listing ion concentrations and pH as a function of relative humidity, temperature, and carbon-dioxide partial pressure.

Brines that develop on the waste packages and drip shields will be the result of either evaporative concentration of seepage water or deliquescence of deposited salts. Deposited salts can be due to entrained matter in the ventilation air, dust and debris deposited within the drifts, or seepage waters that have evaporated to dryness. Seepage waters are not expected to enter the drifts until host rock temperatures fall below 100°C. Dust salts will be able to deliquesce water from the atmosphere to form thin films on waste packages and drip shields above the normal boiling point of water (up to about 140°C) (BSC 2003f).

The water types or bins that have been predicted with the in-drift environment geochemical model for drift crown seepage waters are listed in Table 2-1. (This water binning methodology is discussed in detail in the technical basis document on the in-drift chemical environment.) The crown seepage waters are those anticipated to contact the drip shields and the waste package outer shell after the drip shield failure once the temperature of the drift wall falls below 100°C. The seepage waters have been categorized into 11 bins, or water types, based on their chemical composition (BSC 2003f, Section 6.6). A characteristic water has been determined for each bin. These seepage waters are characterized by their dominant constituents shown in the table near

the beginning of the evaporation process (identified in the table as at 98 percent relative humidity) and under conditions just before dryout. The time-integrated occurrence fraction that water in a particular bin will form at the drift crown is also listed. The associated brine type described and the test solution in which corrosion testing was conducted for each bin are also listed in the table and discussed in the following paragraphs.

Less than 1 percent of the time-integrated drift crown waters fall into Bins 1 through 3, which would be expected to be CaCl_2 -type brines. These brine types are projected to occur in the rocks above the drift during the time when the drift wall temperature is above 100°C . Most of the time-integrated waters (99 percent or more) fall into Bins 4 through 11, which evolve to sodium- and potassium-dominated solutions. The standard solutions used for corrosion testing by the project have also been categorized in terms of the representative bins.

Corrosion testing to determine the response of waste package, drip shield, and other in-drift materials is carried out in environmental conditions consistent with those predicted by in-drift chemical modeling. Corrosion testing environments were chosen based on the three types of natural brines: calcium chloride, carbonate, and sulfate. Initial studies focused on the carbonate-type brine, based on reasoning that carbonate-type waters, typified by J-13 well water from the saturated zone near Yucca Mountain, were the expected types of waters at the repository (Harrar et al. 1990). Details of the aqueous test solutions are given after the discussion of the brine types.

The brine type name reflects a characteristic that distinguishes it from the other brines. In terms of sulfate brines and in other cases where modeling has gone beyond the classic chemical divides (see the in-drift chemical environment technical basis document), it does not necessarily reflect the dominant species in the brine. This characterization of surface brine types has, in part, guided the expected range of brine water chemistry in the repository. However, some differences are expected between brines formed at the earth's surface and brines formed in the repository. These differences are mainly due to differences in the chemistry of seepage waters and surface waters giving rise to brines, and differences between the salt chemistry of dust and the dissolved salt content of such surface waters. Two important general factors specific to the repository brines are the presence of nitrate and more effective mechanisms for the removal of magnesium. It is expected that nitrate will be present in the deliquescent brines owing to multiple potential sources (BSC 2003g, Section 6.7.2.8) and the generally high solubility of nitrate minerals (BSC 2003g, Section 4.1.1.7). It is expected that magnesium will not be significant owing to a combination of low source (for the dust, as well as for at least some groundwaters) and multiple removal mechanisms, most of which are enhanced by elevated temperature (BSC 2003g, Sections 6.7.2.10 and 6.7.2.11).

The calcium-chloride brines have near neutral pH and no significant bicarbonate/carbonate, fluoride, or sulfate content. These brines may contain other cations such as sodium, potassium, and magnesium and other anions such as nitrate, but not carbonate, sulfate, or fluoride. The endpoint of the evaporative concentration of this type of brine would contain Ca-Cl/NO_3 or a mixture of Ca/Mg-Cl/NO_3 . The quantity of magnesium and calcium in this type of brine would be limited due to the precipitation of calcium carbonates and sulfates, and magnesium silicates. This is consistent with information on saline lakes where sodium is the dominant cation with the percentage of calcium varying from insignificant to about 20 percent (Drever 1997). In the

repository, the concentration of magnesium in any type of brine is expected to be insignificant as noted earlier. Thus, a magnesium chloride brine is not expected. Nitrate is expected to be present, and an end-point brine of this type is likely to be dominated by calcium chloride and calcium nitrate. A brine of the calcium chloride type is expected to have a very limited occurrence in the repository, as indicated in Table 2-1. For brine generated by dust deliquescence, the brine is actually expected to be more of a potassium nitrate–sodium chloride brine with only a small probability of calcium present due to the compositional nature of the dust leachate.

Relative humidity dependence of the calcium-chloride brine composition is as follows. At low relative humidity, the aqueous solutions will be dominated by calcium cations (very low sodium and potassium) and chloride and nitrate anions, since both calcium nitrate and calcium chloride are very soluble. At higher relative humidity, chloride and nitrate salts of sodium and potassium become soluble and could dominate the aqueous solution compositions. This would occur at or above the deliquescence relative humidity for salts composed of these ions.

Corrosion test solutions corresponding to this calcium chloride type of brine include calcium chloride, calcium chloride plus calcium nitrate, the simulated saturated water (SSW), and sodium chloride aqueous solutions. The SSW and sodium chloride test solutions simulate the moderate relative humidity scenario where calcium is a minor component in the aqueous solution. Numerous electrochemical studies were performed in these test solutions. Thin film studies were also performed using these types of solutions on coupons of Alloy 22 using an environmental thermogravimetric analyzer. See Appendix A for the corrosion tests performed in these types of solutions.

The carbonate brines are alkaline and do not contain significant calcium or magnesium content. In the early stages of the evaporative concentration, calcium precipitates predominately as carbonate mineral (calcite or aragonite) under equilibrium conditions. Magnesium precipitates as a minor component in the calcium carbonate species and as magnesium silicate. In the repository, it is expected that magnesium will be removed even more efficiently. Potassium may be significant in some of these brines. Nitrate is expected to be an important component, and a brine of this type may evolve through a high extent of evaporation into one in which nitrate is actually the dominant anion. The carbonate brine is likely to be represented as alkali metal (sodium, potassium) carbonate brine.

Relative humidity dependence of carbonate brine composition is as follows. At low relative humidity, the aqueous solutions will be dominated by nitrate and chloride anions with nitrate ions dominating at the lowest relative humidity. At moderate relative humidity (greater than 70 percent relative humidity), chloride ions could dominate the solution composition. The nitrate-chloride solutions are expected to have slightly elevated pH due to residual carbonate in solution. Significant amounts of carbonate and sulfate ion are not expected until the relative humidity is greater than 85 percent.

Corrosion test solutions corresponding to the carbonate type of brine include the simulated dilute water (SDW), simulated concentrated water (SCW), basic saturated water (BSW), and under certain circumstances, SSW and simulated acidic water (SAW) aqueous test solutions (see Table 2-2). The BSW test solution is a highly concentrated alkaline solution and could be

expected under repository conditions where temperatures could be at its measured boiling point of nominally 112°C to 113°C or where the relative humidity is nominally 70 to 75 percent. The SCW test solution is a moderately concentrated alkaline solution and solutions in this concentration range could be expected to form for relative humidity in the range of 90 to 95 percent. The SDW test solution is a dilute alkaline solution and solutions in this concentration range could be expected to form for high relative humidity (greater than 99 percent). These may have characteristics of solutions at the drift wall, that is, typical of in-drift seepage waters.

Under conditions of extreme evaporative concentration (i.e., low relative humidity) this type of brine containing high nitrate and chloride content would evolve into a nitrate-chloride brine with low carbonate content. The SSW test solution has characteristics of this type of brine. Likewise, the SAW test solution has characteristics of low carbonate brine and would have characteristics of solutions in equilibrium with relative humidity of nominally 90 percent. The calcium and magnesium addition to this test solution tends to make it more able to sustain lower pHs due to the hydrolysis properties of these cations.

The sulfate brines have near-neutral pH and no significant bicarbonate/carbonate and calcium content. Calcium precipitates as carbonates and possibly sulfates. In addition, they typically have only a small amount of magnesium, though some surface brines have been observed to have high magnesium (Drever 1997, Table 15-1, p. 333, brines 1-3). The dominant cation is typically sodium. In the repository brines, potassium may be comparable to sodium, and magnesium is expected to be insignificant. A brine of this type may also evolve through a high extent of evaporation into one in which nitrate is the dominant anion.

Relative humidity dependence of the sulfate brine composition is as follows. At low relative humidity, the aqueous solutions will be dominated by nitrate and chloride anions with nitrate ions dominating at the lowest relative humidity. At moderate relative humidity (greater than 70 percent relative humidity), chloride ions could dominate the solution composition. However, unlike the carbonate brines, these brines are expected to have near-neutral to slightly acidic pH because of the lack of a carbonate component. Significant amounts of carbonate and sulfate ion are not expected until the relative humidity is greater than 85 percent because of the increase in solubility of expected sulfate minerals (sodium and potassium sulfates). (Magnesium sulfate is expected to be present in insignificant quantities in these brines.)

The corrosion test solutions corresponding to the sulfate type of brine include the SAW and SSW. This type of brine has near-neutral to slightly acidic pH and, as noted, magnesium is not expected to be present in seepage waters to any significant extent. The SAW test solution has characteristics of solutions in equilibrium with nominally 90 percent relative humidity. The SSW has characteristics of water that have undergone evaporative concentration to the extent that sulfate precipitates out of solution (this is for the magnesium-free situation).

Two important general factors specific to the repository brines are the presence of nitrate and more effective mechanisms for the removal of magnesium. It is expected that nitrate will always be present in the deliquescent brines because of multiple potential sources (BSC 2003g, Section 6.7.2.8) and the generally high solubility of nitrate minerals (BSC 2003g, Section 4.1.1.7). The presence of nitrate is evident in the endpoint brines, as shown in Table 2-1.

It is expected that magnesium ions will never be significant because of a combination of low concentration (for the dust, as well as for at least some groundwaters) and multiple removal mechanisms, most of which are enhanced by elevated temperature (BSC 2003g, Sections 6.7.2.10 and 6.7.2.11).

Table 2-1. Drift Crown Seepage Water Limiting Compositions and Probabilities of Their Formation, the Associated Brine Type, and the Corresponding Corrosion Test Solutions

Bin Water*	Probability of Crown Seepage*	Dominant Constituents in Bin Water at 98% Relative Humidity*	Dominant Constituents in Endpoint Brines*	Brine Type	Corrosion Test Solution
1	0.00	Ca-Cl	Ca-Cl	Calcium chloride	CaCl ₂ ; CaCl ₂ + Ca(NO ₃) ₂
2	0.00	Na-Cl	Ca-Cl	Calcium chloride	CaCl ₂ ; CaCl ₂ + Ca(NO ₃) ₂
3	0.22	Na-Cl	Ca-Cl; K-Cl	Calcium chloride	CaCl ₂ ; CaCl ₂ + Ca(NO ₃) ₂
4	1.42	Na-Cl	K-NO ₃ ; Na-NO ₃	Sulfate	SSW, SAW, NaCl
5	0.79	Na-Cl	Na-Cl; K-Cl	Sulfate	SSW, SAW, NaCl
6	5.46	Na-Cl	Na-Cl; Na-NO ₃ ; K-Cl	Carbonate	SDW, SCW, BSW, SSW, NaCl
7	27.15	Na-Cl	Na-Cl; Na-NO ₃ ; K-Cl	Carbonate	SDW, SCW, BSW, SSW, NaCl
8	16.2	Na-CO ₃	Na-Cl; Na-NO ₃ ; K-Cl	Carbonate	SDW, SCW, BSW, SSW, NaCl
9	15.55	Na-CO ₃	K-NO ₃ ; K-Cl	Carbonate	SDW, SCW, BSW, SSW, NaCl
10	11.7	Na-CO ₃	Na-Cl; Na-NO ₃ ; K-Cl	Carbonate	SDW, SCW, BSW, SSW, NaCl
11	21.5	Na-Cl	Na-Cl; Na-NO ₃ ; K-Cl	Carbonate	SDW, SCW, BSW, SSW, NaCl

Source: BSC 2003f; Table 6.14-8 for columns identified with *.

NOTE: The probability of crown seepage represents the 20,000-year time-integrated occurrence fraction (in percent) of the representative water for each bin. However, the frequency of occurrence can be significantly higher for short durations.

Aqueous corrosion test solutions include several multiionic solutions (Table 2-2) based on a carbonate-base, J-13 well water and test solutions containing the major species expected to effect corrosion. The standardized solutions developed by the project as relevant test environments are presented in Table 2-2. These solutions include SDW, SCW, and SAW at 30°C, 60°C, and 90°C, as well as SSW at 100°C and 120°C. The SSW formulation is based upon the assumption

that evaporation of J-13 eventually leads to a sodium-potassium-chloride-nitrate solution. The absence of sulfate and carbonate in the target composition for this test medium is conservative. For example, carbonate would help buffer pH in any occluded geometry such as a crevice, and sulfate can act as a corrosion inhibitor. The compositions of these environments, as well as the solution known as BSW, are given in Table 2-2. Small amounts of carbonate will form in the SSW, SAW, and BSW solutions by interaction with gas phase carbon dioxide. The amount of carbonate formed was not determined experimentally, since the small amounts were not expected to affect the corrosion processes significantly.

Table 2-2. Target Composition of Standard Test Media Based on J-13 Well Water

Ion	SDW (mg/L)	SCW (mg/L)	SAW (mg/L)	SSW (mg/L)	BSW-12 (mg/L)
K ⁺	3.400×10^1	3.400×10^3	3.400×10^3	1.420×10^5	6.762×10^4
Na ⁺	4.090×10^2	4.090×10^4	3.769×10^4	4.870×10^4	1.0584×10^5
Mg ²⁺	1	<1	1.000×10^3	0	0
Ca ²⁺	5.000×10^{-1}	<1	1.000×10^3	0	0
F ⁻	1.400×10^1	1.400×10^3	0	0	1.470×10^3
Cl ⁻	6.700×10^1	6.700×10^3	2.425×10^4	1.280×10^5	1.3083×10^5
NO ₃ ⁻	6.400×10^1	6.400×10^3	2.30×10^4	1.313×10^6	1.3965×10^6
SO ₄ ²⁻	1.670×10^2	1.670×10^4	3.86×10^4	0	1.470×10^4
HCO ₃ ⁻	9.470×10^2	7.000×10^4	0	0	0
Si	27 (60°C), 49 (90°C)	27 (60°C), 49 (90°C)	27 (60°C), 49 (90°C)	0	0
pH	9.8 to 10.2	9.8 to 10.2	2.7	5.5 to 7	12

Source: DTN: LL000320405924.146.

NOTE: pH measured for actual solutions at room temperature.

BSW can have a pH between 11 and 13, and has a boiling point near 110°C (BSW-12 with a pH of 12 shown in Table 2-2). This test medium was established based on results from a distillation experiment. The total concentration of dissolved salts in the starting liquid was more concentrated than that in the standard SCW solution. After evaporation of approximately 90 percent of the water from the starting solution, the residual solution reaches a maximum chloride concentration and has a boiling point of approximately 110°C, with a pH of about 11. The synthetic BSW solution composition can be slightly modified (mainly by adding sodium hydroxide) to cover a range of pH values, yielding BSW-13, BSW-12, and BSW-11.

Deliquescence of dust deposited on the waste packages and drip shield is another means by which brines can form on these engineered barrier system components. In the absence of salts, condensed water can be present on smooth surfaces only if the relative humidity is 100 percent. At lower relative humidity values, most of the water evaporates, with residual water existing on the surface as a very thin adsorbate layer. Dissolved salts lower the relative humidity at which such dryout occurs. Salt minerals in a dry system lower the relative humidity required for an aqueous solution to form. If the dissolved salt composition of a solution is known, the relative humidity at which dryout occurs at a given temperature can be determined. Conversely, the relative humidity for a given salt or set of salt minerals at which deliquescence occurs at a specified temperature can also be found.

Table 2-3 lists the brines that would develop on the waste packages using the analysis (BSC 2003f) for dust deliquescence in drift thermal environments up to 140°C. Included in the table are the associated brine type and the corresponding aqueous corrosion test solutions.

Table 2-3. Brines from Dust Deposited on the Waste Packages, Including Bromide, the Probabilities of Their Formation, the Associated Brine Type, and the Corresponding Corrosion Test Solutions

Bin Water	Probability of Deliquescence Bin	Dominant Constituents in Bin Water at 98 Percent Relative Humidity	Dominant Constituents in Endpoint Brines	Brine Type	Corrosion Test Solution
1	5.77	Na-NO ₃	Ca-NO ₃	Calcium chloride	CaCl ₂ ; CaCl ₂ + Ca(NO ₃) ₂
2	7.69	Na-NO ₃	K-NO ₃ ; Na-NO ₃	Sulfate	SSW, SAW, NaCl
3	17.31	Na-SO ₄	K-NO ₃ ; Na-NO ₃	Carbonate	SDW, SCW, BSW, SSW, NaCl
4	23.08	Na-NO ₃	Na-NO ₃	Sulfate	SSW, SAW, NaCl
5	44.23	Na-NO ₃	K-NO ₃ ; Na-NO ₃	Sulfate	SSW, SAW, NaCl
6	1.92	Na-Cl	K-NO ₃	Carbonate	SDW, SCW, BSW, SSW, NaCl

Source: BSC 2003f, Tables 6.10-6 and 6.14-9.

NOTE: The probabilities represent the percentage of waste packages subject to dust that may deliquesce into the identified brine type.

In all cases, the nitrate component is the most soluble species and would dominate the solution composition at the deliquescent relative humidity or eutectic point of a mineral assemblage at elevated temperatures. At higher relative humidity, chloride minerals become soluble and could become a dominant ion. It is not until the relative humidity is much higher that the sulfate and carbonate compositions could become appreciable. In essence, solutions will be dominated by chloride and nitrate at low to moderate (less than 70 percent) relative humidity and, at higher relative humidity, sulfate and carbonate could be appreciable. This is discussed in more detail in *Environment on the Surfaces of the Drip Shield and Waste Package Outer Barrier* (BSC 2003g).

INTENTIONALLY LEFT BLANK

3. LONG-TERM THERMAL AGING OF ALLOY 22 IN THE REPOSITORY

As described in Section 1.2, Alloy 22 phase stability issues resulting from exposure at higher temperatures during welding can potentially degrade corrosion resistance and mechanical properties. To minimize potential phase instabilities resulting from waste package fabrication, a solution heat treatment and rapid water quench of the as-fabricated waste package is implemented. Following solution heat treatment in the fabrication shop and the final thermal cycle for the lid closure weld, the temperature of the Alloy 22 waste package outer shell will remain significantly below 200°C as shown in Figure 1-2. With these constraints, the impact of thermal aging and phase instability on the corrosion of Alloy 22 are expected to be minimal consistent with early work (CRWMS M&O 2000b). This previous work indicated that degradation resulting from phase instability for Alloy 22 base metal will not affect waste package performance at less than about 300°C.

3.1 MODEL DEVELOPMENT

More recently, the precipitation kinetics for two of the higher temperature tetrahedrally close packed phases known as P and σ and the lower temperature ordered phase known as oP6-ordered phase have been modeled based on fundamental thermodynamics and kinetic concepts and principles (BSC 2003d). This modeling, benchmarked with thermal aging kinetic measurements, is being used to provide predictive insight into the long-term metallurgical stability of Alloy 22 under repository relevant conditions.

3.2 KINETICS OF TRANSFORMATION IN A NICKEL–CHROMIUM–MOLYBDENUM ALLOY SURROGATE FOR ALLOY 22

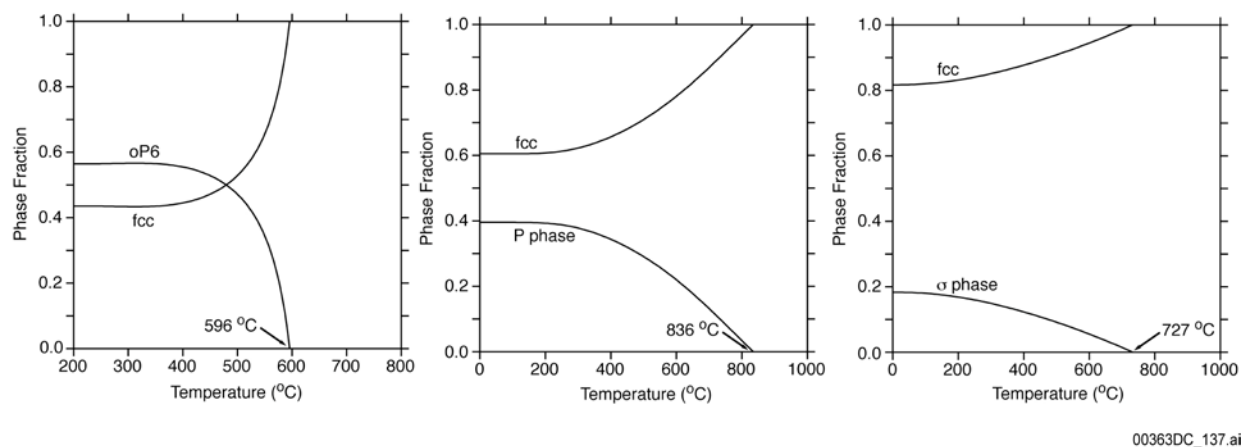
To simulate the kinetic transformations of Alloy 22 over long time periods, a more simplified ternary nickel-chromium-molybdenum alloy that can be considered as a surrogate for Alloy 22 was used. The nominal composition used was 21.1 weight percent chromium, 13.5 weight percent molybdenum, and the remainder nickel. Three transformations were considered: the face-centered cubic matrix to the oP6-ordered phase, the face-centered cubic matrix to the P phase, and the face-centered cubic matrix to the σ phase. The corresponding thermodynamic-model-generated phase-fraction versus temperature diagrams are shown in Figure 3-1. In this study of phase-formation kinetics for the oP6-ordered phase, 7.5 weight percent molybdenum is used instead of 13.5 weight percent in the extreme left panel. This reduction in molybdenum accounts for the role of tungsten in destabilizing the ordered phase, and the relative contribution of tungsten is approximately twice that of molybdenum (1 weight percent tungsten is approximately 2 weight percent molybdenum).

In Figure 3-2, the time-temperature-transformation diagram associated with the face-centered cubic-to-oP6 ordered phase transformation of Ni–21.1Cr–7.5Mo is displayed with 2, 10, and 15 percent transformation rates.

Similarly, the transformation of Ni–21.1Cr–13.5Mo from the face-centered cubic-based matrix to the P phase with 2, 10, and 15 percent transformation rates was predicted (Figure 3-3) as a function of time and temperature. The results are comparable with the qualitative observations cited by Turchi (2001). Finally, the transformation of Ni–21.1Cr–13.5Mo from the

face-centered cubic-based matrix to the σ phase with 2, 5, and 10 percent transformation rates was predicted as a function of time and temperature (Figure 3-4).

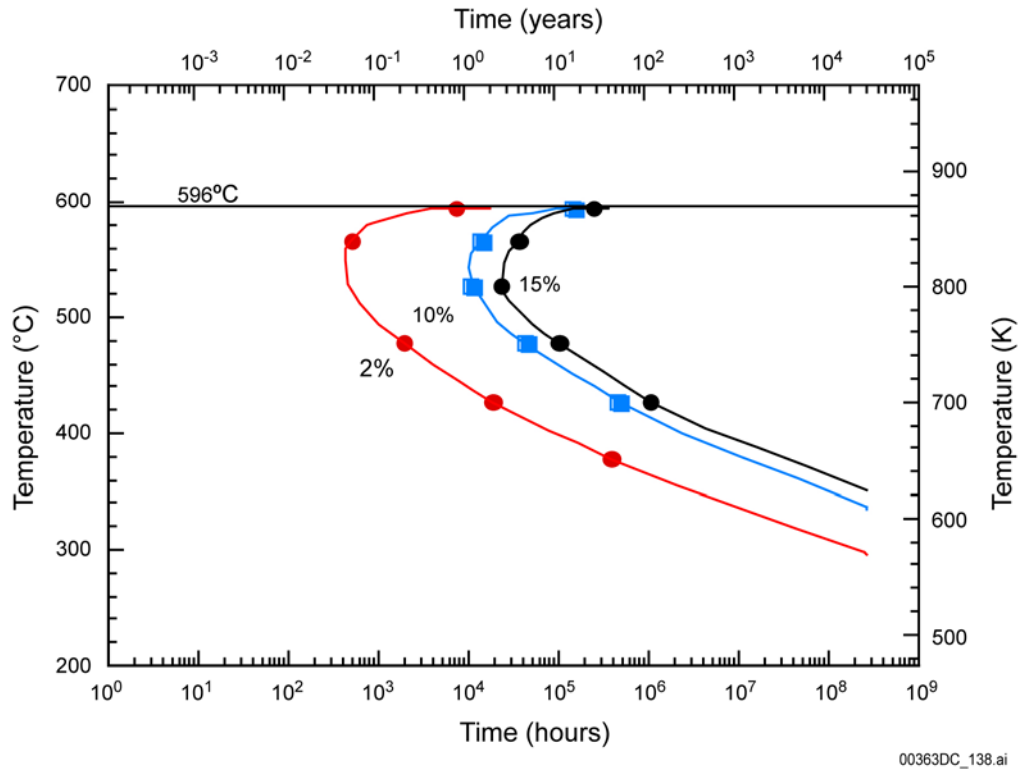
It can be seen from Figures 3-2, 3-3, and 3-4 that extrapolation of each curve to lower temperatures is consistent with the expected low probability of forming less than 2 percent (an insignificant amount) of these phases out of the face-centered cubic-solid solution at less than 200°C for as long as 10,000 years. Thus, phase and time temperature-transformation diagrams predicted for Alloy 22, and validated with experimental data (BSC 2003d), indicate no significant phase instabilities (long-range ordering and tetrahedrally close packed phase precipitation) at temperatures below 200°C for 10,000 years. Further, examination of Figures 3-2, 3-3 and 3-4 indicate that no significant phase formation is expected even for the highest potential waste package temperatures of about 300°C resulting from early drift collapse. The estimated temperature increase due to drift collapse is based on the previously analyzed back fill case (with Overton sand) (BSC 2001a, Section 6.11.1.4 and Figures 6-7 and 6-14). This analysis suggests that the waste package temperature could increase to peak temperatures of about 300°C, but for only decades to centuries.



Source: DTN: LL030106312251.013.

NOTE: The face-centered cubic matrix and the oP6-ordered phase (left panel); in this case, 7.5 weight percent molybdenum, was considered instead of 13.5 weight percent (see text) P phase (middle panel) and σ phase (right panel). All other phases are suspended during the calculations.

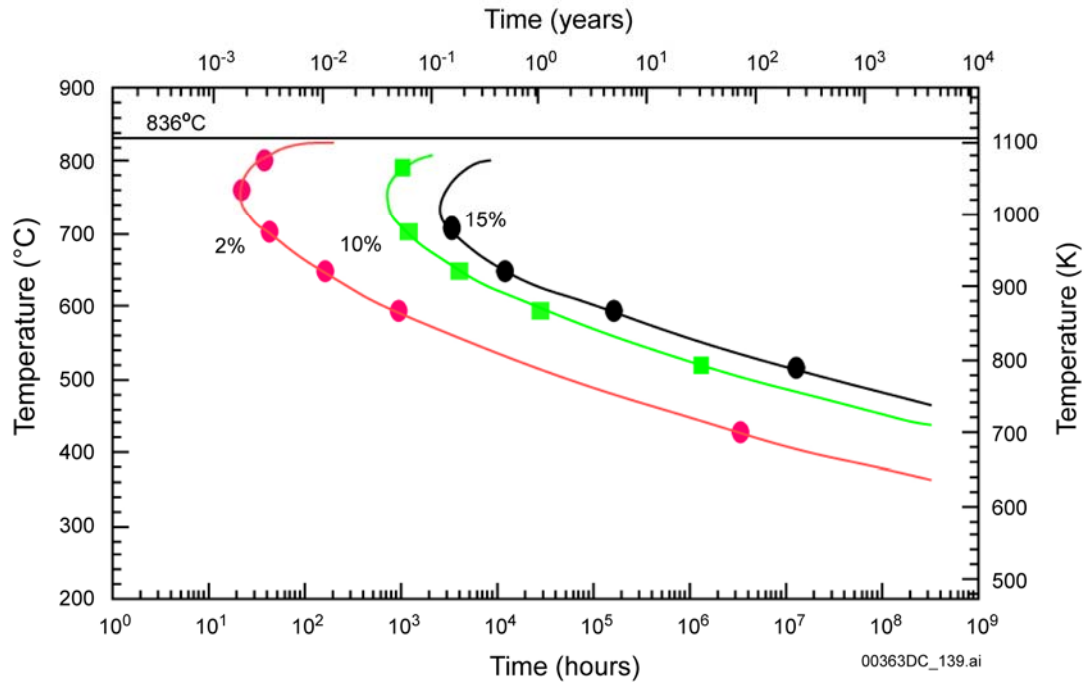
Figure 3-1. Time-Temperature-Transformation Diagram for Ternary Alloy Nickel-21.1 Chromium-13.5 Molybdenum



Source: DTN: LL030106312251.013.

NOTE: At 596°C (see Figure 3-1, left panel), the phase fraction of oP6-ordered phase drops to 0.

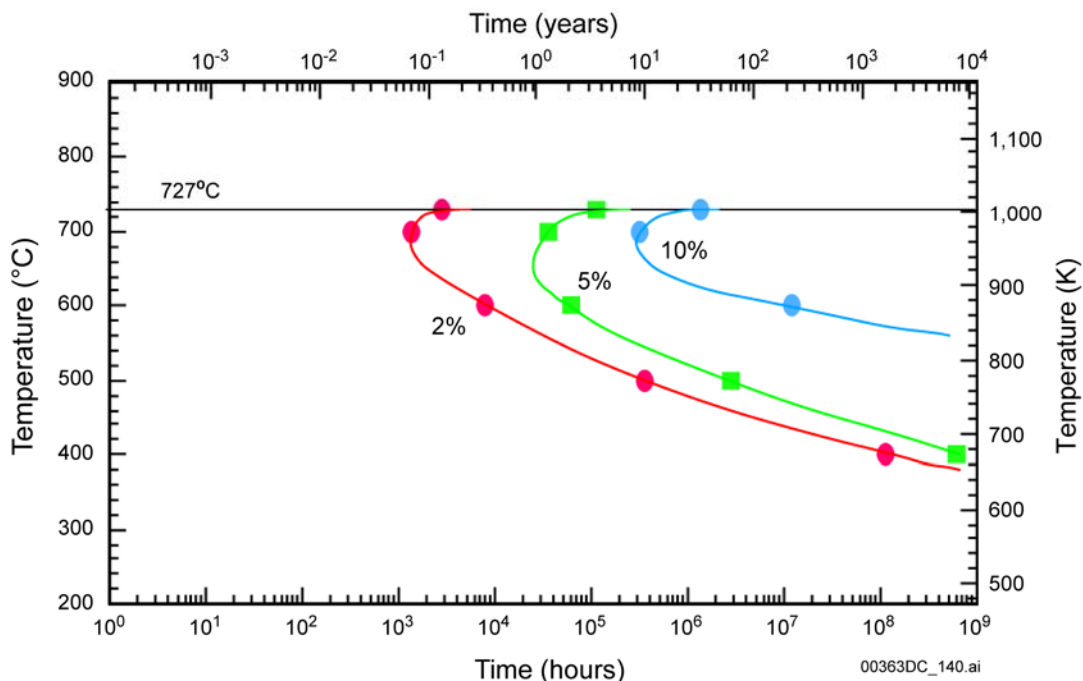
Figure 3-2. Calculated Isothermal Time-Temperature-Transformation for a Face-Centered Cubic-Based Matrix of a Ternary Ni-21.1Cr-7.5Mo (in Weight Percent) Alloy (Surrogate for Alloy 22) Transforming into the oP6-Ordered Phase for 2, 10, and 15 Percent Transformation Rates



Source: DTN: LL030106312251.013.

NOTE: At 836°C (see Figure 3-1, middle panel), the phase fraction of P phase drops to 0.

Figure 3-3. Calculated Isothermal Time-Temperature-Transformation for a Face-Centered Cubic-Based Matrix of a Ternary Ni-21.1Cr-13.5Mo (in Weight Percent) Alloy (Surrogate for Alloy 22) Transforming into the P Phase for 2, 10, and 15 Percent Transformation Rates



Source: DTN: LL030106312251.013.

NOTE: At 727°C (see Figure 3-1, right panel), the phase fraction of σ phase drops to zero.

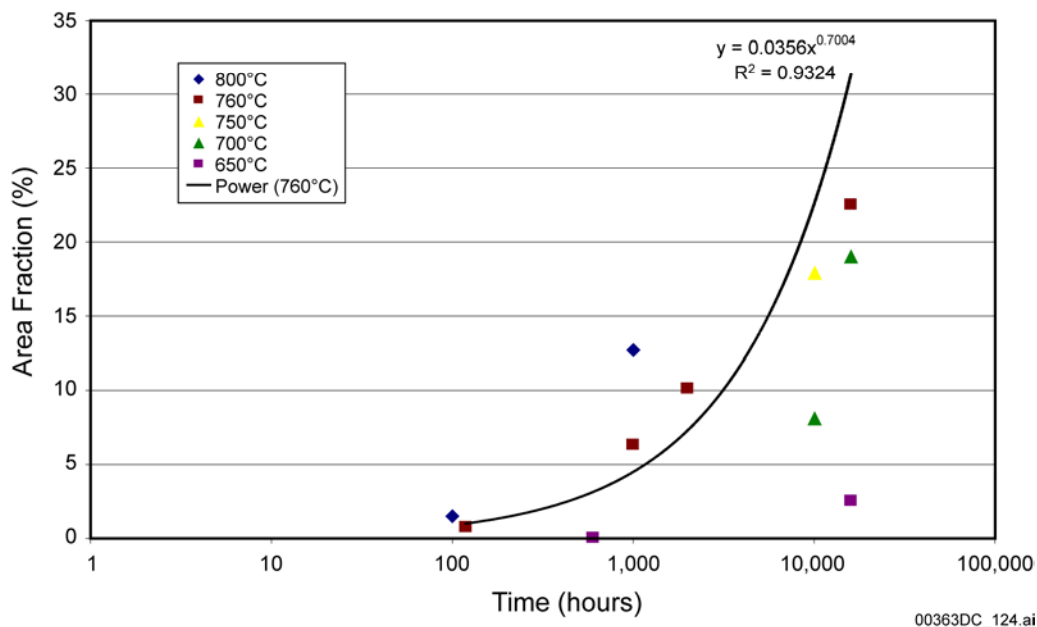
Figure 3-4. Calculated Isothermal Time-Temperature-Transformation for a Face-Centered Cubic-Based Matrix of a Ternary Ni-21.1Cr-13.5Mo (in Weight Percent) Alloy (Surrogate for Alloy 22) Transforming into the σ Phase for 2, 5, and 10 Percent Transformation Rates

3.3 EXPERIMENTAL RESULTS

Volume-Fraction Measurements in Alloy 22—In order to measure the amount of tetrahedrally close packed phase precipitation in Alloy 22 base metal and welds, area-fraction measurements have been made, using scanning electron microscope image analyses as a function of aging time and temperature. Using standard methods of quantitative stereology, it has been shown that area-fraction measurements (and correspondingly, linear-fraction measurements on grain boundaries) are mathematically equivalent to volume-fraction measurements (Vander Voort 2000; Hilliard and Cahn 1961). Thus, the area-fraction measurements or bulk precipitation presented here are equivalent to the volume-fraction values in Alloy 22 as a function of time and temperature which in turn can be related to any potential effects on corrosion and (or) mechanical property degradation. The scanning electron microscope image analyses that were performed measured gross tetrahedrally close packed phase precipitation in the samples as a function of time and temperature. No tetrahedrally close packed phase extraction was conducted to differentiate the types of tetrahedrally close packed phases that may be present in these measurements.

Volume-Fraction Measurements in Base Metal—The measurements of area-fraction of tetrahedrally close packed precipitation for base metal, as a function of time and temperature, are

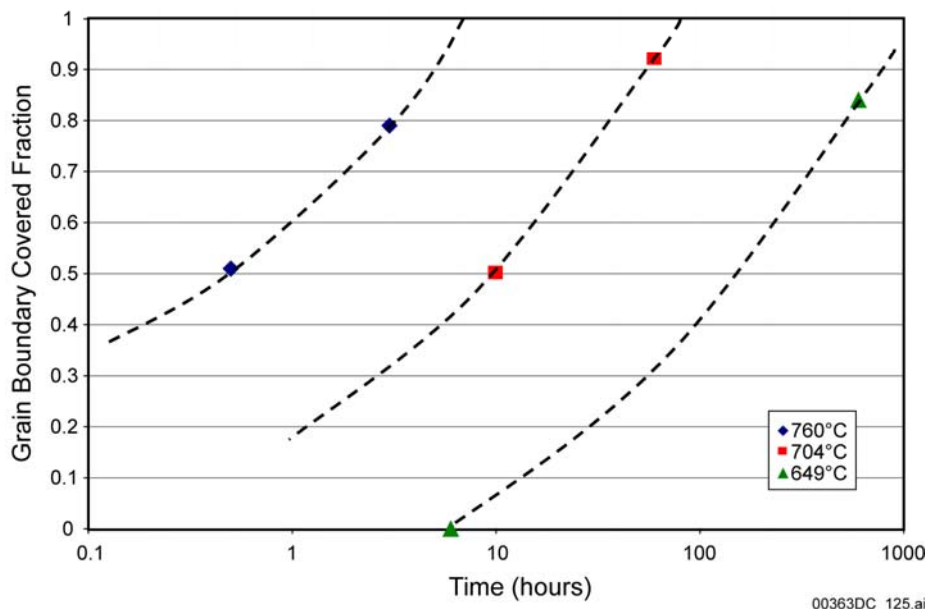
presented in Figure 3-5. A trend line is included for the results at 760°C, where more than two measurements were made. Tetrahedrally close packed phases are seen to readily form at higher temperatures (760°C to 800°C) in less than 1,000 hours. In general, as the temperature is decreased, the onset of tetrahedrally close packed phase precipitation is delayed, and it also appears that the slopes of trend lines at lower temperatures may become shallower, indicating a slower rate of phase precipitation. The measurements presented here are reasonably consistent with model predictions shown in Figure 3-3 which in turn indicate that forming tetrahedrally close packed phases from the face-centered cubic solid solution within 10,000 years at less than 200°C is unlikely.



Source: DTN: LL030606912251.020.

Figure 3-5. Precipitation of Tetrahedrally Close Packed Phases in Alloy 22 Base Metal as a Function of Time and Temperature

Area-Coverage Measurements on Grain Boundaries—Area-coverage measurements (linear-fraction measurements) on grain boundaries have also been performed using scanning electron microscope image analyses, and are shown in Figure 3-6. These measurements are similar to the area-fraction measurements on base metal samples discussed in the previous section and give a quantitative measure of grain boundary precipitation kinetics. Extrapolation of Arrhenius plots or comparison to time-temperature-transformation diagrams in Figure 3-3 indicate that significant precipitation will not occur under repository conditions (BSC 2003d).



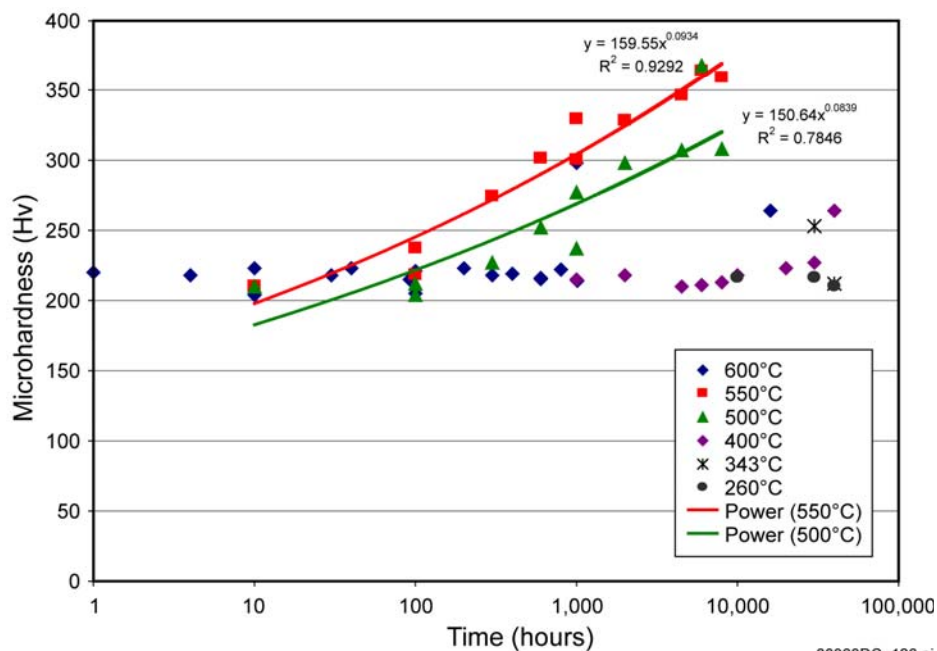
Source: DTN: LL030606912251.020.

Figure 3-6. Precipitation of Tetrahedrally Close Packed Phases at Alloy 22 Grain Boundaries as a Function of Time and Temperature

Long-Range Ordering—The kinetics of long-range ordering are treated in a manner similar to that discussed for tetrahedrally close packed phase precipitation. However, very little kinetic data exist for long-range ordering in Alloy 22. A very fine dispersion of ordered domains was seen after aging for 30,000 and 40,000 hours at 427°C in Alloy 22 base metal, and in a weld similarly aged (BSC 2003d). The ordering in these cases is so fine that it would be difficult to measure the volume fraction of the ordered domains. Long-range ordering was also observed in Alloy 22 base metal aged at 593°C for 16,000 hours and at 538°C and 593°C for 1,000 hours. Alloy 22 base metal samples aged for 40,000 hours at 260°C and 343°C and for 1,000 hours at 482°C were also examined with transmission electron microscopy, but no long-range ordering was observed.

Unlike tetrahedrally close packed phase precipitates, long-range ordering results in very small and finely dispersed precipitates. As a result, scanning electron microscope image analysis is not well suited to determine the extent of long-range ordering kinetics. However, due to the uniformly and finely dispersed nature of long-range ordering, microhardness measurements are indicative of long-range ordering, because analogous to precipitation in age-hardened alloys, hardness increases with the amount of long-range ordering precipitation (Reed-Hill 1973).

Figure 3-7 (BSC 2003d, Figure 96), shows such microhardness (Hv) measurements made on Alloy 22 as a function of time and temperature. Trend lines have been included for the results at 500°C and 550°C. The microhardness of “as-received” material was 217 Hv. The microhardness measurements indicate that long-range ordering has occurred at temperatures in the range of 500°C to 550°C, for up to 40,000 hours. In addition, for results up to 40,000 hours, no long-range ordering is evident for temperatures below 400°C, and little long-range ordering is seen at temperatures around 600°C. The observation of very little long-range ordering near 600°C conforms to the critical order-disorder temperature of the computational model, which is about 596°C (BSC 2003d).

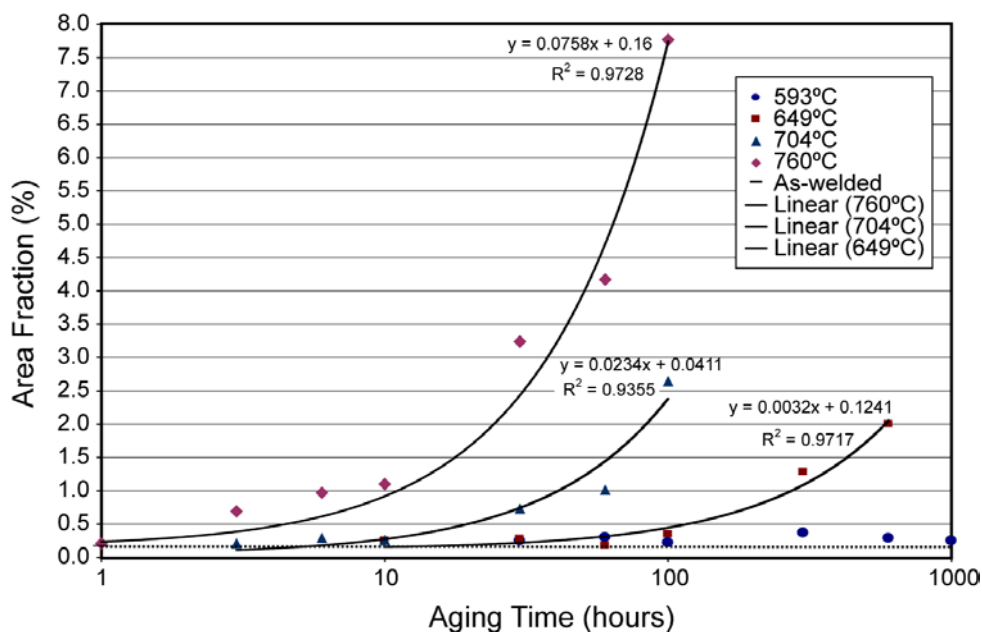


Source: DTN: LL030607112251.021.

NOTE: Microhardness of "as-received" base metal is 217 Hv.

Figure 3-7. Microhardness (Hv) Measurements on Aged Alloy 22 Base Metal Shown as a Function of Time and Temperature and Indicative of Long-Range Ordering

Volume Fraction Measurements in Alloy 22 Welds—As observed by Cieslak et al. (1986), tetrahedrally close packed phases are present in the interdendritic regions of the as-welded structure. After aging, the amount and size of tetrahedrally close packed precipitates increases with both time and temperature up to 760°C. Nucleation of precipitation was also observed to form possibly along grain boundaries in some areas of these samples. The area fraction of precipitates is shown as a function of time in Figure 3-8. Each of the data points in Figure 3-8 represents the average of 20 to 40 measurements. In the as-welded condition, there is approximately 0.02 volume-percent tetrahedrally close packed phase. The average activation energy calculated from the slopes of Arrhenius plots of these data is 241 kJ/mol, which is comparable to but lower than the values of 250 and 260 kJ/mol reported previously for base metal (Rebak et al. 2000). Extrapolations of these data do not indicate that precipitate nucleation and growth in the welds will occur at temperatures below approximately 200°C.



00363DC_127.ai

Source: DTN: LL030606912251.020.

Figure 3-8. Tetrahedrally Close Packed Phase Precipitation Kinetics for Alloy 22 Gas Tungsten Arc Weld as a Function of Temperature

3.4 MODEL CONFIDENCE

In *Aging and Phase Stability of Waste Package Outer Barrier* (BSC 2003d, Section 7.5), the computational phase kinetics results for the phase (from DICTRA, a code that predicts time-temperature-transformation diagram) for the ternary nickel-chromium-molybdenum alloy (a surrogate for Alloy 22) were compared with volume-fraction measurements on Alloy 22 base metal at temperatures of approximately 700°C and 760°C. The computation phase kinetics results are used to construct the computational time-temperature-transformation diagrams for a particular phase. The comparison is somewhat limited because (1) the volume-fraction measurements do not distinguish among the possible tetrahedrally close packed phases (P, μ , and σ) that have formed, and (2) the DICTRA results only display one type of phase fraction at a time. As a result, the P phase formation results from DICTRA were compared with the tetrahedrally close packed volume-fraction measurements, as the P phase is the most likely to form at these temperatures and times. For this comparison, only a few volume-fraction measurements were deemed most likely to contain primarily P phase at the times and temperature shown and thus the available data set was very limited.

However, in both comparisons (i.e., at 700°C and 760°C), the agreement between the computational kinetics results and the volume-fraction measurements is reasonable. The comparison (although based on a limited number of data points) shows that the computational results are conservative compared to the measured data.

3.5 SUMMARY

Analyses documented in *Aging and Phase Stability of Waste Package Outer Barrier* (BSC 2003d) assumed that the precipitation mechanisms that operate at higher temperatures also operated at much lower temperatures, and that the phases seen at the higher temperatures were also stable at the lower temperatures. Information from josephinite, a material that has been proposed as a natural analog for Alloy 22, shows stability of metallic phases after exposure over millions of years. This is fully consistent with model predictions and experimental observations of no low-temperature mechanism with rates significantly greater than those predicted at lower temperatures. This observation provides confidence in the implicit assumption that the high-temperature mechanisms used to extrapolate kinetics are the same as those that occur at lower temperatures (approaching expected repository conditions).

Long-range ordering formation occurs at relatively lower temperatures than for the tetrahedrally close packed phases. However, the associated kinetics based on model predictions and transmission electron microscopy and microhardness measurements support the expected lack of formation of the ordered phase of Ni₂Cr-type at repository temperatures, as the phase formation kinetics are primarily driven by thermally activated diffusion. Thus, alloys homogenized (or annealed) at high temperatures and rapidly quenched should not display any deleterious phases. Extrapolation of computationally derived time-temperature-transformation curves to lower temperatures, which are expected in a repository, indicate that formation of the P phase or oP6-ordered phase from the face-centered cubic solid solution will not occur.

In summary, model predictions and extrapolation of higher temperature results to lower temperatures show that formation of tetrahedrally close packed or ordered phases in Alloy 22 base metal and annealed welds will not occur during the repository period of 10,000 years. Further, as discussed, analysis shows that tetrahedrally close packed and long-range ordering phases would not form even for the unlikely case of early steady state drift collapse (acting like backfill), where the waste package temperature could potentially increase to peak temperatures of about 300°C, but for only relatively short times, decades to centuries. On this basis, neither the waste package outer shell base metal nor weld metal are subject to enhanced degradation due to the effects of thermal aging (BSC 2003b, Section 6.4.6), and this process is not included in total system performance assessment (TSPA) modeling.

4. WASTE PACKAGE OUTER SHELL OXIDATION AND CORROSION IN DRYOUT REGIME

While in the higher temperature dryout regime, Alloy 22 may undergo dry oxidation at relative humidities below the critical value for humid air or aqueous corrosion (CRWMS M&O 2000a, Section 6.4.2). However, the extent of dry oxidation is believed to be insignificant. To confirm the expected low dry oxidation rates at repository temperatures, a bounding calculation using typical literature based oxidation rate laws has been performed.

4.1 DRY OXIDATION ABOVE DELIQUESCENCE POINT

Dry oxidation of Alloy 22 at repository temperatures involves the formation of a relatively thin protective oxide film. To quantify this effect, a simple bounding analysis has been performed that assumes the uniform protective surface oxide film is primarily Cr_2O_3 (other oxides may also be present). The rate of dry oxidation is assumed to be limited by mass transport through this growing metal oxide film. Fick's First Law is applied, assuming a linear concentration gradient across the oxide film of thickness x . Integration shows that the oxide thickness should obey the following parabolic growth law, also known as Wagner's Law (Welsch et al. 1996), where the film thickness is proportional to the square root of time. This is represented by the following equation.

$$x = \sqrt{x_0^2 + k \times t} \quad (\text{Eq. 4-1})$$

where x_0^2 is the initial oxide thickness, x is the oxide thickness at time t , and k is a temperature-dependent parabolic rate constant that follows an Arrhenius type relationship. The rate log term constant in the above equation is determined as follows:

$$\log[k(m^2s^{-1})] = -12.5 \left(\frac{10^3}{T(K)} \right) - 3.5 \quad (\text{Eq. 4-2})$$

where T is defined as the absolute temperature. The highest waste package surface temperature is expected to be less than 200°C , which is well below 350°C (623 K), the boundary temperature used in calculations below (BSC 2003b, Section 6.4.2). The value of k corresponding to this very conservative upper limit of 350°C is $2.73 \times 10^{-24} \text{ m}^2/\text{s}$ ($8.61 \times 10^{-5} \mu\text{m}^2/\text{yr}$). After 1 year, this corresponds to an oxide thickness of $0.0093 \mu\text{m}$ (about $9.3 \text{ nm}/\text{yr}$). As will be seen in subsequent discussion, this estimated rate is comparable to that expected for aqueous phase corrosion at lower temperatures. A logarithmic growth law may be more appropriate for use at low temperatures than the parabolic growth law used above. However, such a logarithmic expression predicts that the oxide thickness (penetration) will asymptotically approach a small maximum level. The parabolic growth law predicts continuous growth of the oxide, which is much more conservative than the logarithmic growth law. To be conservative, the parabolic growth law is used to model the dry oxidation of Alloy 22. Recent measurements (BSC 2003b, Section 6.4.2) of the thickness of the Alloy 22 oxide film exposed to air at 550°C showed the oxide film approaches a limiting thickness of about 0.025 to $0.050 \mu\text{m}$ after about 333 days exposure, which corresponds to a penetration rate of 0.027 to $0.054 \mu\text{m}/\text{yr}$ calculated at 350°C

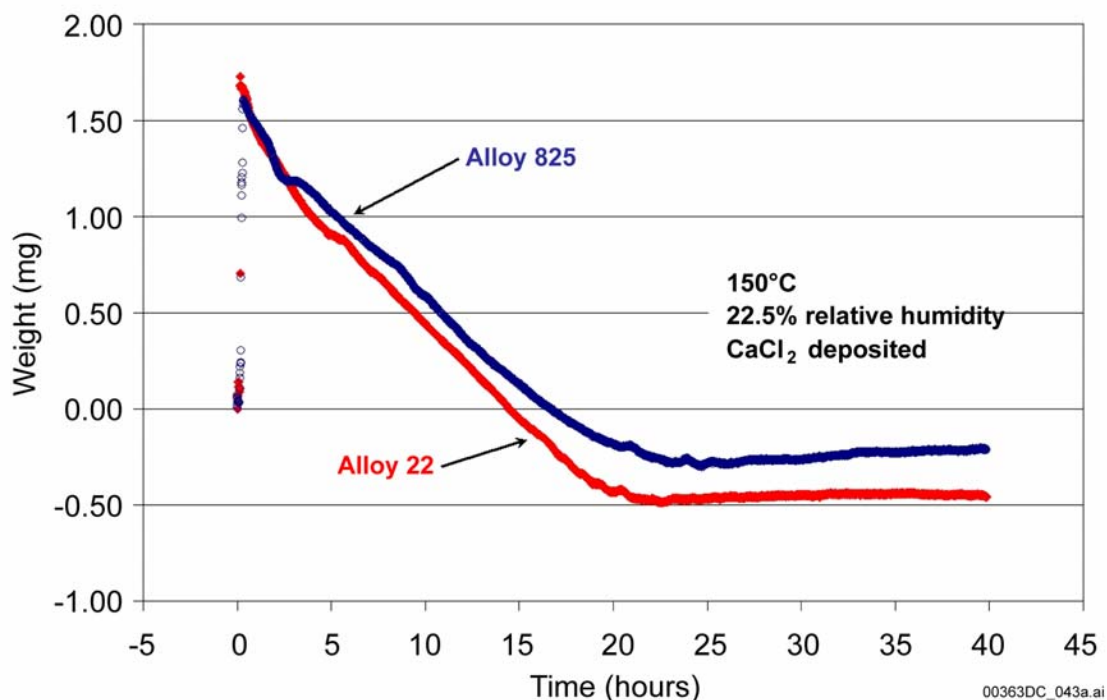
(BSC 2003b). Therefore, the upper bound conservative rate of 0.0093 $\mu\text{m}/\text{yr}$ is consistent with the measurement data considering the higher test temperature. This precludes the need for additional uncertainty bounds. Thus, this analysis indicates dry oxidation will not be a life limiting waste package outer shell degradation mechanism. On this basis, dry oxidation will not have a significant effect on the performance of the waste package outer shell, and this process is not included in TSPA modeling (BSC 2003b, Section 6.4.2).

4.2 CORROSION UNDERNEATH DELIQUESCENT BRINES

At a given surface temperature, the existence of liquid water on the waste package surface depends upon the hygroscopic nature of any salt and mineral deposits on the surface. In the presence of such deposits, a thin liquid-phase surface brine film can be established at a higher temperature and lower relative humidity than otherwise possible. The chemistry–temperature–relative humidity stability range of this liquid phase brine film is modeled. A summary of the results and expected ranges of deliquescent brine compositions and their relative probabilities of occurrence are summarized in the in-drift chemical environment technical basis document.

Environmental thermogravimetric analysis has also been used to study the corrosion of waste package materials underneath deliquescent brines, and the evolution of acid gas due to the thermal decomposition of those brines (BSC 2003g, Section 6.7.2.1.4.2). The subsequent weight loss is due to chemical transformations that are occurring in the aqueous solutions due to volatilization of HCl. The accompanying pH increase causes precipitation of calcium containing species with the loss of the aqueous phase. Because of its lower corrosion resistance, Alloy 825 was tested in parallel to provide insight into localized modes of attack that might occur under deliquescent brine films. Weight change data for the two materials (Alloy 825 and Alloy 22) at 150°C and 22.5 percent relative humidity are shown in Figure 4-1.

Initial weight gains shown in Figure 4-1 are due to the formation of highly concentrated aqueous films due to deliquescence of the deposited CaCl_2 . No sustained oxidation of Alloy 22, usually indicated by an increase in weight due to the addition of oxygen to the surface, is evident from the thermogravimetric analysis data.

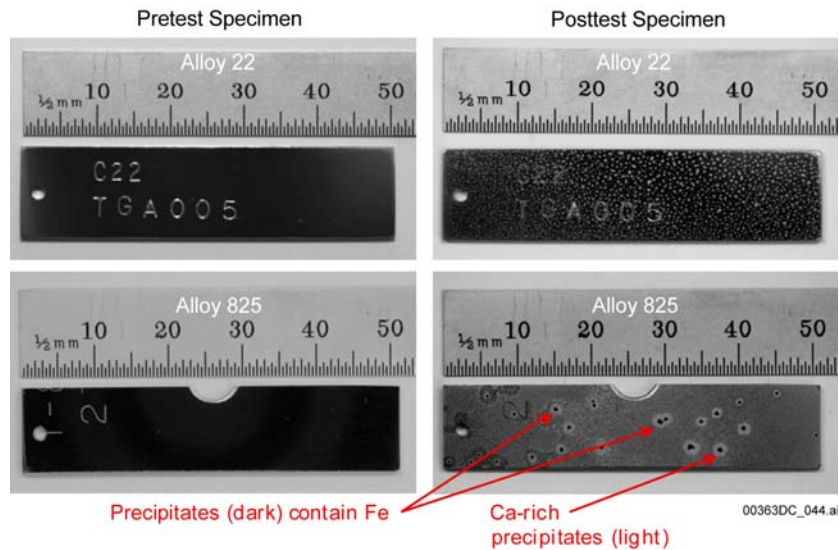


Source: Farmer 2003, Slide 14. Data taken from Hailey and Gdowski 2003.

Figure 4-1. Thermogravimetric Analysis Data Comparing the Weight Gains of Alloy 825 and Alloy 22 at 150°C and 22.5 Percent Relative Humidity

Figure 4-2 shows photographs of the samples after such testing in the thermogravimetric analysis. It is evident that Alloy 22 is highly resistant to localized attack in a deliquescent CaCl_2 brine at 150°C and 22.5 percent relative humidity. There is no evidence of localized corrosion of Alloy 22 (UNS N06022, 55.5 Ni 22 Cr 13 Mo 3 W 4 Fe 2.5 Co) due to deliquescence. The white spots visible are deposits. However, in contrast, substantial attack of a less corrosion resistant material, Alloy 825 (UNS N08825, 42Ni 22Cr 3Mo 0.9 Titanium 2.2Cu 1Mn 28.9Fe) is evident. Thus, Alloy 22 has been shown to be resistant to localized attack under aggressive CaCl_2 -type deliquescent brines at 150°C and 22.5 percent relative humidity.

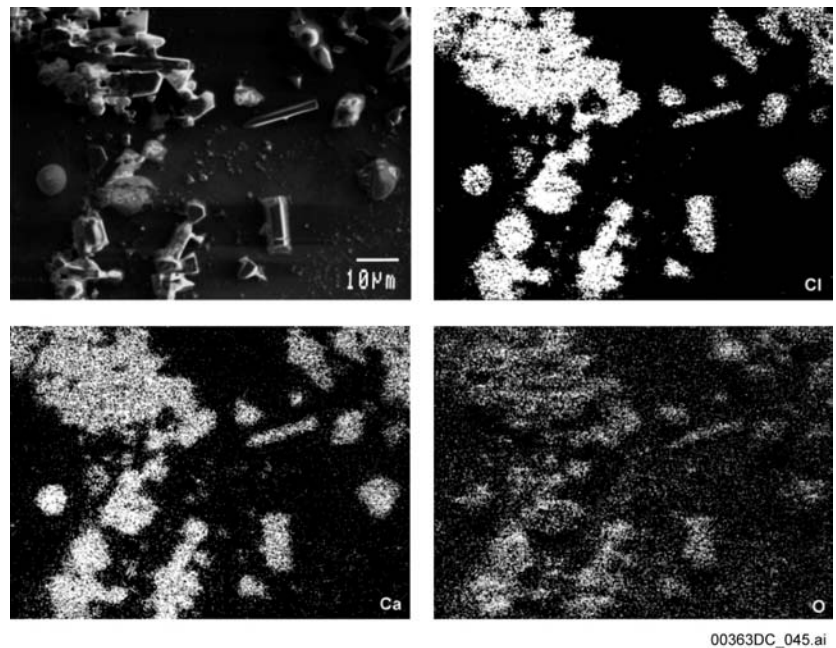
Figure 4-3 (BSC 2003g, Figure 38) shows a scanning electron micrograph of the white precipitates on the Alloy 22 surface, which are formed from the deliquescent brine and are evident in the photographs of Figure 4-2. Elemental analysis of the deposit was done with energy dispersive spectroscopy and indicated that these precipitates contain calcium, chlorine and oxygen. Raman spectroscopy indicates that precipitates are not $\text{Ca}(\text{OH})_2$ or CaCO_3 , but may be CaOHCl (calcium hydroxy chloride). Furthermore, energy dispersive spectroscopy and wet-chemical analyses indicate a loss of chlorine relative to calcium, which is believed to be due to the formation of volatile hydrochloric acid gas (BSC 2003g, Section 6.7.14-2).



Source: Farmer 2003, Slide 15. Data taken from Hailey and Gdowski 2003.

NOTE: No such localized corrosion of Alloy 22 was observed under identical conditions.

Figure 4-2. Localized Corrosion of Alloy 825 Underneath a Deliquescent Brine



Source: Farmer 2003, Slide 16. Data taken from Hailey and Gdowski 2003.

NOTE: Elemental analysis with energy dispersive spectroscopy indicates that the precipitates are probably CaOHCl.

Figure 4-3. Scanning Electron Microscope View of the White Precipitates on the Alloy 22 Surface (Shown in Figure 4-2) Formed from the Deliquescent Brine

5. GENERAL CORROSION OF THE WASTE PACKAGE OUTER SHELL

General corrosion is the uniform thinning of the waste package outer shell at its open-circuit corrosion potential (E_{corr}). The general corrosion rate is temperature dependent, and for a given temperature, is assumed to be constant (i.e., time-independent). Therefore, for a given temperature, the depth of penetration or thinning of the waste package outer shell by general corrosion is equal to the general corrosion rate at that temperature multiplied by the time that the waste package is exposed to the environment under which general corrosion occurs. This assumption is considered conservative because the general corrosion rate of metals and alloys tends to decrease with time. As discussed in the following sections, general corrosion rates of the waste package outer shell have been estimated based on weight-loss and dimensional-change measurements of descaled Alloy 22 samples after a 5-year exposure in the LTCTF. The LTCTF provides a comprehensive source of corrosion data for Alloy 22 in environments relevant to the repository (BSC 2003b, Section 6.4.3). In addition to LTCTF results, general corrosion rates were also measured electrochemically to help model the temperature dependence of this corrosion mode in Alloy 22.

5.1 LONG-TERM WEIGHT LOSS MEASUREMENTS

The LTCTF is equipped with an array of fiberglass tanks. Each tank has a total volume of approximately 2,000 L and is filled with approximately 1,000 L of aqueous test solution. The temperature of the solution in a particular tank is controlled at either 60°C or 90°C, covered with a blanket of air flowing at approximately 150 cm³/min, and agitated. Four generic types of samples, U-bends, crevices samples, weight loss samples, and galvanic couples, are mounted on insulating racks and placed in the tanks. Approximately half of the samples are submersed, half are in the saturated vapor above the aqueous phase, and a limited number are at the water line. It is important to note that condensed water is present on specimens located in the saturated vapor (BSC 2003b, Section 6.4.3.).

The testing includes a wide range of plausible test media, including SDW, SCW, simulated cement-modified water, and SAW. The compositions of three of these solutions are summarized in Table 2-2. In addition, these data along with a detailed discussion of corrosion rate measurement and analysis results are presented in *General Corrosion and Localized Corrosion of Waste Package Outer Barrier* (BSC 2003b, Section 6.4.3). The corrosion rate of Alloy 22 was determined according to applicable ASTM G 1-90 1999. Results from the two types of coupons were used. These were labeled weight loss coupons and crevice coupons (BSC 2003b, Section 6.4.3). Figures 5-1 and 5-2 show the corrosion rate determined on these two types of samples after a 5-year exposure period.

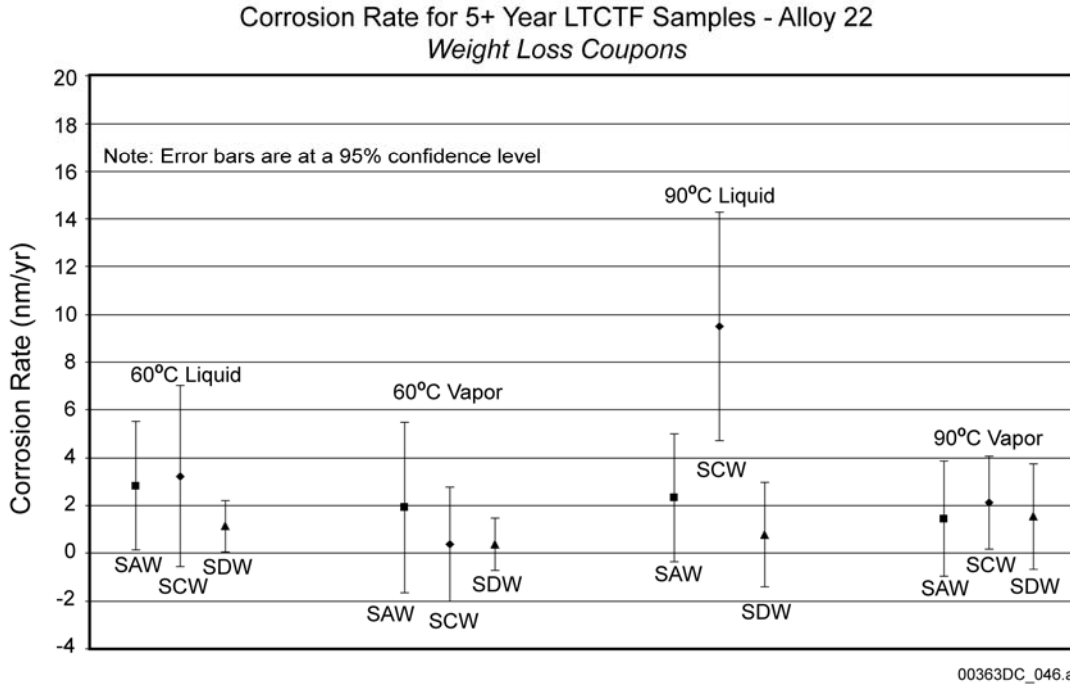
The SCW test medium is about three orders of magnitude (1,000×) more concentrated than J-13 well water and is alkaline (pH approximately 10). The SAW test medium is about three orders of magnitude (1,000×) more concentrated than J-13 well water and is acidic (pH approximately 2.7). These concentrated solutions are intended to mimic the evaporative concentration of the various potential electrolytes on the hot waste package surface. Two temperature levels (60°C and 90°C) are included (BSC 2003b, Section 6.4.3).

After a 5-year exposure to each solution/environmental condition, specimens were removed from their respective test vessel to determine the corrosion rate by weight-loss and dimensional-change measurements. Some samples had been previously removed after 6 month, 1-year and 2-year exposures. In all of the tested conditions, the coupons were covered with deposits. Therefore, the coupons were cleaned prior to final weighing. Cleaning was carried out using ASTM G 1.

A detailed analysis of these results based on weight loss coupons exposed to these environments at 60°C and 90°C for over 5 years is reported in the model report on the general and localized corrosion of the Alloy 22 waste package outer shell (BSC 2003b, Section 6.4.3), and a summary of these Alloy 22 corrosion rate results is presented here. The average corrosion rates and 2σ ranges are presented for the uncreviced (designated as weight loss specimens) and the creviced specimens in Figures 5-1 and 5-2, respectively.

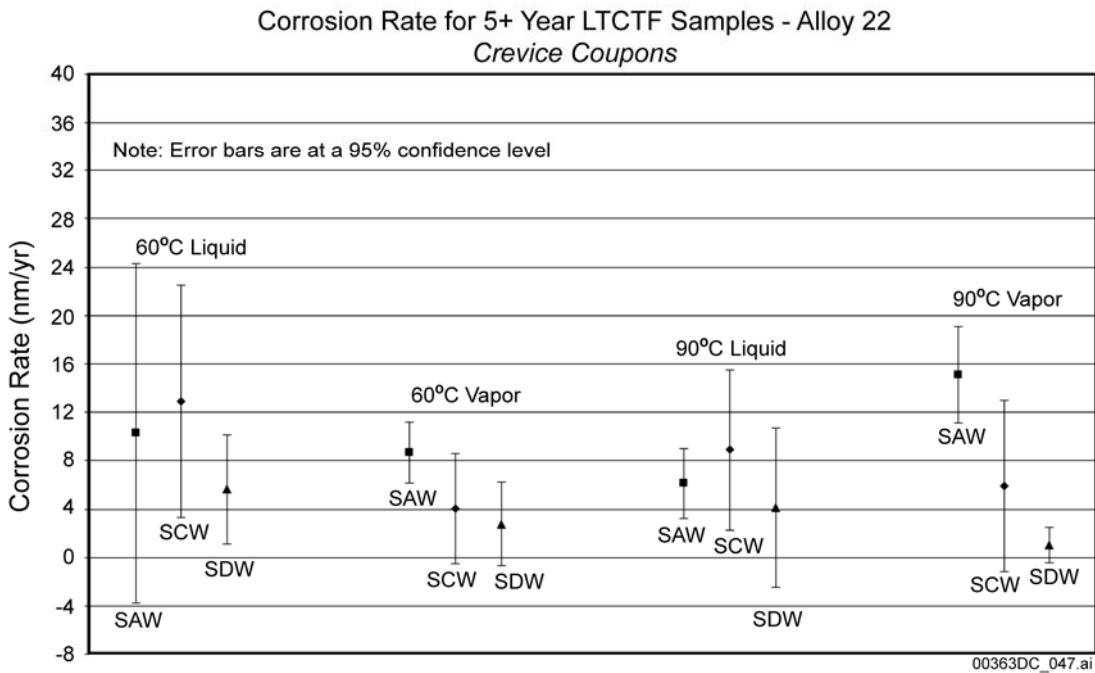
The 2σ range represents a 95 percent confidence level. The individual corrosion rates for the weight loss coupons ranged from 0 to 12 nm/yr, with the lowest rates observed for the coupons in the SDW solution. The individual corrosion rates for the crevice coupons, shown in Figure 5-2, ranged from 0 to 23 nm/yr with the highest rates observed in the SAW solution and, again, the lowest rates observed in the SDW solution. In most cases, the crevice coupons exhibited corrosion rates two to five times higher than the weight loss coupons in the same solutions. Stereomicroscopic, scanning electron microscope and atomic force microscopy observations of both weight loss and crevice specimens indicated little or no corrosion for Alloy 22. The machining grooves remained uniform and sharp throughout each coupon. It is not yet clear why the corrosion rates of the crevice coupons were higher than those of the weight loss coupons because crevice corrosion was not observed in any of the tested coupons. However, it is noteworthy that among all test specimens, a maximum measured corrosion rate of only 23 nm/yr was observed (BSC 2003b, Section 6.4.3).

For both the weight loss and crevice coupons, the corrosion rates were generally lower for those specimens exposed to vapor than immersed in liquid, regardless of the test temperature or electrolyte solution. For the weight loss coupons exposed to liquid, the corrosion rates were generally lower at 90°C than at 60°C. For the weight loss coupons exposed to vapor, the corrosion rates were generally higher at 90°C than at 60°C. Overall, coupons in the SAW solution exhibited slightly lower corrosion rates at the higher temperature. Similar to the weight loss coupons, the corrosion rates for the crevice coupons exposed to liquid were lower at 90°C than at 60°C, while the corrosion rates were generally higher at 90°C than at 60°C for the crevice coupons exposed to vapor. In general, for corrosion processes, the corrosion rate increases with temperature. However, since in this study the corrosion rates were so low and the temperature range studied (60°C to 90°C) is small, a clear dependence with the temperature cannot be established for any set of coupons. Finally, for the weight loss coupons, there appeared to be no effect of the presence of welds on the corrosion rate, however, the nonwelded crevice coupons exhibited slightly higher rates than their welded counterparts (BSC 2003b, Section 6.4.3).



Source: Output DTN: SN0308T0506303.004.

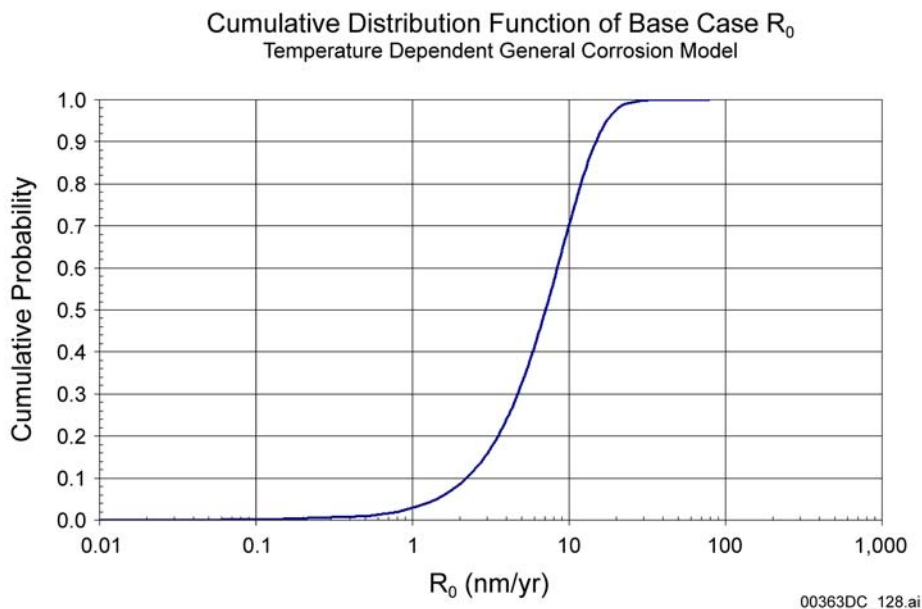
Figure 5-1. Corrosion Rates for Alloy 22 Weight-Loss Coupons in Simulated Acidified Water, Simulated Concentrated Water, and Simulated Dilute Water



Source: Output DTN: SN0308T0506303.004.

Figure 5-2. Corrosion Rates for Alloy 22 Crevice Coupons in Simulated Acidified Water, Simulated Concentrated Water, and Simulated Dilute Water

The empirical cumulative distribution functions for the general corrosion rates of Alloy 22 weight-loss and crevice samples are presented in the model report on the general and localized corrosion of the waste package outer shell (BSC 2003b, Section 6.4.3.2). These provide a comparison of the effect of various experimental factors on the general corrosion rate, such as for the solution chemistry, temperature, and metallurgical condition. For the weight-loss samples, the mean corrosion rate is 2.75 nm/yr and the standard deviation is 2.74 nm/yr. For the crevice samples, the mean corrosion rate is 7.24 nm/yr, and the standard deviation is 4.95 nm/yr (Figure 5-3).



Source: Output DTN: SN0308T0506303.004.

Figure 5-3. Cumulative Distribution Function of R_0 of Base-Case General Corrosion Rate for Alloy 22 Waste Package Outer Shell at 60°C

The crevice coupon rates were used as the base case general corrosion rate of the waste package outer shell. A Weibull distribution, with scale factor of 8.88, shape factor of 1.62, and location factor of 0, best fits the corrosion rate distribution (BSC 2003b, Section 6.4.3).

5.2 GENERAL CORROSION MODEL

The temperature dependence of general corrosion rate can be represented by the logarithm of the Arrhenius relationship.

$$\ln(R_T) = C_o + \frac{C_1}{T} \quad (\text{Eq. 5-1})$$

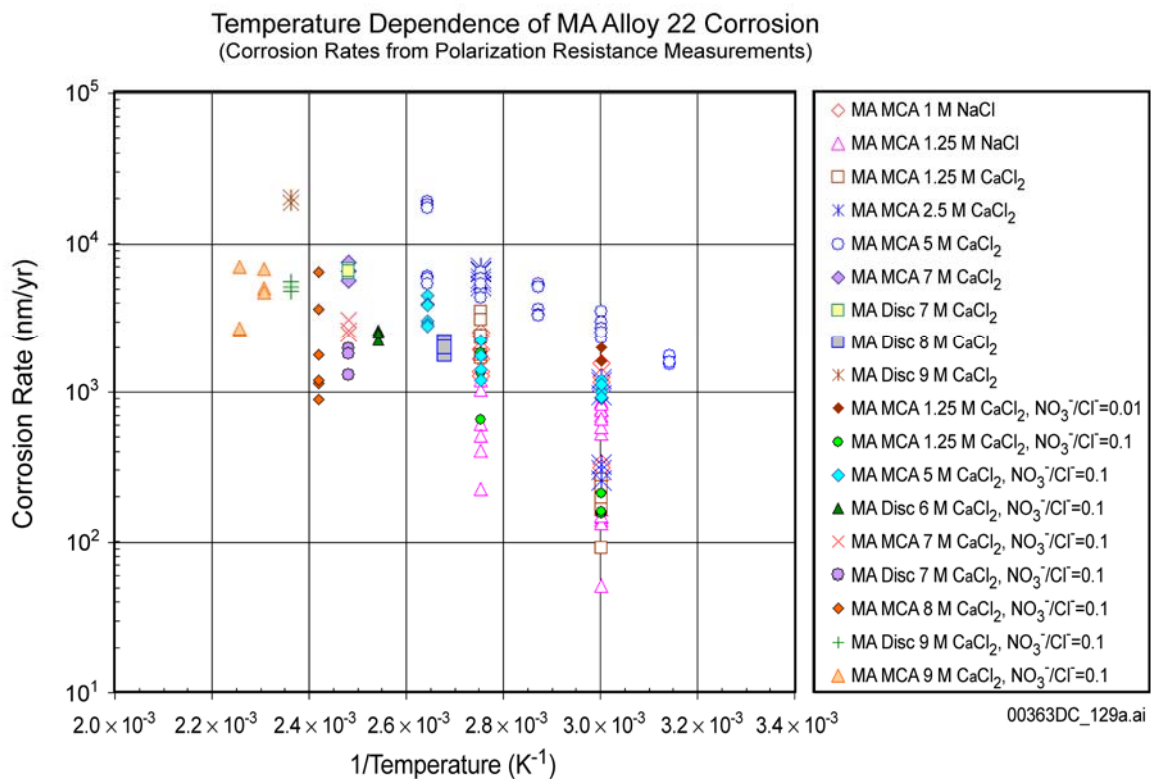
R_T is the temperature-dependent general corrosion rate in nanometers per year, T is the absolute temperature in Kelvin, and C and C_1 are constants. The temperature-dependence term (C_1) is determined from short-term polarization resistance data for Alloy 22 specimens tested for a range of sample configurations, metallurgical conditions, and exposure conditions (temperature

and water chemistry). Figure 5-4 shows the temperature dependence of Alloy 22 corrosion rates measured by the polarization resistance technique over the temperature range from 45°C to 170°C. From fitting the data to the Arrhenius relationship, the temperature-dependence term (C_I) was found to obey a normal distribution with a mean of approximately 3,000 and a standard deviation of approximately 300. This temperature dependence is characterized by the activation energy of 26 kJ/mol. Sample configuration (crevice, disk, or rod), metallurgical conditions (mill-annealed or weld), and water chemistry within the range expected in the repository appear to have no significant effect on the temperature dependence of general corrosion rate.

The Arrhenius relationship is used to predict the temperature-dependent general corrosion rate (R_T) from the general corrosion rate at 60°C (R_0) and the temperature-dependence term (C_I).

$$\ln(R_T) = \ln(R_0) + C_I \left(\frac{1}{T} - \frac{1}{333.15} \right) \quad (\text{Eq. 5-2})$$

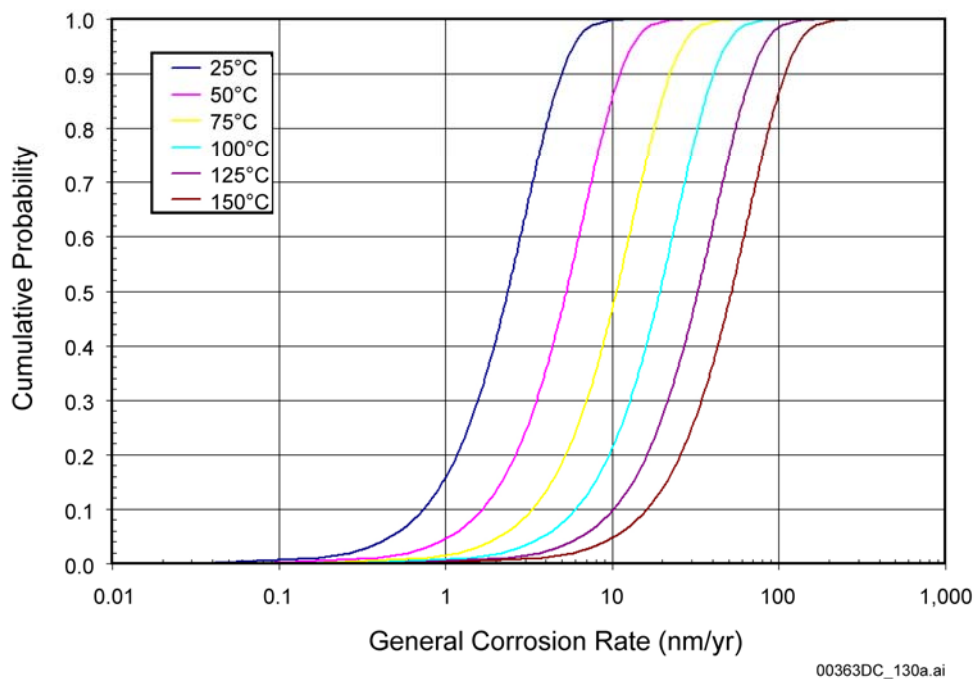
Predictions of the distribution of the temperature-dependent general corrosion rate (R_T) at 25°C, 50°C, 75°C, 100°C, 125°C, and 150°C are shown in Figure 5-5 (BSC 2003b, Figure 6-23).



Source: Output DTN: SN0308T0506303.004.

NOTE: Corrosion rates were determined from 24-hour polarization resistance measurements.

Figure 5-4. Temperature Dependence of Corrosion Rates for Alloy 22 for Various Metallurgical Conditions and Sample Configurations and in a Wide Range of Test Solutions



Source: Output DTN: SN0308T0506303.004.

NOTE: The calculation was performed using the mean value (-3116.47) of the temperature-dependency term (C_1). The calculated general corrosion rate range represents the variability of the rate.

Figure 5-5. Calculated Model Outputs of the Base-Case Temperature-Dependent General Corrosion Model, Based on the Crevice Sample Data at 25°C, 50°C, 75°C, 100°C, 125°C, and 150°C

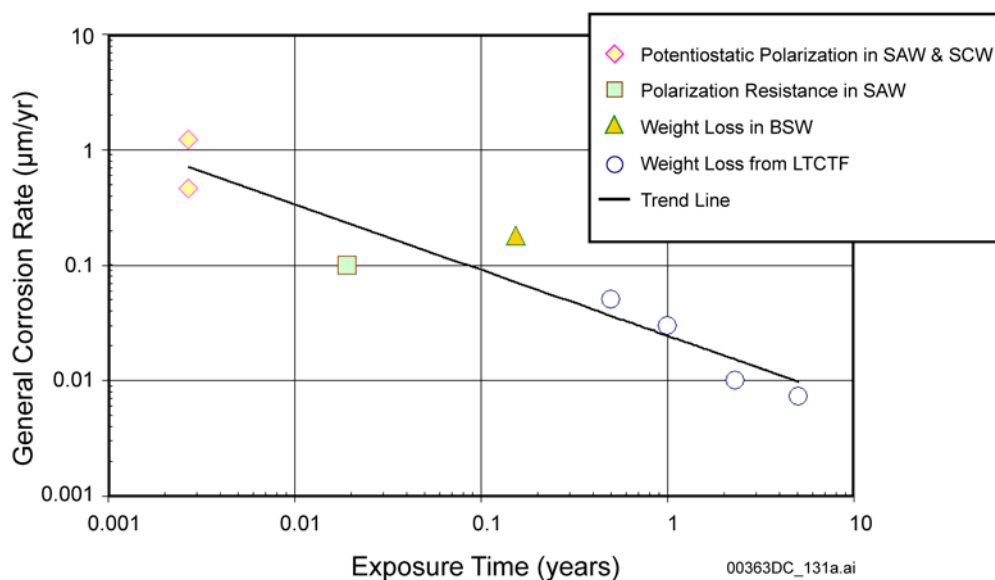
5.3 UNCERTAINTY ANALYSIS OF GENERAL CORROSION RATE DATA

Most of the uncertainties in general corrosion rate of Alloy 22 have resulted from insufficient resolution of the weight-loss and dimensional-change measurements of the samples due to the extremely low corrosion rates of Alloy 22 in the test media. It was concluded that measurement uncertainty was the main source of uncertainty. The combined standard uncertainty is estimated to be approximately 0.185 nm/yr in the case of crevice samples and 0.314 nm/yr in the case of weight-loss samples (BSC 2003b, Section 6.4.3). These estimates correspond to 1 standard deviation (1σ). Therefore, for the crevice samples, about 3 percent of the variation in the measured general corrosion rate is due to the measurement uncertainty, and 97 percent of it is from the variations of the corrosion rate among the specimens. For the weight loss samples, most of the variation (about 89 percent) in the measured corrosion rate is due to variations among the specimens, and the rest is from measurement uncertainty.

5.4 TIME-DEPENDENT GENERAL CORROSION BEHAVIOR OF THE WASTE PACKAGE OUTER SHELL

The general corrosion model implemented in TSPA assumes that general corrosion of the Alloy 22 waste package outer shell progresses uniformly over a large surface. The general

corrosion rate is temperature dependent; for a given temperature, it is assumed to be constant (i.e., time-independent). Therefore, for a given temperature, the depth of penetration or thinning of the waste package outer shell by general corrosion is equal to the general corrosion rate at that temperature multiplied by the time duration that the waste package is at that temperature. In general, however, the corrosion rates of metals and alloys decrease with time. This is shown in Figure 5-6 (BSC 2003b, Figure 6-24) for the mean general corrosion rates of Alloy 22 after 0.5-, 1-, 2-, and 5-year exposures in the LTCTF and for shorter exposure time results based on other measurement techniques such as weight loss, polarization resistance and potentiostatic polarization tests. The mean general corrosion rate after a 5-year exposure in the LTCTF is $0.007 \mu\text{m}/\text{yr}$ ($7 \text{ nm}/\text{yr}$). The trend of decreasing general corrosion rate with time is consistent with the expected corrosion behavior of passive alloys such as Alloy 22 under repository-type aqueous conditions. The time-dependent general corrosion behavior of the waste package outer shell was not included in TSPA because the constant (time-independent) rate model is more conservative and should bound the general corrosion behavior of the waste package outer shell over the repository time period. Since the long-term rates will be lower than the 5-year rates, the 5-year corrosion rates were conservatively selected for extrapolation over the repository time scale.



NOTE: Trend line was obtained by a linear regression fit for the data shown in the figure.

Figure 5-6. Time-Dependent General Corrosion Rate of Alloy 22

5.5 OTHER FACTORS INFLUENCING GENERAL CORROSION OF WASTE PACKAGE OUTER SHELL MATERIAL

Effect of Microbial Activity on General Corrosion—MIC is the contribution to the corrosion rate of a metal or alloy by the presence or activity, or both, of microorganisms (BSC 2003b, Section 6.4.3). MIC most often occurs due to the increase in anodic or cathodic reactions due to the direct impact of microorganisms on the alloy, or by indirect chemical effects on the surrounding solution. Microorganisms can affect the corrosion behavior of an alloy either by acting directly on the metal or through their metabolic products. For example, some types of

aerobic bacteria may produce sulfuric acid by oxidizing reduced forms of sulfur (elemental, sulfide, sulfite), and certain fungi transform organic matter into organic acids (Fontana 1986, Section 8-10).

It has been observed that nickel-based alloys such as Alloy 22 are relatively resistant to MIC (Lian et al. 1999). The impact of microbially influenced corrosion is accounted for by adjusting the rate of general corrosion.

There are no standard tests designed specifically to investigate the susceptibility of an engineering alloy to MIC (Stoecker 1987). One commonly used type of evaluation to determine the MIC factor is to test the alloy of interest in situ (field) using the same variables as for the intended application. However, testing in the laboratory with live organisms can provide more controlled conditions of various environmental variables, and sterile controls can be incorporated to better assess MIC-specific effects (Horn and Jones 2002). This approach was used to evaluate the microbiological processes on general corrosion of the waste package outer shell. For general corrosion of the waste package outer shell, the effect of microbially influenced corrosion can be described as follows:

$$CR_{MIC} = CR_{st} \cdot f_{MIC} \quad (\text{Eq. 5-3})$$

where CR_{MIC} is the general corrosion rate in the presence of microorganisms, CR_{st} is the general corrosion rate of the alloy in the absence of MIC, and f_{MIC} is the microbially influenced corrosion factor. If f_{MIC} is greater than 1, there is an enhancement of the corrosion rate of the alloy as a consequence of the presence or activity of microorganisms.

Lian et al. (1999) showed with polarization resistance measurements that MIC can enhance corrosion rates of Alloy 22 by a factor of at most two. Measurements for Alloy 22 and other similar materials are shown in Table 5-1 (BSC 2003b, Table 6-10). The microbially influenced corrosion factor f_{MIC} is calculated as the ratio of corrosion rates (microbes to sterile) from the table. The value of f_{MIC} for Alloy 22 in sterile media is set to 1 ($f_{MIC} = 1$), whereas the value of f_{MIC} for Alloy 22 in inoculated media is larger ($f_{MIC} = 2$). It is assumed that the microbially influenced corrosion factor f_{MIC} is uniformly distributed between 1 and 2, and that this distribution is all due to uncertainty. The MIC factor is applied to the waste package outer shell general corrosion rate when the relative humidity at the waste package outer shell surface is above 90 percent. This MIC initiation threshold relative humidity is based on the analysis documented in *In-Drift Microbial Communities* (CRWMS M&O 2000c, Sections 6.3.1.6 and 6.5.2, Table 23), which determined that microbial activity would not occur at relative humidity less than 90 percent.

Other environmental factors that could affect bacterial growth include temperature and radiation. These factors, however, are closely coupled to relative humidity; as temperature and radiation decrease in the repository, relative humidity is predicted to increase. At the same time, while there are some types of microorganisms that can survive elevated temperatures (less than or equal to 120°C) and high radiation doses, if there is no available water, then bacterial activity is completely prevented. Thus, because water availability is the primary limiting factor and this factor is coupled to other less critical limiting factors, water availability (as expressed by relative humidity) was used as the primary gauge of microbial activity.

Table 5-1. Alterations in Corrosion Rates and Potentials Associated with Microbial Degradation

Tested Sample Initial Condition	Average Corrosion Rate ($\mu\text{m}/\text{yr}$)	Corrosion Potential E_{corr} (V versus SCE)	
		Initial	Endpoint
CS1020 + YM Microbes	8.80	-0.660	-0.685
Sterile CS 1020	1.40	-0.500	-0.550
M400 + YM Microbes	1.02	-0.415	-0.315
Sterile M400	0.005	-0.135	-0.070
C-22 + YM Microbes	0.022	-0.440	-0.252
Sterile C-22	0.011	-0.260	-0.200
I625 + YM Microbes	0.013	-0.440	-0.285
Sterile I625	0.003	-0.160	-0.130
Stainless Steel Type 304 + YM Microbes	0.035	-0.540	-0.280
Sterile Stainless Steel Type 304	0.003	-0.145	-0.065

Source: DTN: LL991203505924.094.

Effect of Aging and Phase Stability on General Corrosion—The waste package outer shell base metal and all fabrication welds (not including the welds for the closure lids) are fully annealed before the waste packages are loaded with waste (BSC 2003a). The analysis documented in the model report titled *Aging and Phase Stability of Waste Package Outer Barrier* (BSC 2003d, Sections 6.6.5.3 and 8.0) has shown that phase instabilities are not expected in Alloy 22 base metal and welded material as long as the temperature remains below about 200°C. Further, as discussed in Section 3, analysis suggests that even for the case of early steady state drift collapse (acting like backfill), the waste package temperature could potentially increase by about 130°C, leading to peak temperatures of about 300°C but for only relatively short times (decades to centuries).

Mechanical stress mitigation processes, currently planned for the closure weld, however, may introduce cold work into the material. This cold work might accelerate phase transformation kinetics, however the kinetics would have to be at least two orders of magnitude higher before it would be expected to be observed at low temperatures in 10,000 years. For a range of thermal loading designs of the repository, the waste package surface temperature will be always kept below 200°C (BSC 2001b, Section 5.4.1, Figures 5.4.1-2 and 5.4.1-6) in the absence of drift collapse. Although peak temperatures of about 300°C are possible under drift collapse, they would only exist for decades to centuries. These times are too short for significant aging effects at 300°C (Section 3). With this constraint, the effect of aging and phase instability on the corrosion of the waste package outer shell will therefore be insignificant in the repository.

In order to analyze the effects of thermal aging on corrosion of Alloy 22, three metallurgical conditions of Alloy 22 were studied using the multiple crevice assembly samples: mill-annealed, as-welded, and as-welded plus thermally aged (at 700°C for 173 hours). The samples were tested, using electrochemical methods similar to those presented in Sections 6 and 7, in 5 M CaCl₂ and 5 M CaCl₂ + 0.5 M Ca(NO₃)₂ solutions at temperatures up to 120°C. After immersion in the test solution at open-circuit potential for 24 hours, the polarization resistance of the samples was measured. The corrosion rates from the polarization resistance measurements were

only for comparative analysis of the effects of thermal aging on corrosion of Alloy 22; the tests were not intended to obtain the absolute values of the corrosion rate. It is to be noted that the corrosion rates derived from the short-term electrochemical testing are significantly higher than the rates obtained from long-term testing. This is characteristic of short-term tests and the results, therefore, are being used for comparative purposes only.

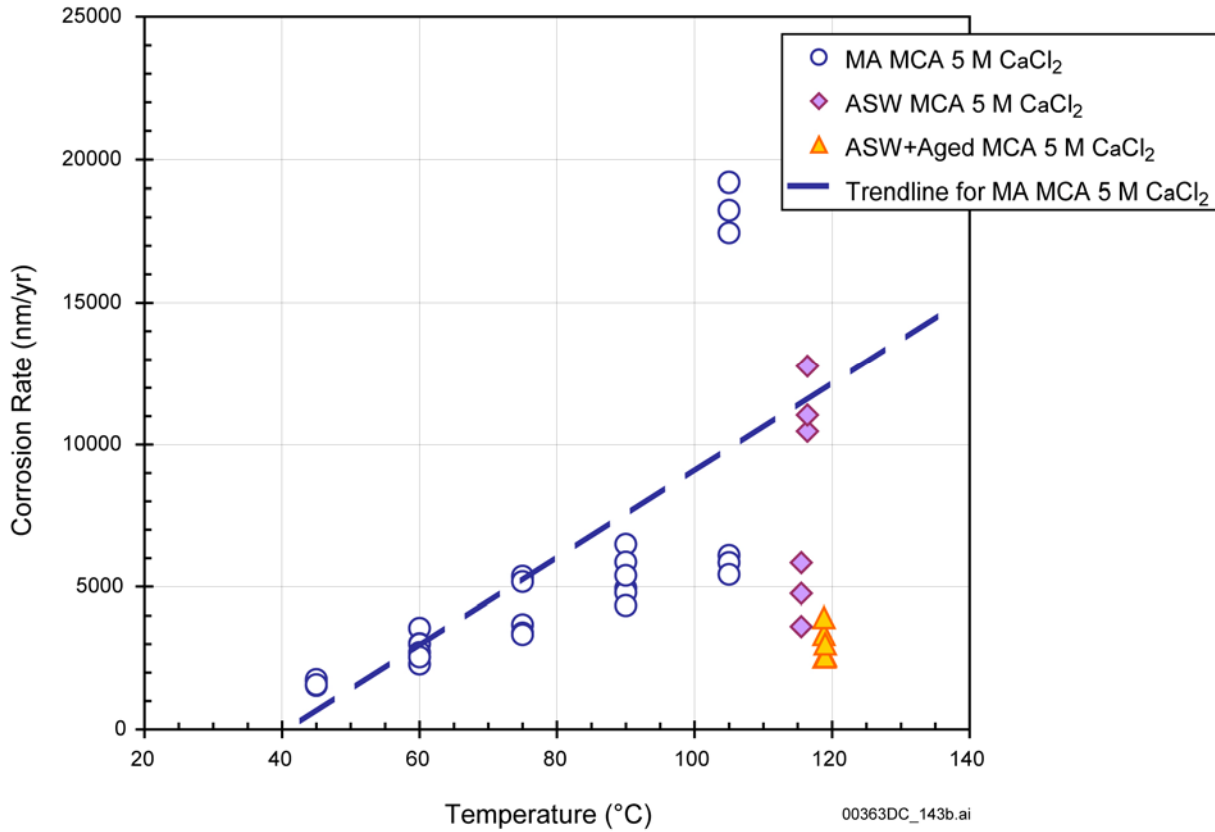
Comparison of the calculated corrosion rates of the mill-annealed, as-welded, and as-welded plus thermally aged samples are shown in Figure 5-7 for 5 M CaCl_2 solutions and Figure 5-8 for 5 M $\text{CaCl}_2 + 0.5 \text{ M Ca(NO}_3)_2$ solutions. The mill-annealed multiple crevice assembly samples in 5 M CaCl_2 solutions at differing temperatures were considered as the baseline condition for the analysis. The baseline condition rates were compared with those of the as-welded and as-welded plus thermally aged multiple crevice assembly samples tested in the same electrolyte solution condition. A data trend-line for the baseline condition data was obtained by linear regression fit for an easier comparison with the as-welded and as-welded plus thermally aged sample data. The comparison shown in Figure 5-7 clearly shows that there is no apparent enhancement of the corrosion rate due to welding or thermal aging of the welded samples for the tested conditions.

As shown in Figure 5-8, a similar comparison was made for the corrosion rates measured in 5 M $\text{CaCl}_2 + 0.5 \text{ M Ca(NO}_3)_2$ solutions. As for the 5 M CaCl_2 solution case, the mill-annealed multiple crevice assembly samples at differing temperatures were considered as the baseline condition, and a data trend-line was drawn for the baseline condition data for an easier comparison. The comparison in Figure 5-8 again clearly shows no apparent enhancement of the corrosion rate due to welding or thermal aging of the welded samples. It is also noted that the corrosion rates of all three type samples (mill-annealed, as-welded, and as-welded plus thermally aged) were reduced by a factor of 3 to 4 in the nitrate containing solutions, compared to those in 5 M CaCl_2 solutions.

The above analyses are consistent with the results by Brossia et al. (2001, Section 3.2.1.3, Figure 3-13) and Rebak et al. (2002). Comparison of the anodic passive current densities of the as-welded Alloy 22 samples to those of the base metal samples showed no significant effect of the welds on the passive corrosion behavior of the alloy (Brossia et al. 2001, Section 3.2.1.3, Figure 3-13).

Based on the above analysis and insignificant aging and phase stability processes under the thermal conditions expected in the repository (BSC 2003d, Sections 6.6.5.3 and 8.0), the corrosion performance of the waste package outer shell is not expected to be affected by the aging and phase stability in the repository. Hence thermal aging and phase instability effects of the waste package outer shell on corrosion are not included in TSPA.

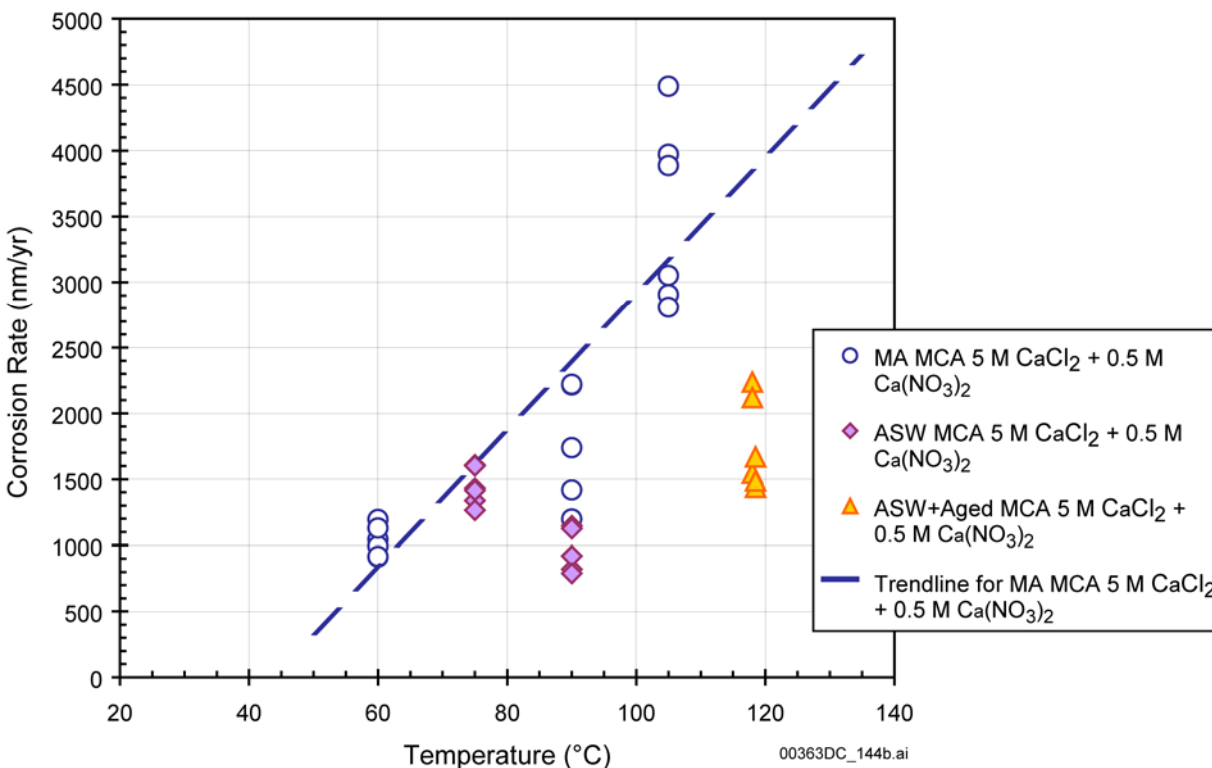
Similarly, analyses described in Section 8 indicate the effects of radiolysis on corrosion performance of Alloy 22 will not be significant enough to lead to corrosion-induced failure of the waste package outer shell under repository relevant conditions. For this reason, the effects of radiolysis on corrosion performance of Alloy 22 are not included in TSPA modeling.



Source: Output DTN: SN0308T0506303.003.

NOTE: The trend line for the mill-annealed samples was obtained by linear regression fit of the data set.

Figure 5-7. Comparison of Corrosion Rates from 24-Hour Polarization Resistance Measurements of Mill-Annealed, As-Welded, and As-Welded Plus Aged Alloy 22 Multiple Crevice Assembly Samples in 5 M CaCl₂ Brines at Varying Temperatures



Source: Output DTN: SN0308T0506303.003.

Figure 5-8. Comparison of Corrosion Rates from 24-Hour Polarization Resistance Measurements of Mill-Annealed, As-Welded, and As-Welded Plus Aged Alloy 22 Multiple Crevice Assembly Samples in 5 M CaCl_2 + 0.5 M $\text{Ca}(\text{NO}_3)_2$ Brines at Varying Temperatures

5.6 SUMMARY OF GENERAL CORROSION OF WASTE PACKAGE OUTER SHELL

Because of extremely slow corrosion rates of Alloy 22, there is little data for Alloy 22 in the scientific literature that could be used to evaluate the general corrosion model presented above. However, similar passive corrosion behavior has also been observed for nickel-chromium-molybdenum type corrosion-resistant alloys. For example, Alloy C is found to retain a very thin passive film, indicated by the retained mirror-like finish after 44 years of exposure at Kure Beach to a marine environment (i.e., salt air with alternate wetting and drying as well as the presence of surface deposits) (Baker 1988, p. 134, Table 6). More recent examination of specimens from this alloy after more than 50 years of exposure indicates that the samples continue to maintain a mirror-like finish and passive film behavior (McCright 1998, Figure ES-1). Under these exposure conditions, the less corrosion-resistant Alloy 600 exhibited a corrosion rate of 8 nm/yr after 36 years of exposure. This long-term corrosion rate is consistent with the model prediction. The 50th and 99.99th percentile rates at 25°C predicted by the model are 2.4 and 11.7 nm/yr respectively. These long-term results provide corroborative support for the expected excellent long-term passive corrosion behavior of Alloy 22 under chloride-containing aqueous environments that are relevant to repository exposure conditions.

In addition, the general corrosion model implemented in TSPA assumes that general corrosion of the waste package outer shell progresses uniformly over a large surface. The general corrosion rate is temperature dependent, and for a given temperature, the depth of penetration or thinning of the waste package outer shell by general corrosion is equal to the general corrosion rate at that temperature multiplied by the time duration that the waste package is at that temperature. However, general corrosion rates of metals and alloys tend to decrease with time. This dependence of the general corrosion rate of Alloy 22 on the exposure time was seen previously for the 6-month, 1-year, and 2-year data from the LTCTF. This is shown in Figure 5-6 for the mean general corrosion rates of Alloy 22 for those data.

The mean general corrosion rate of the crevice samples after 5-year exposure at the LTCTF was 0.0073 $\mu\text{m}/\text{yr}$, and the standard deviation was 0.005 $\mu\text{m}/\text{yr}$. Each data point for up to 2 years is the mean of the measurements on at least 144 samples, and the data point for 5-year is the mean of 59 samples. The trend of decreasing general corrosion rate with time is consistent with the expected corrosion behavior of passive alloys such as Alloy 22 under repository-type aqueous conditions. Therefore, the 5-year corrosion rates were conservatively selected for extrapolation over the repository time scale.

Corroboration of the very low rates obtained from the temperature-dependent general corrosion model with the rates from alternative techniques from the scientific literature confirms that the life of the waste package is not limited by the rate of uniform, general corrosion.

INTENTIONALLY LEFT BLANK

6. LOCALIZED CORROSION OF ALLOY 22 IN AGGRESSIVE BRINES EVOLVED IN THE TRANSITION REGIME

6.1 CRITERION FOR LOCALIZED CORROSION

This section describes the localized corrosion behavior of the corrosion-resistant outer shell of the waste package. The threshold temperature is the temperature above which spontaneous localized corrosion can occur for any given environment, and no localized attack will occur below this temperature. The threshold temperature for localized corrosion can be determined from measurements of the open-circuit corrosion potential (E_{corr}) and the critical potential ($E_{critical}$) as functions of temperature and exposure chemistry. Spontaneous breakdown of the passive film and localized corrosion require that the open-circuit corrosion potential exceed or equal the critical potential (BSC 2003b, Sections 6.4.4 and 6.4.4.1; Farmer, McCright et al. 2000):

$$E_{corr} \geq E_{critical} \quad (\text{Eq. 6-1})$$

Localized corrosion (pitting or crevice corrosion) is a type of corrosion in which the attack progresses at discrete sites or in a nonuniform manner. The alloys under consideration form relatively stable oxide films (passive films) which impede the rate of electrochemical reactions. Under aggressive environmental exposure conditions, the passive films may breakdown locally (typically at defect sites in the film) leading to localized attack of the underlying alloy. The rate of localized corrosion is generally much higher than the rate of general corrosion. The current analysis conservatively considers crevice corrosion as the potential mode of localized corrosion of the waste package outer shell under repository exposure conditions. This is conservative because the initiation thresholds for crevice corrosion of Alloy 22 in terms of water chemistry and temperature are lower than for pitting corrosion (BSC 2003b, Section 6.3)

The localized corrosion model for the waste package outer shell consists of an initiation component and a propagation component. In the initiation component, localized corrosion of the waste package outer shell occurs when the open-circuit corrosion potential (E_{corr}) is equal to or greater than a critical potential ($E_{critical}$), that is ΔE (equal $E_{critical} - E_{corr}$) less than or equal to 0. Both of the crevice corrosion initiation model components (i.e., E_{corr} and $E_{critical}$) are represented as functions of temperature, pH, chloride ion concentration, nitrate ion concentration. When localized corrosion occurs, the rate of localized corrosion propagation is assumed to occur at a (time-independent) constant rate (Section 6.7). This assumption may be conservative (BSC 2003b, Section 6.3).

Section 6.2 focuses on the determination of the long-term open-circuit or corrosion potential (E_{corr}). Section 6.3 discusses cyclic potentiodynamic polarization techniques and their use to determine the critical potential ($E_{critical}$) for breakdown of the passive film. The breakdown potential corresponds to the onset of passive film destabilization and is higher than the critical potentials designated for reformation of the passive film during the negative (cathodic) potential scan. The different types of cyclic potentiodynamic polarization curves relevant to the current analysis are reviewed. In Section 6.4 different methods of choosing the value of $E_{critical}$ are discussed. The localized corrosion initiation model is discussed in Section 6.5 with application

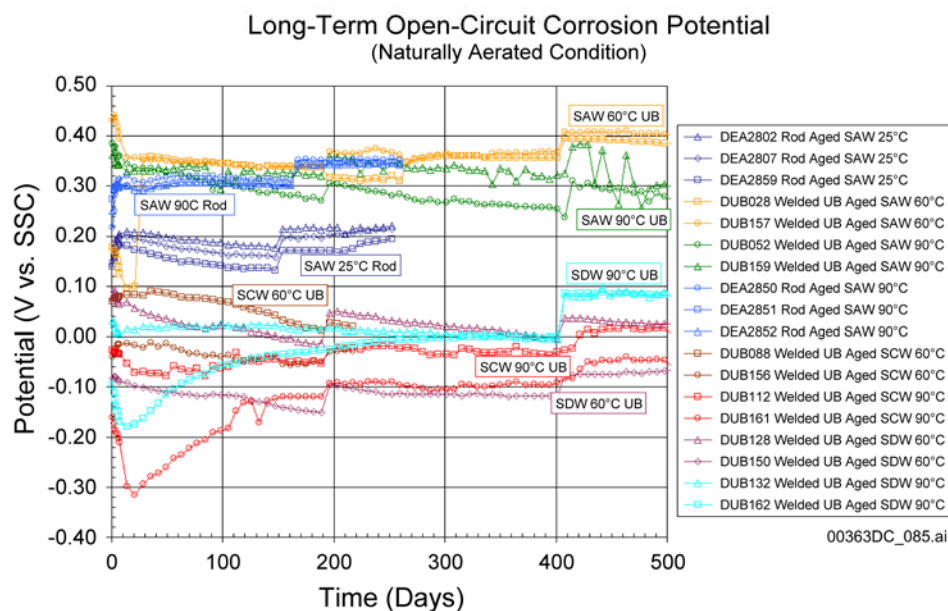
to the characteristic seepage waters presented in Section 6.6. Section 6.7 discusses the localized corrosion penetration rate model.

6.2 LONG-TERM OPEN-CIRCUIT CORROSION POTENTIAL DATA ANALYSIS

Because the corrosion potential of Alloy 22 may change over time, it is important to know the most probable value of long-term corrosion potential (E_{corr}) for Alloy 22 under different environmental conditions and the uncertainty associated with that corrosion potential to evaluate the localized corrosion susceptibility of the waste package outer shell in the repository. The localized corrosion initiation model of the waste package outer shell assumes that localized corrosion will only occur when E_{corr} is equal to or greater than a critical potential (crevice repassivation potential (E_{rcrev}) in the current model analysis) (i.e., $E_{critical}$ equals E_{rcrev}). That is, if E_{corr} is less than E_{rcrev} , general or passive corrosion will occur. General corrosion rates are expected to be exceptionally low.

The specimens used to evaluate E_{corr} of Alloy 22 as a function of immersion time were machined from sheet and bar stock. There were two main groups of specimens, (1) welded U-bend specimens and (2) untested rod specimens. Approximately half of the U-bend specimens tested for long-term corrosion potential were from the LTCTF, and other half of the U-bend specimens were not previously exposed to any electrochemical test condition. The U-bend specimens from the LTCTF already had the passive film and other surface alterations from the exposure in the LTCTF. The data and test details are reported in the source DTN: LL020711612251.017.

Long-term corrosion potential behaviors of some selected Alloy 22 samples in the SDW, SAW and SCW solutions from the LTCTF tanks are shown in Figure 6-1. The figure shows that after initial changes, the corrosion potentials of the Alloy 22 samples become stable after about 100 days of testing. It is shown that the results of the welded U-bend samples (Samples DUB052 and DUB159) and (nonwelded) rod samples (Samples DEA2850, DEA2851 and DEA2852) in aged SAW at 90°C show no significant differences in their long-term open-circuit corrosion potential behaviors.



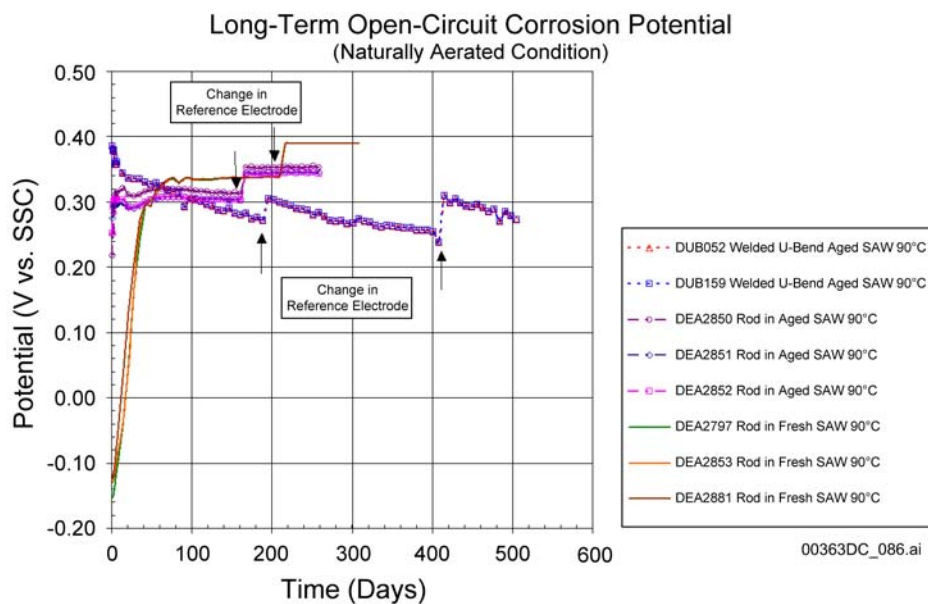
Source: DTN: SN0308T0506303.003.

Figure 6-1. Open-Circuit Corrosion Potential Measurements for Samples of Alloy 22 in Three Types of Long Term Corrosion Test Facility Solutions (Simulated Dilute Water, Simulated Acidified Water, and Simulated Concentrated Water), as a Function of Time

The values of E_{corr} of Alloy 22 in SAW are higher than those in other aged LTCTF solutions. The apparent steady state E_{corr} values of Alloy 22 in SAW (an acidic solution) at 60°C and 90°C are in the order of 300 to 400 mV versus SSC (SSC is Ag/AgCl). Figure 6-2 compares the long-term corrosion potential evolution of freshly polished Alloy 22 rods in freshly prepared SAW at 90°C with the corrosion potential evolution of the welded U-bend and rod samples in aged SAW at 90°C. Because of the long-term nature of the tests, the reference electrodes had to be replaced regularly during the tests due to their operations outside the specified accuracy range. The reference electrode replacements are indicated in the figure. Initially the Alloy 22 rods in the fresh SAW solution had corrosion potentials on the order of about -150 mV versus SSC. However, over approximately 100 days of testing, the corrosion potential increased to a more oxidizing potential value of approximately 330 mV versus SSC. This apparent stable corrosion potential was maintained over the balance of the approximately 300-day test, slowly reaching a maximum oxidizing value near 400 mV versus SSC. This high value of E_{corr} is probably due to the formation of a protective chromium rich oxide film on the surface of the Alloy 22 electrodes. The test results show that, regardless of the initial condition of the metal surface or the age of the electrolyte solution, Alloy 22 eventually undergoes ennoblement in SAW. This ennoblement is probably promoted by both the pH value and the presence of nitrate in the solution (Estill et al. 2003). Such an ennoblement of Alloy 22 with time has also been reported recently, and the ennoblement was significant in acidic solutions (Jayaweera et al. 2003, Figures 9.12 and 9.13; Dunn et al. 2003, Figures 8 and 9).

In addition, the results in Figure 6-2 show that the E_{corr} values of Alloy 22 rods in SAW at 25°C are lower than the values at 90°C by about 150 mV. A similar trend is also observed for the welded U-bend samples in the SDW solutions. This effect could be attributed to kinetic

mechanisms either in the behavior of the oxide film or on the redox reactions in solution. The temperature effect in the SCW solution was not evaluated because the tests at 60°C were terminated early.



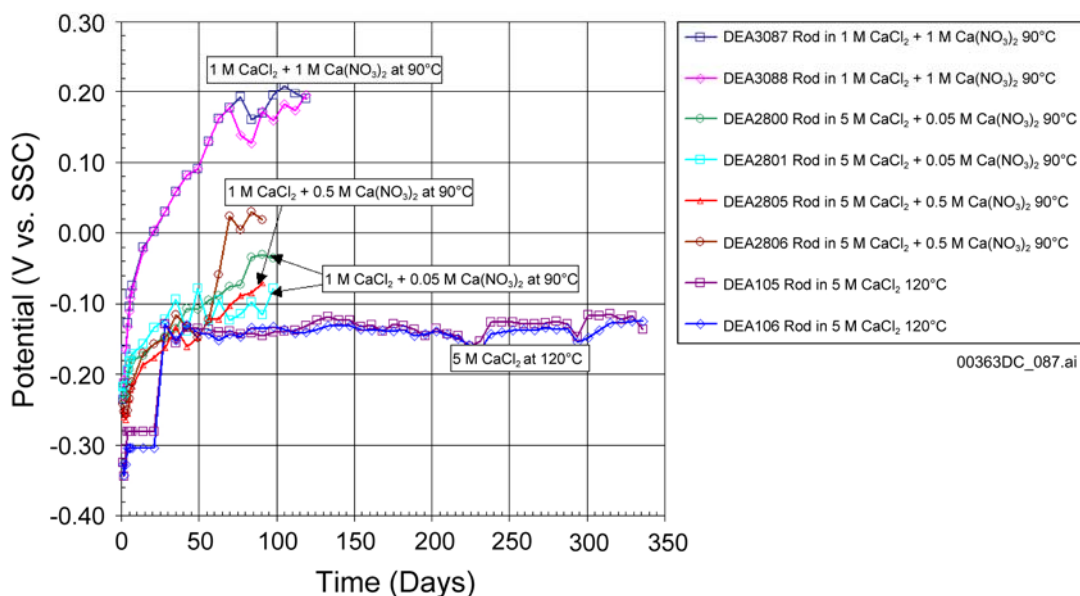
Source: DTN: SN0308T0506303.003.

Figure 6-2. Open-Circuit Corrosion Potential Measurements for Samples of Alloy 22 in Simulated Acidified Water, at Different Conditions, and as a Function of Time

Figure 6-3 shows the test results for the E_{corr} behavior of Alloy 22 in CaCl_2 solutions with varying chloride concentrations and the effect of the addition of nitrate. The data show that E_{corr} of Alloy 22 in the CaCl_2 solutions is affected mostly by the chloride concentration, and addition of nitrate ions slows down the process of attaining steady state. E_{corr} for Alloy 22 in 5 M CaCl_2 solution at 120°C reached steady state in less than 50 days. The average values of E_{corr} after more than 300 days of testing were -129 mV versus SSC (see BSC 2003b, Attachment V for the numerical values of the data).

After approximately 100 days of testing, the E_{corr} values for Alloy 22 in 5 M CaCl_2 solutions with nitrate added seemed to be approaching a steady state value. The average value of E_{corr} for Alloy 22 in 5 M $\text{CaCl}_2 + 0.05$ M $\text{Ca}(\text{NO}_3)_2$ solution at 90°C was -39 mV versus SSC after 100 days of testing. This solution represents a nitrate to chloride ratio of 0.01. A similar behavior was observed for Alloy 22 tested in 5 M $\text{CaCl}_2 + 0.5$ M $\text{Ca}(\text{NO}_3)_2$ solution (nitrate to chloride ratio of 0.1) at 90°C, and the average E_{corr} value was -46 mV versus SSC. For Alloy 22 electrodes immersed in 1 M $\text{CaCl}_2 + 1$ M $\text{Ca}(\text{NO}_3)_2$ solution (nitrate to chloride ratio of 1) at 90°C, it appears that, after 120 days of testing, the E_{corr} values had approached a steady state value, and the average E_{corr} value was 168 mV versus SSC.

Alloy 22 Long-Term Open-Circuit Corrosion Potential
(Naturally Aerated Condition)



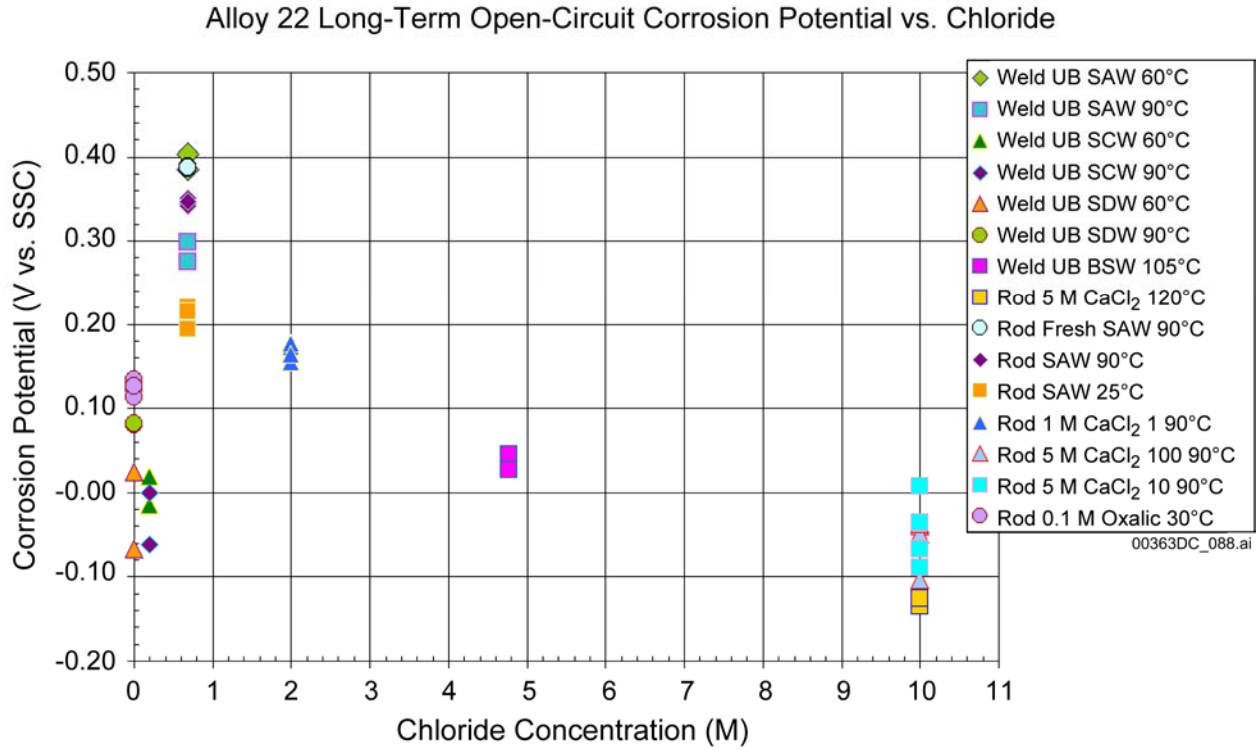
Source: DTN: SN0308T0506303.003.

NOTE: Higher resolution and longer duration data are shown in Figure 6-11 for DEA 105 and DEA 106 and in Figure 6-15 for DEA 2800 and DEA 2801.

Figure 6-3. Open-Circuit Corrosion Potential Measurements for Samples of Alloy 22 in CaCl_2 Solutions, with Various Concentrations and Inhibitor Levels, and as a Function of Time

Figure 6-4 shows the steady state open-circuit potentials (or corrosion potentials) of all the Alloy 22 samples (those shown in the previous figures plus the rest of the data in the input DTN: LL020711612251.017), as a function of chloride concentration. The figure shows that the sample geometry or configuration and the metallurgical condition have negligible effect on the long-term steady-state corrosion potential of Alloy 22. It is shown that the steady state corrosion potential decreases with chloride concentration, which is consistent with the fact that higher chloride concentration makes the metal more active. Also, part of the potential decrease with chloride concentration may be due to the ‘salting out effect’ because the dissolved oxygen decreases with increasing salt concentration.

As discussed later in the model analysis section, the steady-state corrosion potential is affected significantly by the solution pH.

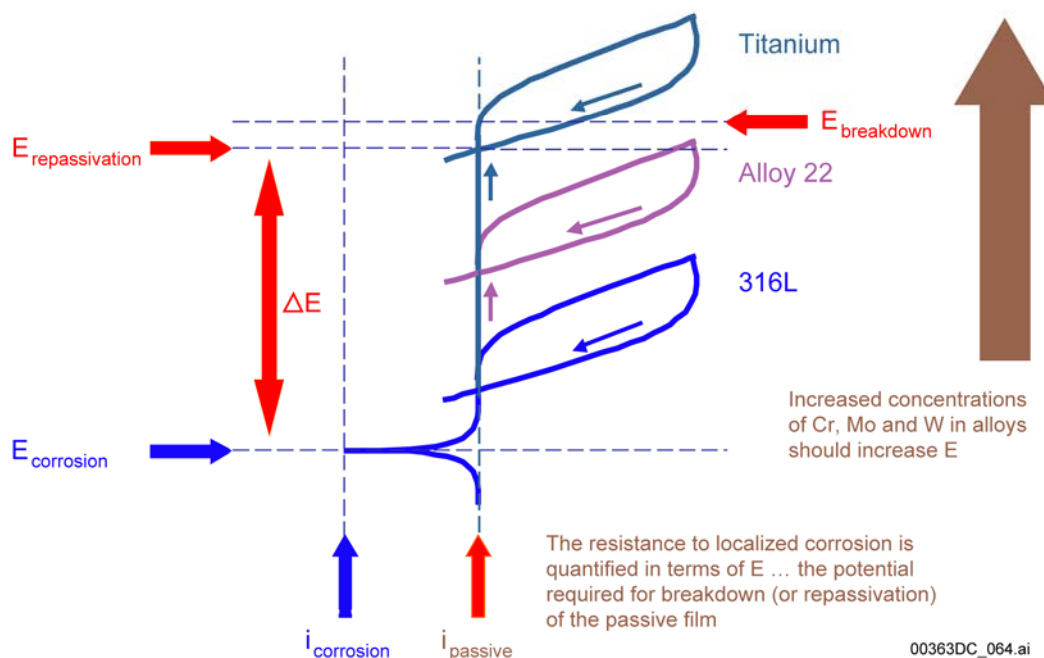


Source: DTN: SN0308T0506303.003.

Figure 6-4. Open-Circuit Corrosion Potential for Alloy 22, with Various Sample Configurations, Metallurgical Conditions, and Chloride Concentration, after Exposure for Extended Periods

6.3 CYCLIC POTENTIODYNAMIC POLARIZATION TECHNIQUES

Initial Approach—Cyclic potentiodynamic polarization has been used by the project for several years as a means of measuring the critical potential of the corrosion-resistant outer layer of waste package ($E_{critical}$), relative to the open-circuit corrosion potential (E_{corr}). Hypothetical cyclic potentiodynamic polarization curves for Type 316L stainless steel, Alloy 22, and titanium are shown in Figure 6-5 to illustrate the differences in the corrosion resistance of these materials. Cyclic potentiodynamic polarization measurements have been based on a procedure similar to ASTM G 5-94, with slight modification. For example, ASTM G 5-94 calls for an electrolyte of 1N H_2SO_4 , whereas SDW, SCW, SAW, SSW, BSW (all aerated) and near-saturation $CaCl_2$ solutions with various levels of nitrate (deaerated) are used here. Use of aerated solutions is also in contrast to the procedure that calls for de-aerated solutions. These choices were made to better replace the expected repository exposure conditions (aerated concentrated solutions). To illustrate the differences in the cyclic potentiodynamic polarization results for Alloy 22 and Type 316L stainless steel, the curves are categorized as Type 1, 2, or 3 (CRWMS M&O 2000a, Section 6.4.1).



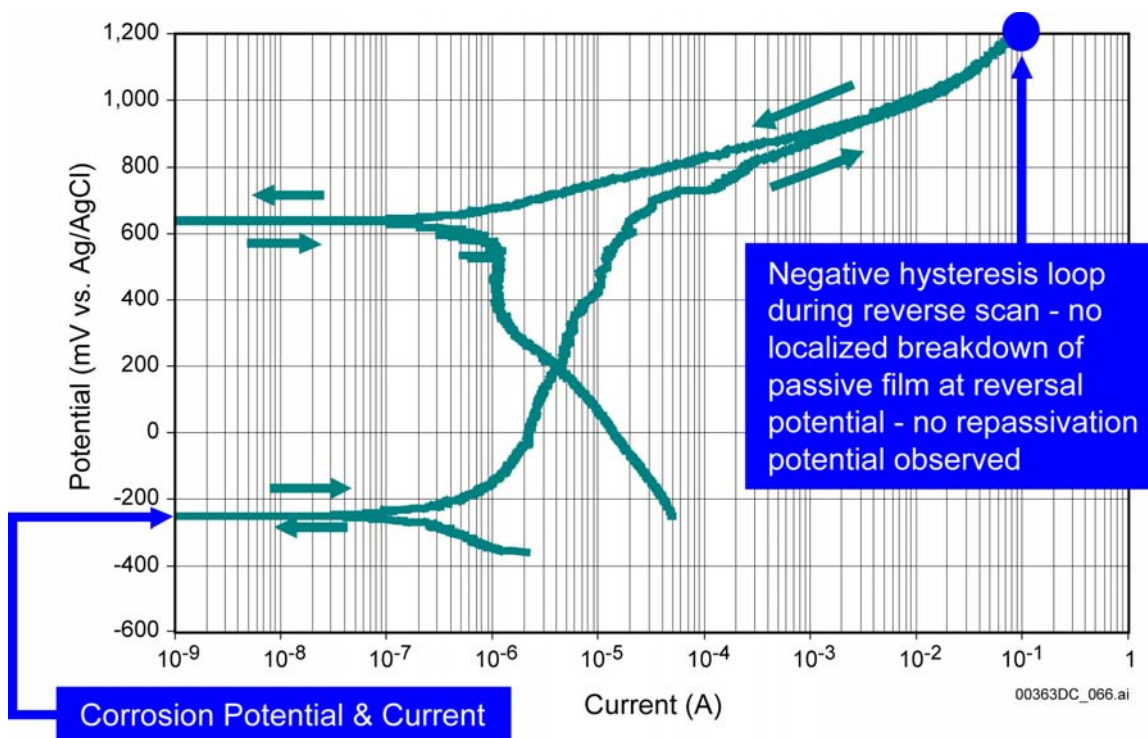
NOTE: The critical potential can be defined as either the breakdown potential, which corresponds to the onset of passive film destabilization, or the repassivation potential evident during the reverse scan.

Figure 6-5. Hypothetical Cyclic Potentiodynamic Polarization Curves for 316L, Alloy 22, and Titanium in High-Chloride Solutions

The initial approach selected threshold potentials for localized corrosion based on the three generic types of cyclic potentiodynamic polarization curves. The characteristics of each type are discussed below. The samples were noncreviced disc samples.

Type 1 Cyclic Potentiodynamic Polarization Curves—A generic Type 1 curve exhibits complete passivity (no passive film breakdown) between the open-circuit corrosion potential and the breakdown potential, or the potential where oxygen evolution begins if no breakdown is

observed (CRWMS M&O 2000a). Type 1 behavior, shown in Figure 6-6, is observed for Alloy 22 in the standardized SSW test medium near its ambient-pressure boiling point of approximately 120°C. This saturated sodium-potassium-chloride-nitrate electrolyte was formulated to represent the type of concentrated electrolyte that might evolve on a hot waste package surface. It is evident from Figure 6-6 that Alloy 22 maintains passivity at potentials up to the reversal potential (1,200 mV versus Ag/AgCl), even under these relatively aggressive conditions.



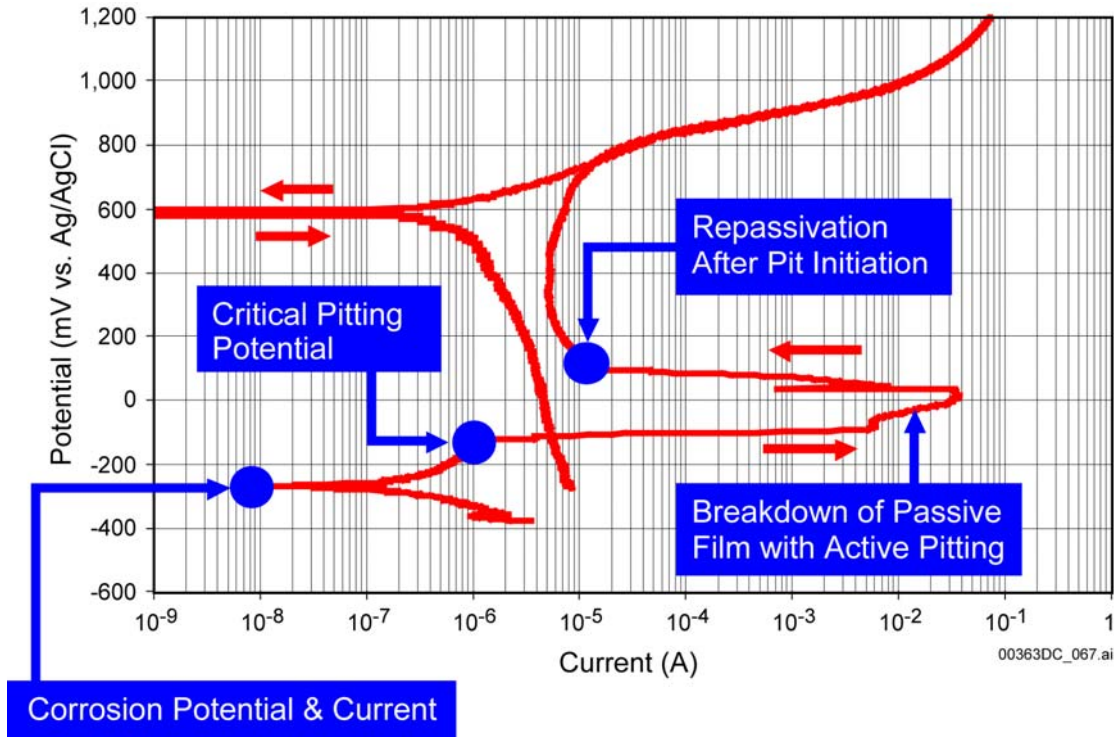
Source: CRWMS M&O 2000a, Figure 3.

NOTE: Data for Alloy 22 in SSW at 120°C show no loss of passivity, even with a voltage reversal of 1,200 mV versus Ag/AgCl, and exhibit Type 1 behavior (nonreviced disc sample).

Figure 6-6. Cyclic Potentiodynamic Polarization Data for Alloy 22 in Simulated Saturated Water at 120°C

Type 2 Cyclic Potentiodynamic Polarization Curves—A generic Type 2 curve (e.g., Section 7, Figure 7-5) exhibits a well-defined oxidation peak between the open-circuit corrosion potential and the breakdown potential, or the potential where oxygen evolution begins if no breakdown is observed (CRWMS M&O 2000a). The anodic oxidation peak (process) is due to the conversion of metals in the passive film to higher, perhaps more soluble, oxidation states. This oxidation process is accompanied by changes in X-ray photoelectron spectroscopy and surface morphology, both of which have been well documented (BSC 2003b, Section 6.4.1).

Type 3 Cyclic Potentiodynamic Polarization Curves—A generic Type 3 curve exhibits a complete breakdown of the passive film and active pitting at potentials relatively close to the open-circuit corrosion potential. The critical pitting potential is evident in Figure 6-7. Type 3 behavior has only been observed with Type 316L stainless steel.



Source: CRWMS M&O 2000a, Figure 8.

NOTE: Data show pitting potential very close to the open-circuit corrosion potential and exhibit Type 3 behavior.

Figure 6-7. Cyclic Potentiodynamic Polarization Data for Type 316L Stainless Steel in Simulated Saturated Water at 120°C (Noncreviced Disc Sample)

The initial approach to evaluate localized corrosion behavior utilized primarily uncreviced specimens with most testing performed in the initially defined set of relevant environments. Subsequent testing indicated these initial test environments were relatively benign (not conducive to initiation of localized corrosion). More recent environmental modeling and experimental assessments have expanded the full range of potential brine environments that could potentially contact the waste package over time resulting in the need to expand the test program to cover the full range of credible environments using creviced specimen configurations.

6.4 CURRENT APPROACH TO MODELING LOCALIZED CORROSION

Currently, three methodologies are used for the interpretation of experimental data for critical potential (threshold potential), and are summarized as follows. Method A identifies the potential where the passive film is breached during the forward (anodic) potential scan. The loss of passivity is indicated by a sudden increase in the measured current density. However, in corrosion-resistant materials, such as Alloy 22, it is not always possible to locate the potential at which there is a sudden increase in current density. As a result, the current density corresponding to loss of passivity is assumed to be $20 \mu\text{A}/\text{cm}^2$. The breakdown potential may be the best estimate of the true critical potential, since it corresponds to the onset of passive film destabilization. Methods B and C identify the potential where the passive film reforms during

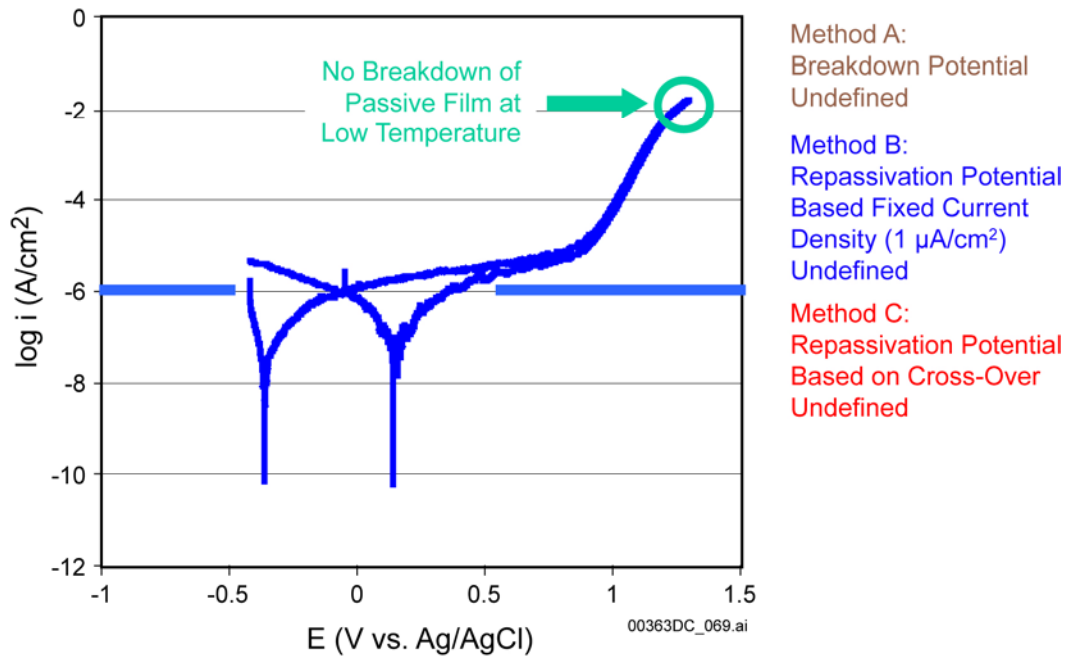
the negative (cathodic) potential scan. Repassivation is indicated by a sudden decrease in the measured current density, to levels indicative of an intact passive film. Again, because of the difficulty in identifying the potential at which the significant decrease in current density occurs, $1 \mu\text{A}/\text{cm}^2$ is assumed in Method B.

- Method A—Initial Breakdown of Passive Film
 - Critical Potential (E_{crit}) = Breakdown Potential (E20)
 - Based on Threshold Current Density of $20 \mu\text{A}/\text{cm}^2$
- Method B—Repassivation of Surface
 - Critical Potential (E_{crit}) = Repassivation Potential (ER1)
 - Based on Threshold Current Density of $1 \mu\text{A}/\text{cm}^2$
- Method C—Repassivation of Surface
 - Critical Potential (E_{crit}) = Repassivation Potential (ERP)
 - Intersection of Forward Scan with Hysteresis Loop (Cross-Over Point).

Cyclic potentiodynamic polarization curves are shown for Alloy 22 multiple crevice assembly samples in 5 M CaCl_2 without nitrate in Figures 6-8 through 6-10, for temperatures ranging from 45°C to 120°C . The samples tested were multiple crevice assembly samples. Since there is no breakdown of the passive film at 45°C , the breakdown and repassivation potentials cannot be determined. However, there are well-defined breakdown and repassivation potentials at 90°C and 120°C , with a large potential margin (ΔE) evident using the initial approach. The repassivation potentials at 90°C and 120°C can be determined with either Methods B or C (similar results are obtained in both cases). The small ennoblement of Alloy 22 in 5 M CaCl_2 without nitrate is shown in Figure 6-11. After 18 months, the open-circuit corrosion potential slightly increased to a steady-state value of approximately -150 to -125 mV versus Ag/AgCl. The critical potentials determined by Method C, which are based upon the crossover point, is shown in Figure 6-12. These data indicate that the criterion for crevice corrosion in pure, concentrated CaCl_2 will probably be met at temperatures above approximately 70°C , which is the apparent threshold temperature for crevice corrosion in the absence of nitrate inhibitor. However, it is noted that significant levels of nitrate will probably be present, even in the most aggressive CaCl_2 -type brines that could be evolved from seepage.

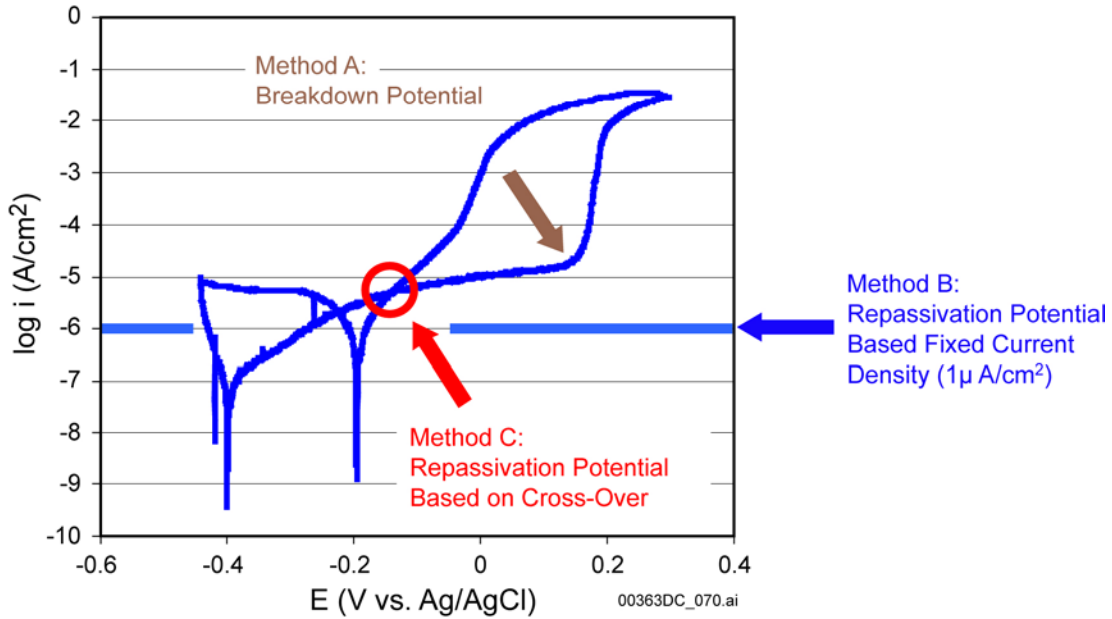
Cyclic potentiodynamic polarization curves are shown for Alloy 22 multiple crevice assembly samples in 5 M CaCl_2 with nitrate inhibitor ($[\text{NO}_3^-]/[\text{Cl}^-]$ about 0.1) at 90°C and 130°C are shown in Figures 6-13 and 6-14. There are well-defined breakdown and repassivation potentials at these temperatures, and a large potential margin (ΔE) at both temperatures. As previously discussed, repassivation potentials can be determined with either Methods B or C. Both methods yield similar results. The ennoblement of Alloy 22 in 5 M CaCl_2 with nitrate is shown in Figure 6-15. After 12 months, the open-circuit corrosion potential increased to a steady-state value of approximately 0 to 200 mV versus Ag/AgCl for base metal, and approximately 200 to 300 mV versus Ag/AgCl for weld metal. As shown in Figures 6-16 and 6-17, this indicates that the criterion for crevice corrosion may be met at temperatures above about 90°C for base metal and at a slightly lower temperature for the weld metal.

From these data, we conclude that localized corrosion of Alloy 22 may occur in pure, concentrated, aqueous-phase CaCl_2 electrolytes at temperatures below the boiling point of approximately 100°C (below which seepage is possible), and above the apparent threshold temperature for crevice corrosion of approximately 70°C (above which crevice corrosion is possible).



Source: DTNs: LL030400112251.043, LL030406212251.044.

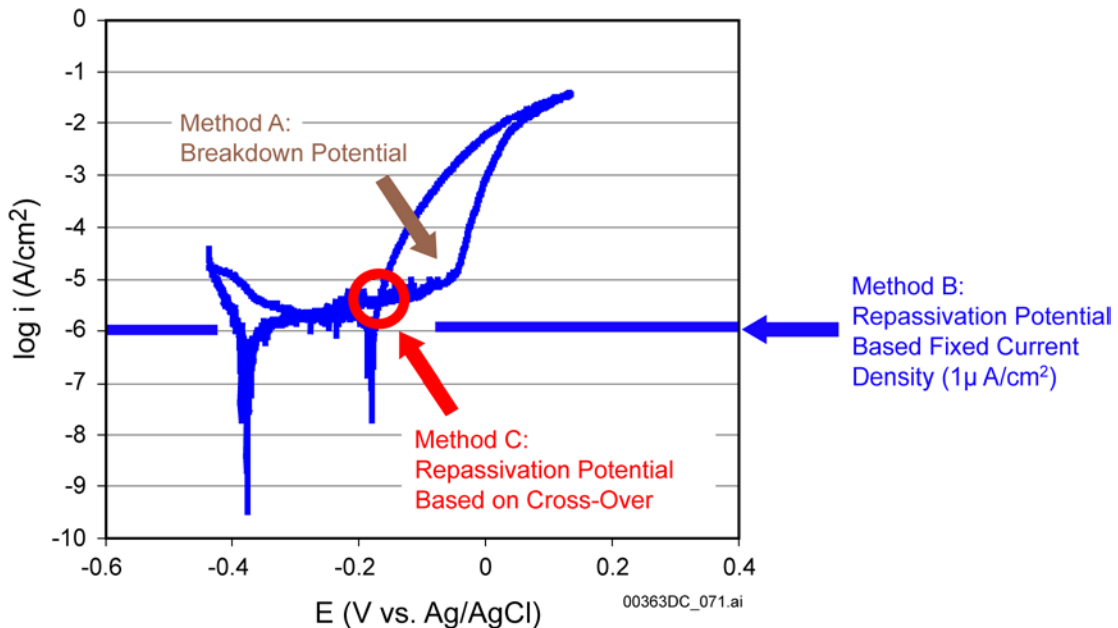
Figure 6-8. Cyclic Potentiodynamic Polarization Data for Creviced Alloy 22 (DEA 3229) in 5 M CaCl_2 Brine at 45°C without NO_3^- Inhibitor



Source: DTNs: LL030400112251.043, LL030406212251.044.

NOTE: E_{crit} approximately 200 mV for Method A; -180 mV for Method B; -150 mV for Method C.

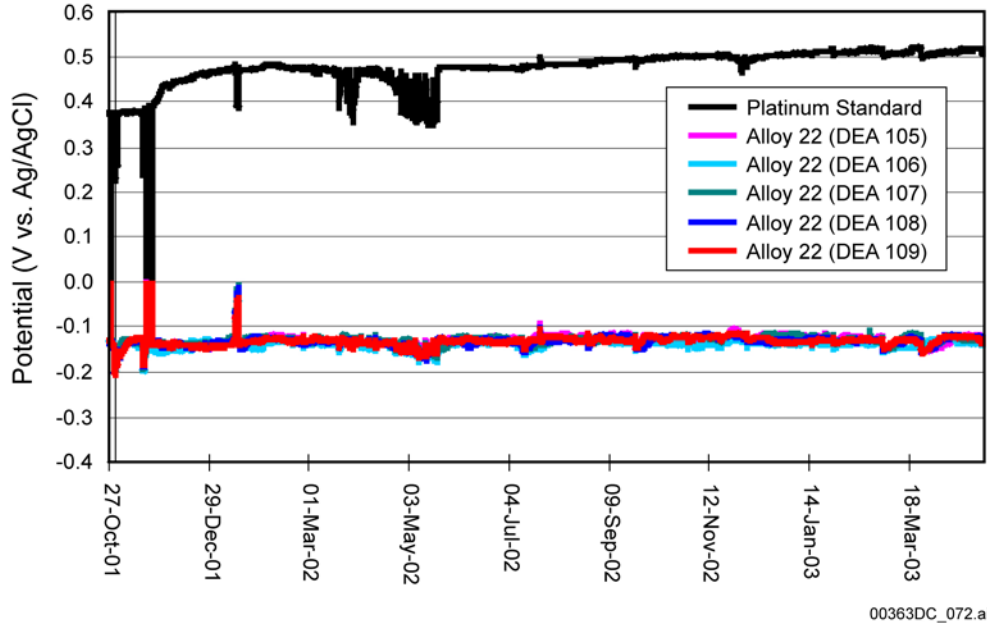
Figure 6-9. Cyclic Potentiodynamic Polarization Data for Creviced Alloy 22 (DEA 3219) in 5 M CaCl₂ Brine at 90°C without NO₃⁻ Inhibitor



Source: DTNs: LL030400112251.043, LL030406212251.044; Farmer 2003, Slide 30.

NOTE: E_{crit} approximately -50 mV for Method A; -180 mV for Method B; -150 mV for Method C.

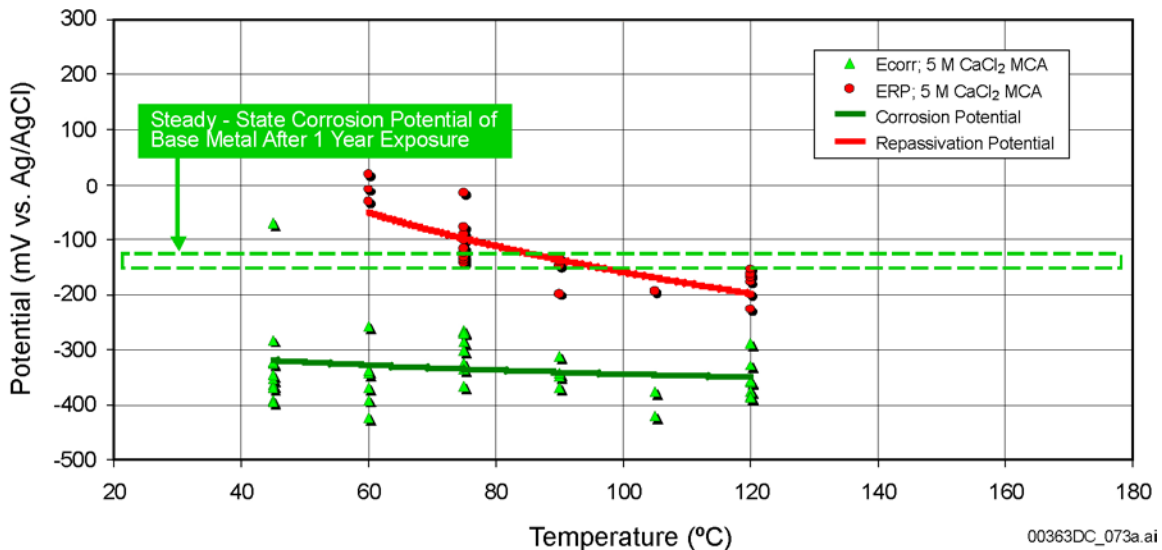
Figure 6-10. Cyclic Potentiodynamic Polarization Data for Creviced Alloy 22 (DEA 3236) in 5 M CaCl₂ Brine at 120°C without NO₃⁻ Inhibitor



Source: Farmer 2003, Slide 32; Estill et al. 2003.

NOTE: Some of these data are repeated in Figure 6-3 but with lower resolution (fewer data points per unit time) and for a shorter period.

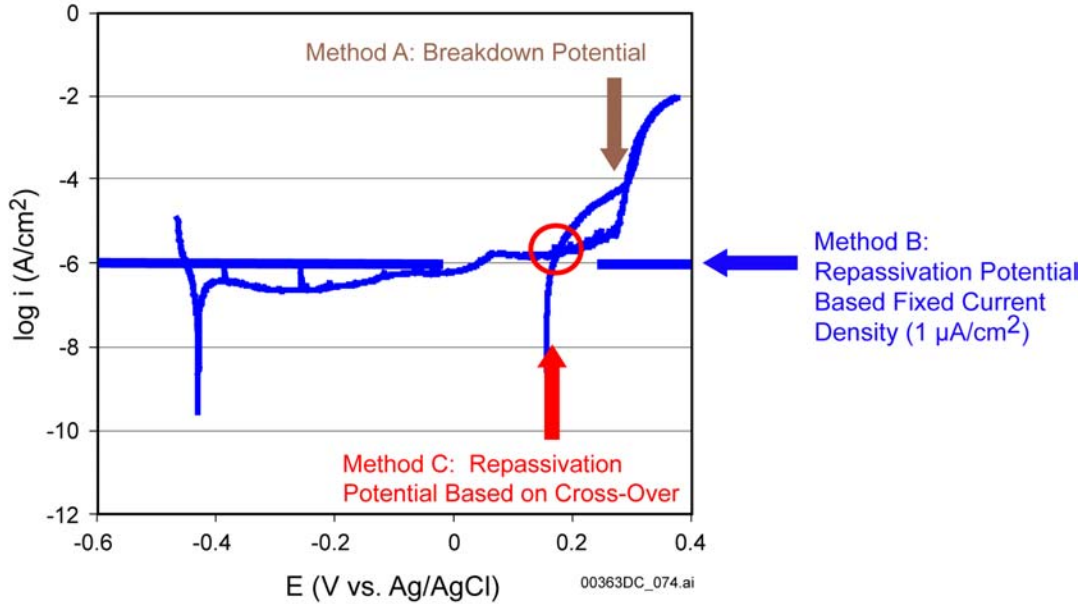
Figure 6-11. Effect of Long-Term Exposure on the Open-Circuit Corrosion Potential of Alloy 22 in High-Temperature CaCl₂ Brine



Source: Farmer 2003, Slide 35; DTN: LL030409512251.051.

NOTE: “Dry Waste Package Surface” applies to seepage conditions. These data were analyzed by Method C, which uses the cross over point to establish the repassivation potential. The dashed box represents a steady-state E_{corr} (▲ short-term (24-hr) E_{corr} measurements). E_{corr} steady state value was measured only at 120°C (from Figure 6-11).

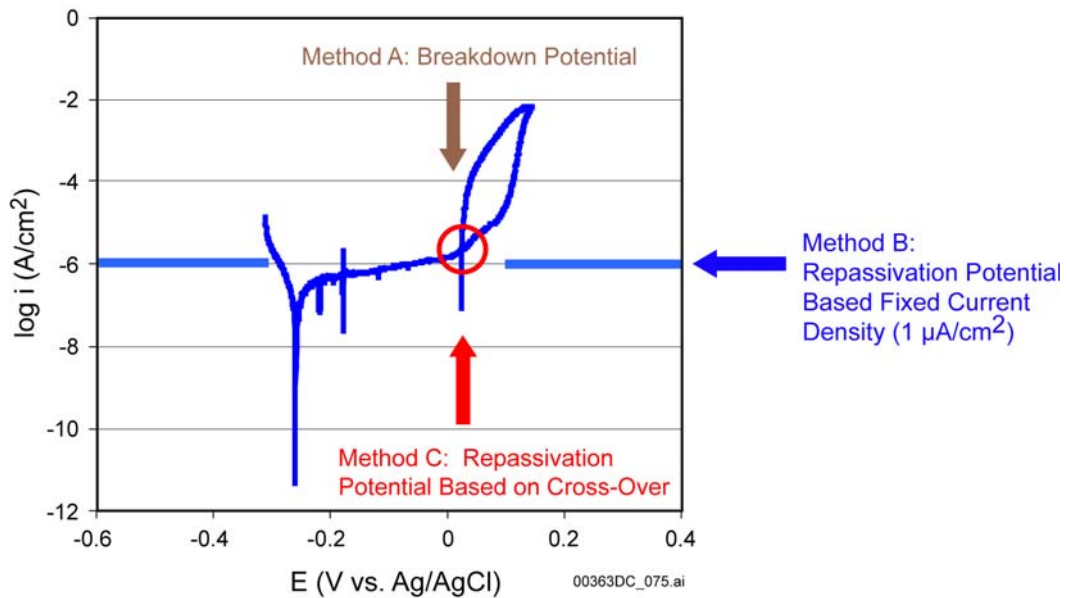
Figure 6-12. Critical Potentials of Creviced Alloy 22 Samples in CaCl₂ Brines, without NO₃⁻ Inhibitor, and at Temperatures Ranging from 45°C to 120°C



Source: DTN: LL030409812251.054; Farmer 2003, Slide 33.

NOTE: E_{crit} approximately 250 mV for Method A; 180 mV for Method B; 190 mV for Method C.

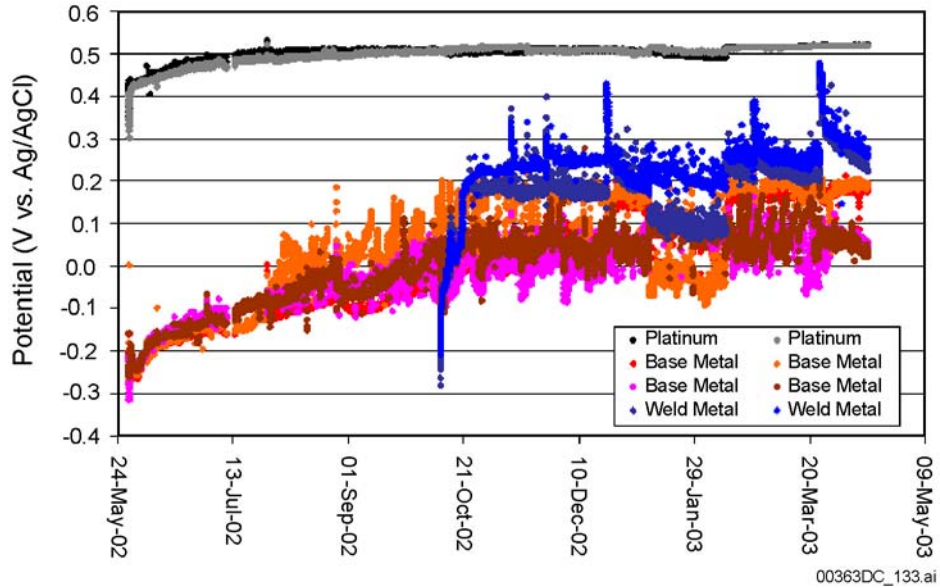
Figure 6-13. Cyclic Potentiodynamic Polarization Data for Creviced Alloy 22 (DEA 3102) in 5 M CaCl₂ Brine at 90°C with NO₃⁻ Inhibitor



Source: DTNs: LL030406212251.044, LL030409812251.054; Farmer 2003, Slide 34.

NOTE: E_{crit} approximately 150 mV for Method A; 50 mV for Method B; 50 mV for Method C.

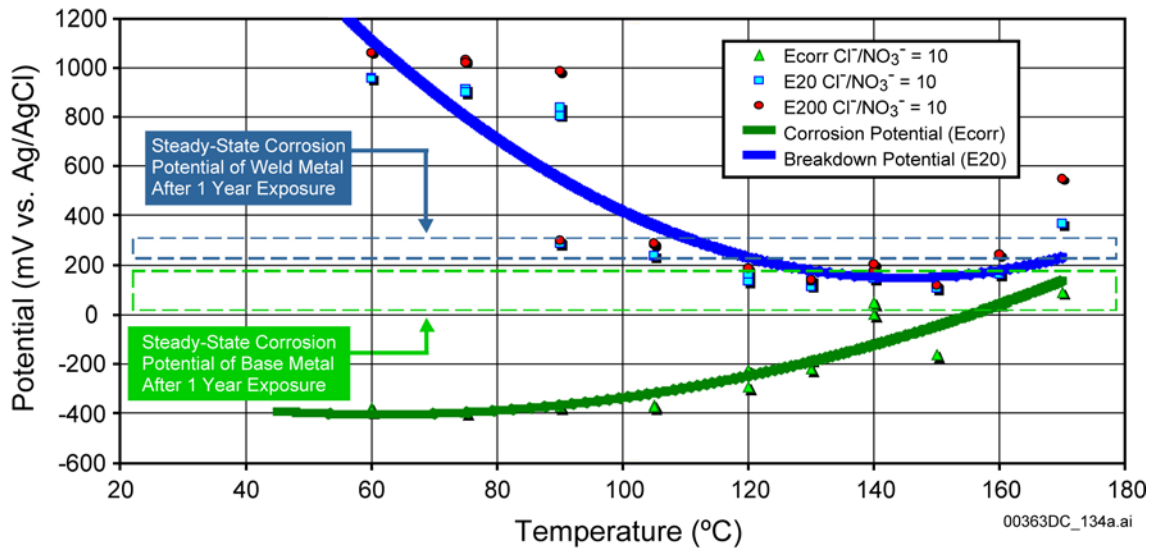
Figure 6-14. Cyclic Potentiodynamic Polarization Data for Creviced Alloy 22 (DEA 3127) in 7 M CaCl₂ Brine at 130°C with NO₃⁻ Inhibitor



Source: Estill et al. 2003.

NOTE: These data are repeated in Figure 6-3 but with lower resolution (fewer data points per unit time) and for a shorter period.

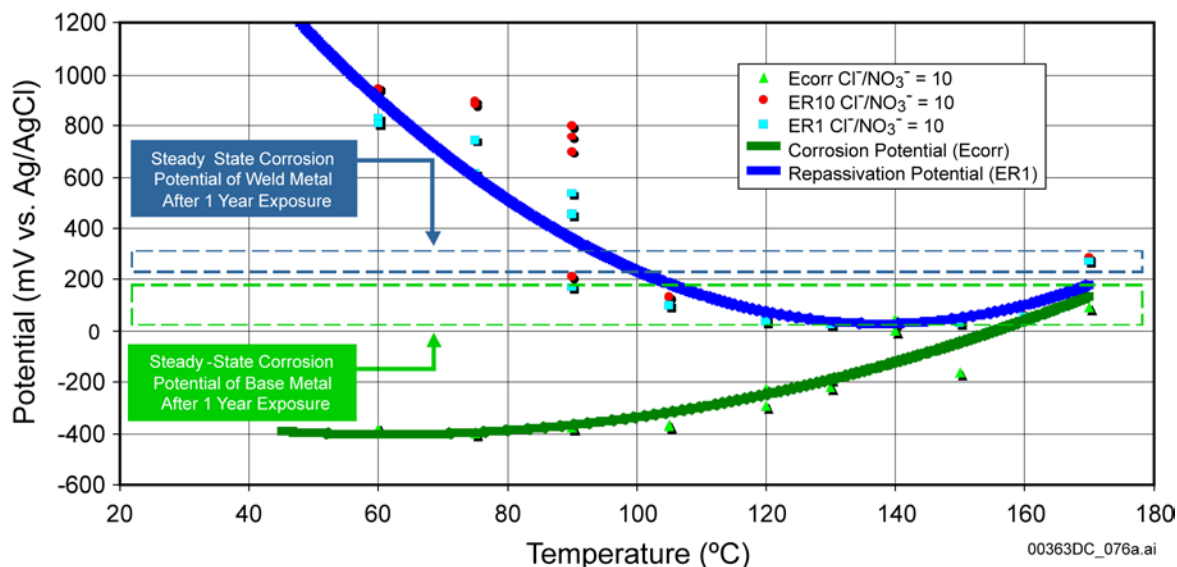
Figure 6-15. Effect of Long-Term Exposure on the Open-Circuit Corrosion Potential of Alloy 22 in High-Temperature CaCl₂ Brine with Nitrate Inhibitor



Source: Farmer 2003, Slide 35; DTN: LL030409512251.051.

NOTE: Short-term (24-hour) E_{corr} measurements. Steady-state E_{corr} values are for one temperature only (Figure 6-15).

Figure 6-16. Critical Potentials of Creviced Alloy 22 Samples in CaCl₂ Brines, with NO₃⁻ Inhibitor, and at Temperatures Ranging from 60°C to 170°C



Source: Farmer 2003, Slide 36; DTN: LL030409512251.051.

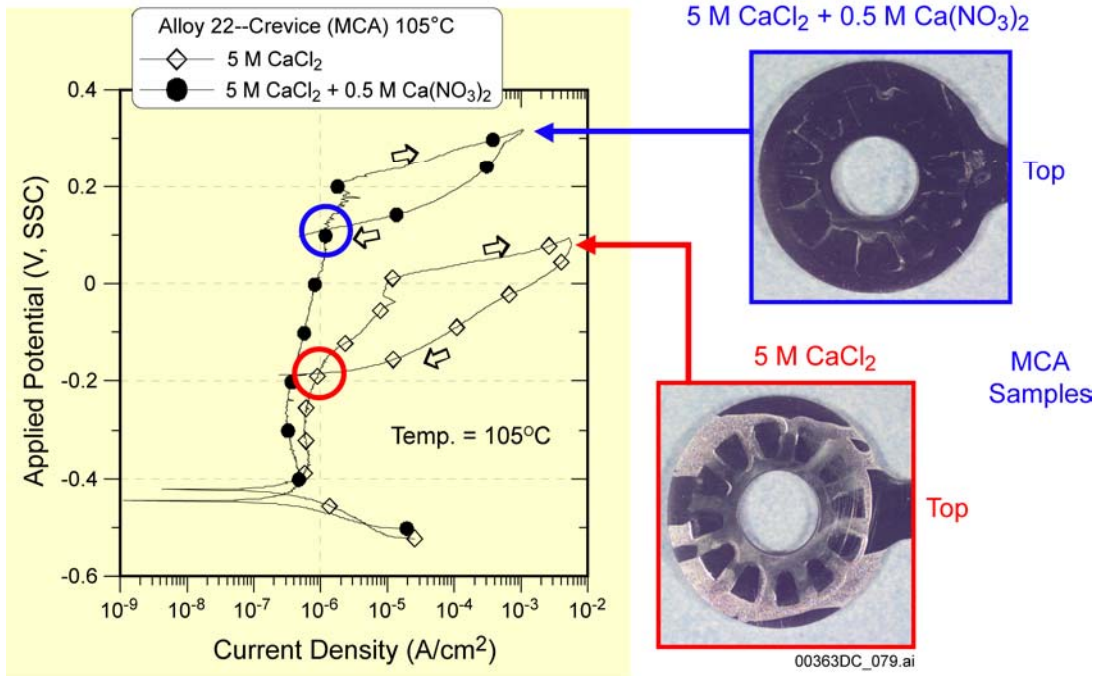
NOTE: These data were analyzed by Method B, which is a determination of the repassivation potential. The dashed boxes represent a range of temperature. Steady-state E_{corr} values are for one temperature only (Figure 6-15).

Figure 6-17. Critical Potentials of Creviced Alloy 22 Samples in CaCl_2 Brines, with NO_3^- Inhibitor, and at Temperatures Ranging from 60°C to 170°C

The strong inhibitory effect of nitrate anion is demonstrated by Figures 6-18 and 6-19. First, consider the shifts in critical potential evident in cyclic potentiodynamic polarization curves. The localized corrosion during cyclic potentiodynamic polarization of Alloy 22 multiple crevice assembly in 5 M CaCl_2 brine at 105°C, with and without inhibition by NO_3^- anion, is shown in Figure 6-18. At a temperature of 105°C, the addition of nitrate ($[\text{NO}_3^-]/[\text{Cl}^-]$ approximately 0.1) shifts the breakdown potential (Method A) by approximately 200 mV, and the repassivation potential (Method C) by approximately 300 mV. The localized corrosion during cyclic potentiodynamic polarization of Alloy 22 disk in 9 M CaCl_2 brine at 150°C, with and without inhibition by NO_3^- anion, is shown in Figure 6-19. At a temperature of 150°C, the addition of nitrate ($[\text{NO}_3^-]/[\text{Cl}^-]$ approximately 0.1) shifts the breakdown potential (Method A) by approximately 200 mV, and the repassivation potential (Method C) by approximately 250 mV.

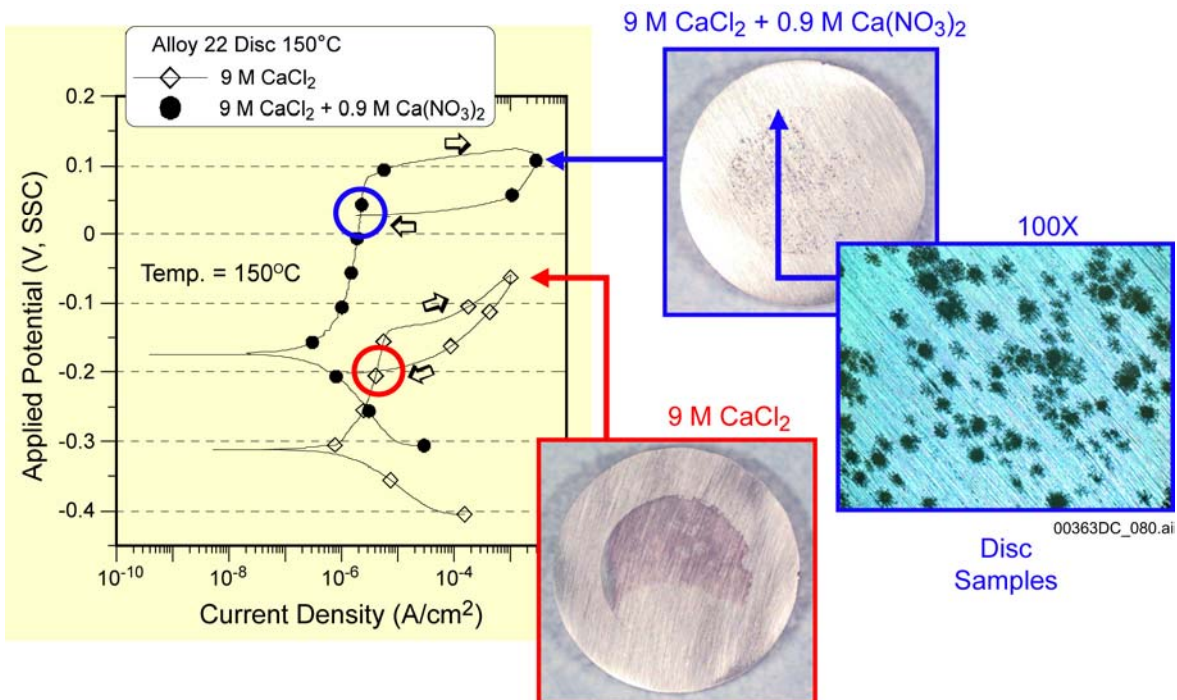
Since CaCl_2 type brines are expected only from seepage waters, they will not be present above about 100°C (i.e., above the boiling point of seepage waters). However, dust leachate derived brines can be present up to 140°C.

Localized corrosion of Alloy 22 has been observed only under polarization conditions.



Source: Farmer 2003, Slide 37; Evans et al. 2003; DTN: LL030409812251.054.

Figure 6-18. Localized Corrosion during Cyclic Potentiodynamic Polarization of Alloy 22 Multiple Crevice Assembly in 5 M CaCl₂ Brine at 105°C, with and without Inhibition by NO₃⁻ Anion



Source: DTN: LL030409812251.054; Farmer 2003, Slide 38.

Figure 6-19. Localized Corrosion during Cyclic Potentiodynamic Polarization of Alloy 22 Disk in 9 M CaCl₂ Brine at 150°C, with and without Inhibition by NO₃⁻ Anion (Specimens DEA 596 and DEA 597)

6.5 LOCALIZED CORROSION INITIATION MODEL

The localized corrosion model for the Alloy 22 waste package outer shell has two components: the initiation model, and the propagation model. The initiation model assumes that localized corrosion of the waste package outer shell occurs when the steady-state corrosion potential, E_{corr} , is equal to or greater than the critical potential, $E_{critical}$. This is expressed mathematically as: $\Delta E \leq 0$ where $\Delta E = E_{critical} - E_{corr}$. The critical potential, $E_{critical}$, is defined as the crevice repassivation potential, E_{rcrev} , the potential at which the Alloy 22 surface undergoes spontaneous repassivation. All potentials are expressed in the units of mV, relative to the standard Ag/AgCl reference electrode (also referred to as SSC). The details of the model are presented in (BSC 2003b, Section 6.4). A summary of the model is described below.

The crevice repassivation potential, E_{rcrev} , is defined in terms of the crevice repassivation potential in the absence of inhibitive nitrate ions, and the change in crevice repassivation potential due to inhibiting nitrate anion, E_{rcrev}^o and $\Delta E_{rcrev}^{NO_3^-}$, respectively, by Equation 6-2.

$$E_{rcrev} = E_{rcrev}^o + \Delta E_{rcrev}^{NO_3^-} \quad (\text{Eq. 6-2})$$

The crevice repassivation potential in the absence of inhibitive nitrate ions, E_{rcrev}^o , is predicted with Equation 6-3.

$$E_{rcrev}^o = a_o + a_1T + a_2pH + a_3 \log([Cl^-]) + a_4T \times \log([Cl^-]) \quad (\text{Eq. 6-3})$$

The adjustable model parameters in this equation are a_o , a_1 , a_2 , a_3 , and a_4 ; the temperature is represented by T , given in the units of °C, and the chloride concentration is represented by Cl^- , given in the units of moles per kilogram of water (molal). The effect of nitrate on the crevice repassivation potential is accounted for with Equation 6-4.

$$\Delta E_{rcrev}^{NO_3^-} = b_o + b_1[NO_3^-] + b_2 \frac{[NO_3^-]}{[Cl^-]} \quad (\text{Eq. 6-4})$$

The adjustable model parameters in this equation are b_o , b_1 and b_2 ; the nitrate concentration is represented by NO_3^- , given in the units of moles per kilogram of water (molal); and the nitrate-to-chloride ratio is represented by NO_3^-/Cl^- , and limited to unity (1.0) by the available data set. This correlation accounts for the competing effects of the aggressive chloride anion and the inhibiting nitrate anion through the nitrate-to-chloride ratio.

An empirical model for the long-term steady-state corrosion potential of the Alloy 22 waste package outer shell has been developed, and is applicable over a broad range of exposure conditions related to the repository. This model is expressed as follows:

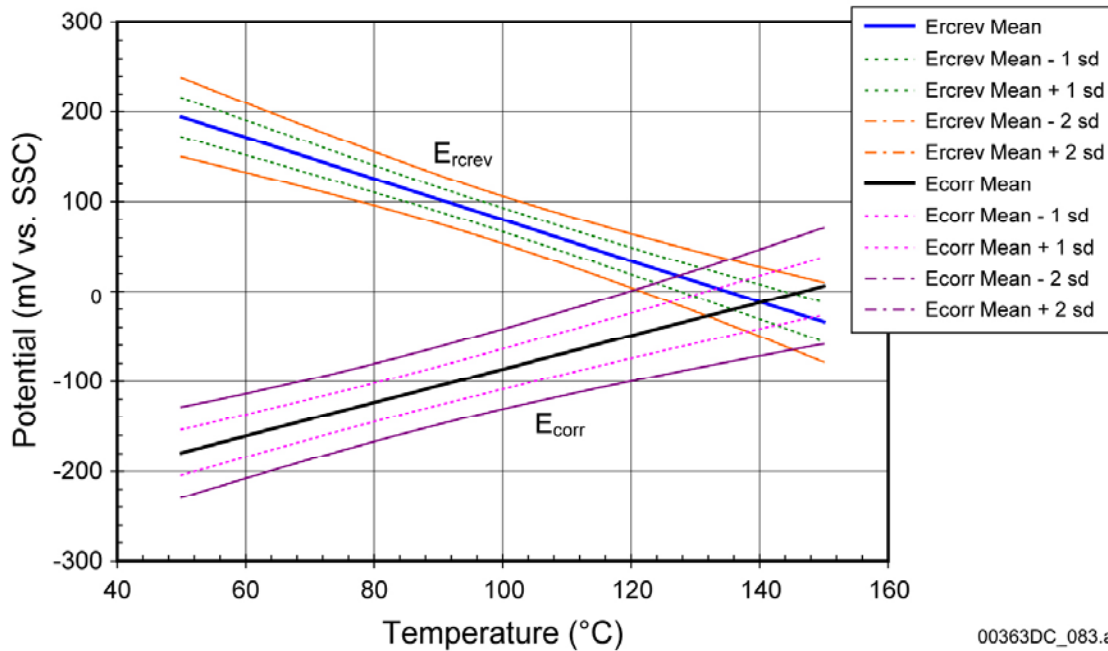
$$E_{corr} = c_o + c_1T + c_2pH + c_3[Cl^-] + c_4 \log\left(\frac{[NO_3^-]}{[Cl^-]}\right) \quad (\text{Eq. 6-5})$$

The predicted value of E_{corr} is expressed in the units of mV, relative to the standard Ag/AgCl reference electrode; adjustable model parameters are c_0 , c_1 , c_2 , c_3 , and c_4 and were determined by fitting Equation 6-5 to the long-term corrosion potential data.

As seen from the dependence of the corrosion potential on the logarithm of the nitrate-to-chloride concentration ratio, the model requires the nitrate concentration be greater than 0. Therefore, for a condition with no nitrate ion present, a small value (such as 0.001 m) can be used for the nitrate ion concentration.

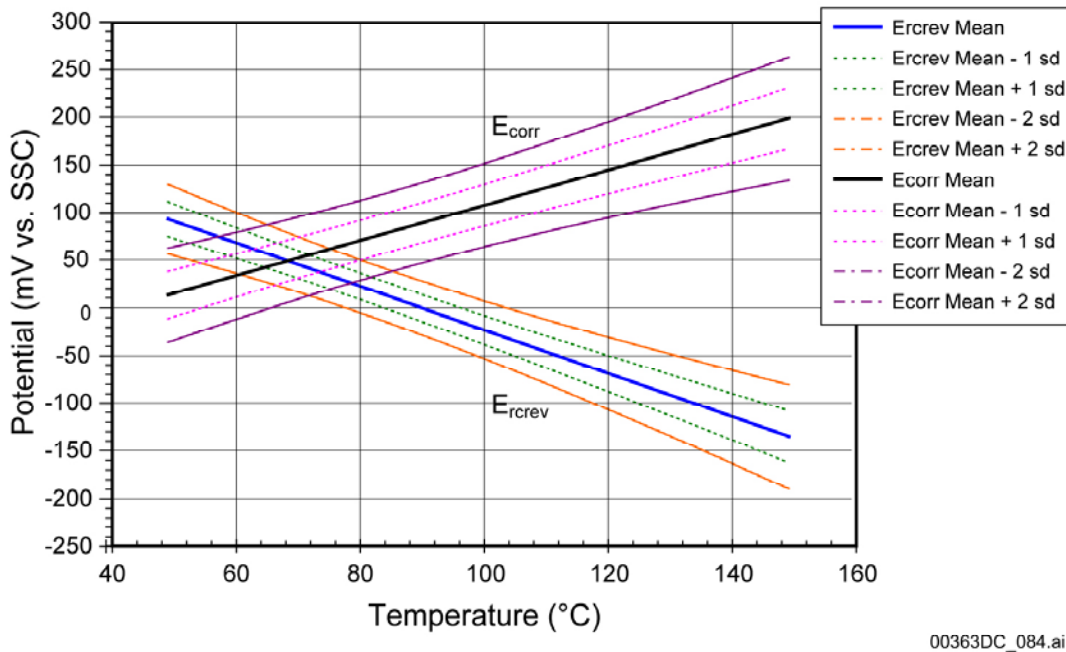
Because only nitrate ions are accounted for in the crevice corrosion initiation model for the inhibitive effect, the model results for solutions with significant amounts of other potentially inhibitive ions such as carbonate and sulfate (in addition to nitrate ions) are believed to be conservative. The model results for the beneficial effects of the inhibitive nitrate anion, combined with the alkaline pH conditions of the typical carbonate waters in the repository, are consistent with the experimental observations of no localized corrosion susceptibility of Alloy 22 in similar waters.

The localized corrosion model for the Alloy 22 waste package outer shell predicts a minimum threshold temperature for crevice corrosion of approximately 120°C in 10-molal chloride solutions with 1-molal nitrate additions ($NO_3^-/Cl^- = 0.1$), at near-neutral pH (pH approximately 7). The mean threshold temperature is predicted to be approximately 140°C. Values of the threshold temperature are determined from the intersection of the E_{corr} versus T regression curve(s) with the E_{rcrev} versus T regression curve(s), as shown in Figure 6-20 (BSC 2003b, Figure 6-44). At lower pH, the threshold temperature for crevice corrosion is predicted to be lower. For example, the localized corrosion model predicts a minimum threshold temperature of approximately 50°C in 10-molal chloride solutions with 1-molal nitrate additions ($NO_3^-/Cl^- = 0.1$), at mildly acidic conditions (pH approximately 3), as shown in Figure 6-21. While such mildly acidic conditions can develop inside crevices, it must be emphasized that the empirical localized corrosion model is highly conservative since hot acidified chloride-dominant brines are not expected to form on the waste package surfaces from the dust leachate that could be present under the drip shield. Also, the beneficial effects of other dominant anions, such as carbonate, bicarbonate, and sulfate, are not accounted for. Furthermore, after 5-year exposures of Alloy 22 crevice samples in SAW (target pH approximately 2.7) at the LTCTF, no crevice attack has been observed. This is consistent with the predictions of the empirical model when actual measured pH, chloride, and nitrate values are used (BSC 2003b, Table 7-2).



Source: DTN: SN0308T0506303.003.

Figure 6-20. Model Results for Crevice Corrosion Susceptibility of the Waste Package Outer Shell as a Function of Temperature for 10 M Chloride, pH 7, and 1 M Nitrate (NO_3/Cl ratio = 0.1)



Source: DTN: SN0308T0506303.003.

Figure 6-21. Model Results for Crevice Corrosion Susceptibility of the Waste Package Outer Shell as a Function of Temperature for 10 M Chloride, pH 3, and 1 M Nitrate (NO_3/Cl ratio = 0.1)

6.6 CONSERVATISM IN THE LOCALIZED CORROSION MODEL FOR THE WASTE PACKAGE OUTER SHELL

The localized corrosion model is very conservative, as mentioned previously. Some of the areas of conservatism are addressed in the following sections.

Conservatism in the Critical Potential for Crevice Corrosion Initiation—The crevice repassivation potentials from the short-term cyclic potentiodynamic polarization tests are a highly conservative measure for the critical potential for localized corrosion initiation of the waste package outer shell. The approach conservatively does not take credit for the fundamental aspects of the localized corrosion processes: localized corrosion initiation (i.e., initial local passive film breakdown), stabilization, and propagation. A more realistic representation of the localized corrosion initiation would be the use of the passive film breakdown potentials (obtained from the forward scan curves of the cyclic potentiodynamic polarization test), coupled with the stabilization and propagation processes of localized corrosion. The more realistic measure of the critical potentials can be obtained using a modified potentiostatic polarization technique (also referred to as a potential step technique). In this technique, (currently underway) the sample is potentiostatically held at a potential and monitored for the corrosion current changes with time.

In addition, discontinuous tortuous thin water films are expected to form on the waste package surface in the nominal-case postclosure repository. The fully immersed condition used to measure the crevice repassivation potentials in the current investigation is considered conservative because, for the same water chemistry, a fully immersed condition is generally more aggressive than a thin water film condition. Kinetics of the cathodic reactions involved in localized corrosion under discontinuous tortuous thin water films is expected to be slower than a fully immersed condition. Such reduced cathodic reaction kinetics are likely to constrain the corresponding anodic reactions at the crevice corrosion site and to limit stabilization of crevice corrosion and slow down the propagation rate. In addition, beneficial effects of other anions (such as carbonates, bicarbonates, and sulfates) are not accounted for in this model. More details concerning conservatism in the critical potential for crevice corrosion initiation are discussed in *General Corrosion and Localized Corrosion of Waste Package Outer Barrier* (BSC 2003b, Section 5).

6.7 LOCALIZED CORROSION PENETRATION RATE MODEL

If the corrosion potential of the waste package outer shell exceeds the critical potential, the waste package outer shell is assumed to be subject to localized corrosion, and penetration of the shell by localized corrosion is modeled. Very little data exist for such localized corrosion under the conditions expected in the repository. Work originally published by Haynes International (1997, p. 8) and later reviewed by Gdowski (1991, Table 22) indicates that the corrosion rate of Alloy 22 in 10 weight percent FeCl_3 at 75°C might be as high as $12.7 \mu\text{m}/\text{yr}$. This rate is significantly higher than those measured by weight loss of the crevice specimens in the LTCTF and may be representative of the types of rates expected for localized corrosion, including crevice corrosion. In a solution composed of 7 volume percent H_2SO_4 , 3 volume percent HCl , 1 weight percent FeCl_3 , and 1 weight percent CuCl_2 , a penetration rate of $610 \mu\text{m}/\text{yr}$ was observed at 102°C . The corrosion rate of Alloy C-276 in dilute HCl at the boiling point is

somewhere between 5 and 50 mils/yr (127 and 1,270 $\mu\text{m}/\text{yr}$) (Sedriks 1996, Figure 9.12; Haynes International 1997, p. 13). Comparable rates would be expected for Alloy 22.

Reasonable Bounds for Rates—The localized corrosion penetration rates for the waste package outer shell were assumed to range from 12.7 to 1,270 $\mu\text{m}/\text{yr}$ with the median value of 127 $\mu\text{m}/\text{yr}$, as shown in Table 6-1. A log-uniform distribution between the bounds was assumed for the penetration rate. The basis for this assumption is that the penetration rate values from the literature span three orders of magnitude, and the percentiles provided are consistent with a log-uniform distribution. This distribution is based on data that bounds those extreme penetration rates found in the literature and are a highly conservative representation of localized corrosion rates of Alloy 22 for the exposure conditions expected in the postclosure repository. The entire variance in the penetration rate is assumed to be due to uncertainty. However, although localized corrosion can be conservatively bounded by this distribution, the expected case is that once initiated, the crevice corrosion propagation rate would be expected to decrease with increasing depth if it were to initiate under realistic environmental conditions.

Table 6-1. Bounding Rates for Localized Corrosion for Alloy 22 (Distribution)

Percentile	Localized Corrosion Rate ($\mu\text{m}/\text{yr}$)
0th	12.7
50th	127
100th	1,270

Source: DTN: SN0308T0506303.003.

Time-Dependent Growth Law for Localized Corrosion—The base case model assumes that, when localized corrosion of the waste package outer shell occurs, it propagates at a (time-independent) constant rate. This assumption is highly conservative because it is known that the localized corrosion rate decreases with time and this is particularly more likely under a thin water film condition that is expected to form on the waste package surface in the postclosure repository. Also, in general, localized corrosion tends to arrest or die shortly after initiation.

An alternative conceptual model for the localized corrosion penetration is a time-dependent growth law. The growth law model can be developed based on a combination of electrochemical and corrosion exposure measurements. A simple pitting model based on hemispherical pit growth yields a penetration law of the form (CRWMS M&O 1998, Table 3-2; Hunkeler and Boehni 1983; McGuire et al. 1998, Section 5.3.1)

$$D = k \cdot t^n \quad (\text{Eq. 6-6})$$

where D is the depth of penetration, t is time, n is time exponent, and k is a growth constant. The growth constant will be dependent on the properties of the material, particularly its susceptibility to anodic dissolution in the acidic environment prevailing in a propagating localized corrosion site. The time exponent, n , would be about 0.5 for both diffusion-controlled (i.e., diffusion of metal ions out of the pit) and ohmically controlled (i.e., rate determined by the ohmic potential drop which develops in the electrolyte in the pit) pit growth (McGuire et al. 1998, Section 5.3.1; Vetter and Strehblow 1974). The above model was used in a separate analysis for the repository by the Electric Power Research Institute (EPRI 2002, Section 5.3.1).

The significance of this pit penetration law has been discussed by Frankel (1998) and leads to a pit growth current density (i) proportional to the inverse square root of time (i.e., $i \propto t^{-1/2}$) in potentiostatic electrochemical experiments. Hunkeler and Boehni (1983) have shown that this growth law is obeyed for both the pitting and crevice corrosion of stainless steels. Newman and Franz (1984) have also observed a similar relationship on stainless steel.

When trying to adapt such a law for practical applications, two main problems arise: (1) insufficient penetration rate data are available, especially for relatively new materials such as Alloy 22, to determine values of k and n ; and (2) the factors that control the form of this apparently simple growth law are complex and, at best, only qualitatively understood. In order to determine values of k and n , it is necessary to employ short-term experiments in which the pit growth process is accelerated electrochemically. In these experiments, those features of the propagation process that enhance growth (the development of critical chemistry; the evolution of pit geometry) are dominant. However, it is necessary to predict penetration behavior after long periods of exposure, when those factors that limit growth (IR drop, loss of critical chemistry, evolution of metallurgical factors, polarization of cathodic processes) are more important.

The literature data available for less corrosion resistant materials (Hunkeler and Boehni 1983; Marsh et al. 1991; Mughabghab and Sullivan 1989; Sharland et al. 1994; Ishikawa et al. 1994) clearly show that a penetration growth law of the form of Equation 6-5 is appropriate, and that a value of n equal to 0.5, the theoretically predicted value, is justifiable. A key point with the materials discussed above (e.g., iron, carbon steel, copper and Titanium Grade 2) is that they are materials that would be expected to undergo rapid propagation. Providing it is not stifled by the accumulation of corrosion product deposits or slow cathodic kinetics, propagation would be limited only by diffusive or ohmic effects, leading to a value of n approaching 0.5.

By contrast, for highly corrosion resistant materials such as Alloy 22 that are designed and fabricated to resist localized corrosion, additional metallurgical features will be important in determining the value of n . One example of such a metallurgical influence that is pertinent to the case of Alloy 22 is the ability of molybdenum to decrease the pitting current densities in stainless steels, possibly by reducing the active dissolution rate within the pit (Frankel 1998; Newman 1985). This prevents the maintenance of the critical pit or crevice chemistry to sustain propagation, leading to repassivation. Again, the n value in the growth law in Equation 6-5 would effectively tend to 0. Evidence to support such a claim has been published by Kehler et al. (2001), who showed that the depth of crevice penetration for Alloy 22 electrochemically driven in extremely saline (5 mol/L LiCl) solutions at 85°C was limited to less than 100 μm . The adoption of such a value assumes that metallurgical features, such as the influence of molybdenum on pit and crevice propagation will suppress penetration.

Localized corrosion rate data are needed to obtain a value for k . The only presently available source of crevice corrosion rate data is that published by Haynes International (1997) and summarized by Gdowski (1991, Table 22). This data was recorded in 10 weight percent FeCl_3 (i.e., under extremely aggressive oxidizing conditions).

The localized corrosion growth law model of the form of Equation 6-5 is not used in TSPA because of lack of data to obtain the values of the model parameters, n and k for Alloy 22 for the exposure conditions relevant to the repository. The base-case model (time-independent constant

penetration rate model) is much more conservative than the growth law model. The base-case model should bound the penetration rate range by localized corrosion of the waste package outer shell when it occurs.

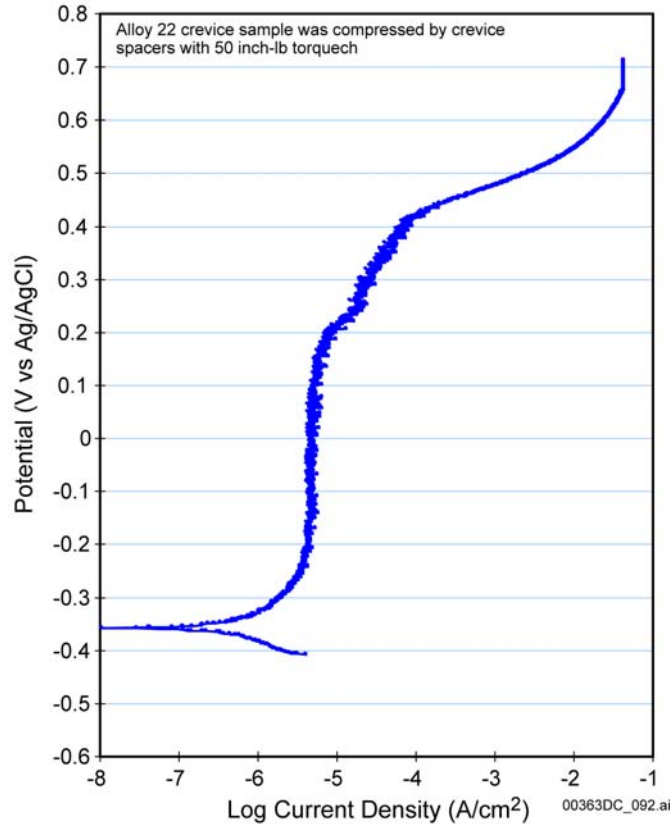
7. LOCALIZED CORROSION OF ALLOY 22 IN CALCIUM-CHLORIDE-FREE BRINES EXPECTED IN THE TRANSITION- AND LOW-TEMPERATURE REGIMES (FREQUENCY GREATER THAN OR EQUAL TO 90 PERCENT)

Section 7 focuses attention on testing in a variety of brines that are believed to be more representative of those that might evolve due to evaporative concentration, brines predicted with a frequency of greater than 90 percent. Such brines include BSW, SAW, and SCW. These test environments have been categorized in terms of the 11 representative water-chemistry bins given in Table 2-1. SSW and SAW are similar to the endpoint waters that evolve from Bins 4 and 5, with a combined time-integrated frequency of about 2 percent. SCW and BSW are similar to the endpoint waters that evolve from Bins 6 through 11, with a combined time-integrated frequency of about 98 percent.

A cyclic potentiodynamic polarization curve for Alloy 22 in BSW at 100°C, as shown in Figure 7-1, exhibits a 550 mV margin between the short-term open-circuit corrosion potential and the anodic oxidation peak (appearing more as a shoulder in this figure). The long-term open-circuit corrosion potential curve for Alloy 22 in BSW at 105°C, as shown in Figure 7-2, demonstrates that the corrosion potential reaches a stable, constant value of below 150 mV versus Ag/AgCl after more than 2 years. Since this value is well below the anodic oxidation peak, destabilization of the passive film is not expected.

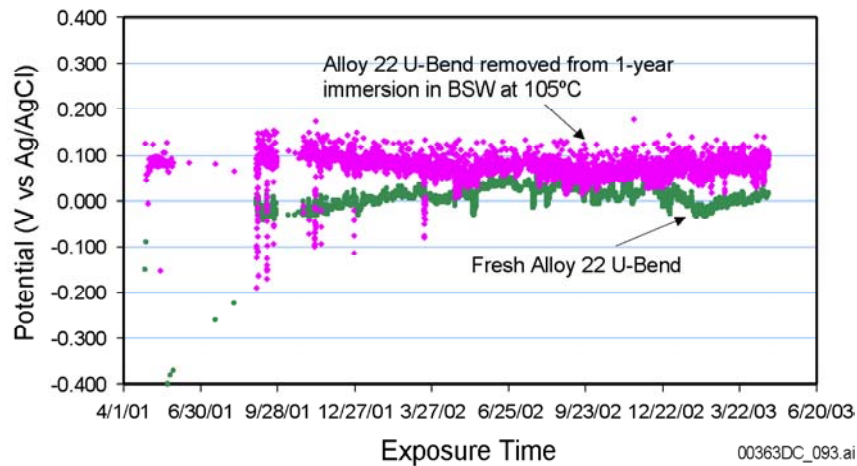
A cyclic potentiodynamic polarization curve for Alloy 22 in SAW at 90°C, as shown in Figure 7-3, exhibits a 650 mV margin between the short-term open-circuit corrosion potential and the breakdown potential. The long-term open-circuit corrosion potential curve for Alloy 22 in SAW at 90°C, as shown in Figure 7-4, demonstrates that the corrosion potential reaches a stable, constant value of below 400 mV versus Ag/AgCl after more than 2 years. Since this value is well below the anodic oxidation peak, destabilization of the passive film is not expected.

A cyclic potentiodynamic polarization curve for Alloy 22 in SCW at 90°C, as shown in Figure 7-5, exhibits a 500 mV margin between the short-term open-circuit corrosion potential and the anodic oxidation peak. Long-term open-circuit corrosion potential curve for Alloy 22 in SCW at 90°C, as shown in Figure 7-6, demonstrates that the corrosion potential reaches a stable, constant value of below 0 mV versus Ag/AgCl after more than 2 years. Since this value is well below the anodic oxidation peak, destabilization of the passive film is not expected.



Source: Farmer, McCright et al. 2000.

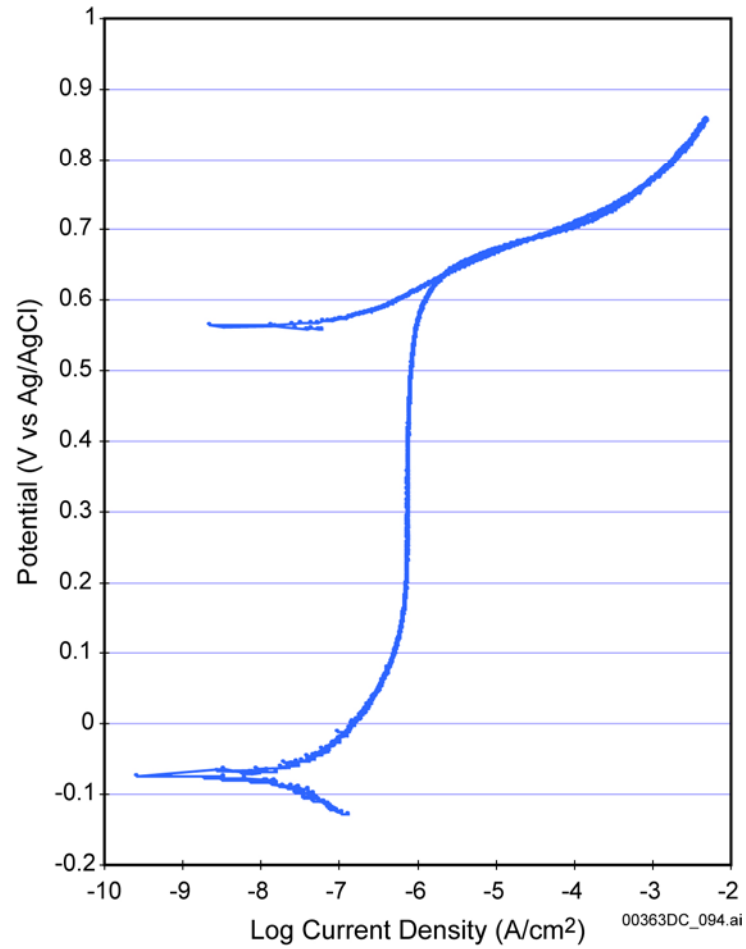
Figure 7-1. Cyclic Potentiodynamic Polarization of Alloy 22 in Basic Saturated Water at 100°C, Showing a 550 mV Margin between the Short-Term Open-Circuit Corrosion Potential and the Anodic Oxidation Peak



Source: Estill et al. 2003, Figure 6.

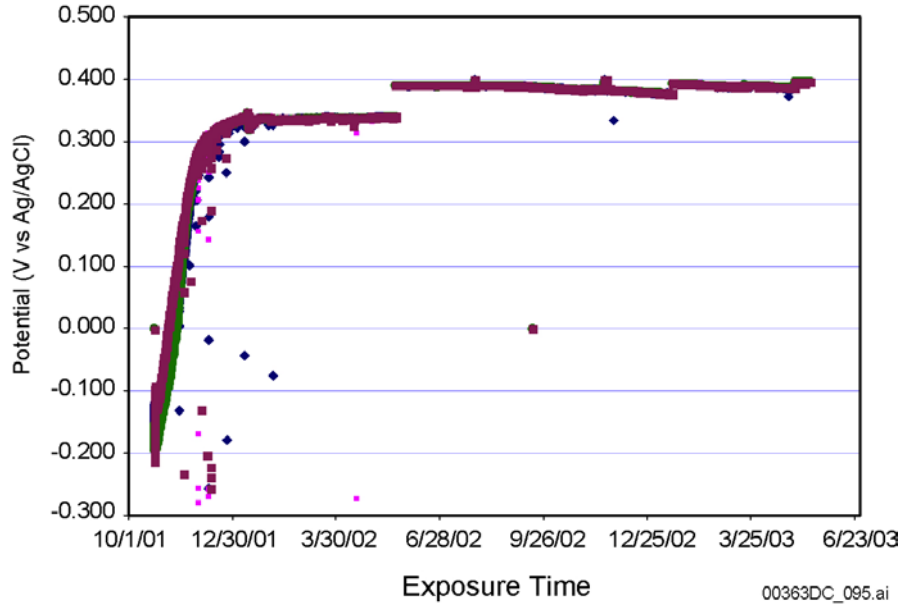
NOTE: Since this value is well below the anodic oxidation peak (shoulder), destabilization of the passive film is not expected, even with ennoblement.

Figure 7-2. Long-Term Open-Circuit Corrosion Potential for Alloy 22 in Basic Saturated Water at 105°C, Showing that the Corrosion Potential Reaches a Stable, Constant Value of below 150 mV after 2 Years



Source: Lian et al. 2003, Figure 2a.

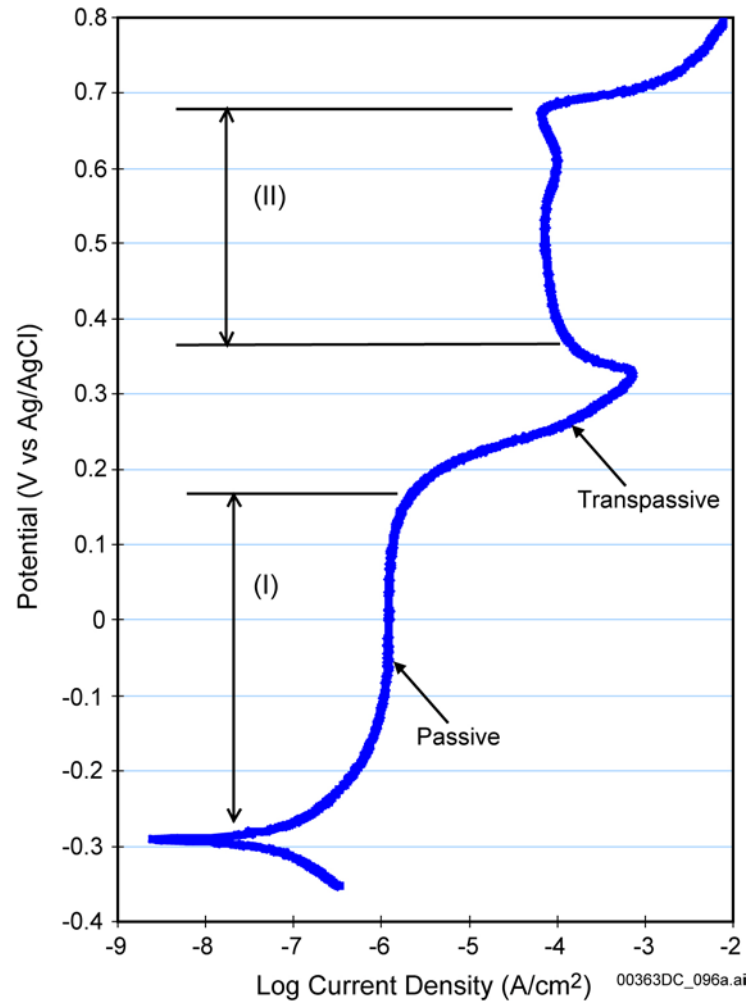
Figure 7-3. Cyclic Potentiodynamic Polarization of Alloy 22 in Simulated Acidified Water at 90°C, Showing a 650 mV Margin between the Short-Term Open-Circuit Corrosion Potential and the Breakdown Potential



Source: Lian et al. 2003, Figure 3a.

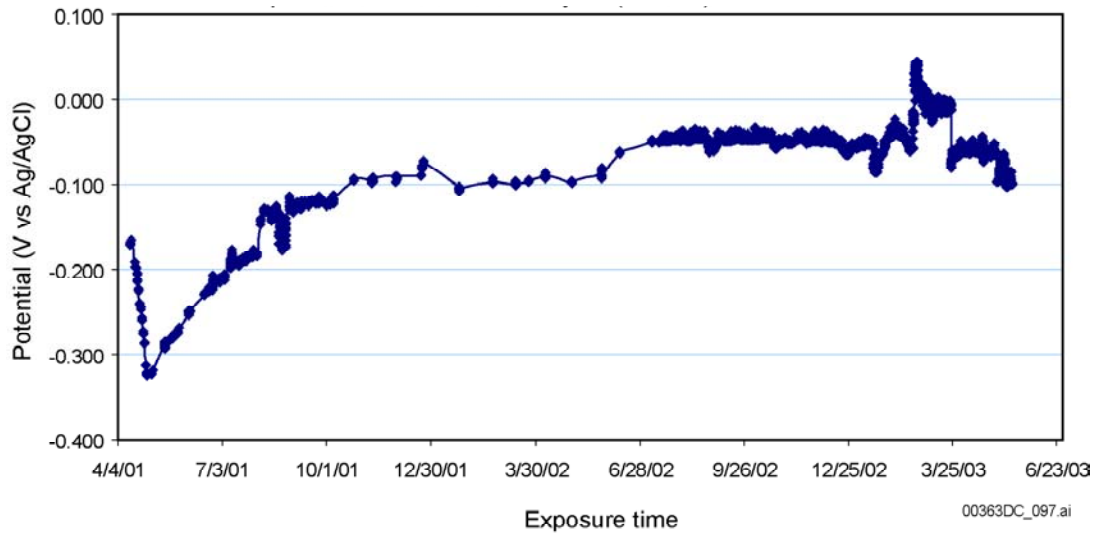
NOTE: Since this value is well below the anodic oxidation peak, destabilization of the passive film is not expected, even with ennoblement.

Figure 7-4. Long-Term Open-Circuit Corrosion Potential for Alloy 22 in Simulated Acidified Water at 90°C, Showing that the Corrosion Potential Reaches a Stable, Constant Value of below 400 mV after 2 Years



Source: Lian et al. 2003, Figure 2b.

Figure 7-5. Cyclic Potentiodynamic Polarization of Alloy 22 in Simulated Concentrated Water at 90°C, Showing a 500 mV Margin between the Short-Term Open-Circuit Corrosion Potential and the Anodic Oxidation Peak



Source: Lian et al. 2003, Figure 3b.

NOTE: Since this value is well below the anodic oxidation peak, destabilization of the passive film is not expected, even with ennoblement.

Figure 7-6. Long-Term Open-Circuit Corrosion Potential for Alloy 22 in Simulated Concentrated Water at 90°C, Showing that the Corrosion Potential Reaches a Stable, Constant Value of below 0 mV versus Ag/AgCl after More than 2 Years

8. THE EFFECTS OF GAMMA RADIOLYSIS IN TRANSITION AND LOW-TEMPERATURE REGIMES

The effects of radiation on waste package materials corrosion differ depending on the amount of liquid present on their surfaces (i.e., humid air or aqueous conditions). Under humid air conditions, a thin film of liquid that may contain trace constituents (e.g., dissolved gases) forms. Irradiation of these films could lead to acidic conditions and to enhanced corrosion rates. Under aqueous conditions (bulk solutions), anodic shifts in the open-circuit potential of stainless steel in gamma irradiated solutions have been experimentally observed. These shifts in potential have been shown to be due to the formation of hydrogen peroxide (BSC 2003c, Section 6.5.1). Glass et al. (1986) performed ambient-temperature cyclic potentiodynamic polarization of 316L samples in 0.018 M NaCl solution during exposure to 3.5 Mrad/hr gamma radiation). They found that the corrosion current shifted in the anodic direction by approximately 200 mV. From inspection of the graphical data in this article, it is concluded that there is very little increase in the corresponding corrosion current density. However, the separation between the corrosion potential and the threshold for localized attack decreased slightly. This shift in corrosion potential was shown to be due to the formation of hydrogen peroxide. This finding was subsequently confirmed by Kim (1988). In this case, ambient-temperature cyclic potentiodynamic polarization of 316 stainless steel in acidic (pH approximately 2) 1.5 M NaCl during exposure to 0.15 Mrad/hr gamma radiation showed a 100 mV anodic shift in the corrosion potential, with very little effect on the corrosion current. Note that Glass et al. (1986) and Kim (1988) worked on stainless steels, not on Alloy 22, which is significantly more corrosion resistant.

Although there is little information available in the literature on the effects of radiation on Alloy 22, some data are available on the corrosion of Alloy C-4, which is compositionally similar to Alloy 22. Gamma irradiation in aggressive $MgCl_2$ brines showed that below approximately 100 rad/hr, irradiation has no observable influence on the corrosion behavior of Alloy C-4. No enhancement of general corrosion and no pitting or crevice corrosion were observed in the material at these dose rates (Shoesmith and King 1998).

Calculations of the expected radiation levels at the surface of the waste package have been performed. For a bounding case waste package containing 21 PWR spent nuclear fuel assemblies (75 GWd/MTU burnup and 5-year decay), the maximum surface radiation level was calculated to be about 1,100 rad/hr at the outer surface of the waste package shell and 1,550 rad/hr at the bottom lid of the shell (BSC 2003h, Figure 6.4-1). These values are at the time of emplacement. During the ventilation period of 50 years, no aqueous or humid air environment and therefore, no radiolysis is expected. After 50 years, the maximum surface radiation level decreases to levels of less than 100 rad/hr for the outer surface and 70 rad/hr for the bottom lid (BSC 2003h, Figure 6.4-1). These values correspond to reduction factors of 0.09 for the outer surface and 0.045 for the bottom lid (BSC 2003h, Figure 6.4-2). One hundred years after emplacement, the calculated levels reduce to about 30 rad/hr for the outer surface and about 20 rad/hr for the bottom lid (BSC 2003h, Figure 6.4-2). Note that these are bounding radiation levels for the highest burnup spent nuclear fuel and are well below the levels at which some effect of radiation has been observed.

On the basis of the above argument, it is concluded that the effects of radiolysis on corrosion performance of Alloy 22 will not be significant enough to lead to corrosion-induced failure of the waste package outer shell under repository relevant conditions. For this reason, the effects of radiolysis on corrosion performance of Alloy 22 are not included in TSPA modeling.

9. STRESS CORROSION CRACKING AND PREVENTION THROUGH STRESS MITIGATION OF THE WASTE PACKAGE OUTER SHELL

SCC in structural materials occurs in the presence of a conducive chemical environment with sustainable tensile stress. Environments that cause SCC are usually aqueous and can be condensed layers of moisture or bulk solutions. The SCC of a particular alloy is usually caused by the presence of a specific chemical species in the environment. For example, the SCC of copper alloys is virtually always due to the presence of ammonia in the environment. Chloride ions cause SCC in stainless steels and aluminum-based alloys. Reduced sulfate is known to promote SCC in nickel-based alloys. Changes in the environmental conditions, which include temperature, dissolved oxygen, and ionic concentrations, will normally influence the SCC process. In some Alloy 22 system/environment combinations, following SCC initiation, propagation can occur at relatively low stress intensity factors (K_I) and at crack growth rates that can lead to through-wall penetration of the waste package outer shell at shorter times than the 10,000-year regulatory time period of importance to the high-level radioactive waste repository at Yucca Mountain. Models to adequately account for SCC have therefore been developed (BSC 2003a, Section 1.2).

The SCC model makes use of a threshold stress for the initiation of stress corrosion cracks on smooth surfaces and a stress intensity factor threshold for the initiation of crack growth. The threshold stress for crack initiation is independent of chemical environment once an aqueous film is formed on the component surface. Manufacturing flaws (e.g., weld defects) are also considered to propagate by SCC. It is conservatively assumed that manufacturing flaws are already initiated; thus, only the stress intensity factor threshold for crack growth is applied to the manufacturing flaws. Both crack initiation and growth are based on the film rupture and slip dissolution theory. The SCC model coupled to the in-drift environment model, the deliquescence model, and the localized and general corrosion models provide all the elements needed for the performance of a lifetime prediction of the waste package outer shell subjected to the effects of SCC. The SCC model is documented in *Stress Corrosion Cracking of the Drip Shield, the Waste Package Outer Barrier, and the Stainless Steel Structural Material* (BSC 2003a).

9.1 INITIAL ASSESSMENT OF ALLOY 22 STRESS CORROSION CRACKING SUSCEPTIBILITY OVER RANGE OF POTENTIAL AND ACCELERATED WASTE PACKAGE OUTER SHELL ENVIRONMENTS

It is important to assess the potential impact on SCC susceptibility of the waste package outer shell over the range of potential and accelerated evolved environments (including aggressive CaCl_2 -type brines that can promote localized corrosion). Thus, a series of slow strain rate tests was performed on Alloy 22 at 73°C to 120°C, and at a strain rate of 1.6×10^{-6} per second. Although slow strain rate testing does not give a direct measure of the threshold stress for SCC initiation, the absence of SCC in tests in which specimens are pulled to failure at a low strain rate is consistent with Alloy 22 being an SCC resistant material and with a high threshold stress used in the SCC initiation model (90 percent of the yield strength) (BSC 2003a, Section 6.2.1).

These slow strain rate test results are summarized in Table 9-1 and cover a broad range of relevant and potentially accelerated environments, with and without lead additions, and with and

without applied potential. Examination of the tabulated results indicates a high degree of SCC resistance at open-circuit potentials in all environments evaluated including approximately 8.5 M (saturated) CaCl₂-type brines at pH approximately 4 and 120°C; as well as lead additions at pH approximately 3-4. The only environment evaluated in which incipient SCC initiation may have been observed was SCW with an applied potential between 300 to 400 mV versus SSC, with a corresponding open-circuit corrosion potential between -94 to -241 mV versus SSC. Clearly, these results, in which the specimens are slowly pulled to the fracture stress, are consistent with the very low SCC susceptibility of Alloy 22.

Table 9-1. Slow Strain Rate Test Results for Annealed Alloy 22 (Strain Rate of 1.66×10^{-6} per second)

Specimen ID	Test Environment	Temperature (°C)	E_{corr} (mV vs. SSC)	$E_{Applied}$ (mV vs. SSC)	Time to Failure of the Specimen (hours)	Max. Stress (MPa)	Reduction in Area (%)	Observation
012	Air	22	N/A	N/A	124	786	74	Inert
123	4M NaCl at pH ~ 6	98	-323	+350	127	758	80	No SCC
004	8.5M CaCl ₂ at pH ~ 6	120	-140 to -180	E_{corr}	127	752	71	No SCC
013	1% PbCl ₂ at pH ~ 4 Aerated	95		E_{corr}	126	765	72	No SCC
015	SAW at pH ~ 3	63	-7 to +360	E_{corr}	118	758	79	No SCC
016	SAW at pH ~ 3 + 0.005% Pb(NO ₃) ₂	76	-6 to +370	E_{corr}	124	772	74	No SCC
017	SAW at pH ~ 3 + 0.005% Pb(NO ₃) ₂	76	0 to +350	E_{corr}	125	772	74	No SCC
003	SAW at pH ~ 3 + 0.005% Pb(NO ₃) ₂	95	-90 to +400	E_{corr}	118	752	85	No SCC
127	BSW at pH ~ 13 with [NO ₃ + SO ₄]	98	-240 to -220	E_{corr}	123	745	72	No SCC
124	BSW at pH ~ 13 with [NO ₃ + SO ₄]	105	-330	+100	100	745	78	No SCC
122	BSW at pH ~ 13 with [NO ₃ + SO ₄]	98	-245	+200	122	752	72	No SCC
120	BSW at pH ~ 13	105	-323	+400	99	745	74	No SCC
119	BSW at pH ~ 13	105	-301	+400	118	745	75	No SCC
115	BSW at pH ~ 13 with [NO ₃]	105	-335	+400	115	752	77	No SCC
129	BSW at pH ~ 13 with [NO ₃]	105	-314	+400	119	731	82	No SCC
020	SCW	22	-109	+400	116	800	85	No SCC
125	SSW at pH ~ 6	100	-154	+400	113	717	71	No SCC
112	SCW at pH ~ 9	73	-94	+400	91	696	71	SCC
021	SCW at pH ~ 9	73	-171	+400	90	662	64	SCC
030	SCW at pH ~ 9	73	-182	+300	98	NA	65	SCC
026	SCW at pH ~ 9	73	-241	+100	120	111	79	No SCC

Source: DTN: LL020603612251.015.

9.2 PREDICTIVE MODELS FOR STRESS CORROSION CRACKING INITIATION AND PROPAGATION

Andresen and Ford (BSC 2003a, Section 6.3.4) have applied the slip-dissolution film-rupture model to the SCC of stainless steels, low-alloy and carbon steel, ductile nickel alloys, and irradiated stainless steel. Specific applications include Types 304 and 316L stainless steel, A533B and A508 low-alloy steels, and nickel-based alloys such as Inconel 600. Therefore, there is ample reason to hypothesize that SCC of nickel-based Alloy 22 occurs by the same fundamental mechanism characterized by the slip-dissolution film-rupture model for SCC propagation.

In regard to assessing the effect of SCC on waste package performance, one model is needed for crack initiation and a second for crack growth. The first is the threshold stress for SCC initiation, while the second is a variation of the slip-dissolution film-rupture model for SCC propagation. In the first model, SCC growth is assumed to start (initiation is assumed to occur) at microscopic surface flaws if the tensile stress at the smooth surface exceeds a threshold stress. Manufacturing flaws (e.g., weld defects) are also considered to propagate by SCC. It is conservatively assumed that manufacturing flaws are already initiated; thus, only the stress intensity factor threshold for crack growth is applied to the manufacturing flaws. Once initiated, crack growth will continue as long as K_I exceeds $K_{I,SCC}$.

Stress Corrosion Cracking: Initiation Threshold Stress—For a given alloy, metallurgical condition, environment, and in the absence of cyclic stresses, initiation of SCC will not occur on a smooth surface (without sharp defects such as weld flaws) if the surface stress is below a threshold value defined as the threshold stress (ASM International 1987, Vol. 13, p. 276). To provide a basis for an Alloy 22 threshold stress value, a series of constant-load crack-initiation tests were performed on 120 Alloy 22 samples by exposing them for 9,600 hours to a 105°C brine, BSW (diluted to approximately 15 percent of full concentration) with a pH approximately 10.3 at test temperature (BSC 2003a, Section 6.2.1). The time-to-failure (or total exposure time without failure) was determined at various applied stress ratios (applied stress to yield strength). Testing was done at applied stress ratios up to 2.1 times the yield strength of the as-received material ($2.1 \times$ yield strength), and up to 2.0 times the yield strength of the welded material ($2.0 \times$ yield strength). These high stress ratios correspond to an applied stress of 89 to 96 percent of the ultimate tensile strength. It is therefore concluded that Alloy 22 exhibited significant resistance to SCC, since no failure was observed in any of the 120 samples, including those in the as-welded state. The SCC resistance of Alloy 22 is corroborated by results of high-magnification visual examination of numerous U-bend specimens (both annealed and as-welded conditions) exposed for 5 years to relevant LTCTF environments (SDW, SCW, SAW) at 60°C and 90°C. These Alloy 22 U-bends showed no evidence of SCC initiation (DTN: LL021105312251.023).

Since the SCC initiation test results are for exposures to about 5 years, an extrapolation scheme is needed to derive a threshold stress value associated with the lifetime of the waste packages and drip shields from the available experimental data. The ASME Boiler and Pressure Vessel code (ASME 1969, p. 80) conservatively assumes a factor of 2 on the runout stress (endurance limit) for defining fatigue lifetime cycles. Using this approach, a threshold stress value (criterion) can be derived from the minimum failure stress (or runout stress without failure) obtained from the

constant load tests (i.e., 2.0× yield strength for Alloy 22 by applying an appropriate safety factor). Based on the assumption that the safety factor used be consistent with the ASME code approach, the resulting threshold stress should not exceed 1.0× yield strength, and, for additional conservatism, a stress reduction factor of 2.2 can be applied to the estimated runout stress to obtain a threshold stress value of 0.9× yield strength. Alternative approaches for developing a threshold stress applicable to the static conditions expected in the repository are being evaluated.

The yield strength appropriate for evaluation of stress threshold is a function of temperature. For conservatism, it is recommended that the yield strength value at the maximum temperature be used for analysis purposes. The estimated maximum temperature of the waste package is 200°C with a corresponding yield strength of 286 MPa.

Stress Corrosion Cracking: Threshold Stress Intensity Factor—For a given alloy, the model assumes that SCC crack growth occurs at preexisting surface flaws if the stress intensity factor (K_I) at that flaw exceeds the threshold stress intensity factor for SCC (K_{ISCC}). If this criterion is not met, no crack will initiate. The criterion is represented by Equation 9-1 (BSC 2003a, Section 1.2, Farmer, Lu et al. 2000).

$$K_I \geq K_{ISCC} \quad (\text{Eq. 9-1})$$

The threshold K_{ISCC} is a material- and environment-dependent property that can be obtained through fracture mechanics testing of the materials in the specified environment. The K_{ISCC} concept has been widely used by engineers to assess the susceptibility of various materials to SCC. Descriptions of this concept are given by Jones and Ricker (1987) and Sprowls (1987). Typical values of K_{ISCC} are 10 to 30 MPa · m^{1/2} (Jones and Ricker 1987).

Stress Corrosion Cracking Propagation: Slip-Dissolution Film-Rupture Model—The slip dissolution/film rupture propagation model relates crack propagation (advance) to the periodic rupture and repassivation of the passive film at the crack tip. In accordance with the slip dissolution and film rupture theory, crack advance is Faradaically related to the metal oxidation that occurs when the protective film at the crack tip is ruptured. This approach has been successfully applied to model SCC crack propagation of stainless steel, low-alloy steel and nickel-based alloys in light-water nuclear reactor environments (BSC 2003a, Section 6.3.1). This model has now been adopted to assess the SCC susceptibility of the materials to be used for the drip shield and waste package. Parameters in this particular model have been quantified through in situ measurements of crack velocity at known stress intensities (BSC 2003a, Section 6.3.4). Calculated values of K_I indicate eventual penetration of the waste package outer shell unmitigated closure weld by through-wall radial cracks (which are driven by circumferential tensile forces) (BSC 2003a, Section 6.5.1).

Initiation of embryonic cracks may occur at microscopic surface flaws or sites of localized corrosion (pitting and inter-granular attack). The coalescence of the embryonic cracks to form larger cracks must also be understood. It has been observed that the crack growth rate increases as small cracks coalesce, and approaches a steady-state value when the mean crack length (depth) is about 20 to 50 μm. Thereafter, the crack propagation rate may be analyzed in terms of linear elastic fracture mechanics, normally applicable to long (deep) cracks (BSC 2003a, Section 6).

As described above, the slip-dissolution film-rupture model has been successfully employed to predict crack extension in boiling-water nuclear reactors. The model is represented by Equation 9-2, which shows the dependence of crack propagation rate (V_t) on the crack tip strain rate ($\dot{\varepsilon}_{ct}$) (BSC 2003a, Section 6.3, Equation 5, Farmer, Lu et al. 2000):

$$V_t = A \left(\dot{\varepsilon}_{ct} \right)^n \quad (\text{Eq. 9-2})$$

The parameters A and n depend upon the material and environment at the crack tip. These two parameters can be determined from the measured rate of repassivation following local rupture of the passive surface film. Such measurements typically involve rapidly straining wires that are fabricated from the material of interest. The initial application of the slip-dissolution or film-rupture model was on the quantitative prediction of cracking in Stainless Steel Type 304 or 316 in high-purity water at 288°C (boiling-water reactor environment). These investigations led to the quantification of the A parameter in the model in terms of n . Further, this slip dissolution and film rupture model (using Stainless Steel Type 304 A versus n relationship in 288°C water) has been statistically validated for the chromium-containing nickel-base alloys 600 and 182 over a range of anionic impurity concentrations (BSC 2003a, Section 6.3.3). Therefore, there is ample reason to hypothesize that SCC of nickel-based Alloy 22 occurs by the same fundamental mechanism characterized by the slip dissolution SCC model (BSC 2003a, Section 6.3.4). The value of A is determined with Equation 9-3 (BSC 2003a, Eq. 11; Farmer, Lu et al. 2000):

$$A = 7.8 \times 10^{-3} (n)^{3.6} \quad (\text{Eq. 9-3})$$

Equations 9-2 and 9-3 have been combined to yield Equation 9-4 (BSC 2003a, Eq. 12; Farmer, Lu et al. 2000):

$$V_t = 7.8 \times 10^{-3} (n)^{3.6} \left(\dot{\varepsilon}_{ct} \right)^n \quad (\text{Eq. 9-4})$$

where V_t is given in centimeters per second and $\dot{\varepsilon}_{ct}$ is given per second. The exponent n is a dimensionless parameter fundamentally related to the crack tip environment (pH, potential, anionic activity) and material properties. In the case of constant load, the crack-tip strain rate in Equation 9-4 is related to the engineering stress or the stress intensity factor (BSC 2003a, Section 6.3.3).

The slip-dissolution film-rupture model has been adapted to Alloy 22 and under constant load conditions (where $\dot{\varepsilon}_{ct}$ is proportional to $(K_I)^4$), the n parameter can be determined empirically directly from Equation 9-5 (BSC 2003a, Section 6.3.4, Equation 19) by measuring the crack growth rate, V_t using fatigue precracked compact tension fracture mechanics specimens exposed to relevant environments under known stress intensity factor, K_I , conditions:

$$V_t = 7.8 \times 10^{-2} n^{3.6} (4.1 \times 10^{-14})^n (K_I)^{4n} \quad (\text{Eq. 9-5})$$

The parameter n was determined for Alloy 22 from Equation 9-5 based on crack growth rates measured under constant load conditions at various levels of applied stress intensity factor, K_I (BSC 2003a, Section 6.3.4). These recent Alloy 22 SCC crack growth rate measurements were obtained at the General Electric Global Research Center (DTN: LL021105312251.023). The test data were developed from three Alloy 22 Compact Tension specimens (c144, c152, c153) tested at 110°C in a concentrated mixed salt environment representative of evaporatively concentrated J-13 and known as BSW. The target composition and solution pH (pH of 13.4 at room temperature) are listed in DTN: LL021105312251.023, pp. 3, 6. The use of one water chemistry and test temperature is not critical since it is conservatively assumed SCC occurs at all chemistries and temperatures. In addition, results of crack growth rates in other environments and slow strain rate tests in a variety of environments and temperatures show that Alloy 22 is resistant to SCC (Table 9-1). Therefore, the assumption of chemistry and temperature independence is conservative. The CT specimens were subjected to cyclic loading in order to initiate crack growth and then followed by constant loading conditions with various hold times. The data from DTN: LL021105312251.023 used as input for establishing the range of n values for Alloy 22 are summarized in Table 9-2 (BSC 2003a, Table 6-1). It is noted in Table 9-2 that a crack growth rate of 10^{-11} mm/s is used to represent the point where crack growth ceases. The choice of 10^{-11} mm/s is judged to be below the limit of measurement sensitivity based on the observation that the lowest growth rate measured in the test program appeared to be 1.4×10^{-10} mm/s (DTN: LL021105312251.023, p. 9).

Based on this experimental approach and the corresponding calculated “ n ” values listed in Table 9-2, the mean value of the repassivation parameter (n) and the standard deviation are 1.304 and 0.160, respectively. By assuming that the parameter (n) was normally distributed, the mean and standard deviation could be used to construct the distribution given in *Stress Corrosion Cracking of the Drip Shield, the Waste Package Outer Barrier, and the Stainless Steel Structural Material* (BSC 2003a, Table 6-2). The lower and upper bounds of n , based upon 2 standard deviations ($\pm 2\sigma$), are 0.984 to 1.624, respectively.

Table 9-2. Determination of the Slip-Dissolution Film-Rupture Model Parameters for Alloy 22 in Basic Saturated Water at 110°C

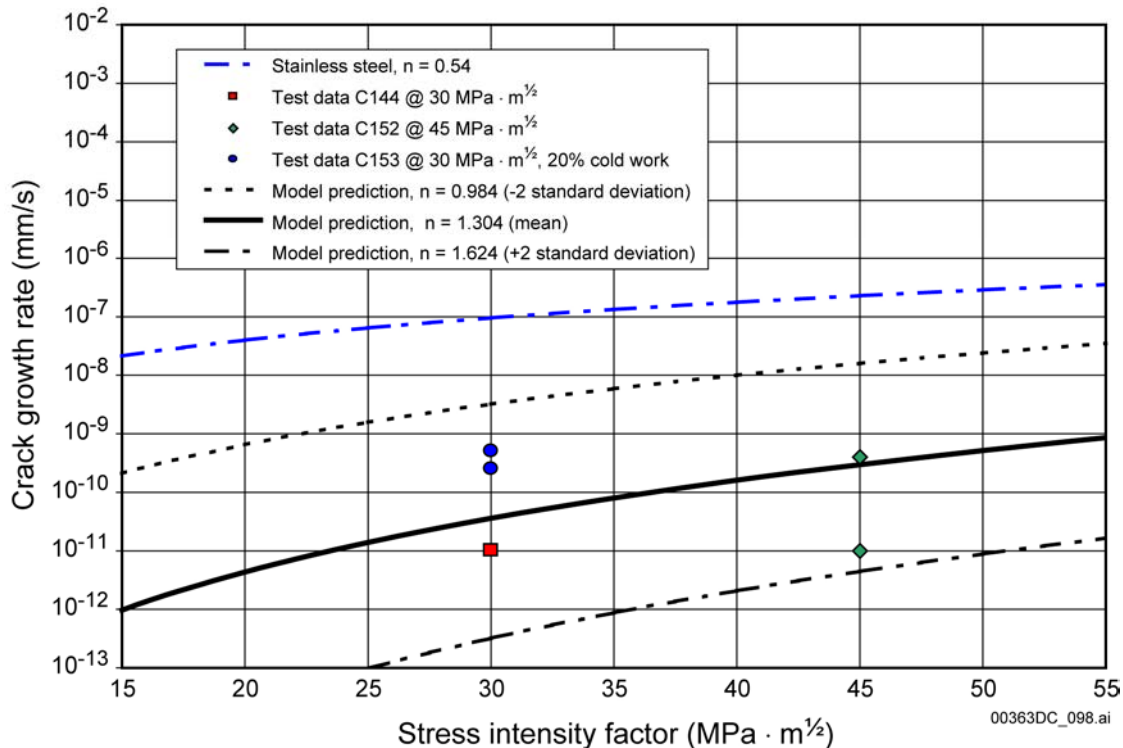
Specimen	Hold Time (hours)	Tested Stress Intensity Factor (MPa · m ^{1/2})	Measured Crack Growth Rate (mm/s)	DTN: LL021105312251.023 (page number)	Calculated Repassivation Parameter (n) ^c
C153	CL ^a	30	2.50×10^{-10}	p. 11	1.168
C153	CL ^a	30	5.00×10^{-10}	p. 11	1.119
C144	1	30	1.00×10^{-11} ^b	p. 7	1.391
C152	24	45	1.00×10^{-11} ^b	p. 10	1.563
C152	24	45	4.00×10^{-10}	p. 10	1.281

NOTE: ^a CL – constant load.

^b Cracking was assumed to cease at a crack growth rate of 10^{-11} mm/s.

^c All values of the repassivation parameter were deduced from crack growth rate data as a function of stress intensity factor.

Figure 9-1 shows predictions of the crack-growth during the SCC of Alloy 22 in BSW at 110°C, as a function of stress intensity factor and for bounding values of the repassivation parameter. Several crack-growth curves are shown in the figure: the lower bound (n equal to 0.984), the mean (n equal to 1.304), and the upper bound (n equal to 1.624) for Alloy 22. It also indicates a crack-growth rate dependency for the mean value for stainless steel (n equal to 0.54). In comparison to stainless steel, Alloy 22 has much higher resistance to SCC.



Source: BSC 2003a, Figure 6.

Figure 9-1. Predicted Crack-Growth Rate for the Stress Corrosion Cracking of Alloy 22 in Basic Saturated Water at 110°C as a Function of Stress Intensity Factor, and for Bounding Values of the Repassivation Parameter (n)

The threshold stress intensity factor is applied to both incipient flaws (once the threshold stress for initiation is exceeded) and for weld flaws. For the waste package outer shell final closure weld, a tightly controlled gas tungsten arc welding process is planned. An experimental confirmation of the expected low weld flaw frequency as well as the correspondingly small flaw size dimensions and their associated size distribution was performed using a series of prototypical Alloy 22 closure weld mockups and results are reported in *Stress Corrosion Cracking of the Drip Shield, the Waste Package Outer Barrier, and the Stainless Steel Structural Material* (BSC 2003a, Section 6.2.2.1). For the model, at each time step, the stress intensity factor, K_I , at a growing initiated crack tip or weld flaw tip will be compared with the K_{ISCC} value. At the point that the K_I value drops below K_{ISCC} , the crack will arrest. Therefore, it is important to develop a basis for assessing K_{ISCC} as discussed below.

9.3 THRESHOLD STRESS INTENSITY FACTOR

As described earlier, the threshold stress intensity factor (K_{ISCC}) is a critical value of stress intensity factor (K_I) such that any preexisting crack will not grow or is in an arrest state if K_I corresponding to the crack size and the applied stress does not exceed K_{ISCC} . Preexisting cracks are usually caused by manufacturing processes (especially welding) or crack initiation (see BSC 2003a, Section 6.2). To apply the method, it is necessary to obtain values of stress intensity factor K_I as a function of crack size correspondent to the stress state at and near the crack site and the threshold stress intensity factor K_{ISCC} .

The threshold stress intensity factor, K_{ISCC} is normally determined experimentally. However, because of the very high SCC resistance of Alloy 22 and correspondingly low measured crack growth rates indicated in Table 9-2, such experiments, which require very long test times and extremely high measurement accuracy, are impractical for Yucca Mountain Project applications. As an alternative conservative approach, a crack blunting criterion is used to define the threshold stress intensity factor. Based on the crack blunting criterion, crack blunting occurs when the corrosion rate of the crack sides approaches the oxidation rate at the crack tip, (i.e., the sharp crack will degenerate to a blunt pit). It follows that an SCC crack will not grow if the general corrosion rate at the crack sides exceeds the crack tip growth rate. If V_{gc} is the general corrosion rate, the threshold stress intensity factor K_{ISCC} can be calculated from Equation 9-5.

Using a mean general corrosion rate of 7.23 nm/yr for Alloy 22 (BSC 2003a, Section 6.3.5), the threshold stress intensity factor for Alloy 22 can be calculated based on the “ n ” values listed in *Stress Corrosion Cracking of the Drip Shield, the Waste Package Outer Barrier, and the Stainless Steel Structural Material* (BSC 2003a, Table 6-2), yielding values shown in Table 9-3.

Table 9-3. Threshold Stress Intensity Factor (K_{ISCC}) Distribution for Alloy 22 in 110°C Basic Saturated Water

Value of n	Value of K_{ISCC} (MPa · m ^{1/2})
0.984 (-2σ)	2.65
1.041	3.65
1.099	4.90
1.139	5.90
1.145 (-1σ)	6.06
1.170	6.76
1.221	8.35
1.264	9.85
1.304 (Mean)	11.38
1.345	13.10
1.388	15.04
1.439	17.56
1.464 (+1σ)	18.87
1.470	19.19
1.509	21.36
1.568	24.89
1.624 (+2σ)	28.50

Source: BSC 2003c.

As stated earlier, at each time step, the stress intensity factor, K_I , at a growing crack tip or defect tip is compared with the K_{ISCC} value. At the point that the K_I value drops below K_{ISCC} , the crack will arrest. The calculations of stress intensity factor for the closure welds in the inner and outer lids of the waste package are described in *Stress Corrosion Cracking of the Drip Shield, the Waste Package Outer Barrier, and the Stainless Steel Structural Material* (BSC 2003a, Section 6.4). The stress intensity factor K_I is usually defined as a function of stress (σ) and crack depth size (a):

$$K_I(a, \sigma) = \beta \sigma (\pi a)^{1/2} \quad (\text{Eq. 9-6})$$

where β is a geometry factor dependent on the size and shape of the crack and the configuration of the structural component and σ is the tensile stress distribution through the wall thickness of the structural component.

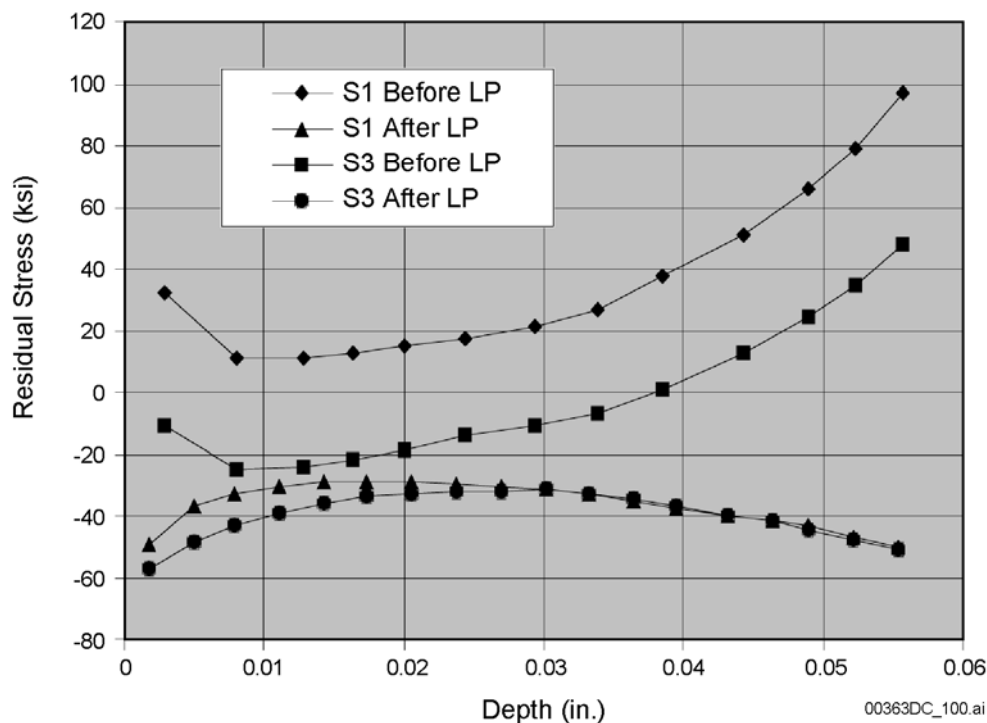
In most practical cases where stresses are nonuniformly distributed across the thickness, the stress intensity factor has to be calculated by some numerical algorithms, such as the finite element method. However, although finite element programs were used to calculate the through-wall stress distributions in each principal direction and can be used to evaluate the stress intensity factor, the latter effort is usually quite time consuming because a series of elaborate finite element analyses must be completed for numerous crack sizes starting from 0 through the thickness of the containment wall. A simplified solution has been developed by using fracture mechanics to evaluate the parameter $(K_I)_{PCCRACK}$ (more detail is given in BSC 2003a, Section 6.4.2.3). Then a geometry correction factor, G , which is usually a function of the crack size, a , is evaluated from the results of finite element analysis. Finally, the true stress intensity factor K_I is derived from $(K_I)_{PCCRACK}$ and G . *Stress Corrosion Cracking of the Drip Shield, the Waste Package Outer Barrier, and the Stainless Steel Structural Material* (BSC 2003a, Section 6.4.2) summarizes the methodology, calculation procedures, and selected results for the waste package outer and middle Alloy 22 lid closure welds in the as-welded condition.

In comparing the multidirectional through-wall residual stress results obtained by finite element analysis with the threshold stress for SCC initiation, it is important to consider that the integrity of components subjected to multiaxial stresses can be assessed with uniaxial stress information. This is an acceptable approach, and is consistent with standard industrial practice. The prediction of stress-strain behavior in sophisticated elastic-plastic analyses typically uses the equivalent (von Mises) stress-strain approach, and uniaxial material stress-strain behavior. The American Society of Mechanical Engineers Boiler and Pressure Vessel Code (ASME 1995) specifies the use of uniaxial materials-strength data for the assessment of materials performance under multiaxial stress conditions. In order to apply the uniaxial stress-strain information to multiaxial conditions, principal stresses are used. This approach recognizes that a combination of stresses can be validly represented by an equivalent, uniaxial stress. Even in a uniaxial stress-strain test (where failure typically occurs along the 45° plane in pure shear), the cross-sections that are not perpendicular to the load line are in a biaxial stress condition that is equivalent to a uniaxial condition. These biaxial stress states can be observed using Mohr's circle.

The output of the calculated through-wall residual stress distributions and resultant stress intensity factor distributions are presented in *Stress Corrosion Cracking of the Drip Shield, the Waste Package Outer Barrier, and the Stainless Steel Structural Material* (BSC 2003a, Tables 6-6 and 6-7) for the outer and middle closure lid welds, respectively for both radial and circumferentially oriented cracks. Further, the impact of time-dependent removal of outer lid surface due to general corrosion is described in *Stress Corrosion Cracking of the Drip Shield, the Waste Package Outer Barrier, and the Stainless Steel Structural Material* (BSC 2003a, Section 6.4.3) where it is indicated the effect of general corrosion on the through-wall stress intensity factor distribution is small. Examination of the calculated range of through-wall K_I values indicates that for both circumferentially and radially oriented flaws, the values of K_I are comparable to or exceed the conservatively calculated K_{ISCC} values given in Table 9-3 indicating that it is prudent to implement a residual stress mitigation process at the outer lid closure weld region to minimize the potential for through-wall SCC to occur during the regulatory period.

9.4 PREVENTION OF STRESS CORROSION CRACKING THROUGH MITIGATION OF RESIDUAL TENSILE STRESS IN CLOSURE WELD

As described earlier, SCC requires tensile stress as a driving force. The highest stress in the waste package outer shell (and the highest probability of SCC) will be in the final closure weld. Postweld tensile stress mitigation processing such as by laser peening or controlled plasticity burnishing can be used to mitigate residual weld tensile stresses in the outer lid surface region. Such stress mitigation must also be accounted for in the SCC model. As described, significant stress can be introduced into Alloy 22 during welding operations. In evaluating weld-induced stress, the effect of each weld pass is determined by simulating the heat being deposited by the welding process through heat generation rate that is deposited over a prescribed time interval. Typical parameters for weld application include the rate of electrical energy input, the speed of welding, and the assumed efficiency of heating (dependent upon heat transfer). Such information was used to determine the heat generation rate for the elements that represent each weld bead. A finite element model was used to calculate weld-induced residual stress, and the corresponding stress intensity factors in the waste package materials. This same approach was used to quantify the expected beneficial effect of postweld stress mitigation on the through-wall residual stress and corresponding stress intensity factor distributions to lower the probability of SCC. As expected the calculated surface stresses in the as-welded condition are at or above yield strength in the weld area (BSC 2003a, Figure 24). The calculated stresses after mitigation are compressive up to a depth of 0.04 to 0.08 in. (1 to 2 mm), consistent with the experimentally measured values shown in Figure 9-2.



Source: DTN: LL000320005924.145.

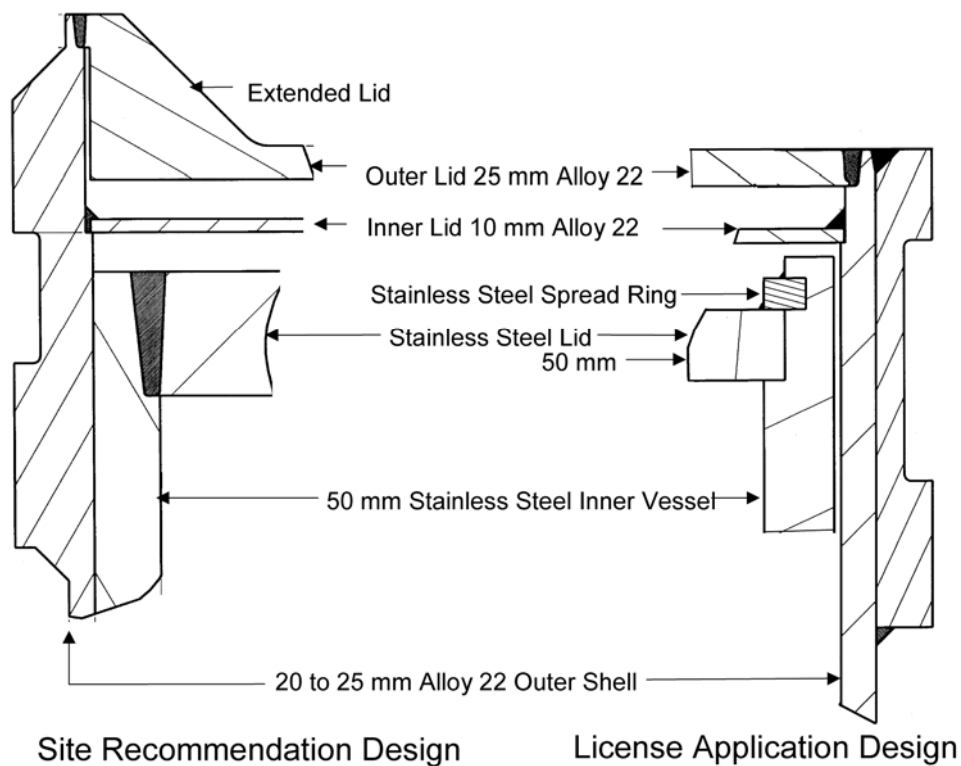
Figure 9-2. Measured Residual Tensile Stress in Alloy 22 Weld Region with and without Laser-Shock-Peening

Based on the modification of the waste package outer lid closure weld configuration as indicated in Figure 9-3, induction annealing is no longer being considered as a residual stress mitigation process for outer lid closure weld. Instead, the current plan is to implement one of two potential mechanical residual stress mitigation processes, (i.e., either laser-shock peening or controlled plasticity burnishing). Laser-shock peening is the baseline process for license application, and utilizes a high-power pulsed laser beam to introduce shock waves into the weld surface (Chen et al. 2002). These pulses produce compressive stress that counter balances the tensile stress caused by welding (due to shrinkage during cooling). Single-pass laser-shock peening has been successfully demonstrated on prototypical Alloy 22 welds. Multiple-pass laser-shock peening can be used to increase the depth of the compressive stress layer. As discussed in a subsequent section, compressive stress can be produced at depths of 2 to 3 mm or greater (Chen et al. 2002).

The waste package design for the license application consists of the following changes from the site recommendation design:

- Replacing the full penetration stainless steel lid weld with a spread ring and seal weld
- Eliminating the outer lid extension
- Changing the outer lid mitigation method from induction annealing to laser-shock peening
- Changing the middle lid weld configuration from a full penetration weld to a seal weld
- Eliminating laser-shock peening of the middle lid.

Sketches of the site recommendation design and the current recommended license application design of the waste package are shown in Figure 9-3.



00363DC_002.ai

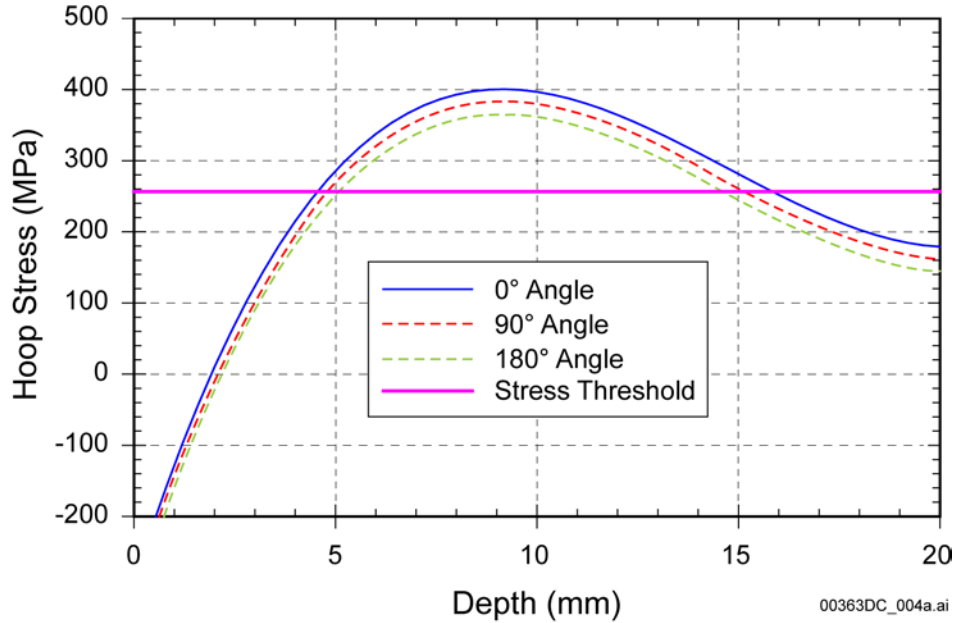
Source: Bokhari 2003, Figure 1.

Figure 9-3. Site Recommendation and License Application Waste Package Closure Lid Designs

Figure 9-3 illustrates a physical separation between the two lids. Thus, any SCC cracks initiated in the outer closure-lid stop after penetrating it, and then the middle closure-lid welds are subject to the external environment and the potential for SCC crack initiation and growth.

Based on the initial very near surface residual stress measurements, analyses of the as-mitigated (by laser-shock peening) through-wall stress and stress intensity factor distributions were performed and are documented in *Stress Corrosion Cracking of the Drip Shield, the Waste Package Outer Barrier, and the Stainless Steel Structural Material* (BSC 2003a, Section 6.4).

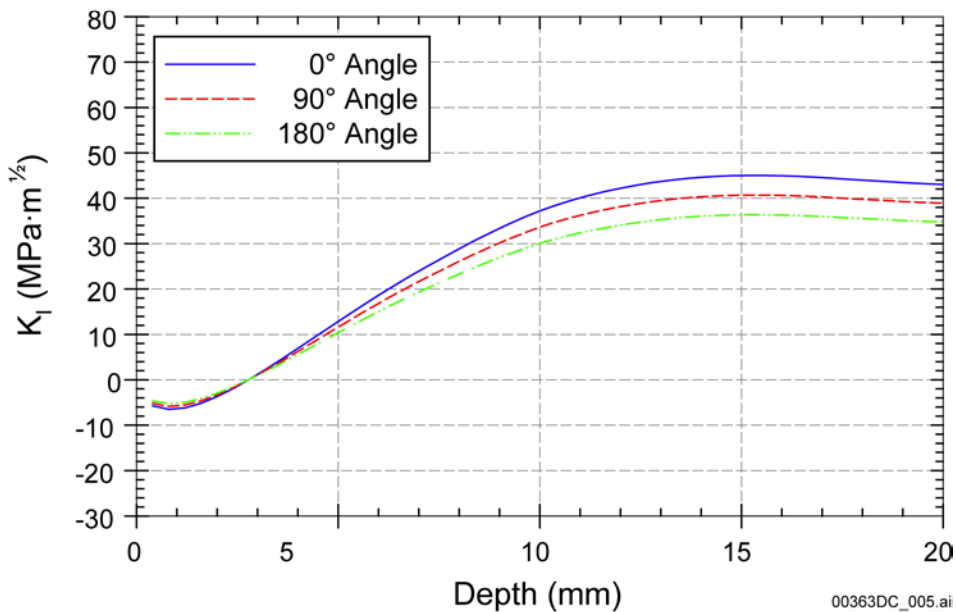
It was concluded that the dominant component of stress in the waste package outer shell closure weld is the hoop stress, which promotes the growth of cracks oriented in the radial direction (BSC 2003a, Section 6.2.2.3). As a direct result of this conclusion, it was only necessary to account for the hoop stress in the current WAPDEG analysis (BSC 2003i). The results of these stress analyses for the laser-shock peening mitigated weld are included in the current WAPDEG analysis (BSC 2003i) including angular variation and the resultant variation in through-wall stress intensity factor, Figures 9-4 and 9-5, respectively. Mitigated compressive stress depths shown in Figure 9-2 are consistent with the calculated compressive stress depth results shown in Figure 9-6.



Source: Input DTN: LL030607012251.065; Output DTN: MO0310MWDWAPAN.002.

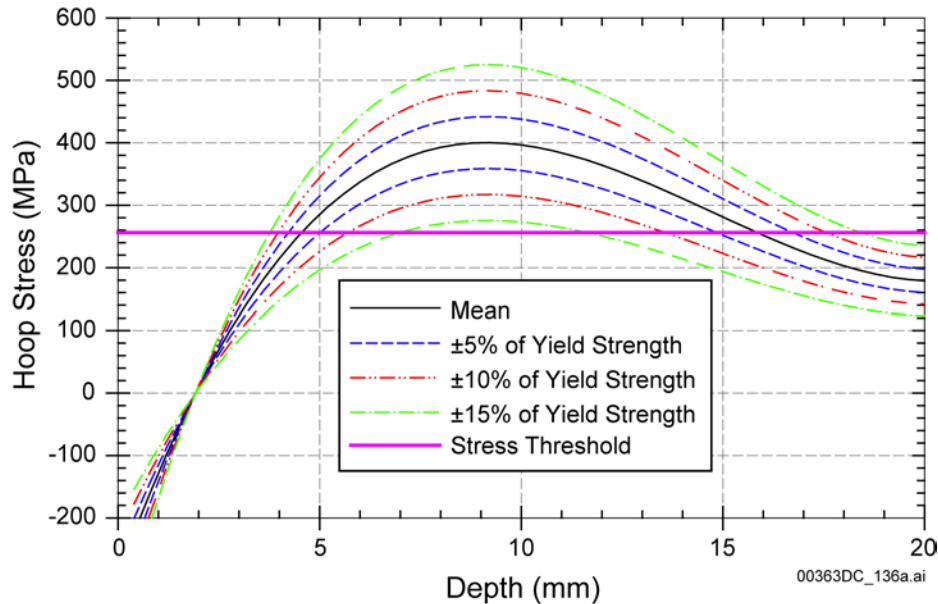
NOTE: Stress threshold is 90 percent of Alloy 22 yield strength of 285 MPa at temperature (200°C).

Figure 9-4. Hoop Stress versus Depth for the Stress-Mitigated Outer Lid of the Waste Package Outer Shell at Various Angles



Source: DTN: LL030607012251.065.

Figure 9-5. Stress Intensity Factor versus Depth for the Stress-Mitigated Outer Lid of the Waste Package Outer Shell



Source: Input DTN: LL030607012251.065; Output DTN: MO0310MWDWAPAN.002.

NOTE: The various curves represent scaling factors that range from 5 to 15 percent of yield strength.

Figure 9-6. Predictions of the Hoop Stress ($\theta = 0$) as a Function of Depth in the Stress-Mitigated Outer Weld of the Waste Package Outer Shell

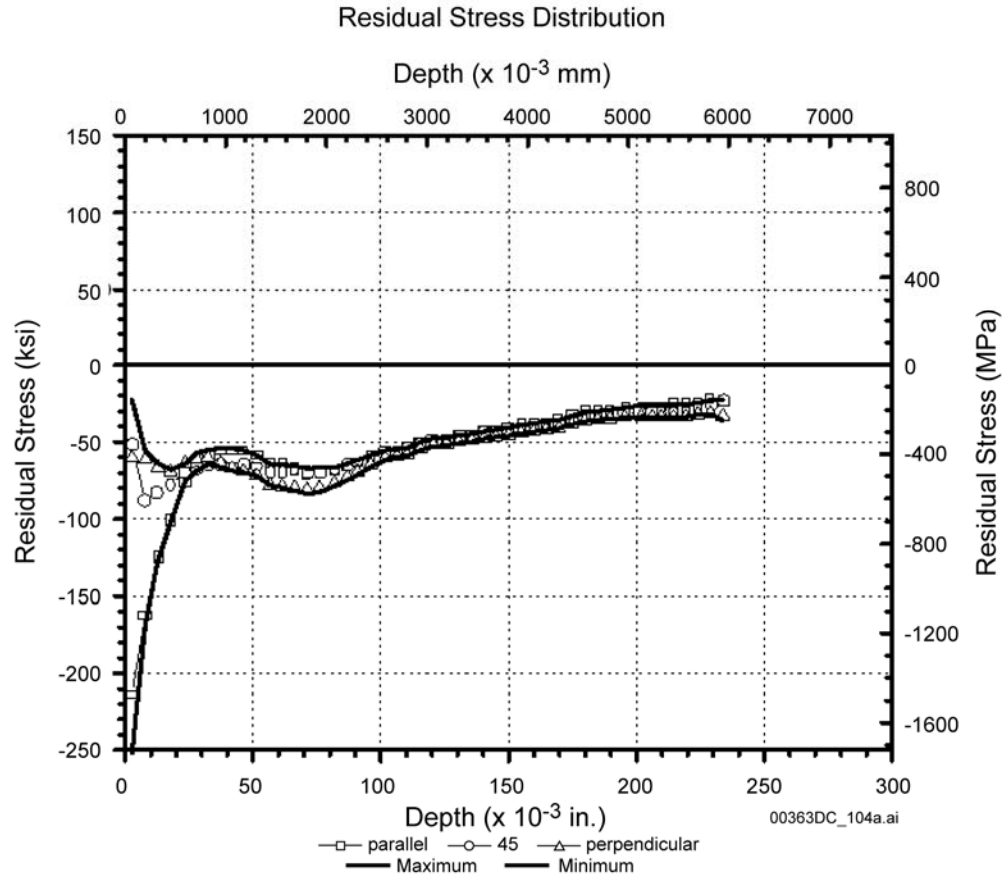
As can be seen, the predicted hoop stress in the stress-mitigated weld in Figure 9-4 is compressive to a depth of approximately 2 mm and rises to the threshold stress (90 percent yield strength) at a depth of approximately 5 mm.

The depth-dependent stress intensity factor, K_I , for a stress-mitigated weld (at three representative angular positions (0°C , 90°C , and 180°C) consistent with the stress distributions shown in Figure 9-4) is shown in Figure 9-5. As a crack propagates, the stresses ahead of the crack tip redistribute, the neutral axis shifts inward, and with increasing depth, the tensile stress starts to decrease. In this case, the depth at which the stress intensity factor in Figure 9-5 reaches 0 is somewhat deeper than for the stress distributions shown in Figure 9-4.

Uncertainty in the stress and stress intensity factor profiles is accounted for with a scaling factor (sz). The scaling factor (sz) is sampled from a normal distribution, with a mean of 0, and a standard deviation of 5 percent of the yield strength, an upper bound of 15 percent of the yield strength, and a lower bound of -15 percent of the yield strength (BSC 2003a, Section 6.4.5). The resultant range of predicted through-wall stress is given in Figure 9-6.

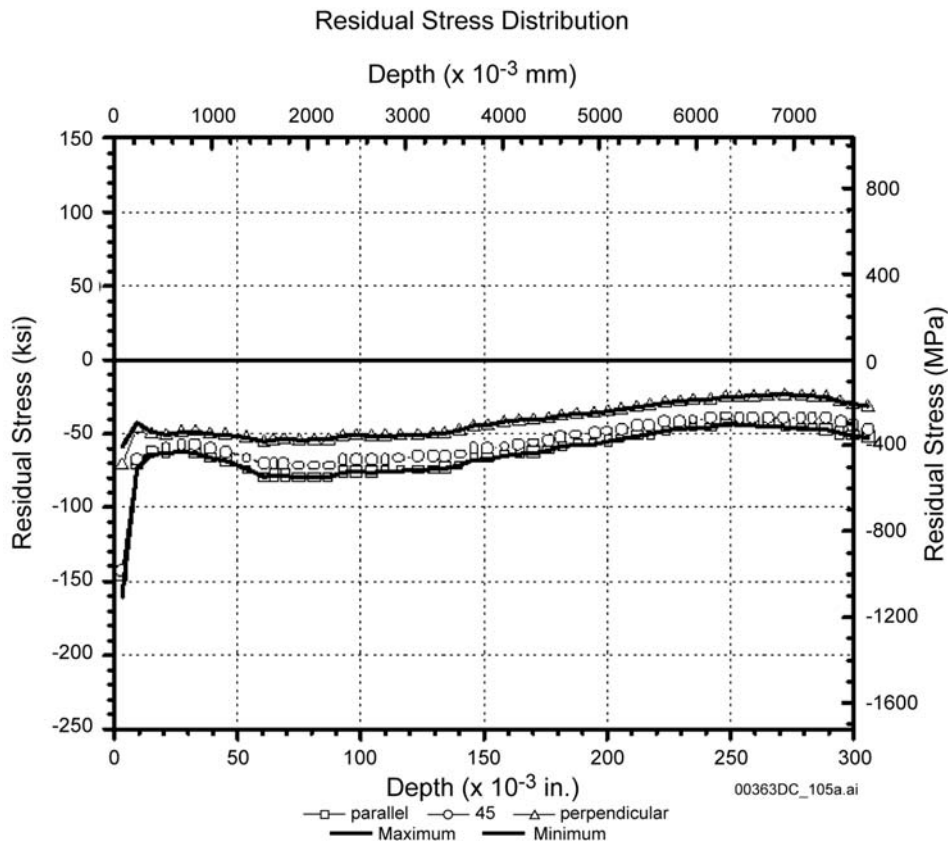
As can be seen, the analysis results predict that the threshold stress (90 percent yield strength) will be reached at a depth of about 5 mm, based upon mean values. More conservatively, the model predicts that the threshold stress will be reached at a depth of only 3.8 mm, based upon the upper bound of uncertainty. Corroborative measurements of the through-wall residual stress have been made on Alloy 22 gas tungsten arc welding welds (1-inch-thick) that were processed with laser-shock peening and controlled plasticity burnishing, and are shown in Figures 9-7 and 9-8. These corroborative measurements show that the predicted values shown in Figure 9-6 are

very conservative estimates of the depth of compression achieved through stress mitigation. These corroborative measurements were obtained with the 1-inch ring-core technique and are reported in DTN: MO0301SPAXRA52.001. Note that stresses parallel to the weld centerline are referred as being in the “parallel direction.”



Source: DTN: MO0301SPAXRA52.001, Figure 4.

Figure 9-7. Residual Stress Distribution in Welded Alloy 22 Plates with Laser-Shock Peening Stress Mitigation



Source: DTN: MO0301SPAXRA52.001, Figure 7.

Figure 9-8. Residual Stress Distribution in Welded Alloy 22 Plates with Controlled Plasticity Burnishing Stress Mitigation

9.5 IMPACT OF CORROSION ON STRESS-MITIGATED WELD (COMPRESSIVE LAYER)

The time-to-failure due to SCC at the stress-mitigated closure weld will be determined by the time required to corrode through the material to a level where the stress exceeds 90 percent of the yield strength added to the time required for the initiated crack to propagate through the remaining lid thickness. Any relaxation of the residual-stress gradient tends to reduce both the compressive surface-stress magnitude and the subsurface tensile-stress magnitude and increases the depth to reach 90 percent of the yield strength. Further, as the outer compressive surface layer is slowly removed by general corrosion, the neutral axis shifts inward, which is beneficial.

The scenario for removal of the compressive layer by corrosion is relatively easy to assess. From Section 5, the general corrosion rate for Alloy 22 is approximately 7.24 ± 4.95 (1σ) nm/yr for crevice samples, and approximately 2.75 ± 2.74 (1σ) nm/yr for weight-loss samples. The wall thickness of the Alloy 22 waste package outer shell is approximately 2 cm, the thickness of the compressive layer at the laser-peened or burnished weld is approximately 2 mm, and the total depth to reach 90 percent of the yield strength is about 5 mm. Estimates of the times-to-failure (t_f) are summarized in Table 9-4. The stress-mitigated layer is deep enough to extend the lifetime of the waste package outer shell well beyond the 10,000-year performance period specified in 10 CFR Part 63.

Table 9-4. Estimates of the Time-to-Failure (t_f) for Stress-Mitigated Closure Weld

	Thickness in Meters	Crevice Sample	Wt. Loss Sample	Crevice Sample	Wt. Loss Sample
		Corrosion Rate (+1 σ) = 12.19×10^{-9} m/yr	Corrosion Rate (+1 σ) = 5.49×10^{-9} m/yr	Corrosion Rate (+2 σ) = 17.14×10^{-9} m/yr	Corrosion Rate (+2 σ) = 8.23×10^{-9} m/yr
		Years	Years	Years	Years
Waste Package Outer Shell Wall	2×10^{-2}	1.64×10^6	3.64×10^6	1.17×10^6	1.43×10^6
Compressive Layer	2×10^{-3}	1.64×10^5	3.64×10^5	1.17×10^5	1.43×10^5
Depth at 90% Yield Strength	5×10^{-3}	4.10×10^5	9.11×10^5	2.92×10^5	6.08×10^5

NOTE: Sample calculations used corrosion rates from Section 5 and assumed mitigated layer thickness.

INTENTIONALLY LEFT BLANK

10. DEGRADATION OF DRIP SHIELD MATERIALS

10.1 BACKGROUND ON TITANIUM GRADE 7 AND CORROSION MODELING

Drip shields will be installed over the waste packages prior to repository closure. Before failure, the drip shields divert any moisture that might seep from the drift walls around the waste packages to the drift floor. The drip shields will be made of titanium alloys, which provide exceptional corrosion resistance in saline environments and structural strength. Such high saline environments may evolve on the drip shield surface under repository exposure conditions. The drip shields also reduce any damage to waste packages in the event of expected rockfall, as the emplacement drifts degrade over time. Titanium alloys are being considered for construction of the drip shield because of their excellent corrosion resistance under the repository conditions. The current recommendation is to use Titanium Grade 7 for the drip shield plates. Titanium Grade 24 (R56405) is used for structural support of the Titanium Grade 7 drip shield plates.

The chemical compositions and mechanical properties, per ASTM B 265-02, of the relevant titanium alloys are shown in Tables 10-1 and 10-2. In Tables 10-1 and 10-2, Titanium Grades 2, 7, 11, and 16 are α -alloys while Titanium Grades 5, 9, 12, and 24 are α - β alloys. The ASTM B 265 specified mechanical properties are identical for Titanium Grades 2, 16, and 7, for Titanium Grades 5 and 24 and for Titanium Grades 9 and 18 (Table 10-2 in ASTM B 265-02). Titanium Grade 16 was used as an analog of Titanium Grade 7 at the LTCTF for the 1-year and 5-year weight loss tests due to its compositional similarity to Titanium Grade 7. Titanium Grade 7 contains slightly higher weight percent of palladium (0.12 to 0.25 weight percent) as compared to Titanium Grade 16 (0.04 to 0.08 weight percent). It is expected that the corrosion performance of Titanium Grade 7, because of its higher palladium content, would be superior to that of Titanium Grade 16. Figure 10-1 shows the relationship among the relevant titanium alloys.

Table 10-1. American Society for Testing and Materials Specifications for Chemical Composition Requirements (Weight Percent) for Relevant Titanium Alloys

Material	UNS	N	C	H	O	Fe	Al	V	Pd	Residual (each)	Residual (total)
Grade 12	R53400	0.03	0.08	0.015	0.25	0.30	-	-	-	0.2-0.4 Mo	0.6-0.9 Ni
Grade 2	R50400	0.03	0.08	0.015	0.25	0.30	-	-	-	0.1	0.4
Grade 16	R52402	0.03	0.08	0.015	0.25	0.30	-	-	0.04-0.08	0.1	0.4
Grade 17	R52252	0.03	0.08	0.015	0.18	0.20	-	-	0.04-0.08	0.1	0.4
Grade 7	R52400	0.03	0.10	0.015	0.25	0.30	-	-	0.12-0.25	0.1	0.4
Grade 11	R52250	0.03	0.10	0.015	0.18	0.20	-	-	0.12-0.25	0.1	0.4
Grade 5	R56406	0.05	0.08	0.015	0.20	0.40	5.5-6.75	3.5-4.5	-	0.1	0.4
Grade 24	R56405	0.05	0.08	0.015	0.20	0.40	5.5-6.75	3.5-4.5	0.04-0.08	0.1	0.4
Grade 9	R56320 ^a	0.03	0.08	0.015	0.12	0.25	2.5-3.5	2.0-3.0	-	0.1	0.4
Grade 18	R56322	0.03	0.08	0.015	0.15	0.25	2.5-3.5	2.0-3.0	0.04-0.08	0.1	0.4

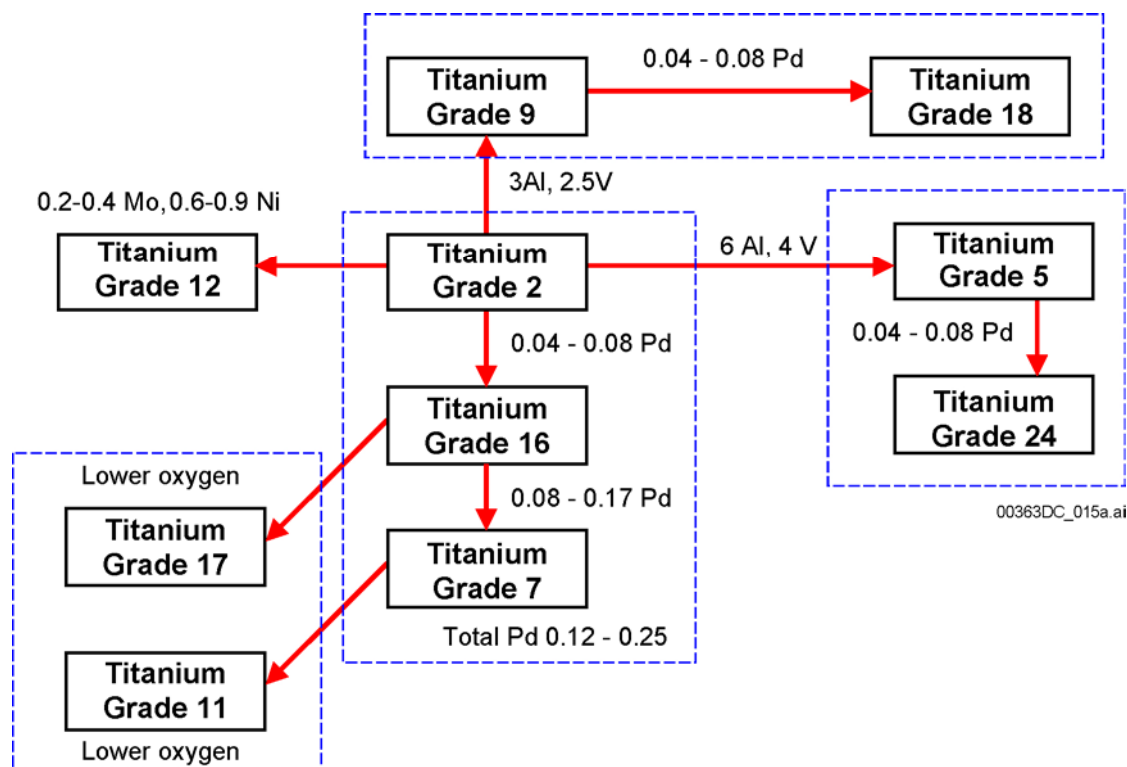
Source: ASTM B 265, Table 2.

NOTE: ^a UNS R56320 requires lower N, C, O, and H.

Table 10-2. American Society for Testing and Materials Specifications for Mechanical Properties of Relevant Titanium Alloys in this Report

Material	UNS Designation	Minimum Tensile Strength		Yield Strength, 0.2% Offset				Minimum Elongation in 2 in., %
		ksi	MPa	Min		Max		
				ksi	MPa	ksi	MPa	
Grade 12	R53400	70	483	50	345	-	-	19
Grade 2	R50400	50	345	40	275	65	450	20
Grade 16	R52402	50	345	40	275	65	450	20
Grade 17	R52252	35	240	25	170	45	310	24
Grade 7	R52400	50	345	40	275	65	450	20
Grade 11	R52250	35	240	25	170	45	310	24
Grade 5	R56406	130	895	120	828	-	-	10
Grade 24	R56405	130	895	120	828	-	-	10
Grade 9	R56320*	90	620	70	483	-	-	15
Grade 18	R56322	90	620	70	483	-	-	15

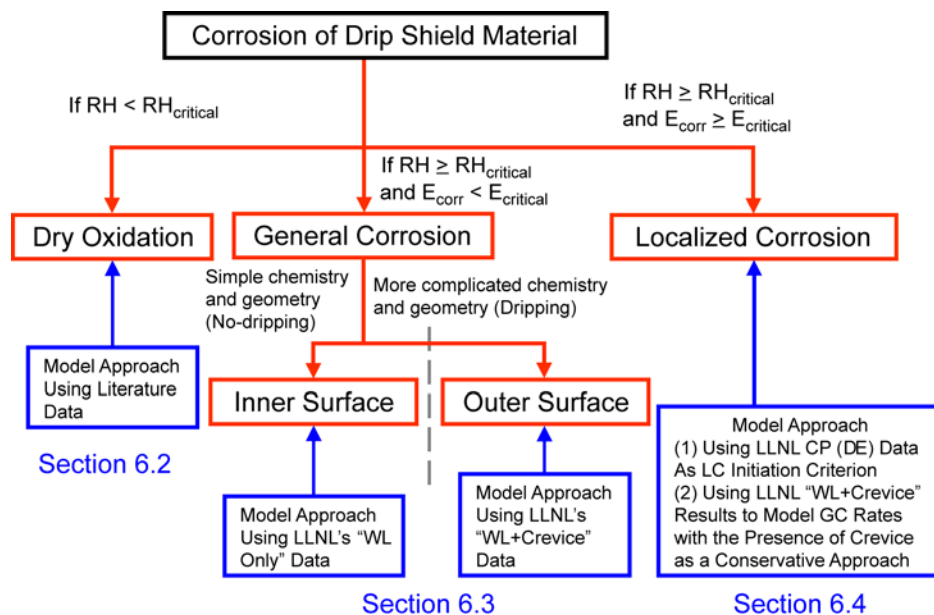
Source: ASTM B 265, Table 1.



NOTE: Alloys grouped by the dashed lines have similar mechanical properties regardless of chemical composition.

Figure 10-1. Relationship between the Relevant Titanium Alloys

In *General Corrosion and Localized Corrosion of the Drip Shield* (BSC 2003c), the corrosion of the inner surface of the drip shield is modeled based on a cumulative distribution function developed from the measured weight loss of specimens with the “weight loss” geometry (i.e., without a creviced area) exposed for 1-year in the LTCTF and validated by using the LTCTF 5-year exposure test data and literature information. The corrosion of the outer surface of the drip shield is represented in a cumulative distribution function developed from the measured weight loss of specimens with both the “weight loss” and “crevice” geometry exposed for 1-year in the LTCTF and validated by using the LTCTF 5-year exposure test data and literature information. The corrosion potential (E_{corr}) and critical potential ($E_{critical}$) are used to determine whether the mode of attack is general corrosion only or both general and localized corrosion. Figure 10-2 illustrates the modeling approaches adopted in the corrosion model of drip shield (BSC 2003c).



* Section 6.1 covers conceptual models of DOX, HAC and APC

00363DC_119.ai

NOTE: Section numbers in this figure refer to *General Corrosion and Localized Corrosion of the Drip Shield* (BSC 2003c).

Figure 10-2. Corrosion Modes and Modeling Approaches in *General Corrosion and Localized Corrosion of the Drip Shield*

Hydrogen induced cracking of drip shield materials is discussed in the model report *Hydrogen Induced Cracking of Drip Shield* (BSC 2003j). Other factors, such as the effects of calcium chloride, fluoride, radiolysis, MIC, aging and phase instability on corrosion of Titanium Grade 7 are also considered in *General Corrosion and Localized Corrosion of the Drip Shield* (BSC 2003c).

10.2 DRY OXIDATION

The rate of dry oxidation will be limited by mass transport through this growing metal oxide film. According to Fick's First Law and assuming a linear concentration gradient across the oxide film of thickness x , the flux can be expressed as

$$J_{oxide} = -D_{oxide} \frac{\partial C}{\partial x} \approx -D_{oxide} \frac{\Delta C}{x} \quad (\text{Eq. 10-1})$$

Manipulation of Equation 10-1 and using the available experimental data obtained by Schutz and Thomas (1987) and applying the Arrhenius relationship leads to Equation 10-2 and Table 10-3.

$$X_{nm} = 7643 e^{-5898/T} t^{1/2} \quad (\text{Eq. 10-2})$$

where X_{nm} is the oxide thickness in nanometers, T is the temperature in Kelvin and t is the time in minutes. A comparison of oxide thickness as calculated by the model with measured values is presented in Table 10-3.

Table 10-3. Dry Oxidation Titanium Oxide Thickness: Measured versus Calculated Using Equation 10-2

Time	Titanium Oxide Thickness (nm)							
	100°C (373 K)	200°C (473 K)	400°C (673 K)		500°C (773 K)		600°C (873 K)	
	Calc'd	Calc'd	Measured	Calc'd	Measured	Calc'd	Measured	Calc'd
10 (min)	0.0	0.1	4.4	3.8	17.8	11.8	31.1	28.2
30 (min)	0.0	0.2	8.9	6.6	23.3	20.4	53.3	48.9
60 (min)	0.0	0.2	11.1	9.3	27.8	28.9	83.3	69.1
120 (min)	0.0	0.3	11.1	13.1	31.1	40.8	96.7	97.8
1 (yr)	0.8	21.3	-	866	-	2691	-	6449
100 (yr)	7.5	212.9	-	8661	-	26910	-	64489
1,000 (yr)	23.8	673.3	-	27387	-	85098	-	203935
10,000 (yr)	75.2	2129.2	-	86605	-	269103	-	644899

Source: Output DTN: MO0306SPAGLCDS.001. Measured oxide thickness values from DTN LL000201305924.120.

Equation 10-2 and Table 10-3 are based on the parabolic law of oxidation. An alternate conceptual model based on the logarithmic law predicts an even lower oxidation rate. While the parabolic law provides a conservative approach and the logarithmic law may provide a liberal approach, both models predict the dry oxidation rates of Titanium Grade 7 to be far less than the roughly 1,500 nm/yr that is required to corrode through the approximately 15 mm thick drip shield in 10,000 years. Therefore, the dry oxidation of Titanium Grade 7 under the repository conditions was excluded from further modeling in TSPA.

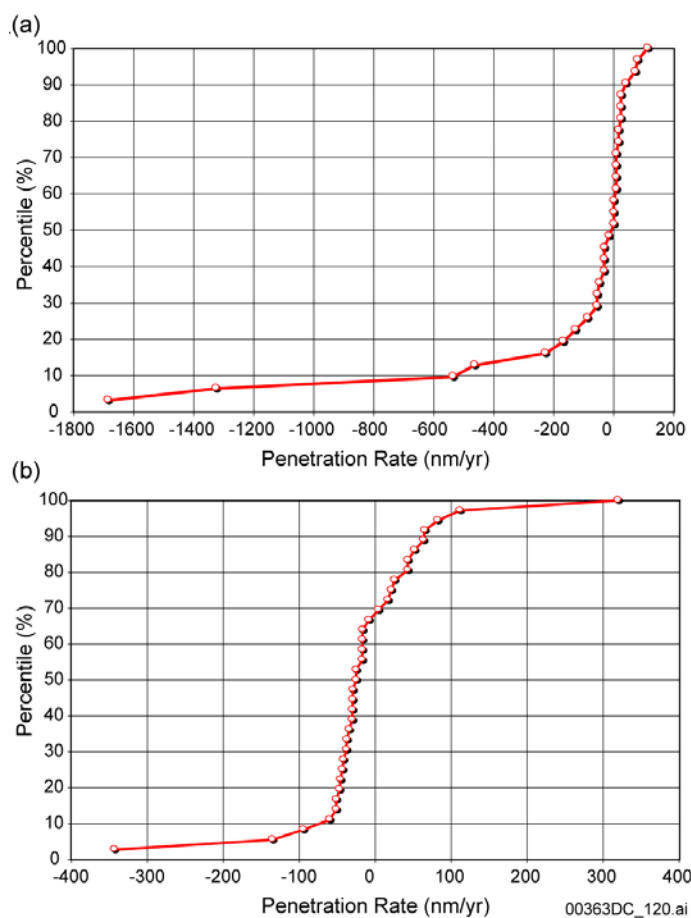
10.3 GENERAL CORROSION

All general corrosion rates, except the dry oxidation rates, are calculated by using weight-loss data obtained at the LTCTF (Estill 1998). The long-term corrosion tests performed at the LTCTF employed two types of specimen geometries, i.e., weight loss specimens and creviced specimens. Both types of specimens were exposed to repository relevant environments for 1 year and 5 years. Correspondingly, there are two types of data treatments in this section. The treatment using corrosion rate data from weight loss specimens only is referred to as the “weight loss only” treatment and that is used to model the general corrosion rates on the inner surfaces of the drip shield. The treatment using a combination of corrosion rate data from both weight loss and creviced specimens is referred to as the “weight loss plus crevice” treatment and is used to represent the general corrosion rates on the outer surfaces of the drip shield.

The weight loss testing includes a wide range of plausible test media, including SDW, SCW, and SAW described in *General Corrosion and Localized Corrosion of the Drip Shield* (BSC 2003c). The SCW test medium is three orders of magnitude (1,000×) more concentrated in some species than J-13 well water and is slightly alkaline (pH approximately 8). The SAW test medium is three orders of magnitude (1,000×) more concentrated in some species than J-13 well water and is acidic (pH approximately 2.7). Two temperature levels (60°C and 90°C) are included in this testing program. The general corrosion measurements and corrosion rate calculation are based upon ASTM G 1-90 1999.

The posttest specimen treatments were different for the 1-year test and 5-year test. The 1-year specimens were cleaned with deionized water and a nylon brush (Estill 1998). In contrast, the 5-year specimens were cleaned more thoroughly and carefully as discussed in DTN: LL030205912251.016 and the scientific notebook referenced therein. Since very little cleaning was performed for the 1-year samples, the incomplete removal of oxide may well account for the large negative values in Figure 10-3. The corrosion rates calculated based on the weight loss show significant scatter. Therefore, the data are presented as cumulative distribution functions.

Corrosion Rates Based Upon 1-Year Weight Loss Measurements—All general corrosion rates for Titanium Grade 16 based on LTCTF 1-year weight loss samples are shown in Figure 10-3. It appears that these measurements are independent of temperature between 60°C and 90°C. Furthermore, the composition of the test medium (SDW, SCW, or SAW) appeared to have little impact on the measurements. With the exception of five outliers, all of the rates plotted in Figure 10-3 are between -200 and +200 nm/yr. The median is at approximately 0. The outliers with large negative rates are believed to be due to improper cleaning and or measurement errors or a combination of both.



Source: DTN: LL000209305924.129.

Figure 10-3. Distribution of General Corrosion Rates of Titanium Grade 16: (a) Long Term Corrosion Test Facility 1-Year Weight Loss Samples and (b) 1-Year Crevice Samples

Similarly, all general corrosion rates for Titanium Grade 16 based on LTCTF crevice samples (DTN: LL000209305924.129) are shown in Figure 10-3. Corrosion rates are calculated based on the areas outside of the crevice. In this case, it also appears that the measurements are independent of temperature and test medium. Most of the rates plotted in Figure 10-3 are between -350 and $+350$ nm/yr. The median is at approximately 0. The largest measured rate shown in Figure 10-3, which is less than $+350$ nm/yr, will not lead to failure of the drip shield during the 10,000-year lifetime. Based upon these data, it does not appear that the life of the drip shield will be limited by the general corrosion of Titanium Grade 16 (an analog of Titanium Grade 7) at temperatures less than those involved in the test (90°C) during a period of 10,000 years.

Corrosion Rates Based Upon 5-Year Weight Loss Measurements—General corrosion rates of Titanium Grade 16 in SCW and SDW at LTCTF for 5 years at the LTCTF were also obtained. The general corrosion rates for Titanium Grade 16 based on LTCTF 5-year weight loss specimens and crevice samples in SDW and SCW are shown in Figure 10-4.

The 5-year weight loss specimen data had a maximum value of about 58 nm/yr with most of the other values under 20 nm/yr. The 5-year crevice specimen data shows a maximum value of about 77 nm/yr with most of the values below about 30 nm/yr. The median is at approximately 5 nm/yr and 10 nm/yr for weight loss specimens and crevice specimens, respectively.

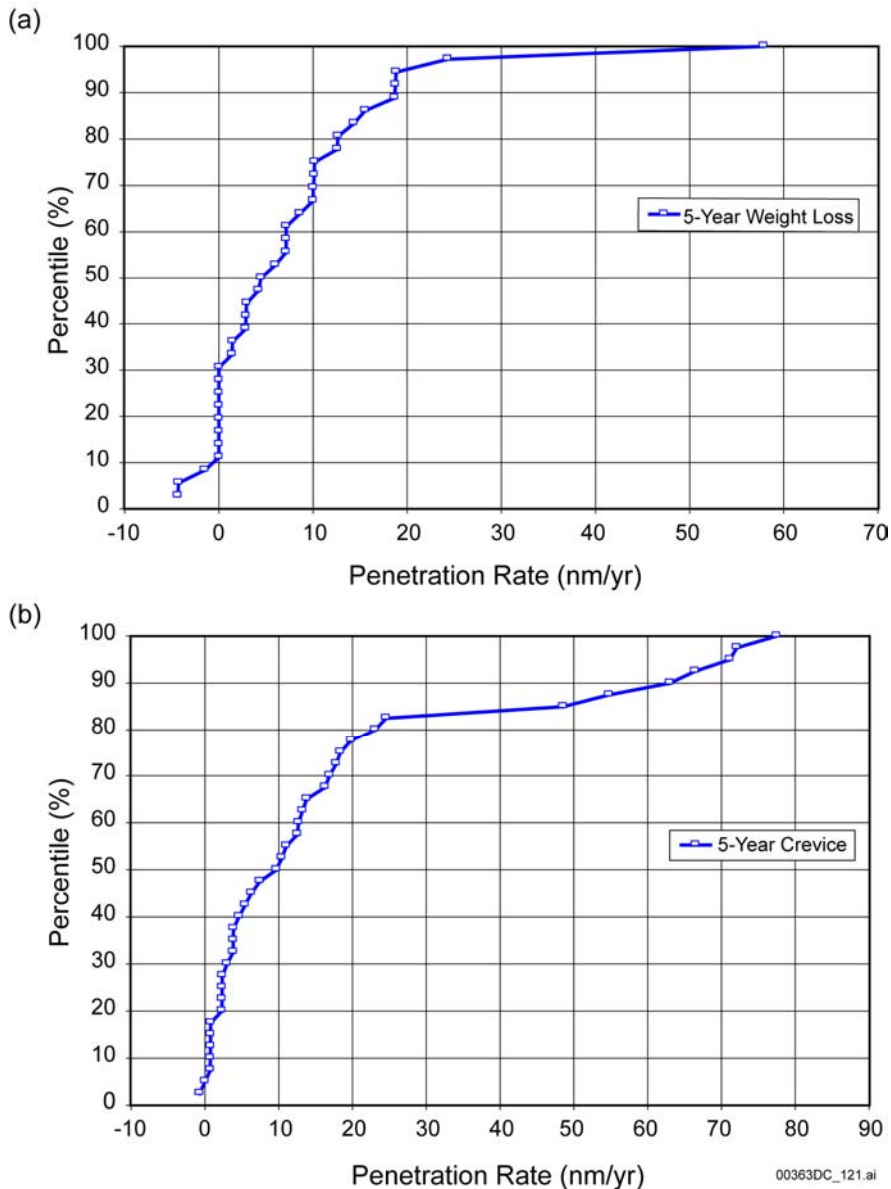
In contrast to the 1-year exposure results, the corrosion rates obtained from the 5-year exposure tests contain very few negative values. The median corrosion rate for the 5-year data is higher than that of the 1-year data. This is not surprising considering the difference in posttest sample treatment in the 1-year tests and 5-year tests. The 1-year specimens were cleaned with deionized water and a nylon brush (Estill 1998). In contrast, the 5-year specimens were cleaned more thoroughly and carefully as discussed in DTN: LL030205912251.016) and the scientific notebook referenced therein. Complete descaling was observed and no corrections for scale deposits were needed.

The maximum and median values of 1-year and 5-year corrosion rate data are summarized in Table 10-4.

Table 10-4. Summary of 1-Year and 5-Year Corrosion Data Comparison

Specimen Type	1-Year (nm/yr)		5-Year (nm/yr)	
	Weight-Loss	Crevice	Weight-Loss	Crevice
Median	0	0	5	10
Maximum	200	350	58	77

Source: Output DTN: MO0306SPAGLCDS.001.



Source: Input DTN: LL030205912251.016; Output DTN: MO0306SPAGLCDS.001.

Figure 10-4. Distribution of General Corrosion Rates of Titanium Grade 16: (a) Long Term Corrosion Test Facility 5-Year Weight Loss Specimens and (b) 5-Year Crevice Specimens

Composite Model for the General Corrosion Rates for Drip Shield—The primary difference between the exposure environments on the inner and the outer surfaces of the drip shield is that the drip shield outer surface may be exposed to a more complicated chemistry and geometry since dust and (or) mineral films (from evaporation of dripping water) may form crevices on the drip shield outer surfaces. In contrast, the inner surfaces of the drip shield will not be exposed to dripping water or significant dust film formation. Therefore, the general corrosion of the inner surface and the outer surface of the drip shield are modeled by using different sets of corrosion data (i.e., the general corrosion of the inner surface of the drip shield is represented by a cumulative distribution function generated from the LTCTF weight-loss samples only, while the general corrosion rates of the outer surface of the drip shield are represented by a cumulative distribution function generated from combining both the LTCTF weight-loss samples and the crevice samples). The negative values of the weight loss for both cases were conservatively removed from the distribution. For the weight loss case, the rate at the 50th percentile is approximately 18 nm/yr, the rate at the 90th percentile is approximately 75 nm/yr, and the maximum rate is less than 120 nm/yr. For the weight loss plus crevice case, the rate at the 50th percentile is approximately 25 nm/yr, the rate at the 90th percentile is approximately 100 nm/yr, and the maximum rate is less than 350 nm/yr. About 10 percent of all the values fall between 100 and 350 nm/yr.

10.4 LOCALIZED CORROSION

The localized corrosion model for the titanium drip shield assumes that localized attack occurs if the open-circuit corrosion potential (E_{corr}) exceeds or is equal to the threshold potential for breakdown of the passive film ($E_{critical}$), i.e.,

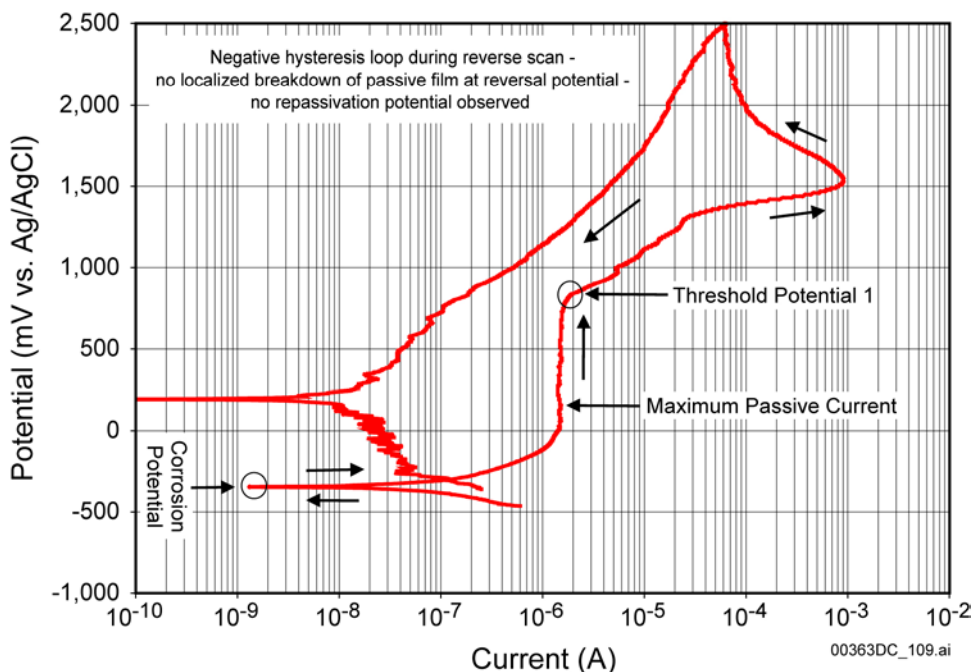
$$E_{corr} \geq E_{critical} \quad (\text{Eq. 10-3})$$

In *General Corrosion and Localized Corrosion of the Drip Shield* (BSC 2003c), the threshold potential is defined as the potential where the current density in a cyclic polarization forward scan significantly increases, rather than the potential at which any specific value of the current density is reached.

Cyclic Polarization in Synthetic Concentrated J-13 Well Waters—The Yucca Mountain Project has used the cyclic polarization method to determine the threshold potentials for titanium alloys in various test media relevant to the environments expected in the repository. Relevant test environments include SDW, SCW, and SAW at 30°C, 60°C, and 90°C, as well as SSW at 100°C and 120°C. The chemical compositions of these test media are detailed in *General Corrosion and Localized Corrosion of the Drip Shield* (BSC 2003c).

The cyclic polarization measurements technique is based on ASTM G 5-94 1997. A representative cyclic polarization curve (DTN: LL010105512251.011 S01009_001) is shown in Figure 10-5. The cyclic polarization data for Titanium Grade 7 in repository-relevant conditions are summarized in DTN: LL010105512251.011 S01009_004.

In general, complete passivity (no passive film breakdown) is shown by these curves between the corrosion potential and the point defined as the threshold potential ($E_{critical}$).



Source: DTN: LL010105512251.011.

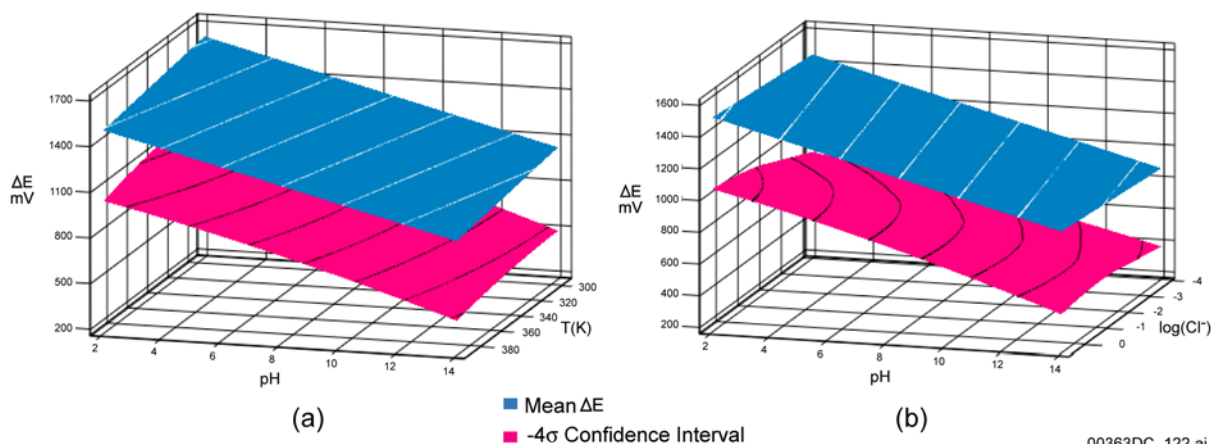
Figure 10-5. Titanium Grade 7 in Simulated Saturated Water at 120°C (NEA031s)

Correlation of Potential versus Temperature and Composition for Various Test Media—The susceptibility of the material to localized corrosion is represented by Equation 10-3. The experimentally obtained E_{corr} and $E_{critical}$ values have been used to fit the difference (ΔE) between the critical potential for localized corrosion initiation, $E_{critical}$, and the corrosion potential, E_{corr} , as a function of absolute temperature, T , solution pH , and the chloride ion concentration, that is,

$$\Delta E = d_0 + d_1 \cdot T + d_2 \cdot \log(Cl^-) + d_3 \cdot pH + \varepsilon \quad (\text{Eq. 10-4})$$

where d_0 , d_1 , d_2 , and d_3 are constants determined from fitting Equation 10-4. The calculation is documented in detail in *Abstraction of Models for Pitting and Crevice Corrosion of Drip Shield and Waste Package Outer Barrier* (BSC 2001c, Attachment I, pp. I-8 to I-12). ε , the model error term, is a term representing data variance not explained by the fitting procedure and has a normal distribution with a mean of 0 (BSC 2001c, Section 5.4) and variance of 10,500 (BSC 2001c, Section 6.4.1). The median values of these parameters are: $d_0 = 2050$, $d_1 = -1.17$, $d_2 = 14.1$, and $d_3 = -48.9$, respectively.

Figure 10-6 contains plots of ΔE versus pH and temperature under constant chloride concentration and ΔE versus pH and chloride concentration under constant temperature using Equation 10-4. The figures taken together show that ΔE is significantly greater than 0 over all ranges of pH , chloride concentration, and temperature.



Source: BSC 2001c, Figures 5 and 6.

Figure 10-6. Plot of the Median ΔE and -4σ Confidence Interval Surface versus pH and Absolute Temperature at $[\text{Cl}^-] = 3 \text{ mol/L}$ (a) and versus pH and Base 10 Logarithm of Chloride Ion Concentration at $T = 300 \text{ K}$ for Titanium Grade 7 Using an Absolute Temperature of 380 K

Crevice Corrosion—Due to the corrosion resistance of Titanium Grade 7 (and Titanium Grade 16), relatively little data exist for crevice corrosion under plausible exposure conditions. Hua et al. (2002) performed tests for crevice corrosion of Titanium Grade 7 in BSW (BSW-12, 50,000 times more concentrated than J-13 well water by evaporation) (DTN: LL000320405924.146) for up to 8 weeks at temperatures from 60°C to 105°C. Although the Titanium Grade 7 specimens became discolored underneath the crevice formers after the test, no crevice corrosion was observed. It was also noticed that the preexisting surface imperfections, possibly due to material processing, remained after 4 and 8 weeks of exposure (Hua and Gordon 2003). The authors concluded that the observed weight losses were due to general corrosion only (Hua et al. 2002). In Lawrence Livermore National Laboratory tests, Titanium Grade 16 crevice specimens were immersed in SSW, SAW, SCW, and SDW at 60°C and 90°C (in SSW also at 120°C) for 1 year and in SAW, SCW, and SDW at 60°C and 90°C for 5 years. No crevice corrosion attack was reported. The critical crevice corrosion temperature, defined as the temperature above which crevice corrosion can occur, may be determined experimentally as, when increasing temperature, the corrosion potential and threshold potential become equal. This critical temperature was not observed in the Lawrence Livermore National Laboratory cyclic polarization tests at temperatures up to 120°C, suggesting that Titanium Grade 16 (Titanium Grade 7) does not suffer from crevice corrosion in repository environments under seepage conditions.

10.5 INFLUENCE OF FLUORIDE ON THE CORROSION OF TITANIUM GRADE 7

Detailed discussions of the possible detrimental effects of fluoride on corrosion of titanium have been provided in *General Corrosion and Localized Corrosion of the Drip Shield* (BSC 2003c, Section 6.3.7). This section briefly review the effects of fluoride on corrosion rates of titanium alloys and the role of oxide film on hydrogen absorption.

Role of Oxide Film on Titanium Alloys—Review of the titanium corrosion literature (BSC 2003c, Section 6.3.7) indicates that the presence of dissolved fluoride in a range of brine solutions may, under certain conditions, significantly increase the general corrosion rate of

titanium alloys including Titanium Grade 7. However, in reviewing the effects of fluoride on enhanced general corrosion, it is important to separate the studies into those using relatively freshly polished specimens and those where the specimens were prefilmed either through longer-term ambient air exposure or through higher temperature exposures prior to corrosion testing.

Effects of fluoride on freshly polished specimens can be significant. For instance, the effects of fluoride were found to decrease the E_{corr} and result in a pseudo active/passive transition with a subsequent potential independent current region with current density considerably higher than those typically encountered during passive dissolution (as high as 10^{-3} to 10^{-1} , as compared to approximately 10^{-6} A/cm² when without fluoride). In a number of environment, temperature, and pH conditions, investigators found a deleterious effect of fluoride ion on general corrosion rates and under some conditions on pitting resistance by using freshly polished specimens.

The importance of the condition of the passive film in resisting corrosion in neutral fluoride-containing solutions is well demonstrated (BSC 2003c). Consistent with the observations on the corrosion resistance benefits from the formation of a stable passive prefilm, excellent corrosion behavior has been observed on both uncreviced and creviced Titanium Grade 16 and Titanium Grade 7 specimens tested in the LTCTF as described previously (BSC 2003c). All of these LTCTF specimens were preexposed for several months to ambient air after polishing at the specimen fabricators shop and before placement in the corrosion tanks. No deleterious effects of fluoride on corrosion resistance of these titanium alloys were observed in any of these tests including tests in the so-called SCW environment (Table 2-2).

In the case of the drip shield application in the repository, there is an early period of ventilation. Under the repository conditions at Yucca Mountain, the Titanium Grade 7 drip shield surface will be covered with an oxide grown relatively slowly under thermal conditions. Such a film is expected to have a low defect density (BSC 2003c) and, hence, should be highly resistant to dissolution including that induced by reaction with F⁻. In addition to the described benefit of forming a stable, low defect density passive film on titanium before immersion in fluoride containing brines, there can be beneficial effect from other ions in the brine solution that are available in the repository environment.

Based on the above discussion, it is not surprising that no influence of F⁻ is observed on the passive corrosion rate of titanium specimens in the LTCTF tests. The concentration of F⁻ in these tests is either limited to low values by precipitation in a high calcium environment, or, even when present in substantial amounts, displaced as an absorbed species from the passive surface by a much higher concentration of the other anions present. Additionally, the presence on the specimens of an air-formed film with a low defect concentration formed prior to immersion in the test would eliminate the possibility of fluoride-induced passivity loss and maintain very low passive corrosion rates.

10.6 INFLUENCE OF CALCIUM CHLORIDE ON LOCALIZED CORROSION OF TITANIUM GRADE 7

The potential for the development of environments containing high concentrations of calcium chloride ions has been proposed (BSC 2001b, Section 7.3.1). As a result, effects of highly concentrated calcium chloride solutions on the Titanium Grade 7 passive film behavior are evaluated.

Table 10-5. General Corrosion Rates of Titanium Grade 7 in Selected Test Media Containing High Concentrations of Chlorides of Ca^{2+} , Mg^{2+} , and Fe^{3+} Ions at Elevated Temperature

Test Medium	Temperature	Corrosion Rate, mm/yr	Source
62% CaCl_2	150°C	nil	Schutz and Thomas 1987, Appendix 2, p. 705
10 and 30% FeCl_3	Boiling	nil	Schutz and Thomas 1987, Appendix 2, p. 705
Saturated MgCl_2	Boiling	nil	Schutz and Thomas 1987, Appendix 2, p. 706

Source: Output DTN: MO0306SPAGLCDS.001.

The effect of Ca^{2+} and Mg^{2+} on general corrosion of Titanium Grade 7 at elevated temperatures is insignificant as shown in Table 10-5. The Ca^{2+} and Mg^{2+} containing environments do not promote the initiation of localized corrosion. This is demonstrated in the Lawrence Livermore National Laboratory cyclic polarization tests. For Titanium Grade 7 in 8 to 9 M CaCl_2 and 9 M $\text{CaCl}_2 + 0.9 \text{ M Ca(NO}_3)_2$ at 100°C and 150°C, the $\Delta E_s (= E_{critical} - E_{corr})$ are in the range of 1.5 to 3.5 V. A more detailed discussion on the mechanism of incorporation of Ca^{2+} and Mg^{2+} into the passive film on titanium alloys can be found in *General Corrosion and Localized Corrosion of the Drip Shield* (BSC 2003c).

10.7 ENVIRONMENTALLY ASSISTED CRACKING OF THE DRIP SHIELD

10.7.1 Stress Corrosion Cracking of Drip Shield

A repository environment is unique in that, in the absence of disruptive events (e.g., rockfall, drift collapse, seismicity), there is no source of dynamic loading. Furthermore, in the repository, the Titanium Grade 7 drip shields will be fully stress-relief annealed before emplacement, meaning there will be no significant residual stress fields to drive SCC initiation and propagation. For this reason, SCC will not occur in the drip shields during the regulatory period.

The effect of rockfall on drip shield performance is considered in *Stress Corrosion Cracking of the Drip Shield, the Waste Package Outer Barrier, and the Stainless Steel Structural Material* (BSC 2003a). It is concluded that SCC could be initiated due to rockfall-induced stresses in the drip shield. However, the SCC cracks tend to be very tight by nature. As the crack grows through-wall, the tensile stresses normal to the crack walls are relieved, and the resulting crack faces continue to corrode by general corrosion. It is estimated that it would take approximately 3,400 years for the crack to fill with corrosion products. In the interim, there could be a small amount of water transport by surface diffusion (film flow) into the crack and through the drip shield. However, the heat differential across the drip shield wall will result in evaporation of the slowly flowing water and formation of a scale deposit (principally calcium carbonate-[calcite]) over the crack where it intersects the upper drip shield surface, as well as within the crack. It is estimated that SCC cracks are sealed in a few hundred years, at most, when water is allowed to flow through the cracks at the expected very low film-flow rate. If the cracks are bridged by water, the sealing process may take longer, but no flow occurs since the water is held by capillary forces. After crack plugging, there is effectively no solution flow through the crack region. Therefore, since the primary role of the drip shield is to keep water from contacting the waste package, SCC of the drip shield does not compromise its intended function.

10.7.2 Hydrogen-Induced Cracking of Drip Shield

Critical Hydrogen Concentration (H_C) of Titanium Grade 7—The only way that an addition of palladium might deteriorate the resistance of titanium alloys to hydrogen induced cracking is through microstructure change. Titanium Grade 16 was developed based on the excellent corrosion performance of Titanium Grade 7 with a more cost effective palladium content (0.04 to 0.08 weight percent). Titanium Grade 7 and Titanium Grade 16 are virtually identical alloys except for their palladium content (Figure 10-1, Tables 10-1 and 10-2). Increasing the palladium content from 0.04 to 0.08 weight percent to 0.12 to 0.25 weight percent does not influence the mechanical properties of the material since addition of palladium does not alter the microstructure of titanium alloys (Schutz and Xiao 1993).

Based on the effect of palladium on hydrogen absorption and microstructure of titanium alloys, it has been concluded that the hydrogen induced cracking behavior of Titanium Grade 7 should be at least as good as, if not superior to, that of Titanium Grade 16 (i.e., H_C approximately 1,000 $\mu\text{g/g}$). Choosing the H_C as 1,000 $\mu\text{g/g}$ for Titanium Grade 7, which was obtained for Titanium Grade 16, is not only appropriate but also sufficiently conservative (BSC 2003j).

Critical Hydrogen Concentration of Titanium Grade 24—The experimentally obtained critical hydrogen concentration for Titanium Grade 24 is not available at this time. However, the comparative corrosion behavior of Titanium Grade 24 and an approximate H_C value of this alloy can be estimated based on the available information on other titanium alloys (e.g., Titanium Grade 5), and based on the relationship between Titanium Grades 2, 16 and 7 as shown in Figure 10-1.

Based on the experimental data of Titanium Grade 5 and the role of palladium in improving resistance to hydrogen induced cracking of titanium alloys, it is clear that the addition of palladium should lead to a higher value of the H_C in Titanium Grade 24 through a similar mechanism to the increase in H_C observed when Titanium Grade 2 is alloyed with the same amount of palladium to produce Titanium Grade 16. The H_C for Titanium Grade 5 was obtained as 200 $\mu\text{g/g}$ with precracked specimens (Hardie and Ouyang 1999). A modest improvement, considering the demonstrated benefit of palladium, to 600 $\mu\text{g/g}$, if not higher, is not an unreasonable H_C value for Titanium Grade 24. However, considering the higher strength of Titanium Grade 24 than Titanium Grade 16 and Titanium Grade 7, it can be estimated conservatively, based on the above analysis, that the H_C of Titanium Grade 24 is at least in the range of 400 to 600 $\mu\text{g/g}$, if not higher. This estimated value of H_C is realistic and conservative. For instance, Kitayama et al. (1992) evaluated the effect of palladium addition to Ti-6Al-4V (Titanium Grade 5) and Ti-3Al-2.5V (Titanium Grade 9) on their hydrogen induced cracking behavior. By cathodically charging hydrogen to palladium-containing Ti-6Al-4V (an equivalent to Titanium Grade 24) to approximately 1,000 ppm, the 0.2 percent proof stress was found to be about 175 ksi (Kitayama et al. 1992), which was similar to ASTM specifications for the minimum 0.2 percent proof stress for Titanium Grade 24 (ASTM B 265). This suggests that no degradation in mechanical properties was observed.

Brief Review of Modeling of Hydrogen Induced Cracking of the Drip Shield—Modeling of hydrogen induced cracking of the drip shield is developed in *Hydrogen Induced Cracking of Drip Shield* (BSC 2003j) by using previously reported 1-year corrosion rates of Titanium

Grade 16 obtained at the LTCTF. After 1-year exposure, the measured corrosion rate at the 50th percentile was approximately 25 nm/yr (25×10^{-6} mm/yr); the rate at the 90th percentile was approximately 100 nm/yr (100×10^{-6} mm/yr); and the maximum rate was less than 350 nm/yr (350×10^{-6} mm/yr) (BSC 2003c). Corrosion data after 5-year exposure have been acquired more recently from the LTCTF and documented in *General Corrosion and Localized Corrosion of the Drip Shield* (BSC 2003c). The maximum possible general corrosion rates of the drip shield are 77 nm/yr (77×10^{-6} mm/yr) and 58 nm/yr (58×10^{-6} mm/yr) for crevice specimen and weight loss specimen, respectively. The average of the corrosion rates of weight loss specimens and weight loss plus crevice specimens is 68 nm/yr (68×10^{-6} mm/yr). It can be seen that these corrosion rates are significantly lower than the 1-year exposure data.

Shoesmith et al. (1997) developed a method to estimate the hydrogen content in titanium alloys due to passive dissolution. The details of the approach can be found in *Hydrogen Induced Cracking of Drip Shield* (BSC 2003j) and the work performed by Greene et al. (2001). Applying the method using the 5-year corrosion rate data and a hydrogen absorption efficiency fraction of 0.015, the hydrogen content in Titanium Grade 7 due to passive dissolution over a time span of 10,000 years can be estimated as:

$$H_A = 124 \mu\text{g/g} \ll H_C = 1,000 \mu\text{g/g}. \quad (\text{Eq. 10-5})$$

where H_A is the hydrogen concentration in the metal absorbed during the passive dissolution.

The hydrogen induced cracking model developed in *Hydrogen Induced Cracking of Drip Shield* (BSC 2003j) is based on the assumption that both the hydrogen generation and diffusion rates are constant. A literature review shows that both of these assumptions are conservative. A considerable amount of literature exists to show that the rate of hydrogen absorption decays following a parabolic relationship. It should be noted that the fractional hydrogen absorption efficiency (f_h) used in the calculation (0.015) is similar to that Okada (1983) obtained experimentally for Titanium Grade 2 under constant applied current conditions with an applied current of 0.5 mA/cm² at 25°C in sodium sulfate solutions (pH of 4). The electrode potential achieved during these experiments was $-1.14 \text{ V}_{(\text{SCE})}$, about -0.5 V more negative than the threshold value of $-0.6 \text{ V}_{(\text{SCE})}$ for significant hydrogen absorption (Okada 1983). This low of a potential is not likely to be achieved by galvanic coupling to less noble metals (e.g., carbon steel). Therefore, the above calculated 124 $\mu\text{g/g}$ in 10,000 years has included the worst case scenario when the titanium alloys are galvanically coupled to less noble metals, although this is not likely to occur in the repository.

Given the high critical hydrogen concentration, the large volume of available titanium in the drip shield into which absorbed hydrogen can diffuse, and other reasons stated above, hydrogen embrittlement of the titanium drip shield is highly unlikely.

10.8 OTHER FACTORS POTENTIALLY AFFECTING DRIP SHIELD CORROSION

Other factors that might potentially influence the corrosion of the drip shield materials such as gamma radiolysis, MIC, aging and phase stability and irregular environmental conditions are also discussed in *General Corrosion and Localized Corrosion of the Drip Shield* (BSC 2003c) and are summarized below.

Gamma Radiolysis—Studies on the effects of gamma radiolysis on corrosion of titanium alloys showed that the effects of radiolysis on corrosion of the drip shield material is insignificant. For instance, Smailos and Köster (1987, Figure 8) observed that even when exposed to a radiation field of 10^5 rad/hr (10^3 Gy/hr) in salt brines containing aggressive oxidants, the corrosion rate of a titanium-palladium alloy after 610 days exposure stabilized at a rate of less than 1 nm/yr. (The maximum radiation field for the drip shield is expected to be about 10^2 Gy/hr). In the absence of the radiation field, the corrosion rate stabilized at about 0.1 nm/yr. Gamma irradiation exposure experiments in aggressive $MgCl_2$ brines showed, even at dose rates above 1,000 rad/hr, only a minor enhancement of film growth rates on Titanium Grade 7 was observed and passivity was not threatened (Shoesmith and King 1998, p. 30). Based on these data, it is concluded that, even in aggressive $MgCl_2$ brines, the radiation levels in the repository are not high enough to result in an enhancement of corrosion processes on Titanium Grade 7.

Microbially Influenced Corrosion—Corrosion handbooks and literature reviews generally state that titanium alloys are immune to microbially influenced corrosion (Revie 2000). It is the remarkable stability of the TiO_2 passive film formed on titanium alloys that confers this immunity. While titanium is susceptible to biofouling in seawater solutions, the biofilm does not compromise the integrity of the passive film and therefore, biofouled titanium maintains its resistance to localized corrosion processes (Revie 2000, Chapter 47). It has been reported that production of nitrates, polythionates, thiosulfates, and oxygen associated with aerobic biologic activity does not significantly increase the corrosion rate of titanium alloys (Brossia et al. 2001, Section 4.1.3). Therefore, MIC is expected to have no significant effect on either general or localized corrosion processes of titanium alloys under the exposure conditions in the repository.

Aging and Phase Instability—Pure titanium is an allotropic element, existing in more than one crystallographic form (Gdowski 1997). Above $883^\circ C$ it has the body-centered cubic crystal structure, which is called the beta (β) phase. Below $883^\circ C$, it transforms to a hexagonal close packed structure, which is called the alpha (α) phase. Both Titanium Grades 7 and 16 are α -phase alloys and have very small additions of palladium. The solubility of palladium in these materials is about 1 weight percent at $400^\circ C$. The nominal concentrations of palladium in both Titanium Grades 7 and 16 are well below the solubility limit at this temperature (Gdowski 1997, pp. 1 to 8). Intermetallic compounds capable of being formed in this system have not been reported to occur in Titanium Grades 7 and 16 with normal heat treatments.

Therefore, the effects of phase instability possibly caused by thermal processes (e.g., welding) on degradation of Titanium Grades 7 and 16 will be insignificant. The effects of nonthermal processing of Titanium alloys on their corrosion resistance and integrity are negligible.

Effects of Irregular Environmental Conditions—A 20-year atmospheric corrosion study has been performed (Covington and Schutz 1981) on titanium in a marine environment. The maximum corrosion rate was found to be 2.5×10^{-5} mm/yr (25 nm/yr). In the tests, approximately half of the samples were submersed and the other half were in the saturated vapor above the aqueous phase. There were a limited number of the samples at the water line. No difference in corrosion rates of these samples was observed because of the different environments.

10.9 SUMMARY OF DEGRADATION OF DRIP SHIELD MATERIALS

- Dry oxidation of the drip shield does not need to be explicitly modeled in TSPA.
- Based upon LTCTF test data, it does not appear that the life of the drip shield will be limited by general corrosion of Titanium Grade 16 (an analog of Titanium Grade 7) at temperatures less than those involved in the test (90°C) during a period of 10,000 years.
- It is also concluded that the presence of a high concentration of CaCl₂ and fluoride ions will not significantly enhance the general corrosion of drip shield material under the repository conditions.
- Based on test results, localized corrosion initiation (and hence propagation) does not need to be implemented in TSPA. It is not likely that calcium chloride will have a significantly detrimental effect on the localized corrosion resistance of Titanium Grade 7. Also, crevice corrosion of Titanium Grade 7 and Titanium Grade 16 is not likely to occur under repository conditions.
- The hydrogen induced cracking behavior of Titanium Grade 7 should be at least as good as, if not superior to, that of Titanium Grade 16 (H_C approximately 1,000 µg/g). Choosing the H_C as 1,000 µg/g for Titanium Grade 7, which was obtained for Titanium Grade 16, is not only appropriate but also sufficiently conservative.
- The H_C of Titanium Grade 24 is at least in the range of 400 to 600 µg/g, if not higher. This estimated value of H_C is conservative.
- Other factors that might potentially influence the corrosion of the drip shield materials such as gamma radiolysis, MIC, aging and phase stability, and irregular environmental conditions are also concluded to be insignificant contributors to the drip shield corrosion.

INTENTIONALLY LEFT BLANK

11. CONCLUSIONS

This technical basis document discusses the degradation processes and models for evaluating long-term performance of the waste package and drip shield materials. Models have been used to analyze the degradation of the Alloy 22 outer shell of the waste package and the drip shield by general and localized corrosion, and SCC under the expected repository exposure conditions, and over the repository performance period.

The cumulative effect of several degradation modes on material performance are included in the waste package and drip shield design process. The design incorporates the effect of general corrosion and structural considerations by determining the appropriate thickness for the corrosion shell. For other modes, fabrication controls and specific design features are instituted to ensure adequate waste package performance during the required regulatory period.

The waste package and drip shield will experience a range of ambient conditions and degradation modes that will determine their overall performance. The modes of degradation are determined by the three thermal regimes of operation, and are summarized below.

11.1 THERMAL REGIMES

During the regulatory period of 10,000 years, the waste package and drip shield materials experience three distinct thermal regimes that are important to the identification of applicable corrosion processes. These three regimes are summarized below.

Dryout Regime (Temperature at the Drift Wall is Greater Than or Equal to the Boiling Point of Seepage Water)—During the preclosure period, the waste package will be kept dry by ventilation air. During the thermal pulse, heat generated by radioactive decay will eventually increase the temperature of the waste package, drip shield and drift wall to a level above the boiling point, where the probability of seepage into drifts will become insignificant. Phase and time-temperature-transformation diagrams predicted for Alloy 22, and validated with experimental data, indicate no significant phase instabilities (long-range ordering and tetrahedrally close packed precipitation) at temperatures below 200°C for 10,000 years. Also, dry oxidation at these elevated temperatures will not limit waste package life. After the peak temperature is reached, the waste package will begin to cool, eventually reaching a point where deliquescent brine formation may occur. While the formation of deliquescent brines may be possible at temperatures above the boiling point of the seepage water, these brines are generally nitrate- and sulfate-rich. No localized corrosion of Alloy 22 has been observed beneath films of CaCl₂ deliquescent brines at 150°C and 22.5 percent relative humidity (close to deliquescence point).

Transition Regime (Temperature at the Drift Wall is at or below the Boiling Point of Seepage Water, and Temperature at the Waste Package and Drip Shield Surfaces is at or above the Boiling Point of the Seepage Water)—Seepage into the drifts will become possible as the waste package cools, as the temperature of the drift wall drops below the boiling point of water, and while the waste package surface temperature is at or above the boiling point of the water. Corrosion in a concentrated, possibly aggressive, liquid-phase brine, evolved through evaporative concentration, is possible while in this regime. However, based upon detailed

modeling of the in-drift water chemistry more than 99 percent of the time-integrated seepage water entering the drift is predicted to evolve as chloride-sulfate or bicarbonate brines at the endpoint. Less than 1 percent will evolve to aggressive calcium chloride brines at the endpoint. Application of the localized corrosion initiation model (Section 7) to the range of water chemistries predicted with the engineered barrier system chemistry model (Section 1) indicates that the initiation of localized corrosion is possible under certain conditions where nitrate-to-chloride ratios in the brines reach low levels. Rates of uniform general corrosion are relatively insignificant, and Alloy 22 has been shown to be very resistant to SCC in a broad range of expected environments, even after 5-year exposures. However, SCC is conservatively assumed to occur if the threshold stress and stress intensity factor criteria are exceeded. The possibility of SCC is further diminished by the application of stress mitigation processes, such as laser-shock peening or controlled plasticity burnishing, and physical isolation of welded regions from corrosive environments.

Low Temperature Regime (Temperature at the Waste Package Surface is less than the Boiling Point of Seepage Water)—Continued cooling will eventually lower the temperature below the boiling point of the seepage water. Once the waste package temperature drops below the critical temperature for crevice corrosion in a given environment, localized corrosion no longer has the potential to occur. However, SCC is still assumed to occur if the threshold stress and stress intensity factor criteria are exceeded. Further, the rates of general corrosion in this regime are extremely low.

11.2 DEGRADATION MODES

As discussed in the preceding section, the waste packages and drip shields are subject to a number of degradation modes. The important aspects of degradation modes are discussed here. At high temperature, in the absence of aqueous films on the surfaces of the engineered barriers, high temperature oxidation is the dominant degradation mode. As the temperature decreases during cooling, aqueous phase electrolytes will develop on the drip shield and waste package surfaces, first through the formation of deliquescent brines, and then through the evaporative concentration of seepage waters. Modes of attack experienced in aqueous electrolytes include general (uniform) corrosion, localized corrosion, and SCC. Finally, the presence of microbes can alter the chemistry of the aqueous films, hence the corrosion rates of the aqueous degradation modes. Each of the degradation modes is summarized below.

Long-Term High-Temperature Phase Stability of Alloy 22—As mentioned in the discussion of the dryout regime, predictions of multicomponent phase diagrams and time-temperature-transformation diagrams are used to calculate the rate at which the phases (precipitates and long-range ordering) develop. These predictions indicate insignificant precipitation and long-range ordering during the 10,000-year lifetime of the repository, for sustained waste package temperatures below 200°C. The peak waste package temperature for the license application design is below 200°C, however, higher temperatures (up to about 300°C) may be possible due to drift collapse, but for only for a period of a few decades to a few centuries, and this will not degrade long-term performance.

High-Temperature Oxidation Processes—Dry oxidation is a high-temperature degradation mode. The reaction of oxygen with Alloy 22 and Titanium Grade 7 can cause a uniform

thickening of the oxide layer on their surfaces. The surface oxide layers can consist of any of the oxides of the alloying elements and (or) constituents. A chromium oxide layer has been assumed as the basis of approximate calculations for Alloy 22. The rate of dry oxidation at the highest temperature in the repository is insignificant compared to other modes of attack.

General Corrosion—For general corrosion, the rate of dissolution is uniform over all surfaces, and is due to the transport of cations from the metal-oxide interface to the oxide-electrolyte interface, where the formation of soluble metal-containing corrosion products can occur. The transport of cations and (or) anions through the passive oxide film is controlled by diffusion and electric field-driven electromigration. Corroboration of the very low rates obtained from the experimentally benchmarked Alloy 22 temperature-dependent general corrosion model with the rates from alternative techniques from the scientific literature confirms the life of the waste package will not be limited by the rate of uniform, general corrosion. Similarly, for the Titanium Grade 7 drip shield material, the lifetime will not be limited by the rate of uniform corrosion, and also, it is concluded based on long-term corrosion test results and relevant literature data that the presence of a high concentration of CaCl_2 and fluoride ions will not significantly accelerate the general corrosion of drip shield material under repository conditions.

Localized Corrosion—Localized corrosion is any type of distributed, nonuniform, corrosive attack of the surface, and is due to localized failure of the passive film. Such localized failure may be due to surface inclusions of relatively soluble species, the precipitation of small soluble halide crystallites on the passive film and destabilization of the passive film within occluded areas such as crevices. For Alloy 22, localized attack may also occur at sites where intermetallic precipitation has occurred.

Localized corrosion margin is defined by the potential difference between the crevice repassivation potential and the long-term corrosion potential. The localized corrosion initiation model indicates that localized corrosion of Alloy 22 is possible over a range of temperatures where brine compositions with low nitrate-to-chloride ratios (approximately 0.2 or less) are present. This could be the case for some seepage brines, which could potentially contact the waste package in the absence of the drip shield.

Also, based on reported test results, the localized corrosion initiation (and hence propagation) for the Titanium Grade 7 drip shield material does not need to be implemented in TSPA. Even for the potentially more aggressive calcium chloride containing brines, it is not likely that they will have a significant detrimental effect on the localized corrosion resistance of Titanium Grade 7.

Stress Corrosion Cracking—Three criteria must be met for SCC to occur: metallurgical susceptibility, a corrosive environment, and static tensile stresses. Initiation and propagation of SCC can occur at low tensile stresses). After initiation, through-wall penetration is essentially instantaneous when compared to the 10,000-year regulatory period for the high-level radioactive waste repository at Yucca Mountain. Environments that cause SCC are usually aqueous and can be aqueous films (condensation on dust) or bulk solutions (seepage). Stress corrosion cracking of a particular stressed alloy is usually caused by the presence of a specific chemical species in the environment. For example, SCC of stressed copper alloys is associated with the presence of ammonia in the environment. Chloride ions cause SCC in stressed stainless steels and aluminum-based alloys. Reduced sulfate is known to promote SCC in nickel-based alloys.

Changes in environmental conditions, which include temperature, dissolved oxygen, and ionic concentrations, will normally influence the SCC process.

SCC requires tensile stress as a driving force. The highest stress in the Alloy 22 (and the highest probability of SCC) is expected to be in the final closure weld. Since analyses based on two SCC models (see Section 9) indicate that through-wall radial cracking is a potential threat to waste package integrity, postweld stress mitigation processes will be implemented for the final closure weld, to lower the probability of SCC. Two options are currently being considered, laser-shock peening or controlled plasticity burnishing, to mitigate residual weld stress. Laser-shock peening is the baseline process for license application; it uses a high-power pulsed laser beam to introduce shock waves into the weld surface. These pulses produce compressive stress that counterbalances the tensile stress caused by welding (due to shrinkage during cooling). Single-pass laser-shock peening has been successfully demonstrated on prototypical Alloy 22 welds. Multiple-pass laser-shock peening can be used to increase the depth of the compressive stress layer. The depth of laser-peened weld-metal with stresses less than the threshold stress (90 percent of the yield strength) has been shown to be about 4.7 mm at the upper uncertainty bound, and about 6 mm for the mean stress value. More recently, stresses have been measured using a 1-inch ring core technique, showing that the depth of the compressive layer achieved with either stress mitigation technique is greater than 5 mm.

The rate of SCC propagation is assumed to be fast enough to penetrate the waste package in one performance assessment time step. The scenario for removal of the compressive layer by corrosion is based on general corrosion rates. Based upon 5-year corrosion rates from the LTCTF, more than the 10,000-year regulatory period will be required to remove the compressive layer by general corrosion (30,000 to 90,000 years).

11.3 RADIOLYSIS

Gamma radiolysis may produce hydrogen peroxide in the aqueous films on the waste package and drip shield. The presence of hydrogen peroxide increases the open-circuit corrosion potential, and, if the increase is large enough, it can cause localized corrosion. However, based on the expected radiation dose levels, it is concluded that the effects of radiolysis on corrosion performance of Alloy 22 will not be significant enough to lead to corrosion induced failure of the outer shell under repository conditions.

11.4 MICROBIALLY INFLUENCED CORROSION

Microbial communities can form on the waste package and drip shield surfaces after temperatures decrease enough that aqueous films develop and the relative humidity exceeds 90 percent. These communities use nutrients from seepage water and dust, and produce biological waste that can change the chemistry of the aqueous film. Such changes can enable localized corrosion. For Alloy 22, MIC is accounted for with an enhancement factor on general corrosion rates, and does not limit lifetime within the 10,000-year period.

11.5 OTHER POTENTIAL DRIP SHIELD DEGRADATION MODES

The resistance of Titanium Grade 7 to hydrogen-induced cracking should be at least as good as, if not superior to, that of experimentally measured Titanium Grade 16 (estimated threshold H_C

approximately 1,000 $\mu\text{g/g}$ for hydrogen induced cracking to occur), which in turn is significantly higher than the predicted hydrogen absorption level after 10,000-year repository exposure. A similar conclusion can be made for the Titanium Grade 24 drip shield structural support material.

Other factors that might potentially influence the corrosion of the drip shield materials such as gamma radiolysis, MIC, and aging and phase stability are also concluded to be insignificant contributions to the drip shield degradation.

INTENTIONALLY LEFT BLANK

12. REFERENCES

12.1 DOCUMENTS CITED

Baker, E.A. 1988. "Long-Term Corrosion Behavior of Materials in the Marine Atmosphere." *Degradation of Metals in the Atmosphere, Proceedings of the Symposium on Corrosion of Metals, Philadelphia, Pennsylvania, 12-13 May 1986*. Dean, S.W. and Lee, T.S., eds. ASTM STP 965. Pages 125-144. Philadelphia, Pennsylvania: American Society for Testing and Materials. TIC: 224019.

Bokhari, S.A. 2003. "Approved Baseline Change Proposal (BCP) YMP-2003-005, Design Changes to Site Recommendation (SR) Waste Package." Memorandum from S.A. Bokhari (DOE) to W.J. Arthur, III (OCRWM/CCB), R.A. Milner (OCRWM/CCB), and R.D. Brown (OCRWM/CCB), January 30, 2003, with attachments. ACC: MOL.20030508.0040.

Brossia, C.S.; Browning, L.; Dunn, D.S.; Moghissi, O.C.; Pensado, O.; and Yang, L. 2001. *Effect of Environment on the Corrosion of Waste Package and Drip Shield Materials*. CNWRA 2001-003. San Antonio, Texas: Center for Nuclear Waste Regulatory Analyses. TIC: 252324.

BSC (Bechtel SAIC Company) 2001a. *Multiscale Thermohydrologic Model*. ANL-EBS-MD-000049 REV 00 ICN 02. Las Vegas, Nevada: Bechtel SAIC Company. ACC: MOL.20020123.0279.

BSC 2001b. *FY 01 Supplemental Science and Performance Analyses, Volume 1: Scientific Bases and Analyses*. TDR-MGR-MD-000007 REV 00 ICN 01. Las Vegas, Nevada: Bechtel SAIC Company. ACC: MOL.20010801.0404; MOL.20010712.0062; MOL.20010815.0001.

BSC 2001c. *Abstraction of Models for Pitting and Crevice Corrosion of Drip Shield and Waste Package Outer Barrier*. ANL-EBS-PA-000003 REV 00 ICN 01. Las Vegas, Nevada: Bechtel SAIC Company. ACC: MOL.20010926.0008.

BSC 2003a. *Stress Corrosion Cracking of the Drip Shield, the Waste Package Outer Barrier, and the Stainless Steel Structural Material*. ANL-EBS-MD-000005 REV 01 ICN 00. Las Vegas, Nevada: Bechtel SAIC Company. ACC: DOC.20030717.0001.

BSC 2003b. *General Corrosion and Localized Corrosion of Waste Package Outer Barrier*. ANL-EBS-MD-000003 REV 01. Las Vegas, Nevada: Bechtel SAIC Company. ACC: DOC.20030916.0010.

BSC 2003c. *General Corrosion and Localized Corrosion of the Drip Shield*. ANL-EBS-MD-000004 REV 01. Las Vegas, Nevada: Bechtel SAIC Company. ACC: DOC.20030626.0001.

BSC 2003d. *Aging and Phase Stability of Waste Package Outer Barrier*. ANL-EBS-MD-000002 REV 01 ICN 0. Las Vegas, Nevada: Bechtel SAIC Company. ACC: DOC.20030807.0004.

BSC 2003e. *Multiscale Thermohydrologic Model Report*. ANL-EBS-MD-000049 REV 01C. Las Vegas, Nevada: Bechtel SAIC Company. ACC: MOL.20030910.0158.

BSC 2003f. *Engineered Barrier System: Physical and Chemical Environment Model*. ANL-EBS-MD-000033 REV 02B. Las Vegas, Nevada: Bechtel SAIC Company. ACC: MOL.20030909.0042.

BSC 2003g. *Environment on the Surfaces of the Drip Shield and Waste Package Outer Barrier*. ANL-EBS-MD-000001 REV 01D. Las Vegas, Nevada: Bechtel SAIC Company. ACC: MOL.20030825.0151.

BSC 2003h. *Dose Rate Calculation for 21-PWR Waste Package*. 000-00C-DSU0-01800-000-00A. Las Vegas, Nevada: Bechtel SAIC Company. ACC: ENG.20030903.0003.

BSC 2003i. *WAPDEG Analysis of Waste Package and Drip Shield Degradation*. ANL-EBS-PA-000001 REV 01D. Las Vegas, Nevada: Bechtel SAIC Company. ACC: MOL.20031009.0225

BSC 2003j. *Hydrogen Induced Cracking of Drip Shield*. ANL-EBS-MD-000006 REV 01. Las Vegas, Nevada: Bechtel SAIC Company. ACC: DOC.20030304.0003.

Chen, H.L.; Evans, K.J.; Hackel, L.A.; Rankin, J.E.; Yamamoto, R.M.; Demma, A.G.; Dewald, A.T.; Lee, M.J.; and Hill, M.R. 2002. *Mitigation of Tensile Weld Stresses in Alloy 22 Using Laser Peening*. OCRL-ID-151 055-LST02-031. Lawrence Livermore National Laboratory, Livermore, California. ACC: MOL.20030911.0252

Cieslak, M.J.; Headley, T.J.; and Romig, A.D., Jr. 1986. "The Welding Metallurgy of Hastelloy Alloys C-4, C-22, and C-276." *Metallurgical Transactions A*, 17A, (11), 2035-2047. Warrendale, Pennsylvania: Metallurgical Society of AIME. TIC: 233952.

Covington, L.C. and Schutz, R.W. 1981. "Resistance of Titanium to Atmospheric Corrosion." *Corrosion/81, International Corrosion Forum, April 6-10, 1981, Toronto, Ontario, Canada*. Pages 113/1-113/7. Houston, Texas: National Association of Corrosion Engineers. TIC: 248534.

CRWMS M&O (Civilian Radioactive Waste Management System Management and Operating Contractor) 1998. *Waste Package Degradation Expert Elicitation Project*. Rev. 1. Las Vegas, Nevada: CRWMS M&O. ACC: MOL.19980727.0002.

CRWMS M&O 2000a. *General Corrosion and Localized Corrosion of Waste Package Outer Barrier*. ANL-EBS-MD-000003 REV 00. Las Vegas, Nevada: CRWMS M&O. ACC: MOL.20000202.0172.

CRWMS M&O 2000b. *Aging and Phase Stability of Waste Package Outer Barrier*. ANL-EBS-MD-000002 REV 00. Las Vegas, Nevada: CRWMS M&O. ACC: MOL.20000410.0407.

CRWMS M&O 2000c. *In-Drift Microbial Communities*. ANL-EBS-MD-000038 REV 00 ICN 01. Las Vegas, Nevada: CRWMS M&O. ACC: MOL.20001213.0066.

Drever, J.I. 1997. "Evaporation and Saline Waters." Chapter 15 of *The Geochemistry of Natural Waters: Surface and Groundwater Environments*. 3rd Edition. Upper Saddle River, New Jersey: Prentice Hall. TIC: 246732.

Dunn, D.S.; Yang, L.; Pan, Y.-M.; and Cragolino, G.A. 2003. "Localized Corrosion Susceptibility of Alloy 22." *Corrosion/2003, 58th Annual Conference & Exposition, March 16-20, 2003, San Diego, California*. Paper No. 03697. Houston, Texas: NACE International. TIC: 254387.

EPRI (Electric Power Research Institute) 2002. *Evaluation of the Proposed High-Level Radioactive Waste Repository at Yucca Mountain Using Total System Performance Assessment, Phase 6*. EPRI TR-1003031. Palo Alto, California: Electric Power Research Institute. TIC: 252239.

Estill, J.C. 1998. "Long-Term Corrosion Studies." 2.2 of *Engineered Materials Characterization Report*. McCright, R.D., ed. UCRL-ID-119564 Volume 3 Rev.1.1. Livermore, California: Lawrence Livermore National Laboratory. ACC: MOL.19981222.0137.

Estill, J.C.; Hust, G.A.; and Rebak, R.B. 2003. "Long Term Corrosion Potential Behavior of Alloy 22." *Corrosion/2003, 58th Annual Conference & Exposition, March 16-20, 2003, San Diego, California*. Paper No. 03688. Houston, Texas: NACE International. TIC: 254387.

Evans, K.J.; Day, S.D.; Ilevbare, G.O.; Whalen, M.T.; King, K.J.; Hust, G.A.; Wong, L.L.; Estill, J.C.; and Rebak, R.B. 2003. "Anodic Behavior of Alloy 22 in Calcium Chloride and in Calcium Chloride Plus Calcium Nitrate Brines." *Transportation, Storage, and Disposal of Radioactive Materials, 2003, Presented at the 2003 ASME Pressure Vessels and Piping Conference, Cleveland, Ohio, July 20-24, 2003*. Hafner, R.S., ed. PVP-Vol. 467. Pages 55-62. New York, New York: American Society of Mechanical Engineers. TIC: 254935.

Farmer, J. 2003. Materials Performance. Presentation to the Nuclear Waste Technical Review Board, May 13, 2003, Washington, D.C. Las Vegas, Nevada: Bechtel SAIC Company. ACC: MOL.20030820.0044.

Farmer, J.C.; Lu, S.; Summers, T.; McCright, D.; Lingenfelter, A.; Wang, F.; Estill, J.; Hackel, L.; Chen, H-L.; Gordon, G.; Pasupathi, V.; Andresen, P.; Tang, S.; Herrera, M. 2000. "Modeling and Mitigation of Stress Corrosion Cracking in Closure Welds of High-Level Waste Containers for Yucca Mountain." *Transportation, Storage, and Disposal of Radioactive Materials, 2000, Presented at the 2000 ASME Pressure Vessels and Piping Conference, Seattle, Washington, July 23-27, 2000*. Hafner, R.S., ed. PVP-Vol. 408, Pages 71-81. TIC: 251259.

Farmer, J.C. and McCright, D. 1998. "Crevice Corrosion and Pitting of High-Level Waste Containers: Integration of Deterministic and Probabilistic Models." *Proceedings of Corrosion 98, March 22-27, 1998, San Diego, California*. Pages 160/1 to 160/24. Houston, Texas: NACE International. TIC: 238172.

Farmer, J.C.; McCright, D.; Gdowski, G.; Wang, F.; Summers, T.; Bedrossian, P.; Horn, J.; Lian, T.; Estill, J.; Lingenfelter, A.; and Halsey, W. 2000. "General and Localized Corrosion of Outer Barrier of High-Level Waste Container in Yucca Mountain." *Transportation, Storage, and Disposal of Radioactive Materials, 2000, Presented at the 2000 ASME Pressure Vessels and Piping Conference, Seattle, Washington, July 23–27, 2000*. Hafner, R.S., ed. PVP-Vol. 408. Pages 53-69. New York, New York: American Society of Mechanical Engineers. TIC: 251259.

Fontana, M.G. 1986. *Corrosion Engineering*. 3rd Edition. New York, New York: McGraw-Hill. TIC: 240700.

Frankel, G.S. 1998. "Pitting Corrosion of Metals, A Review of the Critical Factors." *Journal of the Electrochemical Society*, 145, (6), 2186-2198. Pennington, New Jersey: Electrochemical Society. TIC: 254587.

Gartland, P.O. 1997. "A Simple Model of Crevice Corrosion Propagation for Stainless Steels in Seawater." *Corrosion* 97. 417/1 to 417/17. Houston, Texas: NACE International. TIC: 245216.

Gdowski, G.E. 1991. *Survey of Degradation Modes of Four Nickel-Chromium-Molybdenum Alloys*. UCRL-ID-108330. Livermore, California: Lawrence Livermore National Laboratory. ACC: NNA.19910521.0010.

Gdowski, G.E. 1997. *Degradation Mode Survey Candidate Titanium - Base Alloys for Yucca Mountain Project Waste Package Materials*. UCRL-ID-121191, Rev. 1. Livermore, California: Lawrence Livermore National Laboratory. ACC: MOL.19980120.0053.

Glass, R.S.; Overturf, G.E.; Van Konynenburg, R.A.; and McCright, R.D. 1986. "Gamma Radiation Effects on Corrosion-I. Electrochemical Mechanisms for the Aqueous Corrosion Processes of Austenitic Stainless Steels Relevant to Nuclear Waste Disposal in Tuff." *Corrosion Science*, 26, (8), 577-590. Oxford, Great Britain: Pergamon. TIC: 226179.

Greene, C. A.; Henry, A. J.; Brossia, C. S.; and Ahn, T. M. 2001. "Evaluation of the Possible Susceptibility of Titanium Grade 7 to Hydrogen Embrittlement in a Geologic Repository Environment." *Materials Research Society Symposium Proceedings*. Kaye P. Hart, Gregory R. Lumpkin. 663, Warrendale, Pennsylvania: Materials Research Society. TIC: 254939.

Gruss, K.A.; Cragolino, G.A.; Dunn, D.S.; and Sridhar, N. 1998. "Repassivation Potential for Localized Corrosion of Alloys 625 and C22 in Simulated Repository Environments." *Proceedings of Corrosion 98, March 22-27, 1998, San Diego, California*. Pages 149/1 to 149/15. Houston, Texas: NACE International. TIC: 237149.

Hack, H.P. 1983. "Crevice Corrosion Behavior of Molybdenum-Containing Stainless Steels in Seawater." *Materials Performance*, 22, (6), 24-30. Houston, Texas: NACE International. TIC: 245826.

Hailey, P. and Gdowski, G. 2003. "Thermogravimetric Thin Aqueous Film Corrosion Studies of Alloy 22; Calcium Chloride Solutions at 150°C and Atmospheric Pressure." *Materials Research Society Symposium Proceedings*. 757, 765-770. Warrendale, Pennsylvania: Materials Research Society. TIC: 254940.

Hardie, D. and Ouyang, S. 1999. "Effect of Hydrogen and Strain Rate Upon the Ductility of Mill-Annealed Ti6Al4V." *Corrosion Science*, 41, 1, 155-177, 1999. New York, New York: Elsevier. TIC: 253121.

Harrar, J.E.; Carley, J.F.; Isherwood, W.F.; and Raber, E. 1990. *Report of the Committee to Review the Use of J13 Well Water in Nevada Nuclear Waste Storage Investigations*. UCID-21867. Livermore, California: Lawrence Livermore National Laboratory. ACC: NNA.19910131.0274.

Haynes International 1997. *Hastelloy Alloy C-276*. Kokomo, Indiana: Haynes International. TIC: 238832.

Hilliard, J.E. and Cahn, J.W. 1961. "An Evaluation of Procedures in Quantitative Metallography for Volume-Fraction Analysis." *Transactions of the Metallurgical Society of AIME*, 221, (2), 344-352. New York, New York: American Institute of Mining, Metallurgical, and Petroleum Engineers. TIC: 253830.

Horn, J. and Jones, D. 2002. "Microbiologically Influenced Corrosion: Perspectives and Approaches." *Manual of Environmental Microbiology*. 2nd Edition. Hurst, C.J., ed. Pages 1072-1083. Washington, D.C.: ASM Press. TIC: 254738.

Hua, F. and Gordon, G. 2003. "On Apparent Bi-Linear Corrosion Rate Behavior of Titanium Grade 7 in Basic Saturated Water (BSW-12) Below and Above 80°C." *Corrosion/2003*, Paper No. 03687, Houston, Texas: NACE International. TIC: 254248.

Hua, F.; Sarver, J.; Jevic, J.; and Gordon, G. 2002. "General Corrosion Studies of Candidate Container Materials in Environments Relevant to Nuclear Waste Repository." *Corrosion/2002, 57th Annual Conference & Exposition, April 7-11, 2002, Denver, Colorado*. Paper No. 02530. Houston, Texas: NACE International. TIC: 252067.

Hunkeler, F. and Boehni, H. 1983. "Pit Growth Measurements on Stainless Steels." *Passivity of Metals and Semiconductors, Proceedings of the Fifth International Symposium on Passivity, Bombannes, France, May 30-June 3, 1983*. Froment, M., ed. Pages 655-660. New York, New York: Elsevier. TIC: 236283.

Ishikawa, H.; Honda, A.; and Sasaki, N. 1994. "Long Life Prediction of Carbon Steel Overpacks for Geological Isolation of High-Level Radioactive Waste." *Life Prediction of Corrodible Structures*. Parkins, R.N., ed. Volume 1. Pages 454-483. Houston, Texas: NACE International. TIC: 254834.

Jayaweera, P.; Priyantha, N.; Macdonald, D.D.; Engelhard, G.; and Davydov, A. 2003. *Deterministic Prediction of Localized Corrosion Damage to Alloy C-22 HLNW Canisters*. SRI Project 10333. Menlo Park, California: SRI International. TIC: 253900.

- Jones, R.H. and Ricker, R.E. 1987. "Stress-Corrosion Cracking." In *Corrosion*, Volume 13, Pages 145-163 of *Metals Handbook*. 9th Edition. Metals Park, Ohio: ASM International. TIC: 209807.
- Kehler, B.A.; Ilevbare, G.O.; and Scully, J.R. 2001. "Crevice Corrosion Stabilization and Repassivation Behavior of Alloy 625 and Alloy 22." *Corrosion*, 57, (12), 1042-1065. Houston, Texas: NACE International. TIC: 254305.
- Kim, Y.J. 1987. "Effect of Gamma Radiation on Electrochemical Behavior of 9 Cr-1Mo Alloy in NaCl Solutions." *Journal of the Corrosion Science Society of Korea*, 16, (1), 25-30. Seoul, Korea: Corrosion Science Society of Korea. TIC: 246337.
- Kim, Y-J. 1999a. "Analysis of Oxide Film Formed on Type 304 Stainless Steel in 288°C Water Containing Oxygen, Hydrogen, and Hydrogen Peroxide." *Corrosion*, 55, (1), 81-88. Houston, Texas: NACE International. TIC: 245184.
- Kim, Y-J. 1999b. "In-Situ Electrochemical Impedance Measurement of Oxide Film on 304 SS in 288°C Water." *Corrosion* 99. Paper No. 437, 1-11. Houston, Texas: NACE International. TIC: 246024.
- Kim, Y-K. 1988. "Electrochemical Mechanisms for Radiation Corrosion Processes of 316 Austenitic Stainless Steel in Chloride Environment." *Journal of the Corrosion Science Society of Korea*, 17, (1), 20-26. Seoul, Korea: Korean Corrosion Science Society. TIC: 246622.
- Kitayama, S.; Shida, Y.; Ueda, M.; and Kudo, T. 1992. "Effect of Small Pd Addition on the Corrosion Resistance of TI and TI Alloys in Severe Gas and Oil Environment." *Techniques for Corrosion Measurement, Papers Presented at the Corrosion/92 Symposium*. Paper No. 52. 1992. Houston, Texas: NACE International. TIC: 253165.
- Lian, T.; Estill, J.C.; Hurst, G.A.; and Rebak, R.B. 2003. "Passive and Transpassive Dissolution of Alloy 22 in Simulated Repository Environments." *Corrosion/2003, 58th Annual Conference & Exposition, March 16-20, 2003, San Diego, California*. Paper No. 03694, Houston, Texas: NACE International. TIC: 254906.
- Lian, T.; Martin, S.; Jones, D.; Rivera, A.; and Horn, J. 1999. "Corrosion of Candidate Container Materials by Yucca Mountain Bacteria." *Corrosion* 99, 54th Annual Conference and Expo, San Antonio, Texas, April 25-30, 1999. Paper No. 476. Houston, Texas: NACE International. TIC: 245833.
- Marsh, G.P.; Taylor, K.J.; and Harker, A.H. 1991. *The Kinetics of Pitting Corrosion of Carbon Steel Applied to Evaluating Containers for Nuclear Waste Disposal*. SKB TR-91-62. Stockholm, Sweden: Svensk Kärnbränsleförsörjning AB. TIC: 206582.
- McCright, R.D. 1998. *Corrosion Data and Modeling Update for Viability Assessment*. Volume 3 of *Engineered Materials Characterization Report*. UCRL-ID-119564, Rev. 1.1. Livermore, California: Lawrence Livermore National Laboratory. ACC: MOL.19981222.0137.

- McGuire, R.D.; Vlasity, J.; Kessler, J.; Long, A.; Childs, S.; Ross, B.; Schwartz, F.; Shoesmith, D.; Kolar, M.; Apted, M.; Zhou, W.; Sudicky, E.; Smith, G.; Kozak, M.; Salter, P.; Klos, R.; Venter, A.; Stenhouse, M.; Watkins, B.; and Little, R. 1998. *Alternative Approaches to Assessing the Performance and Suitability of Yucca Mountain for Spent Fuel Disposal*. EPRI TR-108732. Palo Alto, California: Electric Power Research Institute. TIC: 248813.
- Mughabghab, S.F. and Sullivan, T.M. 1989. "Evaluation of the Pitting Corrosion of Carbon Steels and Other Ferrous Metals in Soil Systems." *Waste Management*, 9, (4), 239-251. Elmsford, New York: Pergamon Press. TIC: 254591.
- Newman, R.C. 1985. "The Dissolution and Passivation Kinetics of Stainless Alloys Containing Molybdenum—I. Coulometric Studies of Fe–Cr and Fe–Cr–Mo Alloys." *Corrosion Science*, 25, (5), 331-339. New York, New York: Elsevier. TIC: 254590.
- Newman, R.C. and Franz, E.M. 1984. "Growth and Repassivation of Single Corrosion Pits in Stainless Steel." *Corrosion*, 40, (7), 325-330. Houston, Texas: National Association of Corrosion Engineers. TIC: 254580.
- Okada, T. 1983. "Factors Influencing the Cathodic Charging Efficiency of Hydrogen by Modified Titanium Electrodes." *Electrochimica Acta*, 28, (8), 1113-1120. New York, New York: Pergamon Press. TIC: 246262.
- Plinski, M.J. 2001. *Waste Package Operations Fabrication Process Report*. TDR-EBS-ND-000003 REV 02. Las Vegas, Nevada: Bechtel SAIC Company. ACC: MOL.20011003.0025.
- Rebak, R.B.; Summers, T.S.E.; and Carranza, R.M. 2000. "Mechanical Properties, Microstructure and Corrosion Performance of C-22 Alloy Aged at 260°C to 800°C." *Scientific Basis for Nuclear Waste Management XXIII, Symposium held November 29-December 2, 1999, Boston, Massachusetts*. Smith, R.W. and Shoesmith, D.W., eds. 608, 109-114. Warrendale, Pennsylvania: Materials Research Society. TIC: 249052.
- Rebak, R.B.; Summers, T.S.E.; Lian, T.; Carranza, R.M.; Dillman, J.R.; Corbin, T.; and Crook, P. 2002. "Effect of Thermal Aging on the Corrosion Behavior of Wrought and Welded Alloy 22." *Corrosion/2002, 57th Annual Conference & Exposition, April 7-11, 2002, Denver, Colorado*. Paper No. 02542. Houston, Texas: NACE International. TIC: 254582.
- Reed-Hill, R.E. 1973. *Physical Metallurgy Principles*. 2nd Edition. Boston, Massachusetts: PWS-KENT. TIC: 254402.
- Revie, R.W., ed. 2000. *Uhlig's Corrosion Handbook*. 2nd Edition. New York, New York: John Wiley & Sons. TIC: 248360.
- Schutz, R.W. and Thomas, D.E. 1987. "Corrosion of Titanium and Titanium Alloys." In *Corrosion*, Volume 13, Pages 669-706 of *ASM Handbook*. Formerly 9th Edition, Metals Handbook. Materials Park, Ohio: ASM International. TIC: 240704.

Schutz, R.W. and Xiao, M. 1993. "Optimized Lean-Pd Titanium Alloys for Aggressive Reducing Acid and Halide Service Environments." *Corrosion Control for Low-Cost Reliability, Proceedings, 12th International Corrosion Congress, Houston, Texas, September 19-24, 1993*. 3A, 1213-1225. Houston, Texas: NACE International. TIC: 248725.

Sedriks, A.J. 1996. *Corrosion of Stainless Steels*. 2nd Edition. Corrosion Monograph Series. New York, New York: John Wiley & Sons. TIC: 245121.

Sharland, S.M.; Naish, C.C.; Taylor, K.J.; and Marsh, G.P. 1994. "An Experimental and Modelling Study of the Localized Corrosion of Carbon Steel Overpacks for the Geological Disposal of Radioactive Waste." *Life Prediction of Corrodible Structures*. Parkins, R.N., ed. Volume 1. Pages 402-418. Houston, Texas: NACE International. TIC: 254835.

Shoesmith, D.W.; Hardie, D.; Ikeda, B.M.; and Noel, J.J. 1997. *Hydrogen Absorption and the Lifetime Performance of Titanium Waste Containers*. AECL-11770. Pinawa, Manitoba, Canada: Atomic Energy of Canada Limited. TIC: 236220.

Shoesmith, D.W. and King, F. 1998. *The Effects of Gamma Radiation on the Corrosion of Candidate Materials for the Fabrication of Nuclear Waste Packages*. AECL-11999. Pinawa, Manitoba, Canada: Atomic Energy of Canada Limited. ACC: MOL.19990311.0212.

Smailos, E. and Köster, R. 1987. "Corrosion Studies on Selected Packaging Materials for Disposal of High Level Wastes." *Materials Reliability in the Back End of the Nuclear Fuel Cycle, Proceedings of a Technical Committee Meeting, Vienna, 2-5 September 1986*. IAEA TECHDOC-421, 7-24. Vienna, Austria: International Atomic Energy Agency. TIC: 252877.

Sprowls, D.O. 1987. "Evaluation of Stress-Corrosion Cracking." In *Corrosion*, Volume 13, Pages 245-282 of *Metals Handbook*. 9th Edition. Metals Park, Ohio: ASM International. TIC: 209807.

Stoecker, J.G., II. 1987. "Evaluation of Microbiological Corrosion." In *Corrosion*, Volume 13, Pages 314-315 of *Metals Handbook*. 9th Edition. Metals Park, Ohio: ASM International. TIC: 209807.

Treseder, R.S.; Baboian, R.; and Munger, C.G. 1991. *NACE Corrosion Engineer's Reference Book*. 2nd Edition. 156-181. Houston, Texas: NACE International. TIC: 245834.

Turchi, P.E.A. 2001. "Delivery of Property Diagram (Phase Fraction Versus Temperature) of Alloy 22 at Its Nominal Composition." Memorandum from P.E.A. Turchi (BSC) to RPC = 3, May 21, 2001, PROJ.05/01.051, with enclosure. ACC: MOL.20010522.0158.

Vander Voort, G.F. 2000. "Volume Fraction." *Metallography, Principles and Practice*. Pages 425-435. Materials Park, Ohio: ASM International. TIC: 254149.

Vetter, K.J. and Strehblow, H.H. 1974. "Pitting Corrosion in an Early Stage and its Theoretical Implications." *Localized Corrosion, U.R. Evans Conference on Localized Corrosion, December 6-10, 1971, Williamsburg, Virginia*. International Corrosion Conference Series, NACE-3. Pages 240-251. Houston, Texas: National Association of Corrosion Engineers. TIC: 254803.

Walton, J.C.; Cragnolino, G.; and Kalandros, S.K. 1996. "A Numerical Model of Crevice Corrosion for Passive and Active Metals." *Corrosion Science*, 38, (1), 1-18. Amsterdam, The Netherlands: Pergamon. TIC: 233439.

Welsch, G.; Smialek, J.L.; Doychak, J.; Waldman, J.; and Jacobson, N.S. 1996. "High Temperature Oxidation and Properties." Chapter 2 of *Oxidation and Corrosion of Intermetallic Alloys*. Welsch, G. and Desai, P.D.; eds. West Lafayette, Indiana: Purdue University. TIC: 245280.

12.2 CODES, STANDARDS, AND REGULATIONS

10 CFR 63. Energy: Disposal of High-Level Radioactive Wastes in a Geologic Repository at Yucca Mountain, Nevada. Readily available.

ASME (American Society of Mechanical Engineers). 1969. Criteria of the ASME Boiler and Pressure Vessel Code for Design by Analysis in Sections III and VIII, Division 2. New York, New York: American Society of Mechanical Engineers. TIC: 254727.

ASME 1995. "Materials, Part C — Specifications for Welding Rods, Electrodes, and Filler Metals." 1995 Addenda, Section II of *1995 ASME Boiler and Pressure Vessel Code*. New York, New York: American Society of Mechanical Engineers. TIC: 245287.

ASM International 1987. *Corrosion*. Volume 13 of *ASM Handbook*. 9th Edition. Materials Park, Ohio: ASM International. TIC: 240704.

ASTM B 265-02. 2002. *Standard Specification for Titanium and Titanium Alloy Strip, Sheet, and Plate*. West Conshohocken, Pennsylvania: American Society for Testing and Materials. TIC: 254000.

ASTM G 1-90 (Reapproved 1999). 1999. *Standard Practice for Preparing, Cleaning, and Evaluating Corrosion Test Specimens*. West Conshohocken, Pennsylvania: American Society for Testing and Materials. TIC: 238771.

ASTM G 5-94. *Standard Reference Test Method for Making Potentiostatic and Potentiodynamic Anodic Polarization Measurements*. Philadelphia, Pennsylvania: American Society for Testing and Materials. TIC: 231902.

12.3 DATA, LISTED BY DATA TRACKING NUMBER

LL000201305924.120. General Corrosion and Localized Corrosion of the Drip Shield. Submittal date: 02/07/2000.

LL000209305924.129. General Corrosion and Localized Corrosion of the Drip Shield.
Submittal date: 02/29/2000.

LL000320005924.145. Corrosion Cracking of the Drip Shield, the Waste Package Outer Barrier and the Stainless Steel Structural Material. Submittal date: 03/22/2000.

LL000320405924.146. Target Compositions of Aqueous Solutions Used for Corrosion Testing.
Submittal date: 03/22/2000.

LL010105512251.011. General Corrosion and Localized Corrosion of the Drip Shield.
Submittal date: 01/17/2001.

LL020603612251.015. Slow Strain Rate Test Generated Stress Corrosion Cracking Data.
Submittal date: 08/27/2002

LL020711612251.017. Open Circuit Potential Tests. Submittal date: 10/11/2002.

LL021105312251.023. Stress Corrosion Crack Growth and Initiation Measurements for C-22 and Ti-7, General Electric Global Research Center (GEGRC) 121202. Submittal date: 01/08/2003.

LL030106312251.013. Property and Phase Kinetics Diagrams. Submittal date: 04/09/2003.

LL030205912251.016. Titanium (Ti) Grade 16 Corrosion Rate Data in Simulated Diluted and Concentrated Well Water (SDW and SCW). Submittal date: 02/13/2003.

LL030400112251.043. Electrochemical Behavior of Multiple Crevice Assembly (MCA) Alloy 22 Specimens in 5M CaCl₂. Submittal date: 04/07/2003.

LL030406212251.044. Alloy 22 in 5M CaCl₂ at 75C—Supplemental. Submittal date: 04/08/2003.

LL030409512251.051. Electrochemical Analysis of Alloy 22—CaCl₂ Data at Various Temperatures, Surface Conditions, and Electrolyte Solutions. Submittal date: 05/23/2003.

LL030409812251.054. Electrochemical Data of Alloy 22 in CaCl₂ Solutions—Effect of Nitrate.
Submittal date: 06/26/2003.

LL030606912251.020. Developed Data from Alloy 22 Volume Fraction Measurements.
Submittal date: 06/20/2003.

LL030607012251.065. Output of Stress Corrosion Cracking AMR ANL-EBS-MD-000005 REV. 01 ICN 00. Submittal date: 06/20/2003.

LL030607112251.021. Long-Range Ordering (LRO) of Alloy 22 Base Metal Aged at Various Times and Temperatures Using Vickers Microhardness Measurements. Submittal date: 06/20/2003.

LL991203505924.094. Approach and Supporting Data for MIC Modeling. Submittal date: 12/13/1999.

MO0301SPAXRA52.001. X-Ray Diffraction and Ring Core Determination of the Subsurface Residual Stress Distributions in Two Alloy 22 Welded Plates. Submittal date: 01/30/2003.

MO0306SPAGLCDS.001. General Corrosion and Localized Corrosion of the Drip Shield. Submittal date: 05/28/2003.

MO0310MWDWAPAN.002. WAPDEG Analysis of Waste Package and Drip Shield Degradation. Submittal date: 10/16/2003.

SN0308T0506303.003. Updated Localized Corrosion Model and Analyses of Waste Package Outer Barrier. Submittal date: 08/20/2003.

SN0308T0506303.004. Updated General Corrosion Model and Analyses of Waste Package Outer Barrier. Submittal date: 08/20/2003.

INTENTIONALLY LEFT BLANK

APPENDIX A
MEASUREMENT OF CORROSION RATES OF WASTE PACKAGE MATERIALS
(RESPONSE TO CLST 1.07 AIN-1)

Note Regarding the Status of Supporting Technical Information

This document was prepared using the most current information available at the time of its development. This Technical Basis Document and its appendices providing Key Technical Issue Agreement responses that were prepared using preliminary or draft information reflect the status of the Yucca Mountain Project's scientific and design bases at the time of submittal. In some cases this involved the use of draft Analysis and Model Reports (AMRs) and other draft references whose contents may change with time. Information that evolves through subsequent revisions of the AMRs and other references will be reflected in the License Application as the approved analyses of record at the time of License Application submittal. Consequently, the DOE will not routinely update either this Technical Basis Document or its Key Technical Issue Agreement appendices to reflect changes in the supporting references prior to submittal of the License Application.

APPENDIX A

MEASUREMENT OF CORROSION RATES OF WASTE PACKAGE MATERIALS (RESPONSE TO CLST 1.07 AIN-1)

This appendix is a response to the U.S. Nuclear Regulatory Commission (NRC) additional information needed (AIN) request regarding the U.S. Department of Energy (DOE) response to Key Technical Issue (KTI) Agreement Container Life and Source Term (CLST) 1.07. Agreement CLST 1.07 relates to providing documentation on methods used to measure corrosion rates of the waste package materials.

A.1 KEY TECHNICAL ISSUE AGREEMENT

A.1.1 CLST 1.07 AIN-1

Agreement CLST 1.07 was reached during the NRC/DOE Technical Exchange and Management Meeting on Container Life and Source Term held September 12-13, 2000, in Las Vegas, Nevada. Subissues 1 (effects of corrosion processes on the lifetime of the containers), 2 (effects of phase instability and initial defects on the mechanical failure and lifetime of the containers), 3 (the rate at which radionuclides in spent nuclear fuel are released from the engineered barrier subsystem through the oxidation and dissolution of spent nuclear fuel), 4 (the rate at which radionuclides in high-level radioactive waste glass are released from the engineered barrier subsystem), and 6 (effects of alternate engineered barrier subsystem design features on container lifetime and radionuclide release from the engineered barrier subsystem) were discussed at the meeting (Schlueter 2000).

Wording of the agreement is as follows:

CLST 1.07

Provide documentation for the alternative methods to measure corrosion rates of the waste package materials (e.g., ASTM G-102 testing) or provide justification for the current approach. DOE will document the alternative methods of corrosion measurement in the revision of Alloy 22 AMR (ANL-EBS-MD-000003), prior to LA.

The DOE submitted information in a letter report (Ziegler 2002a) addressing CLST 1.05, CLST 1.06, CLST 1.07, and CLST 2.07. The DOE later submitted a supplement to the letter report (Ziegler 2002b) containing additional information related to CLST 1.06 and CLST 1.07.

The NRC informed the DOE (Schlueter 2003) that it had provided sufficient information to close CLST 1.05 and 2.07. The NRC stated (Schlueter 2003) that neither DOE's letter report nor the supplement to the letter report addressed the following NRC concerns of the beneficial effect or insignificance of silica deposition on the corrosion rates measured in the long-term corrosion testing facility.

The NRC also asked for specific additional information to close the CLST 1.07 agreement (Schlueter 2003), resulting in CLST 1.07 AIN-1.

Wording of the additional information needed is as follows:

CLST 1.07 AIN-1

The use of appropriate standards should be adopted and exceptions should be properly justified. If a standard is mentioned but not used in its entirety, DOE should indicate specifically which parts of the code will be used (example, G1 is used for identification of equipment, G1 is used for data interval, etc.). Better justification for not using alternative techniques is needed. If such a justification cannot be provided, then DOE must provide details on the alternative techniques to be used for corrosion rate measurements.

A.1.2 Related Key Technical Issue Agreements

There are four KTI agreements related to this KTI agreement, specifically to developing corrosion data using test techniques adopted in CLST 1.07. These are Agreements CLST 1.03, CLST 1.04, CLST 1.06, and CLST 6.01.

A.2 RELEVANCE TO REPOSITORY PERFORMANCE

The issue of test methods used in corrosion testing is important, since the accuracy, uncertainty, and confidence in the corrosion rate obtained by the methods used will have significant impacts on the predicted performance of the repository over the 10,000-year regulated life period. Most standard test methods currently used apply to short-term applications. In the Yucca Mountain Project, the time frame for corrosion prediction is over 10,000 years. The Yucca Mountain Project uses ASTM C 1174-97, *Standard Practice for Prediction of the Long-Term Behavior of Materials, Including Waste Forms, Used in Engineered Barrier Systems (EBS) for Geological Disposal of High-Level Radioactive Waste*, as general guidance and other American Society for Testing and Materials standard methods to develop the database with conservative assumptions in the use of the data for corrosion rate prediction.

A.3 RESPONSE

The Yucca Mountain Project's methods for measuring corrosion rates have been justified and documented in *General Corrosion and Localized Corrosion of Waste Package Outer Barrier* (BSC 2003a). Corrosion rate data for Titanium Grade 7 and Grade 16 are documented in *General Corrosion and Localized Corrosion of the Drip Shield* (BSC 2003b). This response explains the standards adopted by the project and justifies exceptions. Details of alternative techniques or justifications for not using alternative techniques will also be discussed.

Corrosion Rate Measurements—The project uses methods for testing and modeling described in ASTM C 1174 to make predictions of the long-term behavior of materials. The validation approach involves testing specimens over long periods of time. In 2002, the corrosion rate of Alloy 22 was measured for more than 100 coupons (specimens) that were exposed for over 5 years in the Long Term Corrosion Test Facility (LTCTF) at the Lawrence Livermore National Laboratory. Two types of coupons were tested under the following conditions: two temperatures, three solutions, two phases, and two metallurgical conditions. The overall corrosion rate obtained after 5 years of immersion was well below 100 nm/yr. The specific

values of the corrosion rates in each condition and the analysis of the results (influencing variables) are documented in *General Corrosion and Localized Corrosion of Waste Package Outer Barrier* (BSC 2003a) and by Wong et al. (2003). The data in *General Corrosion and Localized Corrosion of Waste Package Outer Barrier* (BSC 2003a) show that the uncertainty in the measured corrosion rate continues to decrease with exposure time. The reduction in uncertainty is also due to more sensitive measurements, better cleaning procedures, and no correction for residual silica deposition from the solution.

Immersion Tests—The Yucca Mountain Project used American Society of Testing and Materials standards that address immersion corrosion testing for measuring corrosion rates. These include ASTM G 31-72, *Standard Practice for Laboratory Immersion Corrosion Testing of Metals*, ASTM G 4-01, *Standard Guide for Conducting Corrosion Tests in Field Application*, and ASTM G 1-90, *Standard Practice for Preparing, Cleaning, and Evaluating Corrosion Test Specimen*. ASTM G 31 addresses guidelines for coupon immersion corrosion testing in the laboratory, ASTM G 4 addresses similar testing in plant or in situ, and ASTM G 1 addresses coupon preparation and cleaning prior to and post testing. The two main general standards used here as general guidelines for immersion testing were ASTM G 31 and ASTM G 1.

Accelerated Tests—Comparatively short-term corrosion immersion testing was used to gather corrosion rate data, which was used in the modeling of the degradation of the waste package (BSC 2003a) and drip shield (BSC 2003b). ASTM C 1174 addresses the appropriate use of accelerated testing and establishes that accelerating factors such as solution concentration, temperature, and applied potential may be used to degrade the material faster than would occur under the intended application conditions, provided the degradation mechanisms remain the same.

Limitations of the Standards Used—The American Society of Testing and Materials standards were used based on the following considerations:

- As per ASTM G 31, complete standardization of corrosion testing is not possible. ASTM G 31 is a guide for testing. The Yucca Mountain Project followed ASTM G 31 guidelines during the LTCTF testing except for the recommended time to test. The technical basis is given in Section A.4.
- There were no contradictions between the guidance given in ASTM G 1 and the procedures used by the Yucca Mountain Project, except for one (improved) variance (discussed in Section A.4 of this appendix). The variance was more sensitive in determining the efficacy of cleaning before establishing the posttest weight loss.
- No exceptions or deviations are noted in the application of ASTM G 4.

Alternative Methods (Electrochemical)—Corrosion rates were measured using immersion tests. Alternative techniques for estimating corrosion rates were also used, not to obtain absolute corrosion rate values, but to assess changes in the corrosion rates as a consequence of changes in the environment or the metallurgical condition of the alloy. The alternative (electrochemical) techniques can be grouped into two main categories:

1. Measurement of Rp using:
 - a. Polarization Resistance method per ASTM G 59-97, *Standard Test Method for Conducting Potentiodynamic Polarization Resistance Measurements*, and ASTM G 102-89, *Standard Practice for Calculation of Corrosion Rates and Related Information from Electrochemical Measurements*
 - b. Alternate Current Impedance method per ASTM G 106-89, *Standard Practice for Verification of Algorithm and Equipment for Electrochemical Impedance Measurements*
2. Measurement of the passive current by applying a constant potential to specimens.

Corrosion rates were estimated for Alloy 22 coupons using the Rp method and the constant potential method. Results are published in *General Corrosion and Localized Corrosion of Waste Package Outer Barrier* (BSC 2003a) and in the open literature (Evans and Rebak 2002; Rebak et al. 2002; Rebak and Estill 2003; Lian et al. 2003; DTN: LL030309512251.042). The results showed that the values of corrosion rates obtained with electrochemical methods corroborate results obtained with the immersion tests. For instance, the electrochemical results showed that the corrosion rates calculated via the two electrochemical methods follow known relationships with the temperature or concentration of the electrolyte (BSC 2003a; Rebak and Estill 2003). Values of corrosion rates measured via electrochemical methods are not used to predict the lifetime of the waste packages. Electrochemical methods for corrosion rate evaluation are fast tools that provide insight on factors influencing corrosion rate.

Additional information on corrosion rate measurements can be found in Section 5.1.

The information in this report is responsive to NRC's AIN request CLST 1.07 AIN-1. The report contains the information that the DOE considers necessary for NRC review for closure of the agreement.

A.4 BASIS FOR THE RESPONSE

A.4.1 Corrosion Testing for the Prediction of Long-Term Behavior of Materials

The project used characterization tests defined in ASTM C 1174 to help develop models by understanding the mechanisms of the degradation modes. American Society of Testing and Materials Committee C-26 on Nuclear Fuel Cycle prepared standard ASTM C 1174 to provide guidelines, among other issues, on the corrosion testing of materials. ASTM C 1174 also states that actual data on the long-term behavior of materials under realistic repository conditions will not be available for use in waste package design. Therefore, ASTM C 1174 establishes how short-time data need to be used to support the development of predictive behavior models for

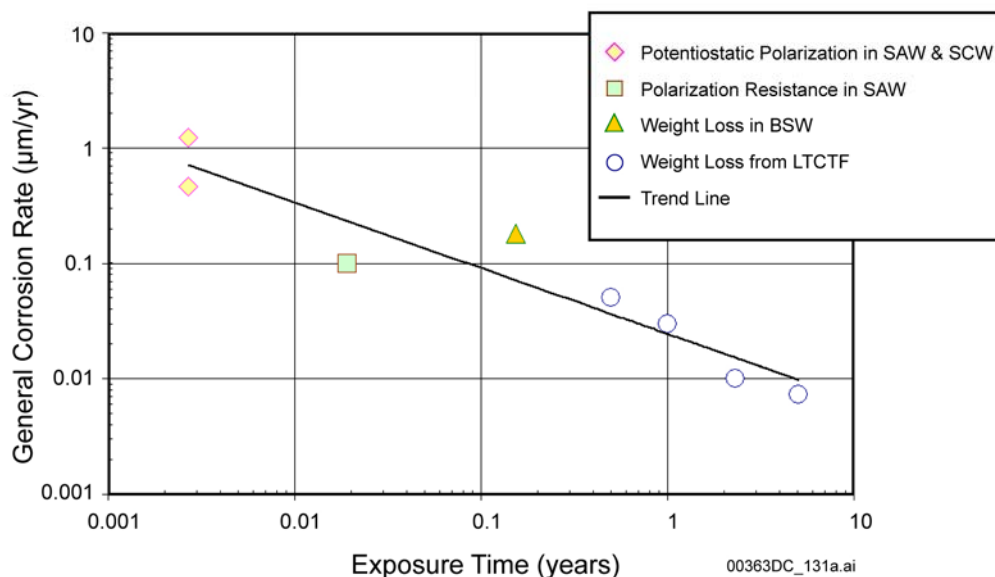
waste packages over times as long as 10,000 years. ASTM C 1174 also provides guidance for performing accelerated corrosion tests to compensate for the shorter testing time. The accelerating factors described in ASTM C 1174 may include the use of more concentrated solutions, higher temperatures, and applied potentials and may be used, provided the degradation (alteration) mechanisms remain the same. The effects of accelerating conditions should be quantified and mechanistically described. Applications to the Yucca Mountain Project include corrosion rate measurements and polarization resistance. The corrosion testing procedures and results described in the following section correspond to American Society of Testing and Materials methods written by the Corrosion of Metals committee. These methods for measuring corrosion rates (e.g., ASTM G 31 and ASTM G 1) are considered short term; however, they employ accelerating factors (e.g., concentrated solutions).

A.4.2 Corrosion Rates Measurements

This section provides the technical basis for the general corrosion rate that can be expected for Alloy 22 (UNS N06022) under repository conditions. In 2002, the corrosion rate of Alloy 22 was measured for more than 100 coupons that were exposed for over 5 years in the LTCTF at the Lawrence Livermore National Laboratory. The testing conditions in the LTCTF included three different electrolyte solutions (simulated acidified water, simulated dilute water, and simulated concentrated water), and two temperatures (60°C and 90°C). For each electrolyte solution the coupons were immersed in the liquid aqueous solution and also exposed to the vapor phase (above the solution) where condensation occurred. Simulated acidified water is approximately 1,000 times more concentrated than well J-13 water and has a pH of approximately 3. Simulated dilute water is approximately 10 times more concentrated than well J-13 water and has a pH of approximately 10. Simulated concentrated water is approximately 1,000 times more concentrated than well J-13 water and also has a pH of approximately 10. Alloy 22 was tested in both the mill-annealed wrought condition and in the as-welded condition. Under each condition mentioned above, Alloy 22 was tested in creviced and noncreviced conditions. Taking into account all the variables mentioned above (two temperatures, three solutions, two aqueous phases, two metallurgical states, and two types of coupons), it is concluded that Alloy 22 was tested in a wide range of repository conditions. The overall general corrosion rate obtained after 5 years of immersion was well below 100 nm/yr. The specific values of the corrosion rates in each condition and the analysis of the results (influencing variables) are fully documented in *General Corrosion and Localized Corrosion of Waste Package Outer Barrier* (BSC 2003a) and in a literature publication (Wong et al. 2003). The corrosion rate values for titanium alloys are documented in *General Corrosion and Localized Corrosion of the Drip Shield* (BSC 2003b).

Figure A-1 shows that the corrosion rate of Alloy 22 follows a logical trend for passive metals; that is, the corrosion rate decreases as the exposure time increases. Figure A-1 also includes corrosion rates for Alloy 22 measured using electrochemical tests (polarization resistance). More corrosion rates measured via electrochemical methods are also reported in *General Corrosion and Localized Corrosion of Waste Package Outer Barrier* (BSC 2003a) and in other publications (Evans and Rebak 2002; Lian et al. 2003; Rebak and Estill 2003). The data in *General Corrosion and Localized Corrosion of Waste Package Outer Barrier* (BSC 2003a) also shows that the uncertainty in the measured corrosion rate continues to decrease with exposure time. This is also due to more sensitive measurements, better cleaning procedures, and no

correction for residual deposition of silica from the solution, all employed in the analysis for the 5-year exposure specimens.



NOTE: BSW = basic saturated water. General corrosion rate of Alloy 22 (N06022) in multi-ionic solutions at 90°C decreases as exposure time increases.

Figure A-1. Alloy 22 Mean General Corrosion Rate versus Exposure Time at 90°C

A.4.3 Immersion Tests

The discussion that follows applies to both Alloy 22 and other nickel alloys (e.g., UNS N06455 or Alloy C-4, UNS N08825 or Alloy 825, UNS N06625 or Alloy 625) as well to Titanium Grade 7 (UNS R52400) and other titanium alloys (e.g., UNS R52402 or Titanium Grade 16 and UNS R53400 or Titanium Grade 12).

During the design of new industrial equipment, the most common and accepted method for measuring corrosion rates is using immersion tests or weight (mass) loss tests. In this method, coupons of the alloy under study are immersed in the corrosive medium in question for a certain period of time. Assuming uniform penetration or thinning of the coupon, the corrosion rate or penetration rate is calculated by dividing the weight loss during immersion by the exposed area and the immersion time (Equation A-1; ASTM G 1, Section 8)

$$CR(mm/year) = 8.76 \times 10^4 \frac{W_i - W_f(g)}{A(cm^2) \cdot t(h) \cdot \delta(g/cm^3)} \quad (\text{Eq. A-1})$$

where W_i is the initial (prior to immersion) weight (mass) of the coupon, W_f is the final weight of the coupon, A is the surface area of the coupon exposed to the corroding electrolyte, t is the

immersion time, and δ is the density of the studied alloy. The constant in the formula accounts for the conversion between centimeters and millimeters and between hours and years.

The most common standards for corrosion testing are provided by the American Society for Testing and Materials through their Corrosion of Metals Committee. The American Society of Testing and Materials has several standards that address immersion testing for measuring corrosion rates. The main standards for general purpose immersion testing include ASTM G 31, ASTM G 4, and ASTM G 1. For example, ASTM G 31 addresses guidelines for coupon immersion corrosion testing in the laboratory, ASTM G 4 addresses similar testing in plant or in situ and ASTM G 1 addresses coupon preparation and cleaning prior to and after testing. Other American Society of Testing and Materials standards for immersion testing such as ASTM G 28-97, *Standard Test Methods of Detecting Susceptibility to Intergranular Corrosion in Wrought, Nickel-Rich, Chromium-Bearing Alloys*, and ASTM G 48-99a, *Standard Test Methods for Pitting and Crevice Corrosion Resistance of Stainless Steels and Related Alloys by Use of Ferric Chloride Solution*, address immersion testing in specific environments such as acidified ferric sulfate and ferric chloride. The two main general standards used for immersion testing were ASTM G 31 (on how to do the test) and ASTM G 1 (on how to handle the coupons).

It should be noted that ASTM C 1174 was written to account for testing geared specifically to the application of materials for long-term geologic repositories. This standard states that acceleration factors, such as temperature, solution composition, and potential, could be used to determine degradation rates in a shorter time. The project is using in its modeling efforts corrosion rate values determined in solutions that are, for example, 1,000 times more concentrated than the groundwater at the Yucca Mountain site. Some of these solutions were purposely acidified to determine material behavior in such conditions. Short-term electrochemical tests were done using forced polarization to determine corrosion response under extreme conditions. All these factors are analyzed and described in detail in the corresponding analysis and model reports. The interpretation of the various results is outside the scope of this CLST 1.07 response.

A.4.4 Limitation of the Standards Used

ASTM G 31, Standard Practice for Laboratory Corrosion Testing of Metals—Because ASTM G 31 is an all-encompassing standard practice for corrosion testing, it is not practical to follow every provision of the standard for a specific test. A disclaimer written into ASTM G 31 states that the complete standardization of corrosion testing is not possible; that is, ASTM G 31 is presented only as a guide for testing. However, most of the items or procedures in ASTM G 31 were strictly followed during the long-term testing in the LTCTF. There were two exceptions from ASTM G 31:

1. Item 7.10: This item states that the preparation of the specimens (coupons) prior to testing should be documented for interpretation by others. The specimens installed in the LTCTF were visually inspected, but detailed (such as scanning electron microscopy) images of the coupons prior to testing do not exist. It is useful to note that ASTM G 31 does not require scanning electron microscope images from the coupons before testing, but it is now understood that this is a good practice. Test specimens for the LTCTF were purchased in 1996 with a specified surface finish of

32 root mean square (in micro inch) for the weight loss coupons (both faces) and 16 root mean square for the label (front) face and 32 root mean square for the opposite (back) face of the crevice coupons. In the LTCTF coupons, the crevice former washer assembly was placed on the label (front) face of the coupon and the smoother machined surface permitted formation of a “tighter” crevice. The coupons were used in the as-received condition; that is, no additional polishing was performed. Each test specimen was handled and examined individually during initial dimensioning and weighing before exposure to the test solution. In all cases, the observed surface was consistent with the surface finish specification and no particular features or anomalies were noted in the “comment” section in the test records. In the 1996 to 1997 period, a high-resolution scanning electron microscope (used later in the analysis of the 5-year exposure specimens) was not available for more detailed characterization of the before-test surface. Therefore, a one-to-one comparison cannot be made of the specimen surfaces between “before” and “after” tests. Nevertheless, careful scanning electron microscope viewing of the cleaned Alloy 22 coupons after the 5-year immersion tests showed no apparent corrosion. That is, the grinding marks typical of grit 120 and 240 appear sharp and noncorroded.

2. Item 8.11.4: This item deals with the recommended exposure time for immersion testing. For moderate to low corrosion rates, ASTM G 31 recommends that the duration of the corrosion test be proportional to the estimated corrosion rate:

$$Hours = \frac{2000}{CR(mpy)} \quad (\text{Eq. A-2})$$

where CR is the corrosion rate in mils per year. In the industry, the lowest corrosion rate that is used for an alloy in a given environment is greater than 1 mpy (or 25 $\mu\text{m}/\text{yr}$). That is, for this corrosion rate of 1 mpy, the longest testing time according to Equation A-2 would be 12 weeks (3 months). However, the application of materials for the Yucca Mountain Project is unique in the length of its design lifetime of 10,000 years. In the Yucca Mountain case, the corrosion rate of the selected alloy has to be extremely low, lower by a factor of 1,000 than industry practice. Estimating a maximum corrosion rate of approximately 100 nm/yr (10^{-4} mm/yr or 4×10^{-3} mpy) for the waste package in Yucca Mountain characteristic environments, the suggested testing time according to Equation A-2 should be approximately 50 to 60 years. These times are unrealistic for laboratory testing and the reason is that the ASTM G 31 standard is aimed to material–environment pairs with higher corrosion rates than the ones required for Yucca Mountain Project. Again, the same ASTM G 31 standard suggests that it a guideline. Therefore, determination of the length of time for conducting the corrosion testing of Alloy 22 and Titanium Grade 7 according to Equation A-2 was deemed impractical. The current design data is for 5 years exposure or approximately 10 percent of the testing time calculated according to Equation A-2. It is expected that continued testing for longer times will only result in lower corrosion rates as supported by the data in Figure A-1. The longer-term tests are ongoing.

ASTM G 1 Standard Practice for Preparing, Cleaning, and Evaluating Corrosion Test Specimen—There were no contradictions between guidance given in ASTM G 1 and the procedures used in long-term testing, except for the following:

1. 7.1.1: This item recommends the use of uncorroded coupons to establish a cleaning procedure that would not remove base material. Yucca Mountain Project performed a thorough study on the cleaning methods used for the 5-year LTCTF samples that were exposed to the different testing conditions. The studies were carried out to determine that the cleaning method does not remove base metal from the sample being cleaned. ASTM G 1 recommends the use of uncorroded replicates to determine that the cleaning procedure posttesting is not removing base metal. These uncorroded coupons were unavailable. Therefore, to replace uncorroded specimens, Alloy 22 foils were used with a thickness of 2 mils (50 μm). The foils used for the cleaning procedure trials were Alloy 22 (N06022), per ASTM B 575-99a, *Standard Specification for Low-Carbon Nickel-Molybdenum-Chromium, Low-Carbon Nickel-Chromium-Molybdenum, Low-Carbon Nickel-Chromium-Molybdenum-Copper, Low-Carbon Nickel-Chromium-Molybdenum-Tantalum, and Low-Carbon Nickel-Chromium-Molybdenum-Tungsten Alloy Plate, Sheet, and Strip*. The heat of the foil was 2277-4-3145 (Alloy 22 produced by Haynes International Inc.) and the composition of the foils was Ni-21.78Cr-13.26Mo-3.05W-4.05Fe-0.33Mn-0.72Co-0.16V. The project did not have replicate samples, and there is no standard to substitute the nontested replicate samples for foils but the foils were deemed to be more efficient than replicate samples. The Alloy 22 foils used had a surface-to-volume ratio 50 times larger than the actual coupons; consequently, the foils were more sensitive to mass removal during cleaning. It can be interpreted that the results obtained by the use of Alloy 22 foils were more accurate than with the use of uncorroded coupons.

A.4.5 Alternative Methods (Electrochemical)

Immersion tests were the main mode of measuring corrosion rates. Alternative techniques for estimating corrosion rates were also used to assess changes in the corrosion rates as a consequence of changes in the environment or the metallurgical condition of the alloy. These alternative techniques can be grouped in two main categories:

1. Measurement of the resistance to polarization, which was done using the polarization resistance method (ASTM G 59, ASTM G 102), and the alternate current impedance method (ASTM G 106) can be used as a reference.
2. Measurement of the passive current by applying a constant potential to specimens (there are no standards for these tests, but they could be ascribed under ASTM G 3-89, *Standard Practice for Conventions Applicable to Electrochemical Measurements in Corrosion Testing*).

Polarization Resistance—The polarization resistance technique is very well established for predicting corrosion rates and monitoring changes (Jones 1996). The principle of measuring the polarization resistance is as follows. When a metal is forcibly polarized in an electrolyte, there is a corresponding current output (i) for each applied potential (E). R_p is defined as the slope of a

dE/di curve in the vicinity of the corrosion potential. Electrochemically, there is a direct inverse relationship between R_p and the corrosion current (i.e., the corrosion rate is inversely proportional to R_p (ASTM G 59, ASTM G 102)). Values needed to convert R_p to corrosion rate include the anodic and cathodic Tafel slopes (β_a and β_c) and the equivalent weight of the alloy. These three values can be calculated or assumed but cannot be known with certainty. For example, the values of the Tafel slopes may change with the temperature, solution composition, or surface preparation.

The other source of uncertainty in the calculation of the corrosion rate from R_p is the value of the equivalent weight. This value changes according to the assumed oxidation state (valence) of the elements in the alloy while corroding. ASTM G 102 gives different values of equivalent weight for Alloy 22 and Titanium Grade 2 as a function of the presumed value of the dissolving elements' valences. Only values of equivalent weight listed in ASTM G 102 for each alloy (titanium and Alloy 22) were used. Therefore, since both equivalent weight and β cannot be exactly known, corrosion rates calculated from R_p are used only to indicate relative changes in the corrosion rate due to changes in the environment or metallurgical condition of the alloy. For example, the R_p method is a fast tool to estimate how much the corrosion rate changes when nitrate is added to a chloride solution, or to determine the activation energy for the corrosion of a certain alloy in a given environment (i.e., to determine changes in the corrosion rate while the temperature changes). R_p can be calculated using the polarization resistance method (ASTM G 59) or alternating current impedance tests (ASTM G 106). The R_p method was used.

Constant Potential or Potentiostatic Tests—Constant potential tests are used to determine the evolution of the passive current density as a function of time. Theoretically, when a constant potential is applied to a passive metal, the current density may decrease as a function of time until a steady state current density is reached. It is assumed that this steady state value of current density represents the dissolution rate of the alloy under passive conditions. Then, this current density can be transformed into corrosion rate using the equivalent weight and the density of the alloy. The major uncertainties here are the actual value of equivalent weight and whether the passive current represents the actual passive dissolution of the alloy. The first point was discussed above. The second point is a source of uncertainty since the true dissolution current cannot be known, due to two reasons: (1) the time for steady state passive current density may not be achieved in laboratory tests and (2) in presence of redox reactions in the solution the measured current density could be a mixture of several different reactions, not only passive dissolution. For example, in the presence of dissolved oxygen, the reduction of oxygen to water may consume electrons short-circuiting the flow to the counter electrode. Thus, the actual passive current density for metal dissolution may be higher than the measured one. The magnitude of this underestimation of the passive current will depend on the system and the value of the applied potential.

A.4.6 Results from Alternative Methods

Corrosion rates were estimated for Alloy 22 using the R_p method and the constant potential method. Some of these results are shown in Figure A-1. Findings obtained are published in *General Corrosion and Localized Corrosion of Waste Package Outer Barrier* (BSC 2003a) and in the open literature (Evans and Rebak 2002; Rebak et al. 2002; Rebak and Estill 2003; Lian et al. 2003; DTN: LL030309512251.042). Results show that the corrosion rates calculated via

these two methods follow known relationships with the temperature or concentration of the electrolyte. That is, the values of corrosion rates obtained with the electrochemical methods corroborate the results obtained with the immersion tests. Values of corrosion rates measured via electrochemical methods are not used to predict the lifetime of the waste packages. Electrochemical methods for corrosion rate evaluation are fast tools that provide insight on factors influencing the corrosion rate.

Moreover, the project has used accelerated tests, as defined in ASTM C 1174, to help develop the predictive models by understanding the mechanisms of the degradation modes. The alternative methods, along with the 5-year general corrosion rate data, including service condition testing and accelerated testing, are sufficient for providing confidence in the models and closure of this agreement.

A.5 REFERENCES

A.5.1 Documents Cited

BSC (Bechtel SAIC Company) 2003a. *General Corrosion and Localized Corrosion of Waste Package Outer Barrier*. ANL-EBS-MD-000003 REV 01. Las Vegas, Nevada: Bechtel SAIC Company. ACC: DOC.20030916.0010.

BSC 2003b. *General Corrosion and Localized Corrosion of the Drip Shield*. ANL-EBS-MD-000004 REV 01. Las Vegas, Nevada: Bechtel SAIC Company. ACC: DOC.20030626.0001.

Evans, K.J.; and Rebak, R.B. 2002. "Passivity of Alloy 22 in Concentrated Electrolytes Effect of Temperature and Solution Composition." *Proceedings of the International Symposium on a Retrospective and Current Status in Honor of Robert P. Frankenthal*. Frankel, G.S.; Isaacs, H.S.; Scully, J.R.; and Sinclair, J.D. *Electrochemical Society Proceedings Volume 2002-13*, 344-354. Pennington, New Jersey: The Electrochemical Society. TIC: 254801.

Jones, D.A. 1996. *Principles and Prevention of Corrosion*. 2nd Edition. Upper Saddle River, New Jersey: Prentice Hall. TIC: 241233.

Lian, T.; Estill, J.C.; Hurst, G.A.; and Rebak, R.B. 2003. "Passive and Transpassive Dissolution of Alloy 22 in Simulated Repository Environments." *Corrosion/2003, [58th Annual Conference & Exposition, March 16-20, 2003, San Diego, California]*. Paper No. 03694. Houston, Texas: NACE International. TIC: 254906.

Rebak, R.B.; Edgecumbe Summers, T.S.; Lian, T.; Carranza, R.M.; Dillman, J.R.; Corbin, T.; and Crook, P. 2002. "Effect of Thermal Aging on the Corrosion Behavior of Wrought and Welded Alloy 22." *Corrosion/2002, [57th Annual Conference & Exposition, April 7-11, 2002, Denver, Colorado]*. Paper No. 02542. Houston, Texas: NACE International. TIC: 254582.

Rebak, R.B. and Estill, J.C. 2003 "Review of Corrosion Modes for Alloy 22 Regarding Lifetime Expectancy of Nuclear Waste Containers," *Mat. Res. Soc. Symp. Proc.* Finch, R.J. and Bullen, D.B. 757, II4.1.1-114.1.9. Warrendale, Pennsylvania: Materials Research Society. TIC: TBD.

Schlueter, J.R. 2000. U.S. Nuclear Regulatory Commission/U.S. Department of Energy Technical Exchange and Management Meeting on Container Life and Source Term (September 12-13, 2000). Letter from J. Schlueter (NRC) to S. Brocoum (DOE), October 4, 2000, with enclosure. ACC: MOL.20010731.0161.

Schlueter, J.R. 2003. "Container Life and Source Term Key Technical Issue Agreement 1.05, 1.06, 1.07, and 2.07, with Request for Additional Information for 1.06 and 1.07." Letter from J.R. Schlueter (NRC) to J.D. Ziegler (DOE/ORD), January 24, 2003, 0129035857, with attachment. ACC: MOL.20030603.0313.

Wong, L.L.; Fix, D.V.; Estill, J.C.; McCright, R.D.; and Rebak, R.B. 2003. "Characterization of the Corrosion Behavior of Alloy 22 after Five Years Immersion in Multi-ionic Solutions." *Mat. Res. Soc. Symp. Proc.* Finch, R.J. and Bullen, D.B. 757, II4.4.1-II4.4.7. Warrendale, Pennsylvania: Materials Research Society. TIC: TBD.

Ziegler, J.D. 2002a. "Transmittal of Information Addressing Key Technical Issue (KTI) Agreement Items Container Life and Source Term (CLST) 1.05, 1.06, 1.07, and 2.07." Letter from J.D. Ziegler (DOE/YMSCO) to J.R. Schlueter (NRC), 0710023266, OL&RC:TCG-1379, with enclosure. ACC: MOL.20020911.0128.

Ziegler, J.D. 2002b. "Transmittal of Supplement to Report Addressing Key Technical Issue (KTI) Agreements Container Life and Source Term (CLST) 1.05, 1.06, 1.07, and 2.07." Letter from J.D. Ziegler (DOE/ORD) to J.R. Schlueter (NRC), November 1, 2002, 1104024968, OLA&S:TCG-0060, with enclosure. ACC: MOL.20030213.0007.

A.5.2 Codes, Standards, and Regulations

ASTM (American Society for Testing and Materials) B 575-99a. 1999. *Standard Specification for Low-Carbon Nickel-Molybdenum-Chromium, Low-Carbon Nickel-Chromium-Molybdenum, Low-Carbon Nickel-Chromium-Molybdenum-Copper, Low-Carbon Nickel-Chromium-Molybdenum-Tantalum, and Low-Carbon Nickel-Chromium-Molybdenum-Tungsten Alloy Plate, Sheet, and Strip.* West Conshohocken, Pennsylvania: American Society for Testing and Materials. TIC: 247534.

ASTM C 1174-97. 1998. *Standard Practice for Prediction of the Long-Term Behavior of Materials, Including Waste Forms, Used in Engineered Barrier Systems (EBS) for Geological Disposal of High-Level Radioactive Waste.* West Conshohocken, Pennsylvania: American Society for Testing and Materials. TIC: 246015.

ASTM G 1-90 (Reapproved 1999). 1999. *Standard Practice for Preparing, Cleaning, and Evaluating Corrosion Test Specimens.* West Conshohocken, Pennsylvania: American Society for Testing and Materials. TIC: 238771.

ASTM G 3-89 (Reapproved 1999). 1989. *Standard Practice for Conventions Applicable to Electrochemical Measurements in Corrosion Testing.* West Conshohocken, Pennsylvania: American Society for Testing and Materials. TIC: 247076.

ASTM G 4-01. 2001. *Standard Guide for Conducting Corrosion Tests in Field Application*. West Conshohocken, Pennsylvania: American Society for Testing and Materials. TIC: 254905.

ASTM G 28-97. 1997. *Standard Test Methods of Detecting Susceptibility to Intergranular Corrosion in Wrought, Nickel-Rich, Chromium-Bearing Alloys*. West Conshohocken, Pennsylvania: American Society for Testing and Materials. TIC: 249897.

ASTM G 31-72 (Reapproved 1999). 1972. *Standard Practice for Laboratory Immersion Corrosion Testing of Metals*. West Conshohocken, Pennsylvania: American Society for Testing and Materials. TIC: 249897.

ASTM G 48-99a. 1999. *Standard Test Methods for Pitting and Crevice Corrosion Resistance of Stainless Steels and Related Alloys by Use of Ferric Chloride Solution*. West Conshohocken, Pennsylvania: American Society for Testing and Materials. TIC: 247546.

ASTM G 59-97. 1998. *Standard Test Method for Conducting Potentiodynamic Polarization Resistance Measurements*. West Conshohocken, Pennsylvania: American Society for Testing and Materials. TIC: 249897.

ASTM G 102-89 (Reapproved 1999). 1989. *Standard Practice for Calculation of Corrosion Rates and Related Information from Electrochemical Measurements*. West Conshohocken, Pennsylvania: American Society for Testing and Materials. TIC: 249897.

ASTM G 106-89 (Reapproved 1999). 1989. *Standard Practice for Verification of Algorithm and Equipment for Electrochemical Impedance Measurements*. West Conshohocken, Pennsylvania: American Society for Testing and Materials. TIC: 249897.

A.5.3 Data, Listed by Data Tracking Number

LL030309512251.042. Low Temperature Operating Mode Electrochemical Test
Data: Corrosion Potential, Linear Polarization, and Cyclic Polarization Tests of Alloy 22 in Oxalic Acid, NaF, NaCl, NaF+NaCl, and CaCl₂ Solutions Recorded at 30, 45, 60, 75, 90 and 105 Deg C. Submittal date: 05/22/2003.

INTENTIONALLY LEFT BLANK

APPENDIX B
DISTRIBUTION OF STRESSES
(RESPONSE TO CLST 1.13 AND GEN 1.01 COMMENT 120)

Note Regarding the Status of Supporting Technical Information

This document was prepared using the most current information available at the time of its development. This Technical Basis Document and its appendices providing Key Technical Issue Agreement responses that were prepared using preliminary or draft information reflect the status of the Yucca Mountain Project's scientific and design bases at the time of submittal. In some cases this involved the use of draft Analysis and Model Reports (AMRs) and other draft references whose contents may change with time. Information that evolves through subsequent revisions of the AMRs and other references will be reflected in the License Application as the approved analyses of record at the time of License Application submittal. Consequently, the DOE will not routinely update either this Technical Basis Document or its Key Technical Issue Agreement appendices to reflect changes in the supporting references prior to submittal of the License Application.

APPENDIX B

DISTRIBUTION OF STRESSES (RESPONSE TO CLST 1.13 AND GEN 1.01 COMMENT 120)

This appendix provides a response to Key Technical Issue (KTI) agreement Container Life and Source Term (CLST) 1.13 and General Agreement (GEN) 1.01 (Comment 120). These KTI agreements relate to providing documentation on methods used to measure corrosion rates of the waste package materials.

B.1 KEY TECHNICAL ISSUE AGREEMENTS

B.1.1 CLST 1.13 and GEN 1.01 (Comment 120)

Agreement CLST 1.13 was reached during the U.S. Nuclear Regulatory Commission (NRC)/U.S. Department of Energy (DOE) Technical Exchange and Management Meeting on CLST held September 12-13, 2000, in Las Vegas, Nevada. Subissues 1 (effects of corrosion processes on the lifetime of the containers), 2 (effects of phase instability and initial defects on the mechanical failure and lifetime of the containers), 3 (the rate at which radionuclides in spent nuclear fuel are released from the engineered barrier subsystem through the oxidation and dissolution of spent nuclear fuel), 4 (the rate at which radionuclides in high-level radioactive waste glass are released from the engineered barrier subsystem), and 6 (effects of alternate engineered barrier subsystem design features on container lifetime and radionuclide release from the engineered barrier subsystem) were discussed at the meeting (Schlueter 2000). There has been no submittal related to this KTI agreement to the NRC.

Agreement GEN 1.01 was reached during the NRC/DOE Technical Exchange and Management Meeting held September 18 to 19, 2001 (Reamer and Gil 2001). At that meeting, NRC provided additional comments that relate to CLST 1.13 including GEN 1.01 (Comment 120) (Reamer and Gil 2001).

Wording of the agreement is as follows:

CLST 1.13

Provide the data that characterizes the distribution of stresses due to laser peening and induction annealing of Alloy 22. DOE will provide the documentation in a revision to AMR (ANL-EBS-MD-000005) prior to LA.

GEN 1.01 (Comment 120)

Page 7-11, the use of the triangular distribution for the residual stress uncertainty dictates that the endpoints of the distribution are well known. Showing the data compared to the distribution would support the selection of a triangular distribution.

DOE Initial Responses to GEN 1.01 (Comment 120):

A triangular distribution is used to represent uncertainty in the residual stress and stress intensity factor profiles in the weld regions of the outer and inner closure lids of the waste package Alloy 22 outer barrier. The triangular distribution was used because the uncertainty bounds used are conservative, considering the strict process control and inspections that will be implemented during the waste package manufacturing process.

If the data currently being obtained under existing CLST KTI agreements 1.12 and 1.13 warrant a change in the assumed distribution, this would be carried forward into a potential TSPA-LA in accordance with KTI agreement TSPA 3.41.

B.1.2 Related Key Technical Issue Agreements

There are five KTI agreements related to KTI agreement CLST 1.13. These are agreements CLST 1.04, CLST 1.12, CLST 1.15, CLST 1.16, and TSPA 3.41. These agreements relate to corrosion data for Alloy 22 altered by stress mitigation processes.

B.2 RELEVANCE TO REPOSITORY PERFORMANCE

Drip shields will be installed over the waste packages prior to repository closure. The drip shields will be made of Titanium Grade 7 seepage diversion plates with Titanium Grade 24 stiffeners and support beams, which provide a mix of corrosion resistance and structural strength. The drip shields divert any moisture (including condensed water vapor) that might seep from the drift walls around the waste packages to the drift floor for thousands of years. The drip shields also protect the underlying waste packages in the event of expected rockfalls, as the emplacement drifts degrade over time. Material microstructure becomes altered during fabrication and stress relief processes, but not all processes generate adverse structural conditions. The detrimental conditions, particularly those that degrade the corrosion performance of Alloy 22, need to be evaluated.

B.3 RESPONSE

Induction annealing is no longer planned for mitigation of waste package closure weld residual stresses. Laser peening is the current baseline residual stress mitigation methodology. The current design specifies the outer and middle Alloy 22 closure lids. Alloy 22 outer-lid closure weld regions will be stress mitigated by either laser peening or controlled plasticity burnishing. Alloy 22 middle-lid closure weld regions will not be stress mitigated.

The analysis of the through-wall stress and stress intensity factor distributions is documented in *Stress Corrosion Cracking of the Drip Shield, the Waste Package Outer Barrier, and the Stainless Steel Structural Material* (BSC 2003a) and the results including the effects of uncertainty are documented in *WAPDEG Analysis of Waste Package and Drip Shield Degradation* (BSC 2003b). It is concluded that the hoop stress, which promotes radially oriented crack growth, is the dominant component of stress in the waste package outer shell closure lid weld regions and, therefore, only the hoop stress profiles were considered in the integrated waste

package degradation model documented in *WAPDEG Analysis of Waste Package and Drip Shield Degradation* (BSC 2003b).

The angular variation is included using the following functional form:

$$\sigma(x, \theta) = \sigma(x, 0) - (17.236893) \cdot (1 - \cos(\theta)) \quad (\text{Eq. B-1})$$

The stress intensity factor variation with angle is given by

$$K(x, \theta) = K(x, 0) \cdot \left(\frac{\sigma(\text{Thck}, \theta)}{\sigma(\text{Thck}, 0)} \right) \quad (\text{Eq. B-2})$$

where *Thck* is taken to be the maximum depth value (about 20 mm). In performance assessment, the stress intensity factor is coupled with the distribution of weld flaws documented in *WAPDEG Analysis of Waste Package and Drip Shield Degradation* (BSC 2003b) to quantify the extent of stress corrosion cracking (SCC) through-wall propagation resulting from these flaws. The uncertainty in the stress and stress intensity factor profiles is introduced through a scaling factor, *sz*. The stress relation, accounting for uncertainty, is given by

$$\sigma_u(x, \theta, z) = \sigma(x, \theta) \cdot \left(\frac{\sigma(\text{Thck}, \theta) + sz}{\sigma(\text{Thck}, \theta)} \right) \quad (\text{Eq. B-3})$$

and the stress intensity factor relation, accounting for uncertainty, is given by

$$K_{1u}(x, \theta, z) = K(x, \theta) \cdot \left(\frac{\sigma(\text{Thck}, \theta) + sz}{\sigma(\text{Thck}, \theta)} \right) = K_1(x, 0) \cdot \left(\frac{\sigma(\text{Thck}, \theta) + sz}{\sigma(\text{Thck}, 0)} \right) \quad (\text{Eq. B-4})$$

More information on distribution of stress and SCC can be found in Section 9 of the technical basis document.

Specific Response for GEN 1.01 (Comment 120)—The median residual stress versus depth distribution is determined using finite element calculations accounting for the thermal perturbations induced by the welding process (BSC 2003a, Section 6.4.2.2). The effects of stress mitigation (laser peening) were then superposed on the results of the finite element calculation (BSC 2003a, Section 6.4.4). The resulting stress profile was fit to a third-order polynomial as a function of depth. Uncertainty in the residual stress profile was evaluated by considering measured data of samples that had undergone laser peening and shot peening. Also, empirical distributions in the published literature were considered. The uncertainty in the residual stress distribution was found to be represented by a multiplicative adjustment factor dependent on an uncertain parameter given by a normal distribution with a mean zero and a standard deviation of 5 percent of the yield strength of Alloy 22 (BSC 2003a, Section 6.4.5). The normal distribution is truncated at ± 3 standard deviations (± 15 percent of the yield strength), which encompasses 99.7 percent of the parameter variation.

The subject agreement also refers to CLST 1.12 and TSPA 3.41. While CLST 1.12 is covered in Appendix G, TSPA 3.41 will be addressed in the future.

The information in this report is responsive to agreements CLST 1.13 and GEN 1.01 (Comment 120) made between the DOE and NRC. The report contains the information that the DOE considers necessary for NRC review for closure of the agreement.

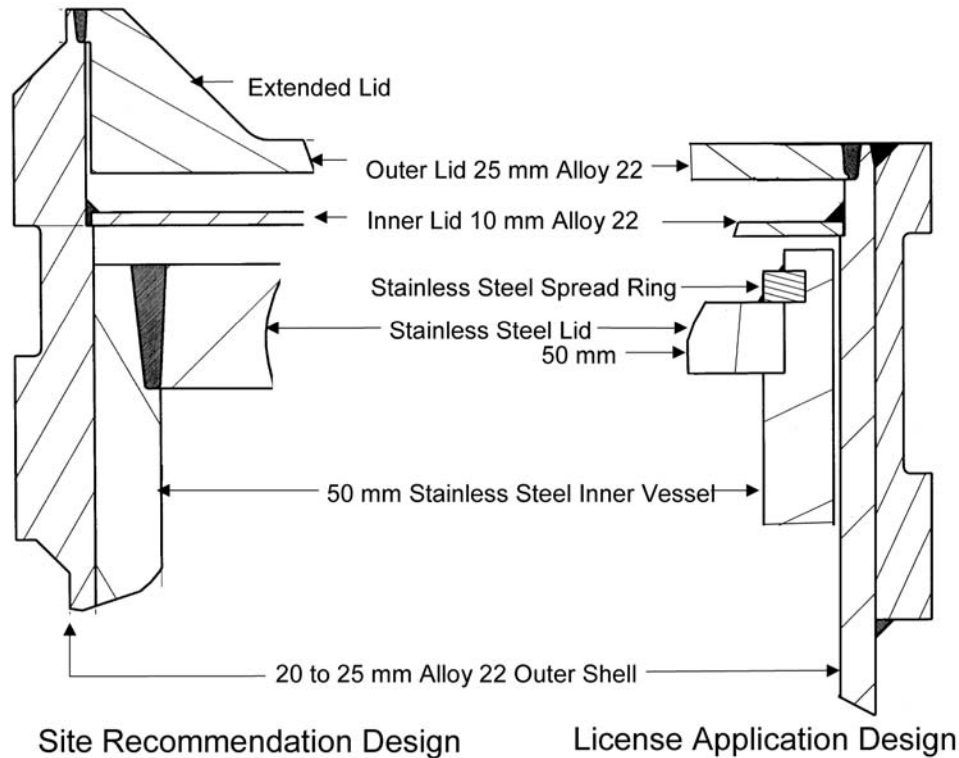
B.4 BASIS FOR THE RESPONSE

Induction annealing is not planned for mitigation of waste package closure stresses. Laser peening is the current baseline method. The current design specifies two Alloy 22 lids for the closure (by welding) of the waste packages. The outer lid closure weld will be stress mitigated by either laser peening or controlled plasticity burnishing. The Alloy 22 middle-lid closure weld will not be stress mitigated. The reasons for the current closure systems are:

- Sufficient time delay for initiation of SCC
- Less possibility of harming Alloy 22 microstructure through heat treatment, reducing performance uncertainty and the probability of early waste package failure
- Greater facility throughput through reduction of waste package closure time
- Removal of dedicated cell required for induction annealing
- Improved operability and reduced rework rates
- Lower utility requirements (primarily electricity).

Sketches of the site recommendation design and the current recommended license application design of the waste package closure lid region of the waste package are shown in Figure B-1.

Figure B-1 indicates a physical separation between the two Alloy 22 lids. Thus, if SCC cracks were to penetrate the outer lid, they would not continue to propagate into the Alloy 22 middle lid. However, if cracks penetrated the outer lid, the Alloy 22 middle-lid closure welds would be subjected to the external environment and the potential for crack initiation and growth.

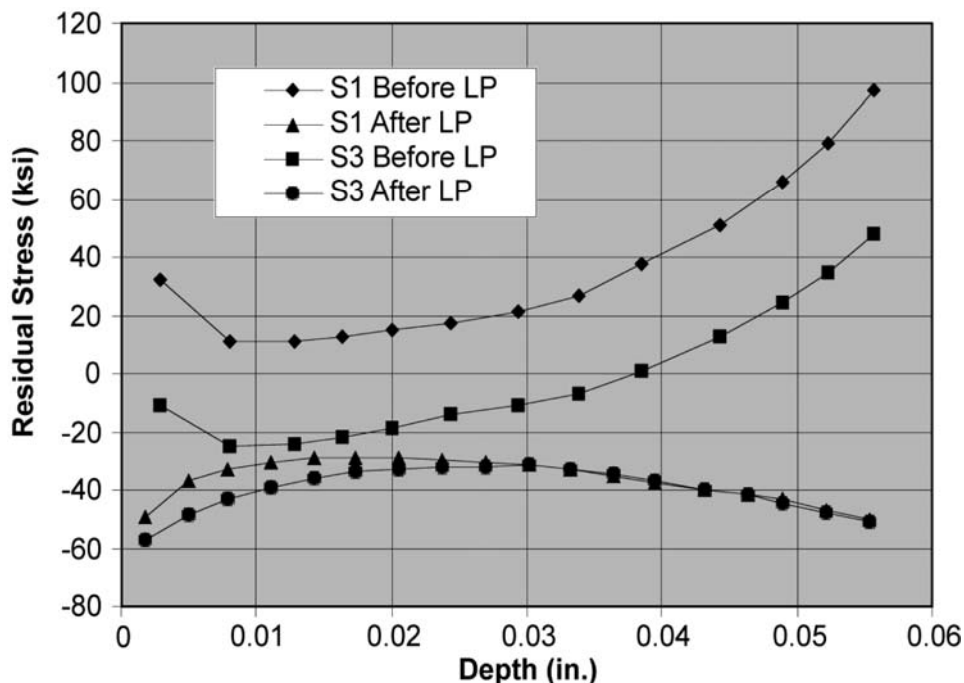


00363DC_002.ai

Source: Bokhari 2003, Figure 1.

Figure B-1. Schematic of the Dual Closure Lids of the Waste Package Outer Shell

Based on the modification of the waste package outer-lid closure weld configuration, as indicated in Figure B-1, induction annealing is not considered as a residual stress mitigation process for outer lid closure weld. Instead, the current plan is to implement one of two mechanical residual stress mitigation processes (i.e., either laser peening or controlled plasticity burnishing). Both of these stress-mitigation processes are commercially available and both processes result in near-surface compressive stresses with a shallow cold-work gradient normal to the outer surface. The selection among the two stress mitigation processes will be based on, practicality of implementation at the Yucca Mountain site welding and stress mitigation hot cell and performance analyses. The decision will be made as part of the hot cell design effort. Currently, for the performance assessment of the waste package subjected to SCC, through-wall stress, and stress intensity factor profiles due to weld residual stress in the waste package closure welds are based on finite element model calculations for a 25-mm-thick Alloy 22 outer-lid closure weld that is subjected to laser peening and an as-welded 10-mm-thick Alloy 22 middle-lid closure weld. The near surface residual stress distribution before and after laser peening for a 1-inch-thick (25.4 mm) welded Alloy 22 plate is shown in Figure B-2.



00363DC_003.ai

Source: DTN: LL000320005924.145.

NOTE: S1 is the Radial Stress and S3 is the Hoop Stress

Figure B-2. Near-Surface Residual Stress Distribution before and after Laser Peening (LP) for a 1-Inch-Thick Welded Alloy 22 Plate

The analysis of the through-wall stress and stress intensity factor distributions is documented in *Stress Corrosion Cracking of the Drip Shield, the Waste Package Outer Barrier, and the Stainless Steel Structural Material* (BSC 2003a, Section 6.4) and the results including the effects of uncertainty are documented in *WAPDEG Analysis of Waste Package and Drip Shield Degradation* (BSC 2003b, Section 6.3.9).

In *Stress Corrosion Cracking of the Drip Shield, the Waste Package Outer Barrier, and the Stainless Steel Structural Material* (BSC 2003a, Section 6.2.2), it is concluded that the hoop stress, which promotes radially oriented crack growth, is the dominant component of stress in the waste package outer-lid closure weld regions (see also BSC 2003a, Table 4.1-3). On this basis, only hoop stress profiles were considered in the integrated waste package degradation model documented in *WAPDEG Analysis of Waste Package and Drip Shield Degradation* (BSC 2003b).

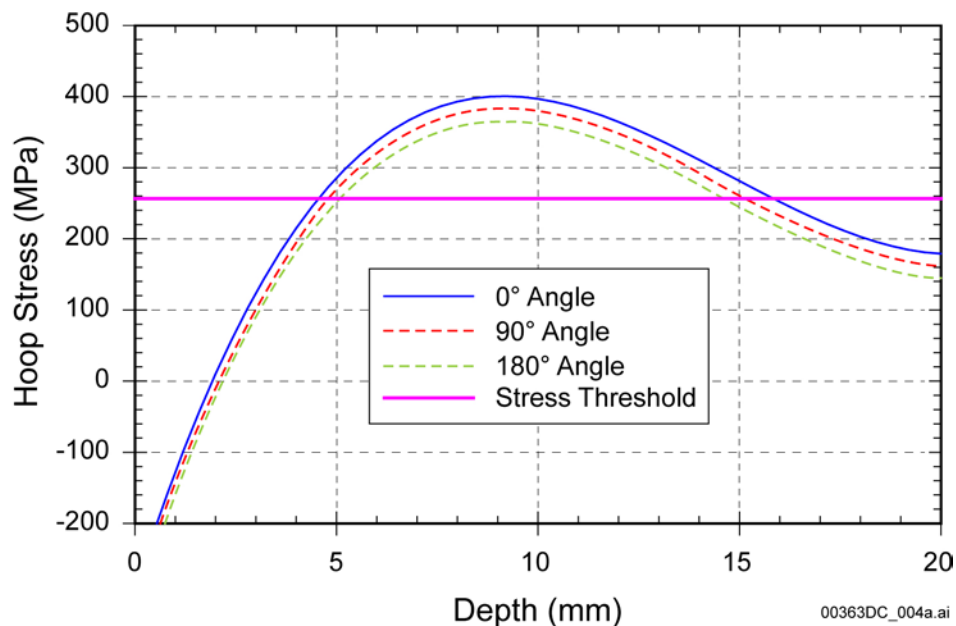
The hoop stress (σ in MPa) as a function of depth (x in mm) in the closure weld regions of the Alloy 22 waste package outer shell is given by a third-order polynomial equation of the form (BSC 2003a; DTN: LL030607012251.065):

$$\sigma(x,0) = A_0 + A_1 \cdot x + A_2 \cdot x^2 + A_3 \cdot x^3 \quad (\text{Eq. B-5})$$

where the values of the coefficients (A_i s) used in the integrated waste package degradation model are given in (BSC 2003b, Table 13) with x in units of mm. The second argument in the stress function is used to represent angular variation ($\theta = 0$ arbitrarily chosen) around the circumference of the Alloy 22 waste package outer- and middle-lid closure welds. The angular variation is included using the following functional form (BSC 2003a, Section 6.4.5; DTN: LL030607012251.065):

$$\sigma(x, \theta) = \sigma(x, 0) - (17.236893) \cdot (1 - \cos(\theta)) \quad (\text{Eq. B-6})$$

Figure B-3 shows the median (not accounting for uncertainty, which is discussed below) stress variation with angle for the laser-peened waste package outer shell outer closure lid weld region. Also included on the graphs is the tensile stress threshold for SCC initiation (discussed in BSC 2003a, Section 6.2.1). This value is 90 percent of the Alloy 22 yield strength. The depth on this graph does not start at zero thickness nor extend to the full lid thickness. For consistency, stress values were calculated at the same depth values as the stress-intensity-factor profile.



Source: DTN: LL030607012251.065; Output DTN: MO0310MWDWAPAN.002.

Figure B-3. Variation of Hoop Stress versus Depth for Waste Package Outer Shell Outer Closure Lid (Stress Threshold at 200°C)

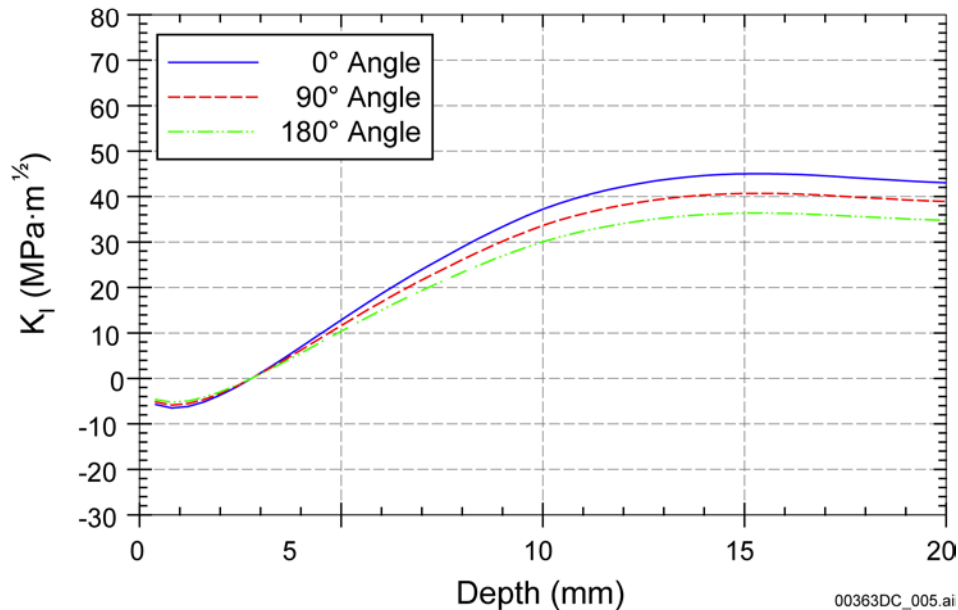
Based on the angular stress variation in Equation B-6, the stress intensity factor variation with angle is given by Equation B-7 (BSC 2003a, Section 6.4.5; DTN: LL030607012251.065):

$$K(x, \theta) = K(x, 0) \cdot \left(\frac{\sigma(Thck, \theta)}{\sigma(Thck, 0)} \right) \quad (\text{Eq. B-7})$$

where $Thck$ is taken to be the maximum depth value shown in the graphs (about 20 mm) (BSC 2003b, Table 14) and $K(x, 0)$ is given by the respective value in this same table. In performance assessment, the stress intensity factor is coupled with the distribution of weld flaws documented

in the *WAPDEG Analysis of Waste Package and Drip Shield Degradation* (BSC 2003b, Section 6.3.9.2) to quantify the extent of SCC through-wall propagation resulting from these flaws.

The small variation of the stress and stress-intensity-factor profiles with angle is due to welding operations (BSC 2003a, Section 6.4.5). Figure B-4 shows the stress-intensity-factor variation with angle for the laser-peened waste package outer-lid closure weld region.



Source: Input DTN: LL030607012251.065; Output DTN: MO0310MWDWAPAN.002.

Figure B-4. Variation of Stress-Intensity Factor versus Depth for Waste Package Outer Shell Outer Closure Lid

The uncertainty in the stress and stress-intensity-factor profiles is introduced through a scaling factor (z), which is sampled from a normal distribution with a mean of zero and a standard deviation of 5 percent of the yield strength, and an upper bound of 15 percent of the yield strength and a lower bound of 15 percent of the yield strength (BSC 2003a, Section 6.4.5).

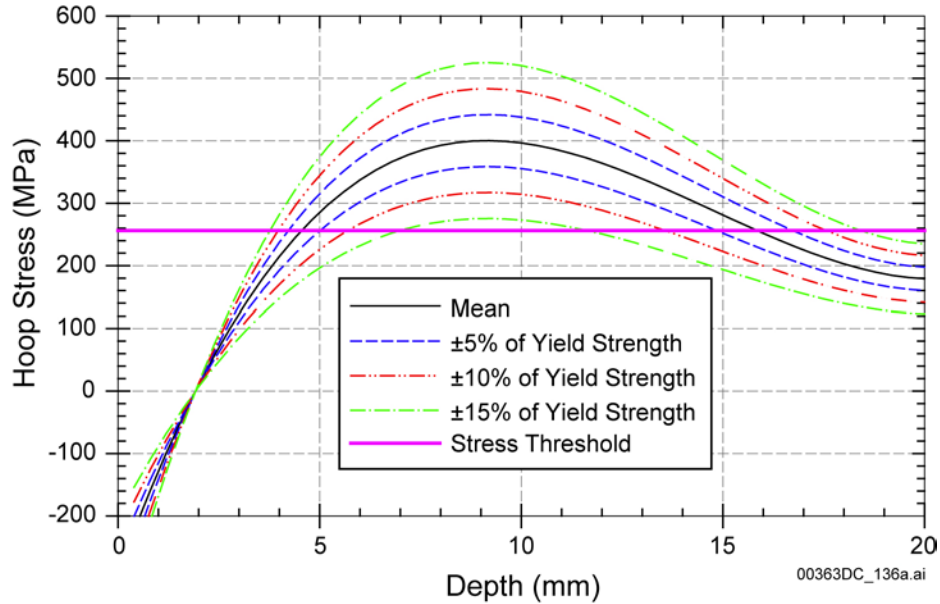
The stress relation, accounting for uncertainty, is given by

$$\sigma_u(x, \theta, z) = \sigma(x, \theta) \cdot \left(\frac{\sigma(\text{Thck}, \theta) + sz}{\sigma(\text{Thck}, \theta)} \right) \quad (\text{Eq. B-8})$$

and the stress intensity factor relation is given by

$$K_{Iu}(x, \theta, z) = K_I(x, \theta) \cdot \left(\frac{\sigma(\text{Thck}, \theta) + sz}{\sigma(\text{Thck}, \theta)} \right) = K_I(x, 0) \cdot \left(\frac{\sigma(\text{Thck}, \theta) + sz}{\sigma(\text{Thck}, 0)} \right) \quad (\text{Eq. B-9})$$

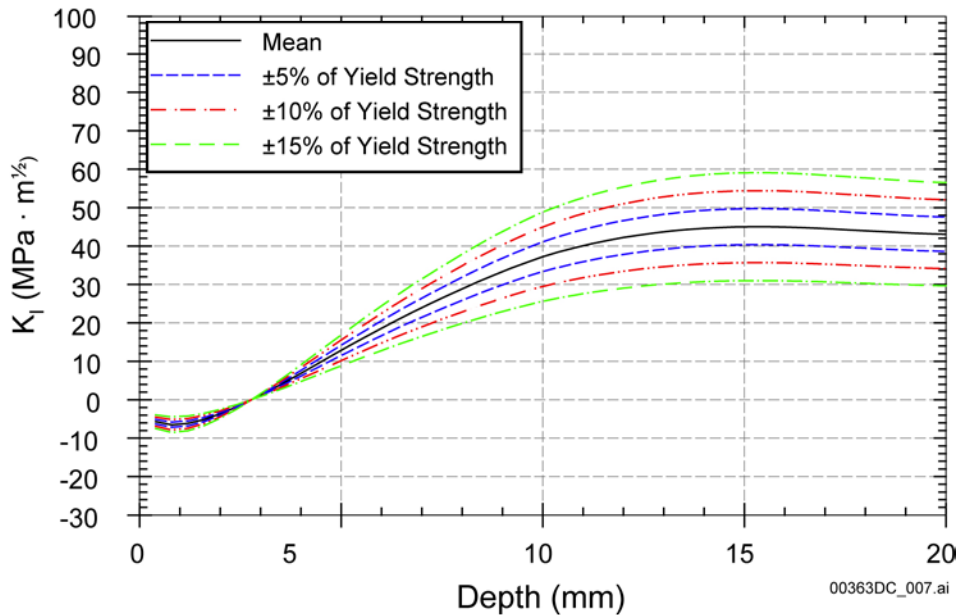
Figure B-5 shows that the depth of the laser-peened layer with stresses less than the threshold stress of 90 percent of the yield strength is about 3.8 mm at the upper bound uncertainty and about 4.5 mm for the mean stress value.



Source: Input DTN: LL030607012251.065; Output DTN: MO0310MWDWAPAN.002.

Figure B-5. Variation of Hoop Stress ($\theta = 0$) versus Depth for Waste Package Outer Shell Outer Closure Lid

The corresponding variation in stress intensity factor is shown in Figure B-6. As can be seen, the stress-intensity factor turns positive at a depth of about 3 mm.



Source: Input DTN: LL030607012251.065; Output DTN: MO0310MWDWAPAN.002.

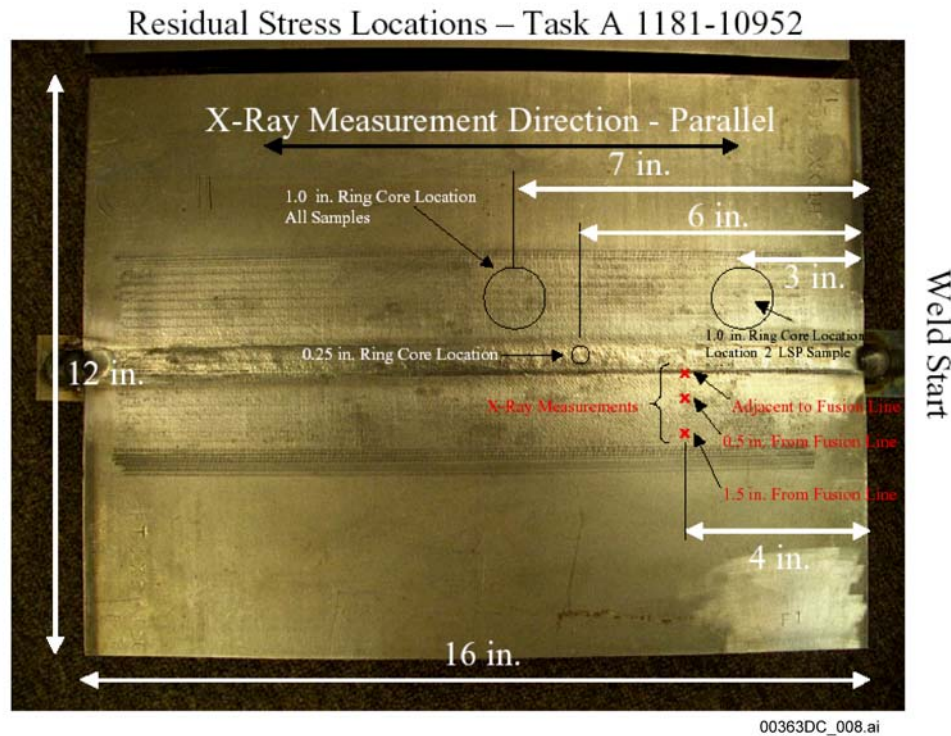
Figure B-6. Variation of Stress-Intensity Factor ($\theta = 0$) versus Depth for Waste Package Outer Shell Outer Closure Lid

Corroborative through-wall residual stress measurements (not included in the analyses in *Stress Corrosion Cracking of the Drip Shield, the Waste Package Outer Barrier, and the Stainless Steel Structural Material* (BSC 2003a)) were obtained from both laser-peened and controlled plasticity burnished one-inch thick gas tungsten arc-welded Alloy 22 plates. Both the laser-peened and the burnished plates were fabricated from the same heat of 1-inch Alloy 22 plate material (HTXX2246BG) and were welded using the same weld preparation geometry and gas tungsten arc-welding process (DTN: MO0301SPAXRA52.001). It is evident from this series of residual stress measurements that the calculated outer lid closure weld residual stress profiles are equivalent to, or more conservative than (i.e., satisfy the stress threshold at lower depths), these corroborative measured stress profiles for both the laser-peened and the controlled plasticity burnished stress mitigated plates.

Figure B-7 is a photograph, showing one of the stress mitigated plates (the laser-peened plate) and indicating the locations where residual stress measurements were made by either X-ray diffraction, or the ring-core technique (using either 0.25-inch cores or 1-inch cores). Typical examples of residual stress versus depth measurements for a laser-peened and a controlled plasticity burnished plate using a 1-inch ring core are shown in Figures B-8 and B-9. These figures demonstrate that the *parallel* direction is parallel to the weld centerline, and thus is equivalent in direction to the calculated hoop stress shown in previous figures. They also show that the depth of compression exceeds 0.2 inches (about 5 mm) with the depth at which the stress exceeds the SCC initiation threshold stress value of 90 percent of yield strength (Figure B-5). The 1-inch-ring core allows measurement down to a significant depth (0.3 = in.) but tends to average the stresses at any given depth over the entire 1-in. circular area. In contrast, the X-ray diffraction measurements cover a much smaller region (spot size about 0.12 in.) but are very near surface (2 mil) measurements. To get the depth profile using the X-ray technique, material is sequentially removed electrolytically to minimize possible surface stress alteration as a result of material removal.

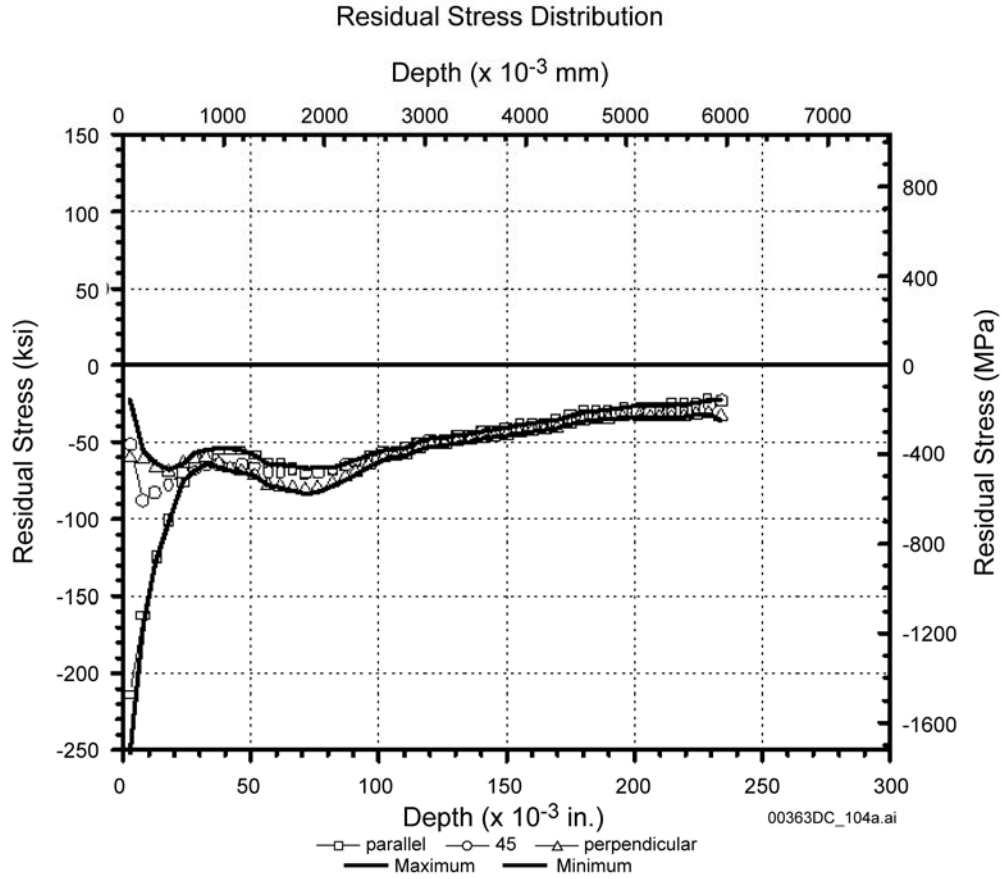
X-ray diffraction measurement results for the burnished plates and laser-peened plates are shown in Figures B-10 and B-11, respectively. In each case, it was reported (DTN: MO0301SPAXRA52.001, p. 2) that with increasing depth, the grain size increased resulting in increased uncertainty in the measurements and limiting the maximum depth of X-ray diffraction measurement to about 0.1 inches for the laser-peened plate and about 0.24 in. (about 6 mm) for the burnished plate. The reason for the apparent larger grain size at a relatively shallow depth for the laser-peened plate is not known. Measurements were made at locations adjacent to the fusion line, and at 0.5 and 1.5 in. from the fusion line as shown in Figure B-7. These measurements indicate (Figure B-10) that the burnished plate has a surface compressive layer depth greater than 0.25 in. (about 6.4 mm). For the laser-peened plate (Figure B-11) the stress remained compressive down to the maximum measurement depth of about 0.12 in. (about 3 mm), except for one measurement made at a location about 1.5 in. from the weld fusion line where the stress became tensile (about 100 MPa) at about 1.5 mm depth and then dropped slightly below zero stress at about 2 mm depth. However, the grain size limitation on depth of measurement precluded the establishment of the depth at which the stress approaches the SCC initiation threshold value although it can be concluded that it exceeds 3 mm. These limited depth X-ray results, combined with the deeper 1-inch ring-core results, are consistent with the calculated stress profiles (shown in Figure B-5 for the laser-peened case) being conservative representations of the expected mitigated stress gradients at both depths where the stress reaches

zero and where it reaches the threshold stress level. It can also be concluded that the expected beneficial stress depth for the controlled plasticity burnished case is at least equivalent to that for the laser-peened case.



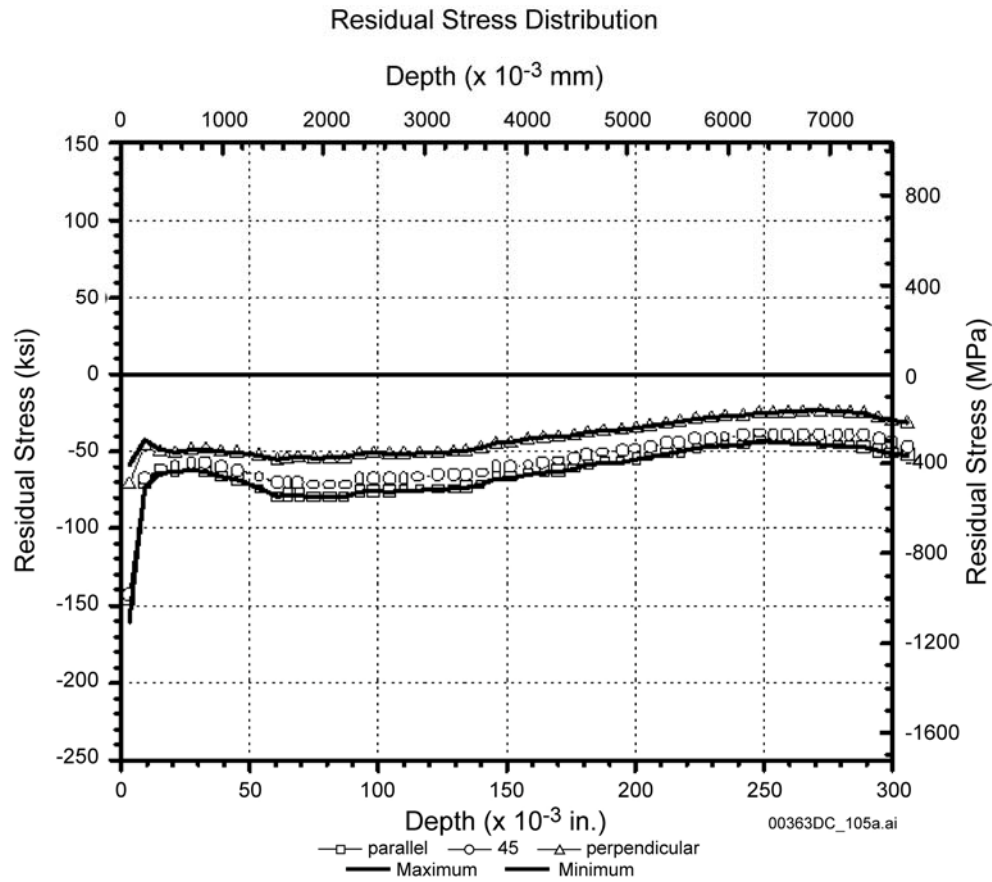
Source: DTN: MO0301SPAXRA52.001, Figure 8.

Figure B-7. Alloy 22 Laser-Peened Welded Plate Showing Residual Stress Measurement Locations Using X-Ray Diffraction and Ring-Core Techniques



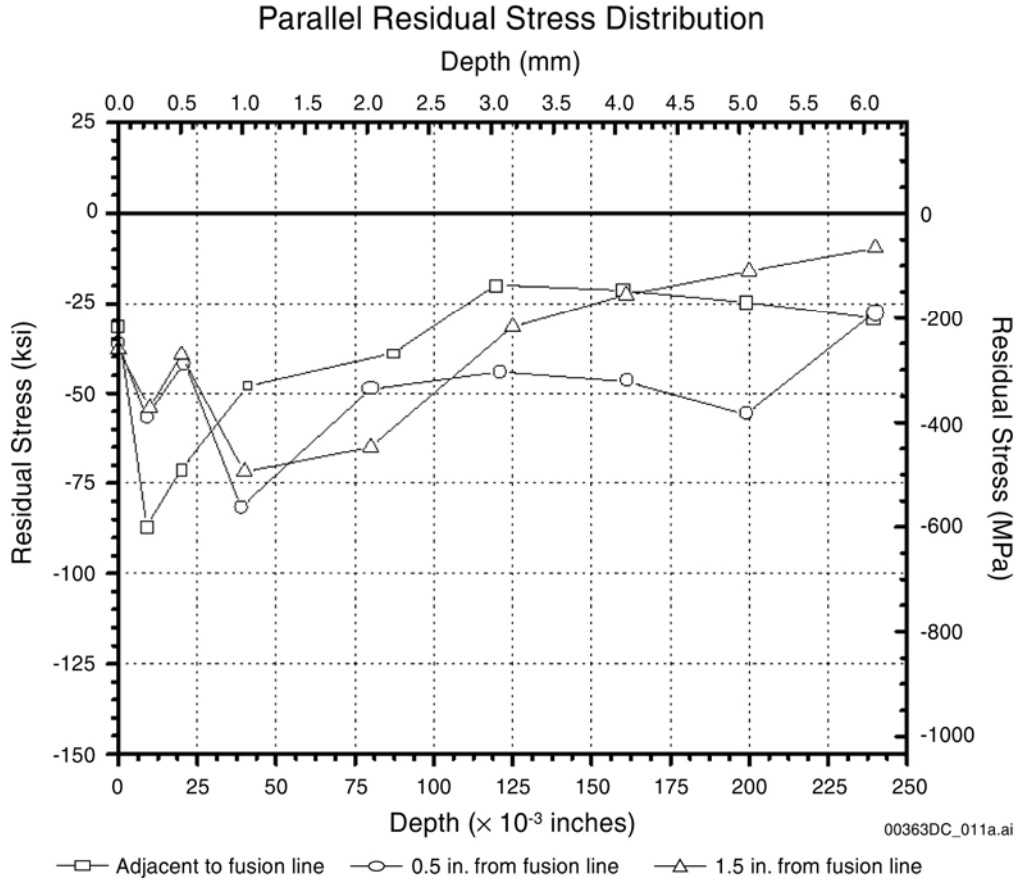
Source: DTN: MO0301SPAXRA52.001, Figure 4.

Figure B-8. Measured Stress (Using 1-Inch Ring Core Method) versus Depth for Alloy 22 Laser Peened 1-Inch-Thick Welded Plate



Source: DTN: MO0301SPAXRA52.001, Figure 7.

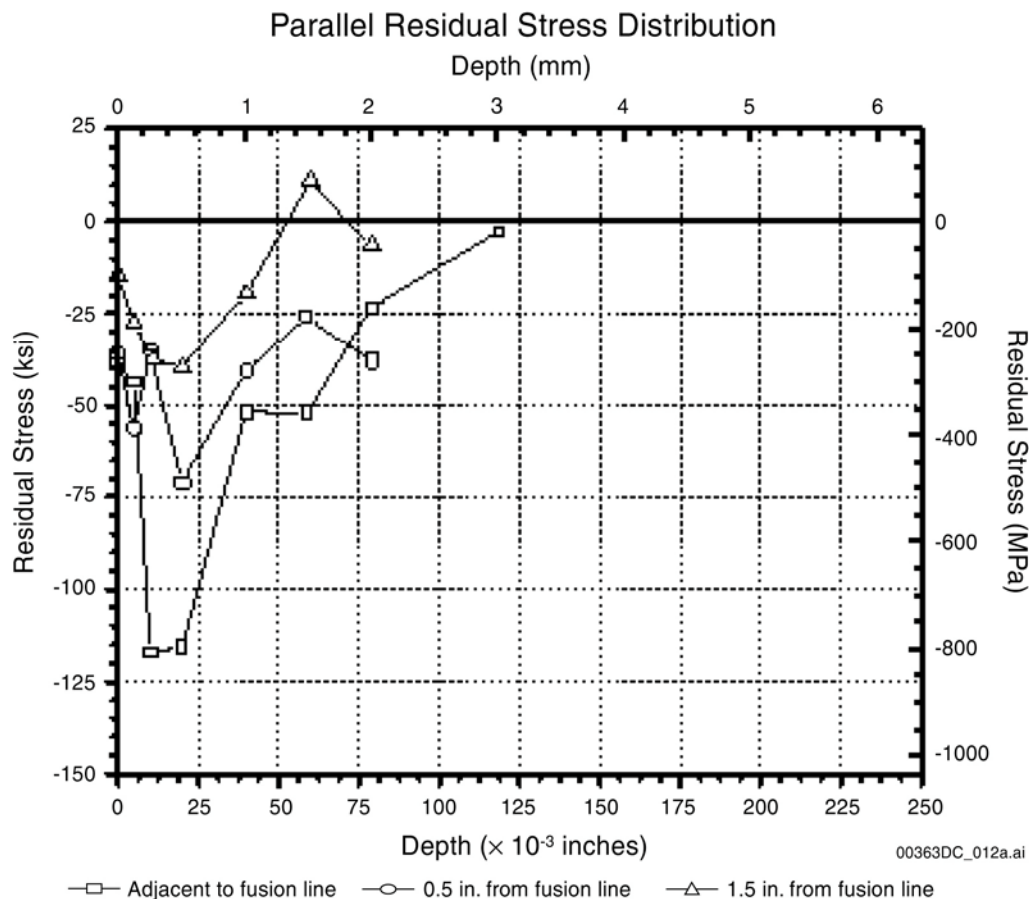
Figure B-9. Measured Stress (Using 1-Inch Ring-Core Method) versus Depth for Alloy 22 Controlled Plasticity Burnished 1-Inch-Thick Welded Plate



Source: DTN: MO0301SPAXRA52.001, Figure 1.

NOTE: Measurements made at fusion line, 0.5 in. from fusion line and 1.5 inch from fusion line.

Figure B-10. X-Ray Diffraction Measured Residual Stress versus Depth for 1-Inch-Thick Controlled Plasticity Burnished Alloy 22 Welded Plate



Source: DTN: MO0301SPAXRA52.001, Figure 2.

NOTE: Measurements made at fusion line, 0.5 in. from fusion line and 1.5 inch from fusion line.

Figure B-11. X-Ray Diffraction Measured Residual Stress versus Depth for 1-Inch-Thick Laser-Peened Alloy 22 Welded Plate

B.5 REFERENCES

B.5.1 Documents Cited

Bokhari, S.A. 2003. "Approved Baseline Change Proposal (BCP) YMP-2003-005, Design Changes to Site Recommendation (SR) Waste Package." Memorandum from S.A. Bokhari (DOE) to W.J. Arthur, III (OCRWM/CCB), R.A. Milner (OCRWM/CCB), and R.D. Brown (OCRWM/CCB), January 30, 2003, with attachments. ACC: MOL.20030508.0040.

BSC (Bechtel SAIC Company) 2003a. *Stress Corrosion Cracking of the Drip Shield, the Waste Package Outer Barrier, and the Stainless Steel Structural Material*. ANL-EBS-MD-000005 REV 01. Las Vegas, Nevada: Bechtel SAIC Company. ACC: DOC.20030717.0001.

BSC 2003b. *WAPDEG Analysis of Waste Package and Drip Shield Degradation*. ANL-EBS-PA-000001 REV 01D. Las Vegas, Nevada: Bechtel SAIC Company. ACC: MOL.20031009.0225.

Reamer, C.W. and Gil, A.V. 2001. Summary Highlights of NRC/DOE Technical Exchange and Management Meeting of Range on Thermal Operating Temperatures, September 18-19, 2001. Washington, D.C.: U.S. Nuclear Regulatory Commission. ACC: MOL.20020107.0162.

Schlueter, J. 2000. "U.S. Nuclear Regulatory Commission/U.S. Department of Energy Technical Exchange and Management Meeting on Container Life and Source Term (September 12-13, 2000)." Letter from J. Schlueter (NRC) to S. Brocoum (DOE/YMSCO), October 4, 2000, with enclosure. ACC: MOL.20010731.0161.

B.5.2 Data, Listed by Data Tracking Number

LL000320005924.145. Corrosion Cracking of the Drip Shield, the Waste Package Outer Barrier and the Stainless Steel Structural Material. Submittal date: 03/22/2000.

LL030607012251.065. Output of Stress Corrosion Cracking AMR. ANL-EBS-MD-000005 REV. 01 ICN 00. Submittal date: 06/20/2003.

MO0301SPAXRA52.001. X-ray Diffraction and Ring-Core Determination of the Subsurface Residual Stress Distributions in Two Alloy 22 Welded Plates. Submittal date: 01/30/2003.

MO0310MWDWAPAN.002. WAPDEG Analysis of Waste Package and Drip Shield Degradation. Submittal date: 10/16/2003.

APPENDIX C
ROCKFALL AND DEAD-WEIGHT EFFECTS
(RESPONSE TO CLST 1.14)

Note Regarding the Status of Supporting Technical Information

This document was prepared using the most current information available at the time of its development. This Technical Basis Document and its appendices providing Key Technical Issue Agreement responses that were prepared using preliminary or draft information reflect the status of the Yucca Mountain Project's scientific and design bases at the time of submittal. In some cases this involved the use of draft Analysis and Model Reports (AMRs) and other draft references whose contents may change with time. Information that evolves through subsequent revisions of the AMRs and other references will be reflected in the License Application as the approved analyses of record at the time of License Application submittal. Consequently, the DOE will not routinely update either this Technical Basis Document or its Key Technical Issue Agreement appendices to reflect changes in the supporting references prior to submittal of the License Application.

APPENDIX C

ROCKFALL AND DEAD-WEIGHT EFFECTS (RESPONSE TO CLST 1.14)

This appendix provides a response to Key Technical Issue (KTI) agreement Container Life and Source Term (CLST) 1.14. This agreement documents rockfall and dead-weight effects on the waste package and drip shield.

C.1 KEY TECHNICAL ISSUE AGREEMENT

C.1.1 CLST 1.14

Agreement CLST 1.14 was reached during the U.S. Nuclear Regulatory Commission (NRC)/U.S. Department of Energy (DOE) Technical Exchange and Management Meeting on CLST, held September 12-13, 2000, in Las Vegas, Nevada. Subissues 1 (effects of corrosion processes on the lifetime of the containers), 2 (effects of phase instability and initial defects on the mechanical failure and lifetime of the containers), 3 (the rate at which radionuclides in spent nuclear fuel are released from the engineered barrier subsystem through the oxidation and dissolution of spent nuclear fuel), 4 (the rate at which radionuclides in high-level radioactive waste glass are released from the engineered barrier subsystem), and 6 (effects of alternate engineered barrier subsystem design features on container lifetime and radionuclide release from the engineered barrier subsystem) were discussed at the meeting (Schlueter 2000). There has been no submittal related to this KTI agreement to the NRC.

Wording of the agreement is as follows:

CLST 1.14

Provide the justification for not including the rockfall effect and deadload from drift collapse on SCC of the waste package and drip shield. DOE will provide the documentation for the rockfall and dead-weight effects in the next revision of the SCC AMR (ANL-EBS-MD-000005) prior to LA.

C.1.2 Related Key Technical Issue Agreements

There are several KTI agreements that are related to KTI agreement CLST 1.14. These include CLST 1.04, CLST 1.13, CLST 1.15 and CLST 1.16.

C.2 RELEVANCE TO REPOSITORY PERFORMANCE

Stress corrosion cracking (SCC) for waste package and drip shield can take place when a sustained load is applied and an appropriate chemical environment exists. Rockfall scenarios are considered in evaluating conditions that may lead to SCC. Data and analysis conducted to date indicate that SCC is not significant to repository performance during the regulatory period (BSC 2003a, Section 7.2).

C.3 RESPONSE

Justification is provided for not including the roles of rockfall and dead-load from drift collapse on SCC of the waste package and drip shield. The documentation for the rockfall and dead-weight effects is provided in model report *Stress Corrosion Cracking of the Drip Shield, the Waste Package Outer Barrier, and the Stainless Steel Structural Material* (BSC 2003a).

Rockfall Effects—The structural design of the drip shield precludes rockfalls from affecting it to the extent that damage is caused to the waste package (BSC 2003a, Section 6.3.7). The calculated maximum vertical displacement in the drip shield due to rockfall is less than the clearance between the drip shield and the waste package. Therefore, no contact between the drip shield and the waste package is expected to occur as a result of rockfall over the drip shield (BSC 2003b, Section 6; CRWMS M&O 2000, p. II-3).

Drip shield structural response to rockfalls induced by seismic events is addressed in *Drip Shield Structural Response to Rock Fall* (BSC 2003b), where the damaged area of the drip shield is calculated for given rock masses. Damaged area is defined as a region of the drip shield where calculated stress exceeds threshold stress. The seismically induced drip shield and waste package degradation models, analyses, and conclusions can be found in *Seismic Consequence Abstraction* (BSC 2003c).

Dead-Load Effect Resulting from Steady State Drift Collapse—SCC could potentially occur at limited areas. However, examination of peak stress locations (BSC 2003d, Figures II-32 and II-44) indicates that the highest tensile stress values exist only over a limited area on the side of the drip shield near the region of the upper curved surface at the junction between the top plate and external plate corners (BSC 2003d). This area is limited to the region of connection between the bulkheads and the top plate. Thus, no impact on the seepage flow diversion function of the drip shield is expected. Creep caused by the dead-load will not occur below 315°C (ASM International 1990, p. 626) (i.e., the deformation of titanium alloys loaded to yield point does not increase with time). Therefore, the dead-load effect has no impact on the closure.

Drift collapse scenarios that may increase drip shield temperatures above 150°C have not been considered in the analysis to date. Such scenarios are being evaluated for both probability of occurrence and possible consequences. However, the information available at this time is adequate for license application.

The information in this report is responsive to agreement CLST 1.14 made between the DOE and NRC. The report contains the information that the DOE considers necessary for NRC review for closure of this agreement.

C.4 BASIS FOR THE RESPONSE

This response considers two separate drip shield and waste package loading effects: the rockfall effect and the dead-load effect resulting from steady state drift collapse.

Rockfall Effects—An analysis of the effect of rockfall on a drip shield and any resulting impact on drip shield performance under long-term static conditions (excluding seismic effects) is

documented in *Stress Corrosion Cracking of the Drip Shield, the Waste Package Outer Barrier, and the Stainless Steel Structural Material* (BSC 2003a, Section 6.3.7).

Because of the structural design of the drip shield, calculations indicate that any rockfall affecting the drip shield will not transfer loads to the waste package that could subsequently result in SCC of the waste package. This conclusion results from the calculated maximum vertical displacement in the drip shield due to rockfall (BSC 2003b, p. 27) being less than the clearance between the drip shield and the waste package (BSC 2003e, Attachment II and 5; BSC 2003f). Therefore, no contact between the drip shield and the waste package is expected to occur as a result of rockfall on the drip shield.

Drip shield structural response to rockfalls induced by seismic events is addressed in *Drip Shield Structural Response to Rock Fall* (BSC 2003b), where the damaged area of the drip shield is calculated for given rock masses. The damaged area is defined as a region of the drip shield where calculated stress exceeds threshold stress.

Dead-Load Effect Resulting from Steady State Drift Collapse—The structural response of a drip shield subjected to statically applied pressure due to natural backfill and loose rock mass in the repository emplacement drift is evaluated in *Drip Shield Statically Loaded by Backfill and Loose Rock Mass* (BSC 2003d).

In this calculation, a finite element analysis was performed for a drip shield statically loaded by backfill and loose rock mass. The results have been provided in terms of component stresses in x (drip shield lateral), y (vertical), and z (axial) directions. The maximum stresses are given in Tables C-1 and C-2 as functions of temperature and decreased thicknesses. In *Drip Shield Statically Loaded by Backfill and Loose Rock Mass* (BSC 2003d, Table 6-3), thickness reductions are specified to account for a corrosion allowance for both surfaces of the drip shield. For instance, a 1.5-mm decrease means that 1.5-mm material thickness is removed from both sides of the plate, which amounts to a reduction of 3 mm in total.

Table C-1. Stresses in the Drip Shield for Various Backfill Heights

		Direction of Stress	Backfill Height #1 0.9 m	Backfill Height #2 1.1 m
Room Temperature	Titanium Grade 7 Components	X	94 MPa (see Figure II-2)	107 MPa (see Figure II-12)
		Y	106 MPa (see Figure II-3)	110 MPa (see Figure II-13)
		Z	117 MPa (see Figure II-4)	119 MPa (see Figure II-14)
	Titanium Grade 24 Components	X	45 MPa (see Figure II-5)	47 MPa (see Figure II-15)
		Y	98 MPa (see Figure II-6)	101 MPa (see Figure II-16)
		Z	91 MPa (see Figure II-7)	92 MPa (see Figure II-17)
150°C	Titanium Grade 7 Components	X	96 MPa (see Figure II-18)	108 MPa (see Figure II-24)
		Y	106 MPa (see Figure II-19)	110 MPa (see Figure II-25)
		Z	117 MPa (see Figure II-20)	120 MPa (see Figure II-26)
	Titanium Grade 24 Components	X	45 MPa (see Figure II-21)	47 MPa (see Figure II-27)
		Y	98 MPa (see Figure II-22)	101 MPa (see Figure II-28)
		Z	91 MPa (see Figure II-23)	93 MPa (see Figure II-29)

Source: BSC 2003d, Table 6-2.

NOTE: Figure cross-references refer to figures in *Drip Shield Statically Loaded by Backfill and Loose Rock Mass* (BSC 2003d).

Table C-2. Stresses in the Drip Shield with Decreased Thicknesses and Backfill Height #2

		Direction of Stress	Decreased 1 mm	Decreased 1.5 mm
Room Temperature	Titanium Grade 7 Components	X	110 MPa (see Figure II-30)	111 MPa (see Figure II-36)
		Y	127 MPa (see Figure II-31)	138 MPa (see Figure II-37)
		Z	159 MPa (see Figure II-32)	185 MPa (see Figure II-38)
	Titanium Grade 24 Components	X	48 MPa (see Figure II-33)	53 MPa (see Figure II-39)
		Y	122 MPa (see Figure II-34)	135 MPa (see Figure II-40)
		Z	121 MPa (see Figure II-35)	137 MPa (see Figure II-41)
150°C	Titanium Grade 7 Components	X	113 MPa (see Figure II-42)	112 MPa (see Figure II-48)
		Y	127 MPa (see Figure II-43)	138 MPa (see Figure II-49)
		Z	159 MPa (see Figure II-44)	181 MPa (see Figure II-50)
	Titanium Grade 24 Components	X	48 MPa (see Figure II-45)	53 MPa (see Figure II-51)
		Y	123 MPa (see Figure II-46)	137 MPa (see Figure II-52)
		Z	120 MPa (see Figure II-47)	134 MPa (see Figure II-53)

Source: BSC 2003d, Table 6-3.

NOTE: Figure cross-references refer to figures in *Drip Shield Statically Loaded by Backfill and Loose Rock Mass* (BSC 2003d).

To assess the potential for SCC initiation at various locations, the calculated stresses indicated in Tables C-1 and C-2 are compared with the SCC initiation threshold stresses (50 percent of the at-temperature yield strength) for either room temperature or 150°C. (Corresponding yield strength values are 362.5 MPa at room temperature and 210.4 MPa at 150°C for Titanium

Grade 7 (DTN: MO0003RIB00073.000).) This results in SCC initiation threshold stress values (50 percent of yield strength) of 181.3 and 105.2 MPa for room temperature and for 150°C, respectively. In considering the issues of temperature and correct corrosion allowance, it must be noted that the drip shield temperature (based on the full range of thermal-hydrologic infiltration used in the multiscale thermal-hydrologic model (DTNs: LL030602723122.027; LL030608723122.028; LL030610323122.029) will approach about 155°C in less than 100 years, drop to about 108°C in 1,000 years, and drop to less than about 65°C in 10,000 years. It must also be noted that local stress risers from angular rock fragments are not considered in this analysis.

Table C-3 shows a Titanium Grade 7 corrosion rate based on recent 5-year corrosion-rate measurement results as compared to earlier results for 1-year Long Term Corrosion Test Facility exposures. As seen, median and maximum 5-year corrosion rates for a creviced condition are 10 and 77 nm/yr, respectively, which results in removal of a maximum of about 0.008 mm per side in 100 years, about 0.077 mm per side in 1,000 years and about 0.77 mm in 10,000 years. The drip shield undergoes dry oxidation rather than aqueous corrosion during the first 100 years without water since the rock temperature is above the boiling point of potential seepage waters. The calculated titanium oxide thickness per side due to dry air oxidation after 100 years of exposure at 200°C (BSC 2003g, Table 4) is about 213 nm per side (actual metal loss would be less), which is significantly less than the maximum aqueous general corrosion metal loss. Therefore, Table C-1, which lists stress values without a corrosion allowance subtracted from the drip shield wall thickness, is conservative for the 150°C case.

Examination of Table C-1 stresses for Titanium Grade 7 indicates that without any corrosion allowance (i.e., with full design thickness), the threshold stress could be exceeded at either temperature. At 1,000 years, the temperature will drop to about 100°C where the yield strength is approximately 271 MPa (BSC 2003a, Table 4.1-4), the value is 93°C and the threshold stress is approximately 136 MPa. For this case, the expected corrosion loss is about 0.08 mm per side.

Examination of Table C-2 indicates a maximum stress of 159 MPa at both room temperature and 150°C with a corrosion allowance of 1 mm per side. However, at this time period, with an expected maximum corrosion wall loss of 0.08 mm per side, SCC initiation is not expected to occur. At times approaching 10,000 years, the general corrosion wall loss per side approaches 1 mm. Thus, the maximum calculated stress of 159 MPa now exceeds the SCC initiation threshold value of about 136 MPa. As a result, SCC could potentially occur at times approaching 10,000 years. However, examination of peak stress locations shown in Figures II-32 and II-44 of *Drip Shield Statically Loaded by Backfill and Loose Rock Mass* (BSC 2003d) indicates that the highest tensile stress values exist only over a limited area on the side of the drip shield near the region of the upper curved surface at the junction between the top plate and external plate corners. This area is limited to the region of connection between the bulkheads and the top plate. SCC crack penetrations in this region will have no significant impact on the seepage flow diversion function of the drip shield.

In conclusion, no significant impact on the seepage flow diversion function of the drip shield is expected. Any SCC cracks formed are expected to be very tight (i.e., have a limited through-wall crack-opening area) and are expected to be plugged with corrosion products and

(or) evaporation-induced scale-formation, thus further limiting any potential for water transport to the underside of the drip shield (BSC 2003a, Section 6.3.7).

Table C-3. Summary of 1-Year and 5-Year Corrosion Data Comparison

Specimen Type	1 Year (nm/yr)		5 Years (nm/yr)	
	Weight Loss	Crevice	Weight Loss	Crevice
Median	0	0	5	10
Maximum	200	350	58	77

DTN Output: MO0306SPAGLCDS.001

Source: BSC 2003g, Table 7.

C.5 REFERENCES

C.5.1 Documents Cited

ASM International 1990. *Properties and Selection: Nonferrous Alloys and Special-Purpose Materials*. Volume 2 of *ASM Handbook*. Formerly 10th Edition, *Metals Handbook*. 5th Printing 1998. [Materials Park, Ohio]: ASM International. TIC: 241059.

BSC (Bechtel SAIC Company) 2003a. *Stress Corrosion Cracking of the Drip Shield, the Waste Package Outer Barrier, and the Stainless Steel Structural Material*. ANL-EBS-MD-000005 REV 01 ICN 00. Las Vegas, Nevada: Bechtel SAIC Company. ACC: DOC.20030717.0001.

BSC 2003b. *Drip Shield Structural Response to Rock Fall*. 000-00C-TED0-00500-000-00A. Las Vegas, Nevada: Bechtel SAIC Company. ACC: ENG.20030327.0001.

BSC 2003c. *Seismic Consequence Abstraction*. MDL-WIS-PA-000003 REV 00. Las Vegas, Nevada: Bechtel SAIC Company. ACC: DOC.20030818.0006.

BSC 2003d. *Drip Shield Statically Loaded by Backfill and Loose Rock Mass*. 000-00C-TED0-00300-000-00A. Las Vegas, Nevada: Bechtel SAIC Company. ACC: ENG.20030224.0004.

BSC 2003e. *Structural Calculations of Waste Package Exposed to Vibratory Ground Motion*. 000-00C-EBS0-00300-000-00B. Las Vegas, Nevada: Bechtel SAIC Company. ACC: ENG.20030520.0003.

BSC 2003f. *Repository/PA IED Interlocking Drip Shield and Emplacement Pallet*. 800-IED-WIS0-00401-000-00Ba. Las Vegas, Nevada: Bechtel SAIC Company. ACC: MOL.20030929.0051.

BSC 2003g. *General Corrosion and Localized Corrosion of the Drip Shield*. ANL-EBS-MD-000004 REV 01. Las Vegas, Nevada: Bechtel SAIC Company. ACC: DOC.20030626.0001.

CRWMS M&O (Civilian Radioactive Waste Management System Management and Operating Contractor) 2000. *Design Analysis for the Ex-Container Components*. ANL-XCS-ME-000001 REV 00. Las Vegas, Nevada: CRWMS M&O. ACC: MOL.20000525.0374.

Schlueter, J. 2000. "U.S. Nuclear Regulatory Commission/U.S. Department of Energy Technical Exchange and Management Meeting on Container Life and Source Term (September 12-13, 2000)." Letter from J. Schlueter (NRC) to S. Brocoum (DOE/YMSCO), October 4, 2000, with enclosure. ACC: MOL.20010731.0161.

C.5.2 Data, Listed by Data Tracking Number

LL030602723122.027. Multiscale Thermohydrologic Model Output to TSPA and WAPDEG for the Upper Infiltration Case. Submittal date: 06/25/2003.

LL030608723122.028. Multiscale Thermohydrologic Model Output to TSPA and WAPDEG for the Lower Infiltration Case. Submittal date: 06/27/2003.

LL030610323122.029. Multiscale Thermohydrologic Model Output to TSPA and WAPDEG for the Mean Infiltration Case. Submittal date: 06/27/2003.

MO0003RIB00073.000. Physical and Chemical Characteristics of Titanium Grades 7 and 16. Submittal date: 03/13/2000.

MO0306SPAGLCDS.001. General Corrosion and Localized Corrosion of the Drip Shield. Submittal date: 05/28/2003.

INTENTIONALLY LEFT BLANK

APPENDIX D

**EFFECTS OF FABRICATION ON THE SUSCEPTIBILITY OF ALLOY 22 AND
TITANIUM GRADE 7 TO CORROSION AND STRESS CORROSION CRACKING
(RESPONSE TO CLST 1.15 AND GEN 1.01 (COMMENT 119))**

Note Regarding the Status of Supporting Technical Information

This document was prepared using the most current information available at the time of its development. This Technical Basis Document and its appendices providing Key Technical Issue Agreement responses that were prepared using preliminary or draft information reflect the status of the Yucca Mountain Project's scientific and design bases at the time of submittal. In some cases this involved the use of draft Analysis and Model Reports (AMRs) and other draft references whose contents may change with time. Information that evolves through subsequent revisions of the AMRs and other references will be reflected in the License Application as the approved analyses of record at the time of License Application submittal. Consequently, the Project will not routinely update either this Technical Basis Document or its Key Technical Issue Agreement appendices to reflect changes in the supporting references prior to submittal of the License Application.

APPENDIX D

EFFECTS OF FABRICATION ON THE SUSCEPTIBILITY OF ALLOY 22 AND TITANIUM GRADE 7 TO CORROSION AND STRESS CORROSION CRACKING (RESPONSE TO CLST 1.15 AND GEN 1.01 (COMMENT 119))

This appendix provides a response to Key Technical Issue (KTI) agreement Container Life and Source Term (CLST) 1.15 and and GEN 1.01 (Comment 119). These KTI agreements relate to providing documentation on the effects of fabrication on the susceptibility of Alloy 22 and Titanium Grade 7 to corrosion and stress corrosion cracking.

D.1 KEY TECHNICAL ISSUE AGREEMENTS

D.1.1 CLST 1.15

Agreement CLST 1.15 was reached during the U.S. Nuclear Regulatory Commission (NRC)/U.S. Department of Energy (DOE) Technical Exchange and Management Meeting on Container Life and Source Term held September 12–13, 2000, in Las Vegas, Nevada. Subissues 1 (effects of corrosion processes on the lifetime of the containers), 2 (effects of phase instability and initial defects on the mechanical failure and lifetime of the containers), 3 (the rate at which radionuclides in spent nuclear fuel are released from the engineered barrier subsystem through the oxidation and dissolution of spent nuclear fuel), 4 (the rate at which radionuclides in high-level radioactive waste glass are released from the engineered barrier subsystem), and 6 (effects of alternate engineered barrier subsystem design features on container lifetime and radionuclide release from the engineered barrier subsystem) were discussed at the meeting (Schlueter 2000). There has been no submittal related to this KTI agreement to the NRC.

Agreement GEN 1.01 was reached during the NRC/DOE Technical Exchange and Management Meeting held September 18–19, 2001 (Reamer and Gil 2001). At that meeting, the NRC provided additional comments that relate to CLST 1.13 including GEN 1.01, Comment 119 (Reamer and Gil 2001).

Wording of the agreements is as follows:

CLST 1.15

Provide the documentation for Alloy 22 and titanium for the path forward items listed on slide 39. DOE will provide documentation for Alloy 22 and Ti path forward items on slide 39 in a revision to the SCC and General and Localized Corrosion Analysis and Model Reports (ANL-EBS-MD-000003, ANL-EBS-MD-000004, ANL-EBS-MD-000005) by license application.

GEN 1.01 (Comment 119)

In p. 7-9 DOE claimed that NRC accepted the slip dissolution model. The DOE must supply the reference for this acceptance.

DOE Initial Response to GEN 1.01 Comment 119

DOE recognizes that the slip dissolution (GE PLEDGE) model has been used for stainless steels and the model needs to be validated for Alloy 22 and titanium for the environmental conditions relevant to the repository. Data generated under existing KTI agreements CLST 1.12 and CLST 1.15 will provide the basis for this validation.

D.1.2 Related Key Technical Issue Agreements

There are four other KTI agreements related to the KTI agreement CLST 1.15. These are KTI agreements CLST 1.04, CLST 1.12, CLST 1.13, and CLST 1.16. All these agreements relate to corrosion studies associated with waste package and drip shield materials.

D.2 RELEVANCE TO REPOSITORY PERFORMANCE

Drip shields will be installed over the waste packages prior to repository closure. The drip shields will be made of Titanium Grade 7 seepage diversion plates with Titanium Grade 24 stiffeners and support beams, which provide a mix of corrosion resistance and structural strength. The drip shields divert any moisture that might seep from the drift walls, including condensed water vapor, around the waste packages to the drift floor for thousands of years. The drip shields protect the underlying waste packages in the event of expected rockfalls, as the emplacement drifts degrade over time. Fabrication processes could affect the susceptibility of Alloy 22 (N06022) (and also the Titanium Grade 7 drip shield material) to environmentally assisted cracking, thermal stability, general corrosion (including microbially influenced corrosion (MIC)) and localized corrosion. These issues are mostly related to effects of multipass welding on the metallurgical stability of the alloy.

Fabrication processes of interest include (1) the welding procedure, (2) the effect of multipass welding, (3) the time/temperature history during welding, (4) cooling-rate effects, and (5) the effect of surface preparation prior to welding.

D.3 RESPONSE

Slide 39 of the Subissue 1 presentation (Gordon 2000) summarized the path forward for fabrication and welding of Alloy 22 that included the following:

- Install specimens cut from welds of site recommendation design mockup in Long Term Corrosion Test Facility and in other SCC test environments, and determine which specimen geometry is most feasible to complement SCC evaluation.
- Evaluate scaling and weld process factors between thin coupons and dimensions in actual welded waste package containers, including thermal/metallurgical structural effects of multipass weld processes.
- Provide representative weld-test specimens for MIC work, thermal aging, and localized corrosion evaluations.

Since Alloy 22 and Titanium Grade 7 are both involved in the three items on Slide 39 (although the materials were not specified), the responses address the two materials separately below.

Alloy 22—A broad array of SCC crack propagation and crack initiation tests have been performed using techniques such as the reversing direct current potential drop technique, constant deformation U-bend specimens, and slow-strain-rate techniques. It was concluded that Alloy 22 is highly resistant but not immune to SCC under potentially relevant repository environments, as well as environments containing potentially deleterious impurities such as lead.

The conclusions from the previous studies show that thermal degradation of Alloy 22 during long-term exposure in the drifts is not an issue (BSC 2003a, Section 8). In addition to corrosion degradation, mechanical degradation due to fabrication processes (welding) is also not expected.

A thermally aged Alloy 22 microstructure does not significantly affect general and localized corrosion resistance (BSC 2003b). It is also concluded that MIC will not significantly increase corrosion rates due to out-of-specification fabrication practices. The corollary is that a significantly aged (with detrimental secondary phases) structure is not expected under repository conditions; but, if this type of microstructure were to unexpectedly form, its corrosion rate would be anticipated to remain unchanged under representative Yucca Mountain repository environments.

Based on the above information, the DOE suggests that CLST 1.15 has been addressed and that the agreement should be closed. Testing is planned for specimens made from mockup containers fabricated according to the current design.

Titanium Grade 7—The possibility of SCC initiation due to weld residual tensile stresses can be eliminated for the Titanium Grade 7 drip shield since the drip shield will be emplaced in a stress mitigated condition (Plinski 2001). Titanium Grade 7 is not susceptible to thermal-aging-type accelerated corrosion or mechanical degradation at the maximum expected drip shield exposure temperature of less than 200°C (BSC 2003c). Literature (ASM International 1990, p. 626) indicates that between 200°C and 315°C (400°F and 600°F), the deformation of many titanium alloys loaded to yield point does not increase with time. Thus, creep strength is seldom a factor for these alloys in this temperature range. Titanium Grade 24 (an alpha-beta alloy) should remain stable if properly fabricated and heat treated. Commercial alpha-beta alloys are generally stable up to about 425°C in heat-treated condition for periods of 1,000 hours or more. Titanium Grade 7 general corrosion rates are low (BSC 2003c). The material is highly resistant to localized corrosion and MIC in a broad range of potential in-drift concentrated brine environments to which the drip shield may be exposed (BSC 2003c).

Specific Responses to GEN 1.01 (Comment 119)—The NRC has accepted the GE PLEDGE model (slip/dissolution model) to calculate crack growth rates numerous times to disposition SCC and to allow BWR utilities to continue to operate for an added time increment before shutting down to repair SCC damage discovered in piping, core shrouds, etc. during an outage. A more recent description of the NRC acceptance status of this model as a formal SCC crack growth rate evaluation method is described by Carpenter and Lund (1999).

The validation of the model is described in the model report *Stress Corrosion Cracking of the Drip Shield, the Waste Package Outer Barrier, and the Stainless Steel Structural Material* (BSC 2003d)

The information in this report is responsive to agreements CLST 1.15 and GEN 1.01 (Comment 119) made between the DOE and NRC. The report contains the information that the DOE considers necessary for NRC review for closure of these agreements.

D.4 BASIS FOR THE RESPONSE

Environmentally Assisted Cracking—For environmentally assisted cracking to occur three conditions are necessary simultaneously: (a) a susceptible metallurgical microstructure, (b) sustained tensile stresses, and (c) a specific aggressive environment. If one (or more) of these conditions is removed, environmentally assisted cracking will not occur. For example, Type 304 stainless steel (the susceptible microstructure) may crack (suffer environmentally assisted cracking) if it is stressed (tensile stresses) in the presence of hot solutions containing chloride ions (the aggressive specific environment). If the tensile stresses are removed, 304 stainless steel will not crack. Environmentally assisted cracking includes phenomena such as SCC and hydrogen embrittlement.

A full-scale Alloy 22 waste package mockup is undergoing a series of residual stress measurements. Once these measurements are completed, preparation and testing of specimens obtained from material removed from the mockup longitudinal seam weld and the bottom closure lid will be accomplished. These mockup specimen tests are expected to confirm existing SCC and general and localized corrosion experimental test results already available on waste package prototypical thickness, gas-tungsten arc-welded Alloy 22 materials (BSC 2003d, Sections 4.1 and 6.2.1). The reasons for this assertion are discussed below.

The Alloy 22 outer cylinder will be fabricated from rolled and welded Alloy 22 plates. It is then planned to “shop solution heat treat” the as-fabricated Alloy 22 cylinder with the bottom lid welded in place prior to loading the high-level radioactive waste into the waste package at the site hot cell (BSC 2003d, Section 8.1). Following waste loading, the waste package will be sealed by gas tungsten arc-welding the final Alloy 22 closure lids in place (BSC 2003d, Section 6.2.2.1). Thus, only the two outer-closure-lid weld regions will potentially have weld-induced residual tensile stresses. Consequently, the potential for SCC is evaluated whenever these high-tensile-stress weld regions are exposed to a potential brine environment.

A broad array of SCC initiation tests have been performed, including constant load tests (BSC 2003d, Section 6.2.1; DTN: LL021105312251.023) of specimens fabricated from 1.25-inch-thick Alloy 22 multipass gas-tungsten arc-welded plate in the as-welded condition as well as in the as-welded plus thermally aged condition. The welding process and material thickness used are representative of the currently planned waste package final closure lid welds. The thermal-aging treatment produced a significant density of topologically (tetrahedrally) close-packed phases (BSC 2003a, Section 6.3.1). These constant load tests evaluated the potential for Alloy 22 welds to exhibit SCC initiation on “smooth” surfaces (i.e., in the absence of surface-breaking weld defects) as well as with machined sharp notches placed in the weld metal and heat-affected zone. These specimens were exposed to a highly concentrated, aerated brine typical of evaporatively

concentrated J-13 type waters heated to 105°C, with no evidence of SCC initiation observed after 9,000 hours of testing. In addition to the constant load tests, U-bend test specimens (BSC 2003d, Section 6.2.1) were removed from the Long Term Corrosion Test Facility (LTCTF) after more than 5 years of testing. These included nonwelded as well as gas tungsten arc-welded specimens machined from thinner plate material. These specimens were exposed to acidified (simulated acidified concentrated water (SAW)) and alkaline (simulated dilute water (SDW) and simulated concentrated water (SCW)) solutions simulating concentrated groundwaters. Exposure was carried out in the vapor phase and in the liquid phase at 60° and 90°C. A number of these U-bend specimens (BSC 2003d, Section 6.2.1) were examined after 5-year exposures and none of them had any indication of environmentally assisted cracking.

In addition, to evaluate the potential for SCC growth at existing defects, the Alloy 22 crack growth rate has been evaluated as a function of applied stress intensity factor using annealed as well as thermally aged compact tension type fracture mechanics specimens. These specimens were aged, to provide a grain boundary network of tetrahedrally close packed phases, to 174 hours at 700°C under both cyclic- and constant-load conditions, and exposed to basic saturated water (BSW) at 110°C (with and without 1,000 ppm lead additions added as Pb(NO₃)₂ to the test environment) (BSC 2003d, Section 6.3.4; DTN: LL021105312251.023, Figures 1-44, 1-45 and 1-46). It was observed in some cases that once crack growth was initiated by cyclic loading, growth was sustained under constant-load conditions although the growth rates were extremely low and did not increase due to the presence of lead, indicating a high degree of SCC resistance.

Based on the above series of test results, it was concluded that Alloy 22 is highly resistant to but not immune to SCC under relevant repository environments as well as environments containing potentially deleterious impurities, such as lead. Consequently—based on the constant load results obtained on specimens machined from prototypical thickness welded plate and U-bend test results on thinner annealed and welded plate materials—an Alloy 22 SCC initiation threshold stress criterion of 90 percent of the at-temperature yield strength was established (BSC 2003d, Section 6.2.1). This criterion provides a design-basis criterion to limit maximum waste package steady-state stresses due to static loads to preclude SCC. Further, the outer waste package final-closure weld will be subjected to a mechanical stress mitigation process (laser peening or controlled plasticity burnishing) to preclude through-wall SCC penetration during the regulatory period as described in the response to KTI Agreement CLST 1.13 (Appendix B).

In addition to the above SCC test results for Alloy 22, constant load SCC results have also been obtained for the drip shield material, Titanium Grade 7. These results include constant load test results for specimens loaded above the at-temperature yield strength in 105°C to 125°C BSW (diluted to about 15 percent of the full BSW concentration). These data were obtained from specimens machined from both mill-annealed (as-received condition) and from 20 percent cold-worked material, which conservatively simulates the plastic strain that can occur in the weld heat-affected zone due to weld shrinkage strains (BSC 2003d, Section 6.2.1; DTN: LL021105312251.023, Tables 2-2 and 2-3). Unlike the Alloy 22 constant-load results described previously, SCC was detected in the Titanium Grade 7 specimens stressed at and above 110 percent of the at-temperature yield strength. In contrast to the observed SCC susceptibility of Titanium Grade 7 in 15 percent BSW at 105° to 125°C, no SCC was observed in Titanium Grade 7 U-bends. This SCC susceptibility is taken into account as described in *Stress*

Corrosion Cracking of the Drip Shield, the Waste Package Outer Barrier, and the Stainless Steel Structural Material (BSC 2003d, Section 6.3.7), where it is shown that through-wall SCC will not degrade the drip shield seepage diversion function. In addition to the constant load tests, 5 year-exposed U-bend test specimens of Titanium Grade 16 (a palladium-containing analog of Titanium Grade 7) and 2 year-exposed Titanium Grade 7 specimens (BSC 2003d, Section 6.2.1) were removed from the LTCTF. These included nonwelded and welded specimens machined from thinner plate material. These specimens were exposed to acidified (SAW) and alkaline (SDW and SCW); pH of approximately 10) solutions simulating concentrated groundwater. Exposure was carried out in the vapor phase and in the liquid phase at 60°C and 90°C. The annealed and the welded titanium alloy specimens removed after 2 to 5 years of exposure were visually examined and none had any indication of environmentally assisted cracking. This indicates that initiation stress threshold value is very likely at or above the at-temperature yield strength. However, a threshold stress of 50 percent of at-temperature yield strength has been selected as a threshold value for Titanium Grade 7 (BSC 2003d, Section 6.2.1).

The information above addresses the potential for environmental cracking of the waste packages and the SCC aspects of the KTI agreement because the full range of potential waste package metallurgical conditions has been evaluated for SCC performance. To corroborate these results, it is planned that samples will be prepared from the fabricated containers and from thick welded plates.

Thermal Aging—The mockup specimen tests are expected to provide supplemental confirmation of the thermal-aging studies and SCC, and general and localized corrosion experimental test results already conducted. These tests were conducted on as-welded as well as thermally aged waste package prototypical thickness gas-tungsten arc-welded Alloy 22 material (BSC 2003d, Sections 4.1 and 6.2.1; DTN: LL021105312251.023, Tables 2-2 and 2-3). The mockup test results are not expected to provide any significant new information relative to waste package corrosion rate. Information on phase stability is also found in *Aging and Phase Stability of Waste Package Outer Barrier* (BSC 2003a). Aging treatments for the constant load SCC specimen tests described previously included 700°C/174 hours (tetrahedrally close packed phases treatment) and 520°C/1,000 hours (long range order treatment) for mill-annealed materials, and 700°C/174 hours (tetrahedrally close packed phases treatment) for as-welded materials with and without notches.

In addition, experimental measurements were made of the extent of precipitation as a function of time/temperature history for both mill-annealed and as-welded (0.5 inch, 9-pass, gas-tungsten arc-welded, Alloy 22 plate material) conditions. The results were compared with theoretical predictions with reasonable agreement (BSC 2003a, Section 7.5). The conclusions from these studies show that the thermal degradation of Alloy 22 during long-term exposure in the drifts is not an issue (BSC 2003a, Section 8). That is, it is predicted that during the long-term emplacement Alloy 22 will not form secondary phases that could hinder its mechanical properties or corrosion resistance.

In addition to corrosion degradation, mechanical degradation during fabrication (welding) is also not expected. Good welding practices and strict preheat and interpass temperature specifications will prevent Alloy 22 from being exposed to high temperatures for long periods of time. Such exposure could cause detrimental second phase precipitation in the alloy. For example, a holding

time of approximately 10 hours at 700°C is needed for Alloy 22 welded plate to start losing its impact energy (this scenario of time and temperature history will not occur under good welding practices). Alloy 22 was designed to be welded and used in the as-welded condition in harsh industrial applications. The primary alloy producers do not recommend postweld annealing treatments since the as-welded condition retains the mechanical and corrosion resistance characteristics of the prewelded plates (Haynes International 1999).

Samples from mock-up fabricated containers are planned to be removed for thermal aging studies to determine if fabrication processes affect the kinetics of second phase precipitation. This testing will be done for corroborative purposes only.

Localized Corrosion and Microbially Influenced Corrosion for Welded Conditions—A thermally aged Alloy 22 microstructure (containing secondary phases such as μ and P) may offer lower resistance to corrosion than an annealed microstructure in aggressive acidic environments (BSC 2003a, Section 1.1). However, small amounts of these phases along with interdendritic segregation of molybdenum and chromium can be present in an as-welded plate, without significantly affecting general and localized corrosion resistance, as demonstrated by LTCTF descaled weight loss results. These corrosion rate results showed no significant differences, for either the boldly exposed or the creviced coupons, between the mill-annealed and as-welded conditions after exposure for 5 years in 60°C and 90°C SAW, SCW, and SDW (BSC 2003b, Section 6.4.3). These welded specimens were fabricated from 0.125-inch thick gas-tungsten arc-welded plate material.

More recently, Yucca Mountain Project-generated polarization-resistance-type corrosion rate measurements were obtained on creviced Alloy 22 specimens machined from thicker plate materials in the mill-annealed condition, the as-welded condition (welded specimens machined from 1.25 inch-thick, gas-tungsten arc-welded plate), and the as-welded plus thermally aged condition (700°C for 173 hours). These creviced specimens were exposed to brines containing concentrated (1 to 5 M CaCl_2) over a range of temperatures. The results indicated no increase in corrosion rates due to the welding process (BSC 2003b, Section 6.4.6). Similarly, a series of cyclic polarization tests on creviced specimens machined from the same 1.25-inch-thick, gas-tungsten arc-welded plate indicated there was no increased susceptibility to localized corrosion due to the welding process (BSC 2003b, Section 6.4.4.3).

The effect of MIC of Alloy 22, for both mill-annealed and as-welded conditions, is currently under investigation at Lawrence Livermore National Laboratory. Considering that no effect of welding on general or localized corrosion resistance was observed in the LTCTF tests over a range of pH values or in the most aggressive CaCl_2 type brines, it is expected that any MIC effect on as-welded Alloy 22 will be minimal. The results from these tests are expected to corroborate the results of previous studies of MIC. Currently, a factor of two acceleration in the general corrosion rate is assumed to account for potential MIC effects for both mill-annealed and as-welded conditions (BSC 2003b, Section 6.4.5). Since there is no significant difference in the general or localized corrosion behavior between the mill-annealed, the as-welded, and the as-welded plus aged materials described above, it is concluded that MIC will not significantly increase corrosion rates due to out-of-specification fabrication practices.

The corollary is that a significantly aged (with detrimental secondary phases) structure is not expected under repository conditions. However, if this type of microstructure were to unexpectedly form, its corrosion rate would remain unchanged under representative Yucca Mountain repository environments.

It is planned to test the localized corrosion susceptibility of samples removed from thick welded plates. This will be carried out in the as-welded condition and in the welded-plus-stress-mitigated condition prior to license application.

Titanium Grade 7—Similar to the waste package Alloy 22 outer shell, the Titanium Grade 7 drip shield will be emplaced in a stress mitigated condition (BSC 2003d, Section 6.3.7) so that the possibility of SCC initiation due to weld residual tensile stresses will be eliminated. Further, Titanium Grade 7 is not expected to be susceptible to thermal-aging-type accelerated corrosion or mechanical degradation at the maximum expected drip shield exposure temperature of less than 200°C (BSC 2003c, Section 6.5.3). Likewise, at temperatures less than 200°C, the drip-shield thicker section structural-support-beam material, Titanium Grade 24 (an alpha-beta alloy), should remain stable. This is because properly fabricated and heat-treated commercial alpha-beta alloys are generally stable up to about 425°C for 1,000 hours or more (ASM International 1990). In addition, Titanium Grade 7 general corrosion rates are low (BSC 2003c, Section 6.3.3.3); the material is highly resistant to localized corrosion and MIC in a broad range of potential drip shield concentrated brine environments (BSC 2003c, Section 6.4 and Section 6.5.2, respectively).

D.5 REFERENCES

D.5.1 Documents Cited

ASM International 1990. *Properties and Selection: Nonferrous Alloys and Special-Purpose Materials*. Volume 2 of *ASM Handbook*. Formerly 10th Edition, Metals Handbook. 5th Printing 1998. Materials Park, Ohio: ASM International. TIC: 241059.

BSC (Bechtel SAIC Company) 2003a. *Aging and Phase Stability of Waste Package Outer Barrier*. ANL-EBS-MD-000002 REV 01 ICN 0. Las Vegas, Nevada: Bechtel SAIC Company. ACC: DOC.20030807.0004.

BSC 2003b. *General Corrosion and Localized Corrosion of Waste Package Outer Barrier*. ANL-EBS-MD-000003 REV 01. Las Vegas, Nevada: Bechtel SAIC Company. ACC: DOC.20030916.0010.

BSC 2003c. *General Corrosion and Localized Corrosion of the Drip Shield*. ANL-EBS-MD-000004 REV 01. Las Vegas, Nevada: Bechtel SAIC Company. ACC: DOC.20030626.0001.

BSC 2003d. *Stress Corrosion Cracking of the Drip Shield, the Waste Package Outer Barrier, and the Stainless Steel Structural Material*. ANL-EBS-MD-000005 REV 01 ICN 00. Las Vegas, Nevada: Bechtel SAIC Company. ACC: DOC.20030717.0001.

Carpenter, C.E., Jr. and Lund, A.L. 1999. "BWR Internals Cracking Issues." *Corrosion 99, 54th Annual Conference and Expo, San Antonio, Texas, April 25-30, 1999*. Paper No. 438. Houston, Texas: NACE International. TIC: 249986.

Gordon, G. 2000. *Subissue 1: The Effects Of Corrosion Processes On The Lifetime Of Containers*. Presented to NRC/DOE Container Life And Source Term Key Technical Issue Technical Information Exchange, Las Vegas, Nevada, September 12-13, 2000. Las Vegas Nevada: Bechtel SAIC Company. ACC: MOL.20001127.0054.

Haynes International 1999. *Fabrication of Hastelloy Corrosion-Resistant Alloys*. 39. Kokomo, Indiana: Haynes International. TIC: 246409.

Plinski, M.J. 2001. *Waste Package Operations Fabrication Process Report*. TDR-EBS-ND-000003 REV 02. Las Vegas, Nevada: Bechtel SAIC Company. ACC: MOL.20011003.0025.

Reamer, C.W. and Gil, A.V. 2001. Summary Highlights of NRC/DOE Technical Exchange and Management Meeting of Range on Thermal Operating Temperatures, September 18-19, 2001. Washington, D.C.: U.S. Nuclear Regulatory Commission. ACC: MOL.20020107.0162.

Schlueter, J., 2000. "U.S. Nuclear Regulatory Commission/U.S. Department of Energy Technical Exchange and Management Meeting on Container Life and Source Term (September 12-13, 2000)." Letter from J. Schlueter (NRC) to S. Brocoum (DOE/YMSCO), October 4, 2000, with enclosure. ACC: MOL.20010731.0161.

D.5.2 Data, Listed by Data Tracking Number

LL021105312251.023. Stress Corrosion Crack Growth and Initiation Measurements for C-22 and Ti-7, General Electric Global Research Center (GEGRC) 121202. Submittal date: 01/08/2003.

INTENTIONALLY LEFT BLANK

APPENDIX E
THERMAL PROFILE OF THE WASTE PACKAGE MATERIAL
DUE TO INDUCTION ANNEALING
(RESPONSE TO CLST 1.16)

Note Regarding the Status of Supporting Technical Information

This document was prepared using the most current information available at the time of its development. This Technical Basis Document and its appendices providing Key Technical Issue Agreement responses that were prepared using preliminary or draft information reflect the status of the Yucca Mountain Project's scientific and design bases at the time of submittal. In some cases this involved the use of draft Analysis and Model Reports (AMRs) and other draft references whose contents may change with time. Information that evolves through subsequent revisions of the AMRs and other references will be reflected in the License Application as the approved analyses of record at the time of License Application submittal. Consequently, the Project will not routinely update either this Technical Basis Document or its Key Technical Issue Agreement appendices to reflect changes in the supporting references prior to submittal of the License Application.

APPENDIX E

THERMAL PROFILE OF THE WASTE PACKAGE MATERIAL DUE TO INDUCTION ANNEALING (RESPONSE TO CLST 1.16)

This appendix provides a response to Key Technical Issue (KTI) agreement Container Life and Source Term (CLST) 1.16. This KTI agreement relates to providing documentation on the measured thermal profile of the waste package material due to induction annealing.

E.1 KEY TECHNICAL ISSUE AGREEMENT

E.1.1 CLST 1.16

Agreement CLST 1.16 was reached during the U.S. Nuclear Regulatory Commission (NRC)/U.S. Department of Energy (DOE) Technical Exchange and Management Meeting on CLST held September 12-13, 2000, in Las Vegas, Nevada. Subissues 1 (effects of corrosion processes on the lifetime of the containers), 2 (effects of phase instability and initial defects on the mechanical failure and lifetime of the containers), 3 (the rate at which radionuclides in spent nuclear fuel are released from the engineered barrier subsystem through the oxidation and dissolution of spent nuclear fuel), 4 (the rate at which radionuclides in high-level radioactive waste glass are released from the engineered barrier subsystem), and 6 (effects of alternate engineered barrier subsystem design features on container lifetime and radionuclide release from the engineered barrier subsystem) were discussed at the meeting (Schlueter 2000). There has been no submittal related to this KTI agreement to the NRC.

Wording of the agreement is as follows:

CLST 1.16

Provide the documentation on the measured thermal profile of the waste package material due to induction annealing. DOE stated that the thermal profiles will be measured during induction annealing, and the results will be reported in the next stress corrosion cracking analysis model report (ANL-EBS-MD-000005) prior to LA.

E.1.2 Related Key Technical Issue Agreements

There are two KTI agreements related to the KTI agreement CLST 1.16. These are agreements CLST 1.13 and CLST 2.14, both of which are related to testing induction annealed specimens for stress corrosion cracking.

E.2 RELEVANCE TO REPOSITORY PERFORMANCE

A change in waste package design and fabrication approach has eliminated the applicability of this agreement.

E.3 RESPONSE

Induction annealing will not be used for the mitigation of waste package closure weld stresses (Bokhari 2003). The information in this report is responsive to agreement CLST 1.16 made between the DOE and NRC. The report contains the information that the DOE considers necessary for NRC review for closure of this agreement.

E.4 BASIS FOR THE RESPONSE

The current design calls for two Alloy 22 lids. The outer Alloy 22 lid closure weld stresses will be mitigated by either laser peening or controlled plasticity burnishing. Laser peening is the current baseline method. The inner Alloy 22 closure lid weld stresses will not be stress mitigated.

A discussion of the distribution of stresses for the waste package closure lid region is provided in the response to CLST 1.13 found in Appendix B.

E.5 REFERENCES

Bokhari, S.A. 2003. "Approved Baseline Change Proposal (BCP) YMP-2003-005, Design Changes to Site Recommendation (SR) Waste Package." Memorandum from S.A. Bokhari (DOE) to W.J. Arthur, III (OCRWM/CCB), R.A. Milner (OCRWM/CCB), and R.D. Brown (OCRWM/CCB), January 30, 2003, with attachments. ACC: MOL.20030508.0040.

Schlueter, J. 2000. "U.S. Nuclear Regulatory Commission/U.S. Department of Energy Technical Exchange and Management Meeting on Container Life and Source Term (September 12-13, 2000)." Letter from J. Schlueter (NRC) to S. Brocoum (DOE/YMSCO), October 4, 2000, with enclosure. ACC: MOL.20010731.0161.

APPENDIX F

**STRESS MEASURE FOR ASSESSING THE SUSCEPTIBILITY
OF VARIOUS ENGINEERED BARRIER SYSTEM MATERIALS
TO STRESS CORROSION CRACKING (RESPONSE TO RDTME 3.18)**

Note Regarding the Status of Supporting Technical Information

This document was prepared using the most current information available at the time of its development. This Technical Basis Document and its appendices providing Key Technical Issue Agreement responses that were prepared using preliminary or draft information reflect the status of the Yucca Mountain Project's scientific and design bases at the time of submittal. In some cases this involved the use of draft Analysis and Model Reports (AMRs) and other draft references whose contents may change with time. Information that evolves through subsequent revisions of the AMRs and other references will be reflected in the License Application as the approved analyses of record at the time of License Application submittal. Consequently, the Project will not routinely update either this Technical Basis Document or its Key Technical Issue Agreement appendices to reflect changes in the supporting references prior to submittal of the License Application.

APPENDIX F

STRESS MEASURE FOR ASSESSING THE SUSCEPTIBILITY OF VARIOUS ENGINEERED BARRIER SYSTEM MATERIALS TO STRESS CORROSION CRACKING (RESPONSE TO RDTME 3.18)

This appendix provides a response to Key Technical Issue (KTI) agreement Repository Design and Thermal-Mechanical Effects (RDTME) 3.18. This KTI agreement relates to providing a technical basis for a stress measure that can be used as the equivalent uniaxial stress for assessing the susceptibility of engineered barrier system materials to stress corrosion cracking (SCC).

F.1 KEY TECHNICAL ISSUE AGREEMENT

F.1.1 RDTME 3.18

Agreement RDTME 3.18 was reached during the U.S. Nuclear Regulatory Commission (NRC)/U.S. Department of Energy (DOE) Technical Exchange and Management Meeting on Repository and Design Thermal-Mechanical Effects (RDTME) held February 6–8, 2001, in Las Vegas, Nevada (Reamer and Williams 2001). There has been no submittal related to this KTI agreement to the NRC.

Wording of the agreement is as follows:

RDTME 3.18

Provide a technical basis for a stress measure that can be used as the equivalent uniaxial stress for assessing the susceptibility of the various EBS materials to stress corrosion cracking. The proposed stress measure must be consistent and compatible with the methods proposed by the DOE to assess SCC of the containers in WAPDEG and in accordance with the agreements reached at the Container Life and Source Term Technical Exchange. DOE will include a detailed discussion of the stress measure used to determine nucleation of stress corrosion cracks in the calculations performed to evaluate waste package barriers and the drip shield against stress corrosion cracking criterion. DOE will include these descriptions in future revisions of the following: Design Analysis for UCF Waste Packages, ANL-UDC-MD-000001, Design Analysis for the Defense High-Level Waste Disposal Container, ANL-DDC-ME-000001, Design Analysis for the Naval SNF Waste Package, ANL-UDC-ME-000001, and Design Analysis for the Ex-Container Components, ANL-XCS-ME-000001. The stresses reported in these documents will be used in WAPDEG and will be consistent with the agreements and associated schedule made at the Container Life and Source Term Technical Exchange (Subissue 1, Agreement 14, Subissue 6, Agreement 1).

F.1.2 Related Key Technical Issue Agreements

The related KTI agreements include CLST 1.14 and CLST 6.01.

F.2 RELEVANCE TO REPOSITORY PERFORMANCE

Stress corrosion cracking (SCC) is a major type of materials degradation that might influence the performance of the waste package and drip shield in the regulatory period. This KTI agreement supports the understanding necessary to determine the state of stress and the susceptibility of the engineered barrier system materials to SCC. Based on the levels of stresses determined, WAPDEG (BSC 2003a) can exercise the appropriate SCC models.

F.3 RESPONSE

A technical basis for a stress measure that can be used as the equivalent uniaxial stress for assessing the susceptibility of the various engineered barrier system materials to SCC is provided in *Stress Corrosion Cracking of the Drip Shield, the Waste Package Outer Barrier, and the Stainless Steel Structural Material* (BSC 2003b) and summarized in Section F.4. This basis is consistent and compatible with the methods proposed to assess SCC of the containers in WAPDEG (CRWMS M&O 2000a, 2000b, 2000c, 2000d) and in accordance with the agreements reached at the Container Life and Source Term Technical Exchange (Schlueter 2000). A detailed discussion of the stress measure used to determine nucleation of stress corrosion cracks in the calculations performed to evaluate waste package barriers and the drip shield against SCC criterion is documented in *Stress Corrosion Cracking of the Drip Shield, the Waste Package Outer Barrier, and the Stainless Steel Structural Material* (BSC 2003b). The stresses reported in these documents have been used in WAPDEG (BSC 2003a) and are consistent with the agreements and associated schedule made at the Container Life and Source Term Technical Exchange (Subissue 1, Agreement 14; Subissue 6, Agreement 1) (Schlueter 2000).

More information on distribution of stress and SCC can be found in Section 9.

The information in this report is responsive to agreement RDTME 3.18 made between the DOE and NRC. The report contains the information that the DOE considers necessary for NRC review for closure of this agreement.

F.4 BASIS FOR THE RESPONSE

The basis for the current stress measure (threshold stress for SCC initiation) used to determine nucleation of stress corrosion cracks in calculations performed to evaluate the Alloy 22 waste package outer shell and the Titanium Grade 7 drip shield is described in detail in *Stress Corrosion Cracking of the Drip Shield, the Waste Package Outer Barrier, and the Stainless Steel Structural Material* (BSC 2003b, Section 6.2.1). Below this threshold stress value, initiation of SCC will not occur on a smooth surface (i.e., without sharp defects such as weld flaws that can generate a significant stress intensity factor). The SCC stress threshold value for Titanium Grade 7 is based on uniaxial constant-load SCC test results obtained primarily at 105°C, but also some results at 125°C in basic saturated water (a highly concentrated J-13 carbonate-dominated groundwater brine with a pH of 10.3 at 105°C) over a range of applied stresses. Metallurgical conditions tested included the mill-annealed and the 20 percent cold-worked conditions. In addition, results were obtained on a series of highly stressed Titanium Grade 16 and Titanium Grade 7 U-bend specimens in the mill-annealed and as-welded conditions. These U-bend specimens were exposed in the Long Term Corrosion Test Facility at 60°C and 90°C in a range

of concentrated brine environments (simulated dilute water, simulated concentrated water, and simulated acidified water) covering a pH range from about 2.7 to about 10. Materials tested included Titanium Grade 7 and Titanium Grade 16 (an excellent analog for Titanium Grade 7). The Titanium Grade 16 specimens were exposed for up to 5 years, and the Titanium Grade 7 specimens were exposed for 2 years. Based on the combination of U-bend results and constant-load Titanium Grade 7 specimen test results out to about 7,000 hours, it was estimated that the Titanium Grade 7 threshold stress for SCC initiation is near the material yield strength at temperature (BSC 2003b, Section 6.2.1). Since the SCC initiation test results are for exposures to about 5 years, an extrapolation scheme is needed to derive a threshold stress value associated with the lifetime of the waste packages and drip shields from the available experimental data. The ASME Boiler and Pressure Vessel code (ASME 1969, p. 80) conservatively assumes a factor of 2 on the runout stress (endurance limit) for defining fatigue lifetime cycles. Using this approach, a threshold stress value (criterion) can be derived from the minimum failure stress (or runout stress without failure) obtained from the constant load tests (i.e., $1.0\times$ yield strength for Titanium Grade 7 by applying an appropriate safety factor). Based on the assumption that the safety factor used be consistent with the ASME code approach, the resulting threshold stress should not exceed $0.5\times$ yield strength. Alternative approaches for developing a threshold stress applicable to the static conditions expected in the repository are being evaluated. Thus, a threshold stress for SCC initiation in Titanium Grade 7 of 50 percent of the material yield strength was selected as the SCC initiation criterion for use in design calculations (BSC 2003b, Section 6.2.1). Similarly, a threshold stress for SCC initiation of Alloy 22 was determined to be 90 percent of its yield (BSC 2003b, Section 6.2.1).

As described above, the development of a threshold stress criterion is based primarily on uniaxial test data plus results obtained on U-bend specimens under a biaxial stress state. In contrast, design calculations that determine the integrity of components under expected loading conditions generally result in stress outputs described in terms of multiaxial stress components. The application of the multiaxial stress condition (e.g., using a result from a three-dimensional finite element model) to assess the potential for crack initiation and failure of a component is consistent with the failure theory used in the ASME Boiler and Pressure Vessel Code (ASME 1969). The ASME code uses the Tresca criteria (maximum shear stress theory) as the failure basis and allows for comparison of multiaxial stresses with allowable stresses that were generated from uniaxial test results (ASME 1969; Bernstein 1988).

For example, the prediction of stress-strain behavior in sophisticated elastic-plastic analyses typically uses the equivalent (von Mises) stress-strain approach and uniaxial material stress-strain behavior. This uses uniaxial-based material strength test data to assess multiaxial stress conditions. In order to apply the uniaxial stress-strain information to multiaxial conditions, principal stresses are used. This approach considers that a combination of stresses can be equivalent to a uniaxial condition. Even in a uniaxial stress-strain test (where failure typically occurs along the 45-degree plane, in pure shear), the cross sections that are not perpendicular to the load line are in a multiaxial stress condition that is equivalent to the uniaxial condition. These multiaxial stress states can be observed using Mohr's circle. Thus, the use of uniaxial stress-strain curves for multiaxial loading conditions is acceptable when used in combination with principal stresses determined from the stress analyses.

SCC initiation can be treated as microscopic crack formation due to the repetitive process of passive film rupture at slip sites followed by a dissolution transient until passivation recurs. The mechanics of this slip dissolution/film rupture process are described in (BSC 2003b, Section 6.3). These microcrack formations are due to the plastic flow in the local state. Yielding occurs by slip or twin formation. These slip or twin formations occur in the plane that is subjected to the maximum stress (Liebowitz 1968).

By analogy to the theories and criteria used in structural type evaluations, initiation test data under the uniaxial test condition could be used to determine the initiation threshold under the triaxial stress state. The data can be used because the slip and twin formations occur perpendicularly to the maximum stress plane. In fact, the use of all stress components to determine principal stress for comparison against allowable stresses (from a uniaxial test) may be conservative, because it appears that initiation and failure is a function of the maximum stress only in a specific direction (BSC 2003a).

Threshold stress intensity factor is another established method of preventing crack propagation. In this case, crack propagation will not occur if the applied stress intensity factor remains below a threshold value (K_{ISCC}) (BSC 2003b, Section 6.3.5). The stress intensity factor is a direct function of the stress perpendicular to the crack plane. Thus, it is a function only of the stress perpendicular to a specific plane and similar to looking at uniaxial test data (for the same stress at the specific plane location).

The use of uniaxial test data to predict crack initiation and failure for a multiaxially loaded component is consistent with industry practice.

F.5 REFERENCES

ASME (American Society of Mechanical Engineers) 1969. *Criteria of the ASME Boiler and Pressure Vessel Code for Design by Analysis in Sections III and VIII, Division 2*. New York, New York: American Society of Mechanical Engineers. TIC: 254727.

Bernstein, M.D. 1988. "Design Criteria for Boilers and Pressure Vessels in the U.S.A." *Journal of Pressure Vessel Technology*, 110, 430-443. New York, New York: American Society of Mechanical Engineers]. TIC: 254806.

BSC (Bechtel SAIC Company) 2003a. *WAPDEG Analysis of Waste Package and Drip Shield Degradation*. ANL-EBS-PA-000001 REV 01D. Las Vegas, Nevada: Bechtel SAIC Company. ACC: MOL.20031009.0225.

BSC 2003b. *Stress Corrosion Cracking of the Drip Shield, the Waste Package Outer Barrier, and the Stainless Steel Structural Material*. ANL-EBS-MD-000005 REV 01 ICN 00. Las Vegas, Nevada: Bechtel SAIC Company. ACC: DOC.20030717.0001.

CRWMS M&O (Civilian Radioactive Waste Management System Management and Operating Contractor) 2000a. *Design Analysis for UCF Waste Packages*. ANL-UDC-MD-000001 REV 00. Las Vegas, Nevada: CRWMS M&O. ACC: MOL.20000526.0336.

CRWMS M&O 2000b. *Design Analysis for the Defense High-Level Waste Disposal Container*. ANL-DDC-ME-000001 REV 00. Las Vegas, Nevada: CRWMS M&O. ACC: MOL.20000627.0254.

CRWMS M&O 2000c. *Design Analysis for the Naval SNF Waste Package*. ANL-VDC-ME-000001 REV 00. Las Vegas, Nevada: CRWMS M&O. ACC: MOL.20000615.0029.

CRWMS M&O 2000d. *Design Analysis for the Ex-Container Components*. ANL-XCS-ME-000001 REV 00. Las Vegas, Nevada: CRWMS M&O. ACC: MOL.20000525.0374.

Liebowitz, H. 1968. *Microscopic and Macroscopic Fundamentals*. Volume 1 of *Fracture, An Advanced Treatise*. New York, New York: Academic Press. TIC: 254807.

Reamer, C.W. and Williams, D.R. 2001. Summary Highlights of NRC/DOE Technical Exchange and Management Meeting on Repository Design and Thermal-Mechanical Effects. Meeting held February 6-8, 2001, Las Vegas, Nevada. Washington, D.C.: U.S. Nuclear Regulatory Commission. ACC: MOL.20010307.0511 through MOL.20010307.0521.

Schlueter J. 2000. "U.S. Nuclear Regulatory Commission/U.S. Department of Energy Technical Exchange and Management Meeting on Container Life and Source Term (September 12-13, 2000)." Letter from J. Schlueter (NRC) to S. Brocoum (DOE/YMSCO), October 4, 2000, with enclosure. ACC: MOL.20010731.0161.

INTENTIONALLY LEFT BLANK

APPENDIX G

**QUANTIFICATION OF THE RESISTANCE OF ALLOY 22 AND TITANIUM GRADE 7
TO ENVIRONMENTALLY ASSISTED CRACKING PHENOMENA
(RESPONSE TO CLST 1.12 AND GEN 1.01 (COMMENTS 9, 10, 119, AND 120))**

Note Regarding the Status of Supporting Technical Information

This document was prepared using the most current information available at the time of its development. This Technical Basis Document and its appendices providing Key Technical Issue Agreement responses that were prepared using preliminary or draft information reflect the status of the Yucca Mountain Project's scientific and design bases at the time of submittal. In some cases this involved the use of draft Analysis and Model Reports (AMRs) and other draft references whose contents may change with time. Information that evolves through subsequent revisions of the AMRs and other references will be reflected in the License Application as the approved analyses of record at the time of License Application submittal. Consequently, the Project will not routinely update either this Technical Basis Document or its Key Technical Issue Agreement appendices to reflect changes in the supporting references prior to submittal of the License Application.

APPENDIX G

QUANTIFICATION OF THE RESISTANCE OF ALLOY 22 AND TITANIUM GRADE 7 TO ENVIRONMENTALLY ASSISTED CRACKING PHENOMENA (RESPONSE TO CLST 1.12 AND GEN 1.01 (COMMENTS 9, 10, 119, AND 120))

This appendix provides a response to Key Technical Issue (KTI) agreements Container Life and Source Term (CLST) 1.12 and GEN 1.01 (Comments 9, 10, 119, and 120). These KTI agreements relate to providing quantification of the resistance of Alloy 22 and Titanium Grade 7 to environmentally assisted cracking phenomena.

G.1 KEY TECHNICAL ISSUE AGREEMENTS

G.1.1 CLST 1.12 AND GEN 1.01 (COMMENTS 9, 10, 119 and 120)

KTI Agreement CLST 1.12 was reached during the U.S. Nuclear Regulatory Commission (NRC)/U.S. Department of Energy (DOE) Technical Exchange and Management Meeting on Container Life and Source Term held September 12 to 13, 2000, in Las Vegas, Nevada. Subissues 1 (effects of corrosion processes on the lifetime of the containers), 2 (effects of phase instability and initial defects on the mechanical failure and lifetime of the containers), 3 (the rate at which radionuclides in spent nuclear fuel are released from the engineered barrier subsystem through the oxidation and dissolution of spent nuclear fuel), 4 (the rate at which radionuclides in high-level radioactive waste glass are released from the engineered barrier subsystem), and 6 (effects of alternate engineered barrier subsystem design features on container lifetime and radionuclide release from the engineered barrier subsystem) were discussed at the meeting (Schlueter 2000). There has been no submittal related to this KTI agreement to the NRC.

Agreement GEN 1.01 was reached during the NRC/DOE Technical Exchange and Management Meeting held September 18 to 19, 2001 (Reamer and Gil 2001). At that meeting, NRC provided additional comments that relate to CLST 1.12, including GEN 1.01 (Comments 9, 10, 119, and 120) (Reamer and Gil 2001).

Wording of the agreements is as follows:

CLST 1.12

Provide the documentation for Alloy 22 and titanium for the path forward items listed on slides 34 and 35. DOE will provide the documentation in a revision to AMRs (ANL-EBS-MD-000005 and ANL-EBS-MD-000006) prior to LA.

The “path forward items listed on slides 34 and 35” are summarized below:

- Quantify and optimize mitigation processes
- Generate stress corrosion cracking (SCC) data for mitigated material over full range of metallurgical conditions (base metal, as-welded, welded and aged, cold worked)

- New vessels for Long Term Corrosion Test Facility (LTCTF) will house many of the SCC specimens
- Continue slow strain rate testing in same environments as above, specimens in the same range of metallurgical conditions
- Determine repassivation constants needed for film rupture SCC model to obtain value for the model parameter ' n '
- Continue reversing direct current potential drop crack propagation rate determinations in same types of environments and same metallurgical conditions as for slow strain rate testing and LTCTF tests
- Evaluate SCC resistance of welded and laser peened material versus nonwelded unpeened material
- Evaluate SCC resistance of induction annealed material
- Evaluate SCC resistance of full thickness material (with welds) obtained from demonstration prototype cylinder of Alloy 22 (mock-up site recommendation design).

GEN 1.01 Comment 9

Data supporting the residual stress calculations as a result of welding, after laser peening and after induction annealing are not provided.

Basis: The distribution of residual stresses in the waste package final closure welds is based on Finite element modeling. Details of the Model are provided in the *Stress Corrosion Cracking of the Drip Shield, the Waste Package Outer Barrier, and the Stainless Steel Structural Material* AMR. The effects of induction annealing on the residual stresses in the final closure are detailed in the *Residual Stress Minimization of Waste Packages from Induction Annealing* AMR. Several assumptions are made in the models that are not supported by data. These include the assumed temperature profile during welding, the cooling rates during welding and the residual stress during induction annealing.

The distribution of residual stress in the inner closure weld after laser peening is estimated in the SSPA using a shot-peened Incoloy 908 specimen. The technical basis for using a shot-peened specimen is not provided. Differences in the residual stress mitigation methods (i.e., mechanical shot-peening vs. laser peening) may result in significantly different stress distributions.

DOE Initial Response to GEN 1.01 Comment 9

This response is provided as a clarification. The residual stress profiles for the post-induction annealing conditions are based on ANSYS calculations using the induction annealing temperatures, temperature distributions and the cooling rates. These calculations are not dependent on the welding conditions and as-welded

stress distributions. Preliminary measurements of residual stresses in mock-ups that have been subjected to induction annealing have confirmed the effectiveness of this process. These measurements show that the resulting surface stresses are compressive.

The stress profiles for the laser-peened samples are based on actual measurements. The use of shot peening data on Incoloy 908 was only to get uncertainty distribution for the process. The actual magnitude of the stress values were not used in the analysis

Under existing CLST KTI agreements 1.12 and 2.05, DOE is in the process of generating relevant data for use in a potential LA model for SCC.

GEN 1.01 Comment 10

The modified stress corrosion cracking parameters are based in recent tests that may not consider the range of possible environments and the effects of fabrication processes.

Basis: The SSPA uses modified parameters for the stress corrosion cracking including the repassivation rate for the slip dissolution model and the minimum threshold stress for stress corrosion cracking. The SSPA indicates that these new parameters are based on recent data. The particular importance is the change in the minimum threshold stress which has been increased from 20-30 to 80-90 percent of the yield strength. The value of this parameter which is used in the model abstraction as the critical parameter for the occurrence of SCC is likely to be dependent on several factors that have not been investigated such as chemical composition of the environment and the effects of fabrication processes (only a limited number of cold worked and welded specimens has been evaluated).

DOE Initial Response to GEN 1.01 Comment 10

The initial threshold stress range was selected as 20-30 percent of yield to be conservative in the absence of significant Alloy 22 specific results. This range of threshold values was for stainless steels in boiling magnesium chloride and in a NaCl drip test on stressed specimens heated to 200°C. However, more recent Alloy 22 specific results are now available on stressed (significantly over yield) U-bends in boiling magnesium chloride and on two-year (and more limited 4-year) exposed samples in SCW, SDW and SAW at 60 and 90°C (the LTCTF tank environments) (including welded specimens). In addition, results are now available on creviced double U-bends exposed 17 months to approximately 50,000X J-13, pH approximately 13 (BSW) as well as constant load tests in approximately 2800X J-13, pH approximately 12.2 at stresses up to just below the ultimate tensile stress on annealed, welded, cold-worked and aged materials. These Alloy 22 specific results form the basis for the increase in threshold stress range to 80-90 percent of yield which is still well below the stress levels in the

various tests with all results being positive, i.e. no SCC. The high resistance to SCC initiation in this fairly broad range of relevant and accelerated test environments is also consistent with the crack growth test results obtained on compact tension specimens to BSW, SAW, and SCW where SCC is only initiated at pre-existing flaws at relatively high K values (30 and 45 MPa/m) under slow cyclic loading. When the very slow cyclic loading is changed to constant load, the crack front may continue to grow for a while at a very low rate (approximately $1\text{-}3\text{E}\text{-}10$ mm/s) but the growth generally tapers off to zero. Thus, even if SCC were to initiate, it is unlikely to continue to propagate. Thus, there is a significant basis for increasing the initiation stress threshold as done for the SSPA.

GEN 1.01 (Comment 119)

In p. 7-9 DOE claimed that NRC accepted the slip dissolution model. The DOE must supply the reference for this acceptance.

DOE Initial Response to GEN 1.01 Comment 119

DOE recognizes that the slip dissolution (GE PLEDGE) model has been used for stainless steels and the model needs to be validated for Alloy 22 and titanium, for the environmental conditions relevant to the repository. Data generated under existing KTI agreements CLST 1.12 and CLST 1.15 will provide the basis for this validation.

GEN 1.01 Comment 120

Page 7-11, the use of a triangular distribution for the residual stress uncertainty dictates that the endpoints of the distribution are well known. Showing the data compared to the distribution would support the selection of a triangular distribution.

DOE Initial Responses to GEN 1.01 (Comment 120)

A triangular distribution is used to represent uncertainty in the residual stress and stress intensity factor profiles in the weld regions of the outer and inner closure lids of the waste package Alloy 22 outer barrier. The triangular distribution was used because the uncertainty bounds used are conservative, considering the strict process control and inspections that will be implemented during the waste package manufacturing process.

If the data currently being obtained under existing CLST KTI agreements 1.12 and 1.13 warrant a change in the assumed distribution, this would be carried forward into a potential TSPA-LA.

G.1.2 Related Key Technical Issue Agreements

There are several KTI agreements that are related to KTI Agreement CLST 1.12. These include CLST 1.04, CLST 1.13, CLST 1.15, and CLST 1.16.

G.2 RELEVANCE TO REPOSITORY PERFORMANCE

This agreement is related to the quantification of the corrosion resistance of Alloy 22 (UNS N06022) and Titanium Grade 7 (UNS R52400) to environmentally assisted cracking phenomena such as SCC and hydrogen embrittlement. An understanding of the corrosion behavior of waste package materials is important both from the scientific and engineering points of view. Corrosion of the waste package and drift shield materials has direct impact on the performance of the repository over the regulatory life.

G.3 RESPONSE

The resolution of this agreement involves addressing multiple metallurgical variables such as stress mitigation, welding, and thermal aging, and environmental variables such as temperature, electrolyte composition, and applied potential. The current waste package design precludes environmentally assisted cracking in the absence of tensile stresses or under compressive stresses. After the fabrication of the waste packages (except for the final closure by welding), the waste packages will be solution-annealed to eliminate residual tensile stresses resulting from fabrication. After the final closure, tensile stresses due to welding will be mitigated by laser peening (burnishing is also under consideration). In the absence of tensile stresses, the issues relative to environmentally assisted cracking contained in KTI agreement CLST 1.12 are not significant since the possibility of SCC initiation due to weld residual tensile stresses can be eliminated except in the low-probability event of improper heat treatment. Note that laser peening is the current baseline method.

The Alloy 22 outer lid closure weld stress mitigation process will be one of two mechanical stress mitigation processes (i.e., laser peening or controlled plasticity burnishing) instead of the previously considered local induction annealing process. SCC testing of samples subjected to either of the stress mitigation processes is not considered necessary since SCC does not occur under compression. Based on the determination of near-surface compressive stress, as described in Appendix B and as corroborated in the boiling $MgCl_2$ test results for Stainless Steel Type 316, SCC testing of mechanically stress mitigated Alloy 22 mockups is not necessary.

Preliminary general corrosion testing (by polarization resistance measurements) and localized corrosion testing (by cyclic polarization measurements), both using laser-peened Alloy 22 plate material, show that negative effects from surface cold work (due to peening) per se are unlikely (Section G.4).

Nevertheless, confirmatory corrosion tests are planned on specimens fabricated from the outer stress-mitigated surfaces of a laser-peened plate and a controlled plasticity burnished plate at a range of locations. These include base metal, heat-affected zone material and weld metal. Other confirmatory tests (Appendix D) include (1) reversing direct current-crack growth rate tests, (2) constant-load SCC initiation studies, and (3) slow-strain-rate tests. These tests will address mainly metallurgical effects such as welding, cold work, and thermal aging on specimens produced from 1.25-inch-thick welded Alloy 22 plates. Additionally, the slow-strain-rate tests will also assess environmental effects such as electrolyte composition, temperature, and applied potential both on Alloy 22 and Titanium Grade 7.

More information on environmentally assisted cracking for Alloy 22 and drip shield materials, respectively, can be found in Sections 9 and 10.

The information in this report is responsive to agreements CLST 1.12 and GEN 1.01 (Comments 9, 10, 119, and 120) made between the DOE and NRC. This report contains the information that the DOE considers necessary for NRC review for closure of these agreements.

G.3.1 Specific Response to GEN 1.01 Comment 9

The response described under the DOE initial response is valid and sufficiently addresses the comment. Additional information is provided in Section G.4.

G.3.2 Specific Response to GEN 1.01 Comment 10

The DOE initial response to GEN 1.01 Comment 10 is current and has sufficiently addressed the issue. Moreover, as discussed in this report, confirmatory corrosion tests are planned on specimens fabricated from the outer stress-mitigated surfaces of a laser-peened plate and a controlled plasticity burnished plate at a range of locations. Additional information is provided in Section G.4.

G.3.3 Specific Response to GEN 1.01 Comment 119

The response to this comment is discussed in Appendix D where it is indicated that the report contains the information that the DOE considers necessary for NRC review for closure of the comment.

G.3.4 Specific Response to GEN 1.01 Comment 120

The median residual stress versus depth distribution is determined using finite element calculations accounting for the thermal perturbations induced by the welding process (BSC 2003a, Section 6.4.2.2). The effects of stress mitigation (laser peening) were then superposed on the results of the finite element calculation (BSC 2003a, Section 6.4.4). The resulting stress profile was fit to a third-order polynomial as a function of depth. Uncertainty in the residual stress profile was evaluated by considering measured data of samples that had undergone laser peening and shot peening. Also, empirical distributions in the published literature were considered. The uncertainty in the residual stress distribution was found to be represented by a multiplicative adjustment factor dependent on an uncertain parameter given by a normal distribution with a mean of zero and a standard deviation of 5 percent of the yield strength of Alloy 22 (BSC 2003a, Section 6.4.5). The normal distribution is truncated at ± 3 standard deviations (± 15 percent of the yield strength) which encompasses 99.7 percent of the parameter variation.

G.4 BASIS FOR THE RESPONSE

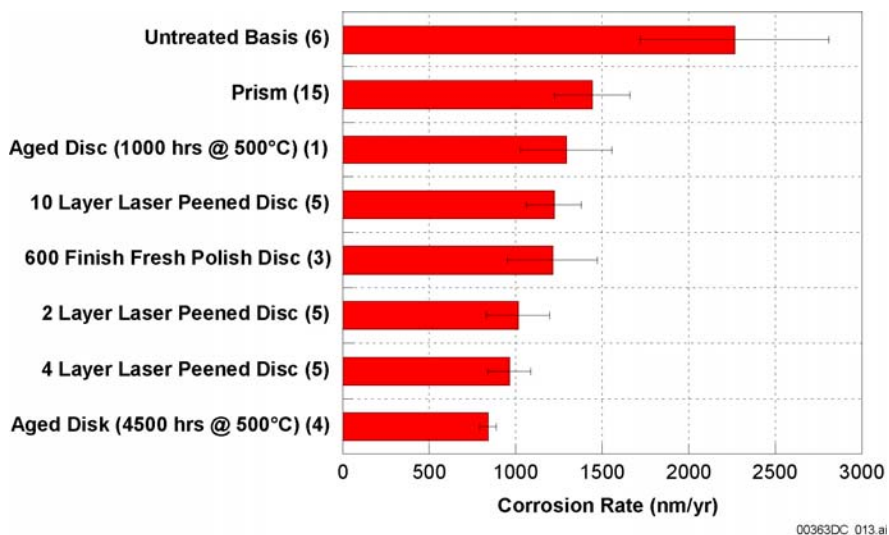
As described in Appendix B, the outer lid closure weld stress mitigation process will be one of two mechanical stress mitigation processes (i.e., either laser peening or controlled plasticity burnishing). Laser peening is the current baseline method. Both these processes are commercially available and result in near-surface compressive residual stresses along with a

shallow cold-work gradient normal to the outer surface. A decision on the process selection will be based on practicality of implementation at the Yucca Mountain site, welding and stress mitigation hot cell, and performance analyses.

SCC testing of laser-peened or other nonthermal mitigation-processed Alloy 22 weld samples is not considered necessary since SCC does not occur under compression. Tests have shown that in both the laser-peened and controlled plasticity burnished welded plate mockups, compressive stresses can be achieved to a depth greater than 3 mm (Appendix B). This thickness of metal with compressive stresses precludes its removal by general corrosion during the regulatory period. The expected absence of SCC in mechanically stress-mitigated welded plate has been corroborated at Lawrence Livermore National Laboratory using a stainless steel Type 316 butt-welded plate submerged in boiling $MgCl_2$ and containing a laser-peened section of weld- and heat-affected zone and nonpeened as-welded region (Hill et al. 2003). Stainless steel Type 316 was used in place of Alloy 22 since Alloy 22 does not suffer SCC in a boiling $MgCl_2$ environment. Posttest examination indicated no SCC damage on the laser-peened section of the weld, but extensive SCC damage on nonpeened sections with crack arrest near the boundary of the laser-peened zone.

Both laser peening and burnishing produce cold work in the near surface. This condition could potentially affect the precipitation kinetics of detrimental tetrahedrally close packed and long-range-ordering phases in the stress-mitigated Alloy 22 weld region. It has been explained in Section 8 of *Aging and Phase Stability of Waste Package Outer Barrier* (BSC 2003b) that precipitation of secondary phases reduces the toughness of the material and may lead to accelerated corrosion in aggressive acidic conditions. However, electrochemical tests of thermally aged Alloy 22 in simulated concentrated water, possibly representative of in-drift water at Yucca Mountain, showed no enhancement to general corrosion or local corrosion as compared to nonaged material. The thermally aged material was produced from a 1.25-inch-thick welded plate and aged at 700°C for 173 hours (BSC 2003c, Sections 6.4.4.3 and 6.4.6). The welding process and material thickness used are representative of the waste package Alloy 22 outer-lid closure weld. Indirectly, any effect of cold work on acceleration of aging kinetics for this thermal cycle will also have been observed in the series of tests just described. This is because the heat-affected zone regions near the weld fusion line for this type of relatively thick section weld can contain 10 to 25 percent cold work induced by weld shrinkage stresses generated during the welding process (Angeliu 2001).

Preliminary electrochemical-polarization-resistance-corrosion rate measurement results obtained in simulated acidic water (pH 2.7), Figure G-1, show an increase in corrosion resistance for laser-peened Alloy 22 base metal samples relative to their untreated controls as indicated by a lower average corrosion rate. Figure G-1 is a comparison of average-corrosion rates of various Alloy 22 sample types exposed to simulated acidic water at 90°C. In each case, 1 hour of open-circuit monitoring occurred before polarization resistance experiments were carried out. The number in parentheses to the far right refers to the number of tests performed on each sample type. The values shown in Figure G-1 should not be perceived as absolute corrosion rates but as relative values for providing a means of comparison.



Source: Chen et al. 2002, Figure 9.

NOTE: Numbers in parentheses represent number of tests on each sample.

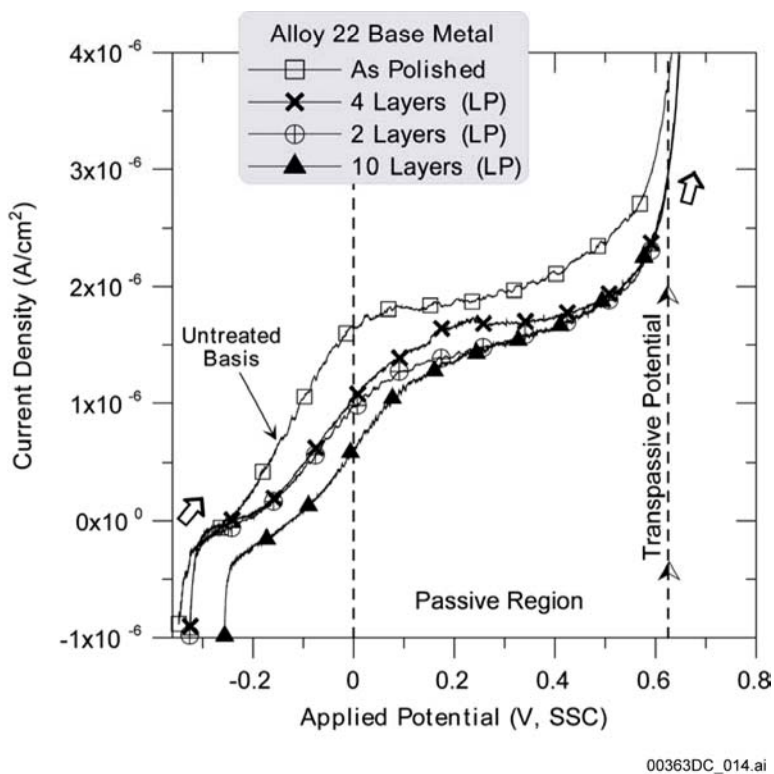
Figure G-1. Average Corrosion Rates for Alloy 22 in 90°C Simulated Acidified Water

According to Figure G-1, average-corrosion-rate values are approximately the same for the 2-layer, 4-layer, and 10-layer laser-peened surfaces. However, in general, average-corrosion rates for the untreated controls used in this study show higher corrosion rates.

In addition to the above polarization resistance measurements of the effect of peening on general corrosion, the potentiodynamic polarization curves shown in Figure G-2 exhibit lower passive current densities for the laser-peened samples compared to polished controls. There is no apparent decrease in passive current density between the sample that received four layers versus two layers of laser peening. However, a slightly lower passive current density can be seen for the 10-layer-treated sample when examining the active-passive region.

None of the Alloy 22 materials shown in Figure G-2 showed localized corrosion after cyclic polarization tests. Instead, transpassive breakdown results because of high applied anodic potential. For each curve shown in Figure G-2, transpassivity occurs at roughly the same potential, slightly beyond 600 mV, SSC.

As described earlier, the final closure weld mechanical stress mitigation processes can produce cold work, which could accelerate aging kinetics. However, no related corrosion degradation effects are expected, either from cold work or the aging process. It is planned to perform confirmatory tests on specimens fabricated from the outer-stress-mitigated surfaces of a laser-peened plate and a controlled plasticity burnished plate at a range of locations to include base metal, heat-affected zone material and weld metal. Selected specimens from each location will be thermally aged to evaluate the effect of process-generated cold work on aging kinetics and the resultant effect on general and localized corrosion resistance. This testing (cyclic polarization evaluations for localized corrosion and aging kinetic measurements for phase stability assessment) will not deleteriously affect waste package performance.



Source: Chen et al. 2002, Figure 10.

NOTE: LP = laser peening.

Figure G-2. Potentiodynamic Polarization of Alloy 22 in 90°C Simulated Acidified Water

In addition to the planned localized corrosion and thermal-aging tests on specimens machined from the laser-peened and controlled-plasticity burnished 1-inch welded plates at Lawrence Livermore National Laboratory, reversing direct current crack growth-rate-tests and constant-load SCC initiation tests (Appendix D) are planned for fiscal year 2004. These tests will emphasize welds and cold-worked and aged materials using specimens machined from 1.25-inch-thick gas-tungsten arc welding Alloy 22 plates. The welding process and material thickness tested will be representative of the currently planned waste package final closure lid weld. Reversing obtained direct current data establishes the threshold stress intensity factor, K_{ISCC} , and constant-load testing on samples with a range of relevant metallurgical conditions offers a basis for stress threshold on smooth surfaces. Results from the testing will be used for reducing uncertainties in the SCC model and confirming the expected lack of negative impact of the stress mitigation processes.

Some SCC specimen testing is included in fiscal year 2004 as part of the restock plan discussed in CLST 1.04. Only slow-strain-rate testing supplementary to reversing direct current testing is planned. This testing will be another component of continuing slow-strain-rate testing that investigates metallurgical (welded and welded plus aged) and environmental (trace impurities, temperature, and applied potential effects). By covering a broader range of metallurgical conditions and test environments and demonstrating that the Alloy 22 SCC initiation does not occur, these slow-strain-rate testing results are consistent with and corroborate the high

resistance to SCC of material observed in other tests. The repassivation constants needed for the film rupture SCC model (e.g., the model parameter “n”) have been determined indirectly from Alloy 22 SCC data and are used as inputs to the SCC model (BSC 2003b).

The Titanium Grade 7 drip shield will be emplaced in a stress-mitigated condition (Appendix D). Consequently, it is not planned to implement an additional stress-mitigation process on drip shield welded regions. As with Alloy 22, Titanium Grade 7 SCC initiation and crack growth test results have been used to develop an SCC initiation threshold stress criterion for use in drip shield design. The criterion requires that applied stresses be less than 50 percent of the at-temperature yield strength as described in Appendix D.

G.5 REFERENCES

Angeliu, T.M. 2001. “Microstructural Characterization of L-Grade Stainless Steels Relative to the IGSCC Behavior in BWR Environments.” *Corrosion/2001 56th Annual Conference & Exposition, March 11-16, 2001, Houston, Texas, USA*. Paper No. 01121. Houston, Texas: NACE International. TIC: 254941

BSC (Bechtel SAIC Company) 2003a. *Stress Corrosion Cracking of the Drip Shield, the Waste Package Outer Barrier, and the Stainless Steel Structural Material*. ANL-EBS-MD-000005 REV 01 ICN 00. Las Vegas, Nevada: Bechtel SAIC Company. ACC: DOC.20030717.0001.

BSC 2003b. *Aging and Phase Stability of Waste Package Outer Barrier*. ANL-EBS-MD-000002 REV 01 ICN 0. Las Vegas, Nevada: Bechtel SAIC Company. ACC: DOC.20030807.0004.

BSC 2003c. *General Corrosion and Localized Corrosion of Waste Package Outer Barrier*. ANL-EBS-MD-000003 REV 01. Las Vegas, Nevada: Bechtel SAIC Company. ACC: DOC.20030916.0010.

Chen, H.L.; Evans, K.J.; Hackel, L.A.; Rankin, J.E.; Yamamoto, R.M.; Demma, A.G.; Dewald, A.T.; Lee, M.J.; and Hill, M.R. 2002. *Mitigation of Tensile Weld Stresses in Alloy 22 Using Laser Peening*. UCRL-ID-151055. Lawrence Livermore National Laboratory, Livermore, California. ACC: MOL.20030911.0252.

Hill, M.R.; DeWald, A.T.; Demma, A.G.; Hackel, L.A.; Chen, H-L.; Dane, C.B.; Specht, R.C.; and Harris, F.B. 2003. “Laser Peening Technology.” *Advanced Materials & Processes*, 161, (8), 65-67. Materials Park, Ohio: ASM International. TIC: 254943.

Reamer, C.W. and Gil, A.V. 2001. Summary Highlights of NRC/DOE Technical Exchange and Management Meeting on Range of Thermal Operating Temperatures, September 18-19, 2001. Washington, D.C.: U.S. Nuclear Regulatory Commission. ACC: MOL.20020107.0162.

Schlueter, J. 2000. “U.S. Nuclear Regulatory Commission/U.S. Department of Energy Technical Exchange and Management Meeting on Container Life and Source Term (September 12-13, 2000).” Letter from J. Schlueter (NRC) to S. Brocoum (DOE/YMSCO), October 4, 2000, with enclosure. ACC: MOL.20010731.0161.

APPENDIX H

**EXPECTED BEHAVIOR OF ALPHA TITANIUM ALLOYS
(RESPONSE TO CLST 6.02 AIN-1 AND CLST 6.03 AIN-1)**

Note Regarding the Status of Supporting Technical Information

This document was prepared using the most current information available at the time of its development. This Technical Basis Document and its appendices providing Key Technical Issue Agreement responses that were prepared using preliminary or draft information reflect the status of the Yucca Mountain Project's scientific and design bases at the time of submittal. In some cases this involved the use of draft Analysis and Model Reports (AMRs) and other draft references whose contents may change with time. Information that evolves through subsequent revisions of the AMRs and other references will be reflected in the License Application as the approved analyses of record at the time of License Application submittal. Consequently, the Project will not routinely update either this Technical Basis Document or its Key Technical Issue Agreement appendices to reflect changes in the supporting references prior to submittal of the License Application.

APPENDIX H

EXPECTED BEHAVIOR OF ALPHA TITANIUM ALLOYS (RESPONSE TO CLST 6.02 AIN-1 AND CLST 6.03 AIN-1)

This appendix provides a response to additional information needed (AIN) by U.S. Nuclear Regulatory Commission (NRC) based on its review of U.S. Department of Energy (DOE) submittals on Key Technical Issue (KTI) agreements CLST 6.02 and 6.03. These KTI agreements relate to the expected behavior of alpha titanium alloys.

H.1 KEY TECHNICAL ISSUE AGREEMENT

H.1.1 CLST 6.02 and CLST 6.03

Agreements CLST 6.02 and CLST 6.03 were reached during the NRC/DOE Technical Exchange and Management Meeting on Container Life and Source Term held September 12 to 13, 2000, in Las Vegas, Nevada. Subissues 1 (effects of corrosion processes on the lifetime of the containers), 2 (effects of phase instability and initial defects on the mechanical failure and lifetime of the containers), 3 (the rate at which radionuclides in spent nuclear fuel are released from the engineered barrier subsystem through the oxidation and dissolution of spent nuclear fuel), 4 (the rate at which radionuclides in high-level radioactive waste glass are released from the engineered barrier subsystem), and 6 (effects of alternate engineered barrier subsystem design features on container lifetime and radionuclide release from the engineered barrier subsystem) were discussed at the meeting (Schlueter 2000).

Wording of the agreements is as follows:

CLST 6.02

Provide additional justification for the use of a 400 ppm hydrogen criterion or perform a sensitivity analysis using a lower value. DOE stated that additional justification will be found in the report "Review of Expected Behavior of Alpha Titanium Alloys under Yucca Mountain Condition" TDR-EBS-MD-000015, which is in preparation and will be available in January 2001.

CLST 6.03

Provide the technical basis for the assumed fraction of hydrogen absorbed into titanium as a result of corrosion. DOE stated that additional justification will be found in the report "Review of Expected Behavior of Alpha Titanium Alloys under Yucca Mountain Condition" TDR-EBS-MD-000015, which is in preparation and will be available in January 2001.

The DOE has provided documents to the NRC pertaining to Container Life and Source Term agreements (Brocoum 2001; CRWMS M&O 2000). The NRC reviewed *Review of Expected Behavior of Alpha Titanium Alloys under Yucca Mountain Conditions* (CRWMS M&O 2000) and found that although additional justification and results were presented, the agreements had not been fully satisfied (Reamer 2001) and additional information was needed.

Though the subject report did contain additional information and justification for the use of a critical hydrogen concentration for cracking (H_C), NRC staff indicated the new critical hydrogen concentration of 1,000 ppm lacked sufficient justification for use. NRC staff requested additional justification and verification of the critical hydrogen concentration, citing that the majority of the testing reported was for Titanium Grade 16, not Titanium Grade 7. Furthermore, NRC staff expressed concerns about the possible detrimental effects of fluoride on hydrogen uptake and its effects on critical hydrogen concentration and subsequent cracking. Finally, analyses of Titanium Grade 24 structural drip shield components were requested.

Additional information needs follow:

CLST 6.02 AIN-1

1. Provide better justification to verify the critical hydrogen concentration chosen is a realistic and representative value for the onset of cracking in Titanium Grade 7. An evaluation of the critical hydrogen concentration for Titanium Grade 24 should also be given.
2. Provide an evaluation of possible detrimental effects of the fluoride on hydrogen uptake and its effects on the critical hydrogen concentration and subsequent cracking.
3. Provide the results for the Titanium Grade 24 structural drip shield components.

CLST 6.03 AIN-1

Provide an evaluation of the possible detrimental effects of fluoride on possible hydrogen uptake rates, as well as enhanced corrosion resulting in higher than currently estimated hydrogen generation rates.

The additional information needed by the NRC includes a better justification on the value selected for the threshold concentration of hydrogen, both for Titanium Grade 7 and Grade 24. The NRC also requested information on how the presence of fluoride in the environment could affect hydrogen uptake by the two titanium alloys. These AINs are addressed below in Sections H.3 and H.4.

H.1.2 Related Key Technical Issue Agreements

None.

H.2 RELEVANCE TO REPOSITORY PERFORMANCE

Titanium alloys may suffer a loss of ductility (embrittlement) due to hydrogen ingress into the metal. It is generally acknowledged that there is a minimum or threshold value on the concentration of hydrogen, below which the embrittlement of titanium will not occur (Shoosmith et al. 1995). The degradation of drip shield materials has an impact on the performance of the waste package. Embrittlement of titanium alloys could affect analytical results where strength of the drip shield is important (e.g., rockfall, seismic studies, etc.).

H.3 RESPONSE

CLST 6.02 AIN-1 and CLST 6.03 AIN-1 have been addressed and the following conclusions reached:

- The value of H_C , which is at least 1,000 $\mu\text{g/g}$, obtained from Titanium Grade 16 is applicable to Titanium Grade 7 (CLST 6.02).
- The H_C of Titanium Grade 24 is estimated to be around 400 to 600 $\mu\text{g/g}$, if not higher (CLST 6.02).
- The possible detrimental effect of fluoride is only functional when the specimens are freshly polished. In the presence of the thermally formed oxide layer on titanium alloys, the influence of fluoride is minor (CLST 6.03).
- The hydrogen content in Titanium Grade 7 due to passive dissolution over a timespan of 10,000 years is conservatively estimated as:

$$H_A 124 \mu\text{g/g} \ll H_C = 1,000 \mu\text{g/g} \quad (\text{Eq. H-1})$$

More information on corrosion and environmentally assisted cracking of the drip shield materials can be found in Section 10 of the technical basis document.

This information in this report is responsive to AIN requests CLST 6.02 AIN-1 and CLST 6.03 AIN-1. This report contains the information that the DOE considers necessary for NRC review for closure of these agreements.

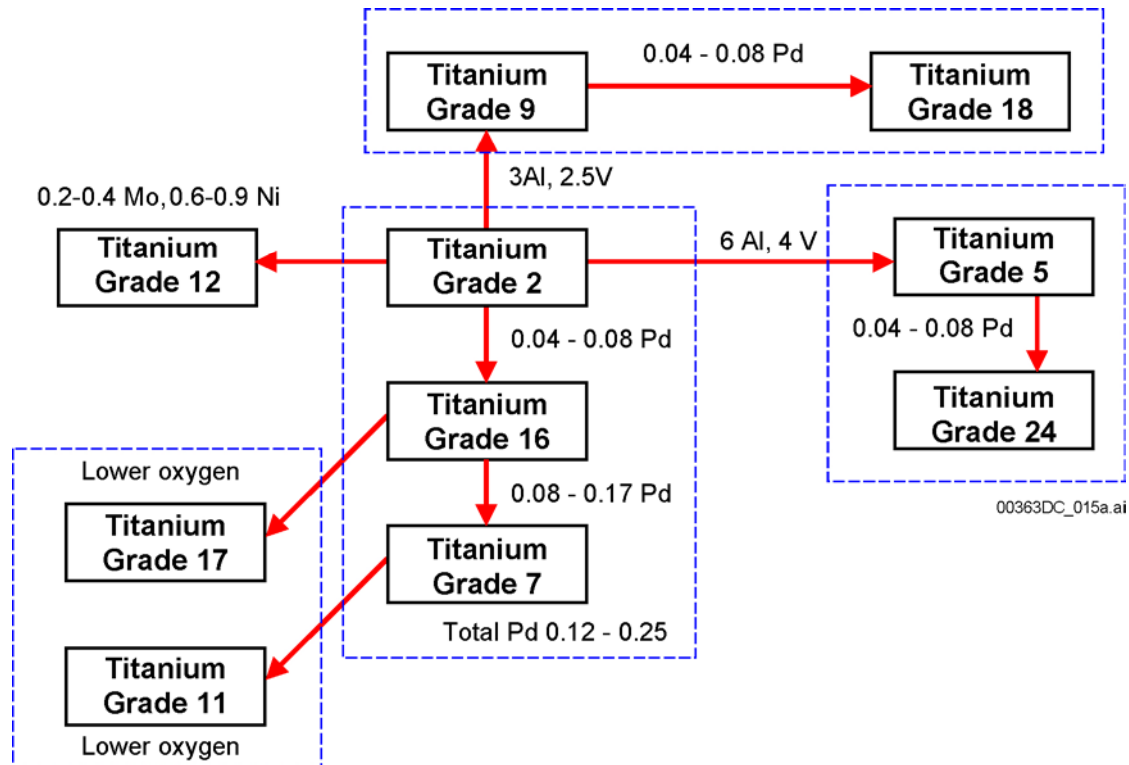
H.4 BASIS FOR THE RESPONSE

H.4.1 Justification for Critical Hydrogen Concentration of Titanium Grade 7 (CLST 6.02 AIN-1 Item 1)

Chemical Compositions and Mechanical Properties of Titanium Alloys—The properties of materials, including mechanical properties and corrosion resistance, largely depend on microstructures that depend on the chemical compositions of the materials. The chemical compositions and mechanical properties, per ASTM B 265-02, *Standard Specification for Titanium and Titanium Alloy Strip, Sheet, and Plate*, of the relevant titanium alloys, are shown in Tables H-1 and H-2. Titanium Grades 2, 12, 16, and 7 are α -alloys while Titanium Grades 5 and 24 are α - β alloys. Titanium Grade 7 contains slightly higher wt% of palladium (0.12 to 0.25 wt%) as compared to Titanium Grade 16 (0.04 to 0.08 wt%). The ASTM B 265-02 (2002) specified mechanical properties are identical for Titanium Grades 2, 16, and 7. They are also identical for Titanium Grades 5 and 24 and for Titanium Grades 9 and 18 (Table H-2) (ASTM B 265).

While certain alloying elements, such as oxygen, significantly influence microstructure and, consequently, mechanical properties of materials (e.g., comparing Titanium Grade 7 and Titanium Grade 11 and comparing Titanium Grade 16 and Titanium Grade 17 in Tables H-1 and H-2), palladium does not influence the microstructure, as can be seen from Tables H-1 and

H-2 by comparing the mechanical properties of Titanium Grades 2, 16, and 7 and by comparing the mechanical properties of Titanium Grades 5 and 24. The relationship between the major alloys discussed in this report is schematically shown in Figure H-1. The alloys grouped by dotted lines in Figure H-1 have identical mechanical properties regardless of their chemical compositions (an example is palladium), implying that these alloys have very similar, if not exactly the same, microstructures.



NOTE: Alloys grouped by the dashed lines have same mechanical properties, regardless of the chemical compositions.

Figure H-1. Relationship between the Relevant Titanium Alloys

Table H-1. ASTM B 265 Specifications for Chemical Composition Requirements (wt%) of Relevant Titanium Alloys in this Report

Material	UNS Designation	N	C	H	O	Fe	Al	V	Pd	Residual (each)	Residual (total)	Ti
Titanium Grade 12	R53400	0.03	0.08	0.015	0.25	0.30	—	—	—	0.2 to 0.4 Mo	0.6 to 0.9 Ni	balance
Titanium Grade 2	R50400	0.03	0.08	0.015	0.25	0.30	—	—	—	0.1	0.4	balance
Titanium Grade 16	R52402	0.03	0.08	0.015	0.25	0.30	—	—	0.04 to 0.08	0.1	0.4	balance
Titanium Grade 17	R52252	0.03	0.08	0.015	0.18	0.320	—	—	0.04 to 0.08	0.1	0.4	balance
Titanium Grade 7	R52400	0.03	0.10	0.015	0.25	0.30	—	—	0.12 to 0.25	0.1	0.4	balance
Titanium Grade 11	R52250	0.03	0.10	0.015	0.18	0.20	—	—	0.12 to 0.25	0.1	0.4	balance
Titanium Grade 5	R56406	0.05	0.08	0.015	0.20	0.40	5.5 to 6.75	3.5 to 4.5	—	0.1	0.4	balance
Titanium Grade 24	R56405	0.05	0.08	0.015	0.20	0.40	5.5 to 6.75	3.5 to 4.5	0.04 to 0.08	0.1	0.4	balance
Titanium Grade 9	R56320*	0.03	0.08	0.015	0.12	0.25	2.5 to 3.5	2.0 to 3.0	—	0.1	0.4	balance
Titanium Grade 18	R56322	0.03	0.08	0.015	0.15	0.25	2.5 to 3.5	2.0 to 3.0	0.04 to 0.08	0.1	0.4	balance

Source: ASTM B 265, Table 2.

NOTE: * UNS R56320 requires lower N, C, O, and H.

Table H-2. ASTM B 265 Specifications for Mechanical Properties of Relevant Titanium Alloys in this Report

Material	UNS Designation	Minimum Tensile Strength		Yield Strength, 0.2 % Offset				Minimum Elongation in 2 in., %
		ksi	MPa	Min		Max		
				ksi	MPa	ksi	MPa	
Titanium Grade 12	R53400	70	483	50	345	—	—	19
Titanium Grade 2	R50400	50	345	40	275	65	450	20
Titanium Grade 16	R52402	50	345	40	275	65	450	20
Titanium Grade 17	R52252	35	240	25	170	45	310	24
Titanium Grade 7	R52400	50	345	40	275	65	450	20
Titanium Grade 11	R52250	35	240	25	170	45	310	24
Titanium Grade 5	R56406	130	895	120	828	—	—	10
Titanium Grade 24	R56405	130	895	120	828	—	—	10
Titanium Grade 9	R56320	90	620	70	483	—	—	15
Titanium Grade 18	R56322	90	620	70	483	—	—	15

Source: ASTM B 265, Table 1.

Justification for H_C of Titanium Grade 7—The previously estimated H_C (400 $\mu\text{g/g}$) for Titanium Grade 7 was based on the results obtained for Titanium Grades 2 and 12 (CRWMS M&O 2000; Shoesmith et al. 1997). Based on more recently obtained experimental results (Ikeda and Quinn 1998, BSC 2003a) the reestimated critical hydrogen concentration of Titanium Grade 7 would at least be 1,000 $\mu\text{g/g}$.

The technical bases for this finding are:

- The only possibility that addition of palladium might deteriorate the resistance of titanium alloys to hydrogen-induced cracking is microstructural change. Titanium Grade 16 was developed based on the corrosion performance of Titanium Grade 7 with a more cost effective palladium content (0.04 to 0.08 wt%). Titanium Grade 7 and Titanium Grade 16 are virtually identical alloys except for palladium content (Figure H-1, Tables H-1 and H-2). Further increases of the palladium content from 0.04 to 0.08 wt% to 0.12 to 0.25 wt% does not influence the mechanical properties of the material since addition of palladium does not alter the microstructure of titanium alloys (Schutz and Xiao 1993).
- It is generally agreed that the titanium-palladium alloys should exhibit a higher H_C than titanium alloys without palladium (Greene et al. 2001). This is due predominantly to the prevention of hydrides formation in the matrix as a result of the higher solubility of hydrogen in the palladium-containing intermetallic particles (Shoesmith et al. 1997; Ikeda et al. 2000).
- H_C is a function of the stress intensity factor (Shoesmith et al. 1995) and, therefore, is determined by both the hydrogen solubility and response to material stress. Both Titanium Grades 7 and 16 are α -alloys containing minimal amounts of β -phase. It is reasonable to expect that both alloys will exhibit very similar responses to applied stresses in an acidic environment. Thus, the controlling factor in determining the H_C will be the solubility of the hydrogen in the alloy, which increases with palladium content. Titanium Grade 7 contains more intermetallic particles that can absorb more hydrogen.

The above evidence clearly suggests that the hydrogen-induced cracking behavior of Titanium Grade 7 should be at least as good as, if not superior to, that of Titanium Grade 16 (i.e., approximately 1,000 $\mu\text{g/g}$). Choosing the H_C as 1000 $\mu\text{g/g}$ for Titanium Grade 7, which was obtained for Titanium Grade 16, is not only appropriate but also conservative (BSC 2003a).

H.4.2 Justification for H_C of Titanium Grade 24 (CLST 6.02 AIN-1 Item 3)

The experimentally obtained critical hydrogen concentration for Titanium Grade 24 is not available at this time. However, the comparative corrosion behavior of Titanium Grade 24 and an approximate H_C value of this alloy can be estimated based on available information about other titanium alloys, including Titanium Grade 5, and on the relationship between Titanium Grades 2, 16, and 7.

Both Titanium Grade 5 and Titanium Grade 24 are high strength titanium alloys. Their chemical compositions and mechanical properties are shown in Tables H-1 and H-2. The ASTM B 265 specifications list identical minimum tensile strength and yield strength for Titanium Grade 5 and Titanium Grade 24 (895 and 828 MPa, respectively) (ASTM B 265). Both Titanium Grade 5 and Titanium Grade 24 contain 5.5 to 6.75 wt% of aluminum and 3.5 to 4.5 wt% of vanadium. The only difference between Titanium Grade 5 and Titanium Grade 24 is that Titanium Grade 24 contains 0.04 to 0.08 wt% of palladium. Titanium Grade 9 and Titanium Grade 18 are similar to Titanium Grade 5 and Titanium Grade 24 in that Titanium Grade 18 contains 0.04 to 0.08 wt% palladium while both contain 2.5 to 3.5 wt% aluminum and 2.0 to 3.0 wt% vanadium. The chemical compositions and mechanical properties of Titanium Grade 9 and Titanium Grade 18, with leaner aluminum and vanadium, are also listed in Tables H-1 and H-2.

The technical bases for these conclusions are:

- From Tables H-1 and H-2, addition of palladium to titanium alloys does not influence their mechanical properties, but aluminum and vanadium contents do. Three groups of titanium alloys listed in Tables H-1 and H-2 (Titanium Grades 2, 16, and 7; Titanium Grades 5 and 24; and Titanium Grades 9 and 18) have identical tensile and yield strength, and share other mechanical properties within their respective group. On the other hand, other alloying elements alter their mechanical properties, implying that addition of palladium to the level of interest does not modify the microstructure of titanium alloys.
- Testing of Titanium Grade 5 and its palladium-modified version, Titanium Grade 24, showed that the addition of palladium to Titanium Grade 5 improves the alloy's corrosion resistance in an analogous manner to that observed when palladium is added to the Titanium Grade 2 alloy to produce Titanium Grade 16 (Schutz 1995; Schutz and Xiao 1993; Kitayama et al. 1992). The mechanism by which palladium improves the corrosion resistance of Titanium Grade 24 as compared to Titanium Grade 5 is expected to be similar to that for Titanium Grade 7 as compared to Titanium Grade 16, where the accumulation of palladium in the corroding surface ennobles the corrosion potential of the alloys and increases the hydrogen solubility in the metal.
- The H_C has been established for Titanium Grade 5 by using similar experimental techniques as those used to determine the critical hydrogen concentrations for Titanium Grades 2, 12, and 16 (Hardie and Ouyang 1999). Using the slow-strain-rate technique on precracked compact tension specimens precharged with known amounts of hydrogen, Hardie and Ouyang showed that the fracture toughness of Titanium Grade 5 was not significantly altered until the hydrogen level in the alloy exceeded 200 $\mu\text{g/g}$ (Hardie and Ouyang 1999). For smooth tensile specimen, the authors showed that the reduction in area and elongation of Titanium Grade 5 did not decrease until the hydrogen concentration reached about 1,500 ppm (Hardie and Ouyang 1999).

Based on the above, it is clear that the addition of palladium should lead to a higher value of H_C in Titanium Grade 24. A similar increase in H_C was observed when Titanium Grade 2 was alloyed with same amount of palladium to produce Titanium Grade 16. A modest improvement

to 600 $\mu\text{g/g}$, if not higher, is not an unreasonable H_C value for Titanium Grade 24. However, considering the higher strength of Titanium Grade 24 than Titanium Grade 16 and Titanium Grade 7, it can be estimated conservatively, based on the above analysis, that the H_C of Titanium Grade 24 is at least in the range of 400 to 600 $\mu\text{g/g}$, if not higher. This estimated value of H_C is realistic and conservative. To support of this assertion, Kitayama et al. (1992) evaluated the effect of palladium added to Ti-6Al-4V (Titanium Grade 5) and Ti-3Al-2.5V (Titanium Grade 9) on their hydrogen-induced cracking behavior. By cathodically charging hydrogen to palladium-containing Ti-6Al-4V (an equivalent to Titanium Grade 24) to a level of approximately 1,000 and 1,100 ppm, the 0.2 percent proof stress was found to be about 175 and 145 ksi (Kitayama et al. 1992), respectively suggesting that no degradation in mechanical properties occurred. This implication corresponds to ASTM specifications for Titanium Grade 24 (ASTM B 265).

H.4.3 Effects of Fluoride (CLST 6.02 AIN-1 Item 2 and CLST 6.03 AIN-1)

The possible effect of fluoride on hydrogen uptake is expected to be primarily due to its enhancement of corrosion and subsequent enhanced hydrogen generation. Detailed discussions of the possible detrimental effects of fluoride on corrosion of titanium have been provided in *Hydrogen-Induced Cracking of Drip Shield* (BSC 2003a, Section 1.2.2) and in *General Corrosion and Localized Corrosion of the Drip Shield* (BSC 2003b, Section 6.3.7). This section briefly reviews the effects of fluoride on corrosion rates of titanium alloys and the role of oxide film on hydrogen absorption.

Role of Oxide Film on Titanium Alloys—Review of titanium corrosion literature indicates that the presence of dissolved fluoride in a range of brine solutions may, under certain conditions, significantly increase the general corrosion rate of titanium alloys, including Titanium Grade 7. However, in reviewing the effects of fluoride on enhanced general corrosion, it is important to separate the studies into those using relatively freshly polished specimens and those where the specimens were prefilmed either through longer-term ambient air exposure or through higher temperature exposures prior to corrosion testing.

Effects of fluoride on freshly polished specimens can be significant. For instance, the effects of fluoride were found to decrease the E_{corr} and result in a pseudo active/passive transition, with a subsequent potential independent current region displaying a current density considerably higher than that typically encountered during passive dissolution (as high as 10^{-3} to 10^{-1} , as compared to approximately 10^{-6} A/cm^2 when without fluoride). In a number of environment/temperature/pH conditions, investigators found a deleterious effect of fluoride ion on general corrosion rates and, under some conditions, on pitting resistance when freshly polished specimens were used. These have been summarized in BSC 2003a and BSC 2003b).

The importance of the condition of the passive film in resisting corrosion in neutral fluoride-containing solutions is demonstrated in the studies of Brossia et al. (2001) and Lorenzo de Mele and Cortizo (2000). Consistent with the observations on corrosion-resistance benefits from the formation of a stable passive prefilm, excellent corrosion behavior has been observed on both uncreviced and creviced Titanium Grade 16 and Titanium Grade 7 specimens tested in the Long Term Corrosion Testing Facility (BSC 2003b). All of these Long Term Corrosion Testing Facility specimens were preexposed to ambient air for several months after polishing at

the specimen fabricators shop and before placement in the corrosion tanks. No deleterious effects of fluoride on corrosion resistance of these titanium alloys were observed in any of these tests, including those in the so-called simulated concentrated water environment (approximately $1,000\times$ J-13 ionic concentration with approximately 1,619 mg/L F^- , 5,047 mg/L Cl^- , 5,482 mg/L NO_3^- , 13,209 mg/L SO_4^{2-} , and 27 to 49 mg/L $SiO_2(aq)$ at a pH of approximately 8-10).

For passive conditions, the rate of hydrogen absorption will be extremely low because the passive oxide film is highly impermeable to hydrogen unless the material is strongly cathodically polarized either by galvanic coupling to an active metal (e.g., carbon steel) or by the application of a large cathodic protection potential (Ikeda et al. 2000). These results strongly suggest that the influence of F^- is via the same mechanism as that involved for Cl^- and requires that F^- utilize defects within the oxide in order to initiate oxide breakdown rather than chemically attacking the outer oxide surface. Dissolution within such flaws then leads to the hydrolysis of dissolved titanium, and the required acidic conditions for the formation of HF, which leads to film destruction.

In the case of the drip shield application in the repository, there is an early period of ventilation (DOE 2002, Section 2.1.2.2). Under the repository conditions at Yucca Mountain, the Titanium Grade 7 drip shield surface will be covered with an oxide grown relatively slowly under thermal conditions. Such a film is expected to have a low defect density (Pan et al. 1997; Blackwood et al. 1988) and, hence, should be highly resistant to dissolution including that induced by reaction with F^- . Moreover, the repository environment at Yucca Mountain contains a significant amount of silica (e.g., 27 to 49 mg/L in simulated concentrated water), along with a variety of metal ions that have the potential to consume F^- ions, and thereby reduce the deleterious effects of fluoride on the Titanium Grade 7 drip shield to a low level. In addition to the described benefit of forming a stable, low-defect-density passive film on titanium before immersion in fluoride-containing brines, there can be a beneficial effect from other ions in the brine solution that are available in the repository.

Based on the above discussion, it is not surprising that no influence of F^- is observed on the passive corrosion rate of titanium specimens in the Long Term Corrosion Testing Facility tests. The concentration of F^- in these tests is either regulated to a low value by precipitation in a high-calcium environment, or, even when present in substantial amounts (1,619 mg/L in simulated concentrated water), displaced as an absorbed species from the passive surface by the much higher concentration of the other anions present. Additionally, the presence on the specimens of an air-formed film with a low-defect concentration formed prior to immersion in the test is expected to both eliminate the possibility of fluoride-induced passivity loss and maintain low passive-corrosion rates.

On the other hand, no catalytic effect of fluoride on hydrogen uptake has been reported. Therefore, for passive titanium and its alloys in the presence of fluoride, the rate of hydrogen absorption is expected to be proportional to the rate of the passive corrosion process, as it is under active corrosion conditions within a crevice (Noel et al. 1996). Even under these conditions, there is electrochemical evidence to show that the hydrogen absorption efficiency decreases with time (Noel et al. 1996). This can be attributed to the formation of a surface hydride layer leading to control of the hydrogen absorption process by transport across this layer.

The approximate hydrogen concentration in titanium due to passive dissolution is estimated below.

Brief Review of Modeling of Hydrogen-Induced Cracking of the Drip Shield–Drip shield hydrogen-induced cracking was modeled by using previously reported 1-year corrosion rates of Titanium Grade 16 obtained at Long Term Corrosion Testing Facility (BSC 2003a). After 1 year of exposure, measured corrosion rate at the 50th percentile was approximately 25 nm/yr (25×10^{-6} mm/yr); the rate at the 90th percentile was approximately 100 nm/yr (100×10^{-6} mm/yr); and the maximum rate was less than 350 nm/yr (350×10^{-6} mm/yr) (BSC 2003b). Corrosion data after 5-year exposure have been acquired more recently from the Long Term Corrosion Testing Facility and documented in *General Corrosion and Localized Corrosion of the Drip Shield* (BSC 2003b). The maximum possible general corrosion rates of the drip shield are 77 nm/yr (77×10^{-6} mm/yr) and 58 nm/yr (58×10^{-6} mm/yr) for crevice specimen and weight loss specimen, respectively. The average of the corrosion rates of weight loss specimens and weight loss plus crevice specimens is 68 nm/yr (68×10^{-6} mm/yr). It can be seen that these corrosion rates are significantly lower than the 1-year exposure data.

Shoesmith et al. (1997) developed a method of estimating the hydrogen content in titanium alloys due to passive dissolution. The details of the approach can be found in *Hydrogen Induced Cracking of Drip Shield* (BSC 2003a) and the work performed by Greene et al. (2001). Applying the method using the 5-year corrosion rate data and a hydrogen absorption efficiency fraction of 0.015, the hydrogen content in Titanium Grade 7 due to passive dissolution over a time span of 10,000 years can be estimated as:

$$H_A = 124 \mu\text{g/g} \ll H_C = 1,000 \mu\text{g/g} \quad (\text{Eq. H-2})$$

where H_A is the hydrogen concentration in titanium absorbed during the passive dissolution.

It should be pointed out that Greene et al. (2001) performed similar calculations on the H_A of Titanium Grade 7 based on “long-term” (up to a month) and “short-term” (a day) corrosion tests results in chloride-only and chloride-and-fluoride-only environments at 95°C. A hydrogen absorption fractional efficiency of 0.02 was used in the calculation ($f_h = 0.02$). The H_C used was 400 $\mu\text{g/g}$. The authors concluded that the Titanium Grade 7 drip shield will become embrittled in 700 years. However, it is a well-known fact that the general corrosion rates decrease with time. This is confirmed by corrosion rates of Titanium Grade 16 documented in *General and Localized Corrosion of the Drip Shield* (BSC 2003b). The average corrosion rate of the weight loss and creviced specimens was found to be only 68×10^{-6} mm/yr (68 nm/yr), much lower than the corrosion rates obtained in the 1-year tests. For time period beyond 5 years, it can be expected that the corrosion rates of Titanium Grade 16 and Titanium Grade 7 will decrease to an insignificant value. Use of short-term (a day to a month) corrosion rate data, as in the case of Greene et al. (2001), will result in an overly conservative prediction and is not appropriate. In addition, the test environments used by Greene et al. (2001) are highly conservative due to the absence of inhibiting anions such as NO_3^- .

The hydrogen-induced cracking model (BSC 2003a) is based on the assumption that both hydrogen generation and diffusion rates are constant. A literature review shows that both of the assumptions are conservative. The review shows that the rate of hydrogen absorption decays

following a parabolic relationship. It should be noted that the fractional hydrogen absorption efficiency (f_h) used in the calculation (0.015) is similar to that Okada (1983) obtained experimentally for Titanium Grade 2 under consistently applied current of 0.5 mA/cm² at 25°C in sodium sulfate solutions (pH = 4). The electrode potential achieved during these experiments was -1.14 V_(SCE), about -0.5 V more negative than the threshold value of -0.6 V_(SCE) for significant hydrogen absorption (Okada 1983). This kind of low potential is not likely to be achieved by galvanic coupling to less noble metals (e.g., carbon steel). Therefore, the above calculated 124 µg/g in 10,000 years has included the worst case scenario where titanium alloys are galvanically coupled to less noble metals; although, this is not likely to occur in the repository.

Given the high critical hydrogen concentration, the large volume of available titanium in the drip shield into which absorbed hydrogen can diffuse, and other reasons stated above, hydrogen embrittlement of the titanium drip shield is unlikely.

H.5 REFERENCES

H.5.1 Documents Cited

Blackwood, D.J.; Peter, L.M.; and Williams, D.E. 1988. "Stability and Open Circuit Breakdown of the Passive Oxide Film on Titanium." *Electrochimica Acta*, 33, (8), 1143-1149. New York, New York: Pergamon Press. TIC: 248517.

Brocoum, S. 2001. "Second Transmittal of Analysis and Model Reports (AMR), Calculations and Other Items Addressing Key Technical Issues (KTI) Technical Exchanges." Letter from S. Brocoum (DOE/YMSCO) to C.W. Reamer (NRC), February 2, 2001, OL&RC:TCG-0791, with enclosure. ACC: MOL.20010501.0238.

Brossia, C.S.; Browning, L.; Dunn, D.S.; Moghissi, O.C.; Pensado, O.; and Yang, L. 2001. *Effect of Environment on the Corrosion of Waste Package and Drip Shield Materials*. CNWRA 2001-003. San Antonio, Texas: Center for Nuclear Waste Regulatory Analyses. TIC: 252324.

BSC (Bechtel SAIC Company) 2003a. *Hydrogen Induced Cracking of Drip Shield*. ANL-EBS-MD-000006 REV 01. Las Vegas, Nevada: Bechtel SAIC Company. ACC: DOC.20030304.0003.

BSC 2003b. *General Corrosion and Localized Corrosion of the Drip Shield*. ANL-EBS-MD-000004 REV 01. Las Vegas, Nevada: Bechtel SAIC Company. ACC: DOC.20030626.0001.

CRWMS M&O (Civilian Radioactive Waste Management System Management and Operating Contractor) 2000. *Review of the Expected Behavior of Alpha Titanium Alloys Under Yucca Mountain Conditions*. TDR-EBS-MD-000015 REV 00. Las Vegas, Nevada: CRWMS M&O. ACC: MOL.20010108.0011.

DOE (U.S. Department of Energy) 2002. *Yucca Mountain Science and Engineering Report*. DOE/RW-0539, Rev. 1. Washington, D.C.: U.S. Department of Energy, Office of Civilian Radioactive Waste Management. ACC: MOL.20020404.0042.

Greene, C.A.; Henry, A.J.; Brossia, C.S.; and Ahn, T.M. 2001. "Evaluation of the Possible Susceptibility of Titanium Grade 7 to Hydrogen Embrittlement in a Geologic Repository Environment." *Scientific Basis for Nuclear Waste Management XXIV, Symposium held August 27-31, 2000, Sydney, Australia*. Hart, K.P. and Lumpkin, G.R., eds. 663, 515-523. Warrendale, Pennsylvania: Materials Research Society. TIC: 254939.

Hardie, D. and Ouyang, S. 1999. "Effect of Hydrogen and Strain Rate Upon the Ductility of Mill-Annealed Ti6Al4V." *Corrosion Science*, 41, 1, 155-177, 1999. New York, New York: Elsevier. TIC: 253121.

Ikeda, B.M. and Quinn, M.J. 1998. *Hydrogen Assisted Cracking of Grade-16 Titanium: A Preliminary Examination of Behaviour at Room Temperature*. 06819-REP-01200-0039 R00. Toronto, Ontario, Canada: Ontario Hydro. TIC: 247312.

Ikeda, B.M.; Quinn, M.J.; Noël, J.J.; and Shoesmith, D.W. 2000. "The Hydrogen-Induced Cracking and Hydrogen Absorption Behaviour of Grade-16 Titanium." *Environmentally Induced Cracking of Metals, Proceedings of the International Symposium, August 20-23, 2000, Ottawa, Ontario, Canada*. Elboujdaini, M.; Ghali, E. and Zheng, W.; eds. Pages 235-248. Montreal, Quebec, Canada: Canadian Institute of Mining, Metallurgy and Petroleum. TIC: 252836.

Kitayama, S.; Shida, Y.; Ueda, M.; and Kudo, T. 1992. "Effect of Small Pd Addition on the Corrosion Resistance of Ti and Ti Alloys in Severe Gas and Oil Environment." *Techniques for Corrosion Measurement, Papers Presented at the Corrosion/92 Symposium*. Paper No. 52. Houston, Texas: NACE International. TIC: 253165.

Lorenzo de Mele, M.F. and Cortizo, M.C. 2000. "Electrochemical Behaviour of Titanium in Fluoride-Containing Saliva." *Journal of Applied Electrochemistry*, 30, (1), 95-100. Dordrecht, The Netherlands: Kluwer Academic Publishers. TIC: 253126.

Noel, J.J.; Bailey, M.G.; Crosthwaite, J.P.; Ikeda, B.M.; Ryan, S.R.; and Shoesmith, D.W. 1996. *Hydrogen Absorption by Grade-2 Titanium*. AECL-11608. Pinawa, Manitoba, Canada: Atomic Energy of Canada Limited, Whiteshell Laboratories. TIC: 246232.

Okada, T. 1983. "Factors Influencing the Cathodic Charging Efficiency of Hydrogen by Modified Titanium Electrodes." *Electrochimica Acta*, 28, (8), 1113-1120. New York, New York: Pergamon Press. TIC: 246262.

Pan, J.; Leygraf, C.; Thierry, D.; and Ektessabi, A.M. 1997. "Corrosion Resistance for Biomaterial Applications of TiO₂ Films Deposited on Titanium and Stainless Steel by Ion-Beam-Assisted Sputtering." *Journal of Biomedical Materials Research*, 35, 309-318. New York, New York: John Wiley & Sons. TIC: 253215.

Reamer, C.W. 2001. "Container Life and Source Term Key Technical Issue Agreements." Letter from C.W. Reamer (NRC) to S.J. Brocoum (DOE/YMSCO), December 21, 2001, 0111021102, with enclosure. ACC: MOL.20020402.0608.

Schlueter, J. 2000. "U.S. Nuclear Regulatory Commission/U.S. Department of Energy Technical Exchange and Management Meeting on Container Life and Source Term (September 12-13, 2000)." Letter from J. Schlueter (NRC) to S. Brocoum (DOE/YMSCO), October 4, 2000, with enclosure. ACC: MOL.20010731.0161.

Schutz, R.W. 1995. "Recent Titanium Alloy and Product Developments for Corrosive Industrial Service." *Corrosion 95, The NACE International Annual Conference and Corrosion Show, March 26-31, 1995, Orlando, Florida*. Paper No. 244. Houston, Texas: NACE International. TIC: 245067.

Schutz, R.W. and Xiao, M. 1993. "Optimized Lean-Pd Titanium Alloys for Aggressive Reducing Acid and Halide Service Environments." *Corrosion Control for Low-Cost Reliability, Proceedings, 12th International Corrosion Congress, Houston, Texas, September 19-24, 1993*. 3A, 1213-1225. Houston, Texas: NACE International. TIC: 248725.

Shoesmith, D.W.; Hardie, D.; Ikeda, B.M.; and Noel, J.J. 1997. *Hydrogen Absorption and the Lifetime Performance of Titanium Waste Containers*. AECL-11770. Pinawa, Manitoba, Canada: Atomic Energy of Canada Limited. TIC: 236220.

Shoesmith, D.W.; Ikeda, B.M.; Bailey, M.G.; Quinn, M.J.; and LeNeveu, D.M. 1995. *A Model for Predicting the Lifetimes of Grade-2 Titanium Nuclear Waste Containers*. AECL-10973. Pinawa, Manitoba, Canada: Atomic Energy of Canada Limited. 1995. TIC: 226419.

H.5.2 Codes, Standards, and Regulations

ASTM B 265-02. 2002. *Standard Specification for Titanium and Titanium Alloy Strip, Sheet, and Plate*. West Conshohocken, Pennsylvania: American Society for Testing and Materials. TIC: 254000.

INTENTIONALLY LEFT BLANK